CAPABILITIES OF DIAGONALLY-CRACKED GIRDERS REPAIRED WITH CFRP

Final Report

SPR 619

CAPABILITIES OF DIAGONALLY-CRACKED GIRDERS REPAIRED WITH CFRP

Final Report

SPR 619

by

Christopher Higgins, Grahme Williams, and Lori Elkins
Kiewit Center for Infrastructure and Transportation
Department of Civil, Construction, and Environmental Engineering
Oregon State University
Corvallis, OR 97331

for

Oregon Department of Transportation
Research Unit
200 Hawthorne SE, Suite B-240
Salem OR 97301-5192

and

Federal Highway Administration
400 Seventh Street, SW
Washington, D.C. 20590-0003

June 2006

Technical Report Documentation Page

1. Report No.	2. Government Accession No.	3. Recipient's Catalog No.
FHWA-OR-RD-06-16		

4. Title and Subtitle	5. Report Date
Capabilities of Diagonally-Cracked Girders Repaired with CFRP	June 2006
	6. Performing Organization Code

7. Author(s)	8. Performing Organization Report No.
Christopher Higgins, Grahme Williams, and Lori Elkins Kiewit Center for Infrastructure and Transportation Department of Civil, Construction, and Environmental Engineering Oregon State University Corvallis, OR 97331	

9. Performing Organization Name and Address	10. Work Unit No. (TRAIS)
Oregon Department of Transportation Research Unit 200 Hawthorne Ave. SE, Suite B-240 Salem, OR 97301-5192	11. Contract or Grant No. SPR 619

12. Sponsoring Agency Name and Address	13. Type of Report and Period Covered
Oregon Department of Transportation Research Unit 200 Hawthorne Ave. SE, Suite B-240 Salem, OR 97301-5192 and Federal Highway Administration 400 Seventh Street, SW Washington, DC 20590-0003	Final Report
	14. Sponsoring Agency Code

15. Supplementary Notes

16. Abstract

The technique of using carbon fiber reinforced polymer (CFRP) for strengthening conventionally reinforced concrete (CRC) girders in flexure is well understood, but strengthening girders for shear is a newer application and less data are available. A literature review and survey were conducted to document the state of understanding and experience with respect to using CFRP for shear reinforcement of CRC girders. A laboratory investigation using full-size T- and inverted T-girder specimens with diagonal (shear) cracks was conducted to investigate the shear capacity improvement due to CFRP reinforcement and the effect of cyclic loading on CFRP shear strengthening. National and international code provisions for the design of CFRP in shear were used to compare the predicted shear capacity with the experimental results. An example application was included for using external CFRP strips to strengthen a bridge girder.

Strengthening with carbon CFRP strips provided a significant increase in load capacity and stiffness compared to unrepaired beams, and the improved capacity was maintained even after being exposed to the equivalent of twenty years of traffic-induced fatigue. At high load levels prior to failure, progressive debonding of multiple strips provided a clear, visual warning of distress.

The ACI 440 methodology provided a reasonably simple approach for shear capacity prediction of RC girders with externally bonded CFRP shear reinforcing for T-beams and is recommended for design. However, the ACI 440 method was unconservative where the CFRP strips terminate in the flexural tension zone. To provide a consistent level of reliability between T- and inverted T- conditions, the CFRP stress should be reduced by a factor of 2 for conditions when the CFRP strip is terminated in the flexural tension zone.

Placement of at least one CFRP strip across the diagonal crack with an anchorage length of at least one-half the height of the web is critical. An equation for strip layout is presented. In addition, girder shear strength can be increased using a targeted repair approach, applying CFRP material only to key critical sections rather than over the entire member. Thus, better economy may be achieved by judiciously applying CFRP materials just to those sections that are understrength for shear.

17. Key Words	18. Distribution Statement
Carbon reinforced polymer, composite, FRP, reinforced concrete, shear, repair, strengthen, beam, girder, fatigue	Copies available from NTIS, and online at http://www.oregon.gov/ODOT/TD/TP_RES/

19. Security Classification (of this report)	20. Security Classification (of this page)	21. No. of Pages	22. Price
Unclassified	Unclassified	18 + appendices	

SI* (MODERN METRIC) CONVERSION FACTORS

APPROXIMATE CONVERSIONS TO SI UNITS

Symbol	When You Know	Multiply By	To Find	Symbol
		LENGTH		
in	inches	25.4	millimeters	mm
ft	feet	0.305	meters	m
yd	yards	0.914	meters	m
mi	miles	1.61	kilometers	km
		AREA		
in^2	square inches	645.2	millimeters squared	mm^2
ft^2	square feet	0.093	meters squared	m^2
yd^2	square yards	0.836	meters squared	m^2
ac	acres	0.405	hectares	ha
mi^2	square miles	2.59	kilometers squared	km^2
		VOLUME		
fl oz	fluid ounces	29.57	milliliters	ml
gal	gallons	3.785	liters	L
ft^3	cubic feet	0.028	meters cubed	m^3
yd^3	cubic yards	0.765	meters cubed	m^3
NOTE: Volumes greater than 1000 L shall be shown in m^3.				
		MASS		
oz	ounces	28.35	grams	g
lb	pounds	0.454	kilograms	kg
T	short tons (2000 lb)	0.907	megagrams	Mg
		TEMPERATURE (exact)		
°F	Fahrenheit	(F-32)/1.8	Celsius	°C

APPROXIMATE CONVERSIONS FROM SI UNITS

Symbol	When You Know	Multiply By	To Find	Symbol
		LENGTH		
mm	millimeters	0.039	inches	in
m	meters	3.28	feet	ft
m	meters	1.09	yards	yd
km	kilometers	0.621	miles	mi
		AREA		
mm^2	millimeters squared	0.0016	square inches	in^2
m^2	meters squared	10.764	square feet	ft^2
m^2	meters squared	1.196	square yards	yd^2
ha	hectares	2.47	acres	ac
km^2	kilometers squared	0.386	square miles	mi^2
		VOLUME		
ml	milliliters	0.034	fluid ounces	fl oz
L	liters	0.264	gallons	gal
m^3	meters cubed	35.315	cubic feet	ft^3
m^3	meters cubed	1.308	cubic yards	yd^3
		MASS		
g	grams	0.035	ounces	oz
kg	kilograms	2.205	pounds	lb
Mg	megagrams	1.102	short tons (2000 lb)	T
		TEMPERATURE (exact)		
°C	Celsius	1.8C+32	Fahrenheit	°F

*SI is the symbol for the International System of Measurement

ACKNOWLEDGEMENTS

Support for this research by Oregon Department of Transportation and Federal Highway Administration is gratefully acknowledged. The authors wish to especially thank Mr. Steven M. Soltesz for assistance in the performance of this research and Mr. Alan R. Kirk in the preparation of the final report.

All repair materials and procedures were donated by MBrace of Cleveland, Ohio and Pioneer Waterproofing of Portland, Oregon, with the help of Mr. Neil Antonini. Reinforcing steel and rebar fabrication were donated by Cascade Steel Rolling Mills of McMinnville, Oregon, and Farwest Steel of Eugene, Oregon, respectively.

The authors would also like to thank Dr. Tanarat Potisuk, Mr. Richard Forrest, Mr. Thomas Schumacher, Ms. Michelle Chavez, and Ms. Angela Rogge for their assistance in experimental testing and data reduction. The findings and conclusions are those of the authors and do not necessarily reflect those of the project sponsors or the individuals acknowledged.

DISCLAIMER

CAPABILITIES OF DIAGONALLY-CRACKED GIRDERS REPAIRED WITH CFRP

TABLE OF CONTENTS

1.0 INTRODUCTION

Diagonal cracks, typical of shear distress, have been identified in large numbers of reinforced concrete deck girder (RCDG) bridges in Oregon built between the late 1940's and early 1960's. Many of the cracked bridges are near the end of their original design life, and wholesale replacements would be costly. To extend their service lives, various repair methods have been considered. One repair technique is the application of carbon fiber reinforced polymer (CFRP) wraps.

The technique of using CFRP for strengthening girders in flexure is reasonably well understood, but strengthening girders for shear is a newer application and less data are available. In order to further the understanding of the contribution of the CFRP shear repair to conventionally reinforced concrete (CRC) girders, a research project was undertaken at Oregon State University.

There were several components to this research project.

- A literature review was conducted to examine fatigue of FRP as well as effects of environmental conditioning on the strength and response of the FRP materials and repaired structural components (Appendix A).

- A survey of state transportation departments was conducted to gather data on the experience of agencies with CFRP in shear for CRC and identify field performance related issues (Appendix B).

- A two-part laboratory investigation using full-size T- and inverted T- girder specimens was conducted to investigate the shear capacity improvement due to FRP reinforcement and the effect of cyclic loading on CFRP shear strengthening (Appendices C, D, and E).

- National and international code provisions for the design of FRP in shear were used to compare the predicted shear capacity with the experimental results (Appendix F).

- Lastly, an example application was included for using external CFRP strips to strengthen an Oregon Department of Transportation (ODOT) bridge girder to withstand ODOT Weight Table 4 trucks (Appendix G).

2.0 EXPERIMENTAL APPROACH

The laboratory investigation used full-scale beams with considerations made for typical details and material properties in order to reproduce the behavior of 1950's vintage CRC bridge deck girders as closely as possible. Five specimens were tested monotonically and three specimens were tested under fatigue loading to study the behavior of girders repaired for shear using CFRP u-wraps. Two designs were used to test shear behavior in both positive moment bending regions (T-beam) and negative moment bending regions (inverted-T (IT)), with various flexural bar cut-off, hook, and stirrup spacing details.

Specimens were initially loaded to produce diagonal cracking representative of that observed from field inspections of existing Oregon highway bridges. After cracking, the girders were repaired using two different unidirectional high-strength carbon fiber fabric strips applied in a wet lay-up procedure. The monotonic specimens were incrementally loaded to failure. The fatigue specimens were cyclically loaded based on the strains measured in a bridge that had been repaired with CFRP. After one million cycles, these beams were also incrementally loaded to failure.

Instrumentation was applied to each specimen to capture local and global behaviors. Strain gages were used to monitor internal steel reinforcing and external CFRP strains. Displacement transducers were used to measure diagonal deformations, local crack motions, and support displacements at each corner of the reaction plates. String potentiometers were used to measure centerline displacement.

The five design methods used for comparison to the experimental results were as follows (Appendix F):

- ACI-440.2R-02 (2004) with the ACI-318-05 (2005);
- the Canadian Standards Association's CSA S806-02 (2002);
- the International Federation of Structural Concrete's FIB Bulletin 14 (2001) with the European standard, Eurocode 2, (British Standard, BS EN 2004);
- the Japan Society of Civil Engineer's (JSCE) Concrete Engineering Series #41, (2001); and
- the approach developed by Monti & Liotta in Italy (2005).

Based on the results of the comparison, the ACI 440 method was applied to an Oregon bridge as a case study.

3.0 RESULTS

3.1 LITERATURE REVIEW

Details of the literature review are included in Appendix A. The results may be summarized as follows:

- Far fewer fatigue studies of girders with FRP shear reinforcement have been conducted compared to girders with FRP flexural reinforcement. Most fatigue tests on beams with FRP shear and flexural reinforcement have been conducted on small-scale specimens. The effect of scale is not well understood.

- In general, the literature shows that fatigue has little impact on the ultimate load capacity of FRP-strengthened beams.

- Results from environmental durability studies have had conflicting conclusions. Synergistic effects due to multiple environmental factors are not well understood.

3.2 DOT SURVEY

Details of the survey of state transportation agencies are included in Appendix B. The results may be summarized as follows:

- Responses from state transportation departments indicated that FRP has seen limited field applications for shear strengthening and wide variability in the practice, installation methods, post-installation inspection, and monitoring.

- The in-service history of externally bonded FRP reinforcing for shear has been relatively short, but to date, no performance issues have yet been identified.

3.3 LABORATORY AND FIELD TESTS

Details of the laboratory and field tests are included in Appendices C, D, E and G. The results may be summarized as follows:

- Superimposed dead load of the magnitude considered (typical for moderate span vintage RCDG bridges) and with ductile stirrups did not impact the ultimate strength of the specimens. For longer span bridges with higher dead to live load ratios or different material properties, the impact of dead load could be significant.

- Repair schemes for shear using discrete CFRP strips provided a significant increase in shear capacity compared to otherwise unrepaired members.

- Specimen response after application of CFRP strips was noticeably stiffer in terms of midspan displacement and diagonal deformations.

- The girders with CFRP exhibited strain compatibility between external CFRP strips and internal stirrups. Addition of the CFRP strips reduced the live-load demand in the internal stirrups at similar load levels but did not reduce flexural steel stresses.

- Addition of longitudinal CFRP strips alone did not increase shear capacity due to debonding and bending of fibers at the poorly constrained diagonal cracks. The combined effect of longitudinal and transverse strips was not investigated, although some synergistic benefits are anticipated.

- Failure was controlled by debonding of CFRP strips initiating near the deck/stem interface for both fatigued and nonfatigued specimens. Terminating edges of the CFRP strips located near the compression zone did not exhibit debonding under fatigue load although debonding and peeling did occur during follow-up strength testing.

- The CFRP repaired members tended to exhibit steeper crack angles than similar unrepaired specimens. At the point of failure, only a single u-wrap was still acting across the failure diagonal crack.

- Thicker CFRP material exhibited reduced amounts of debonding and cracking and achieved higher bond stress than the thinner material. The full effectiveness of thicker CFRP material could not be achieved for the IT specimens due to debonding and peeling at the terminating strip edges in the flexural tension zone.

- Shear strengths were similar for the specimens with CFRP strips applied over the entire length and with CFRP strips targeted to a single critical region.

- Prior to failure, significant areas of debonded CFRP material were observed. Progressive debonding of multiple strips over the loading history provided a visual indication of distress prior to failure.

- Debonded areas of CFRP material tended to occur at and around concrete cracking locations and were easily identified visually by inspection and infrared thermography or by tapping on the CFRP material and listening for a change in sound frequency.

- Under ambient traffic loading, the single largest field measured strain range for an instrumented CFRP strip on an in-service bridge was approximately 34 με. Based on ambient traffic induced strain ranges, the equivalent constant amplitude strain range was below 15 με for all CFRP locations. Using the highest field measured strain location, a CFRP strain range required to produce an estimated equivalence of 20 years of service-

life damage in 1,000,000 cycles for laboratory specimens was determined as approximately 20.5 με.

- Service-level fatigue loading histories, higher than those observed in the field, did not produce significant changes in ultimate shear capacity, and no substantial visual differences between fatigued and unfatigued specimens prior to failure were observed.

- Under repeated loading, small areas of the CFRP strips debonded along diagonal cracks and at the terminating edges of the strips in the flexural tension zone at the deck/stem interface. These small debonded areas had little effect on the load capacity of the beams. Field inspections for large debonded regions that could indicate significant damage to the CFRP should focus on these regions.

3.4 ANALYSIS METHODS AND IMPLICATIONS FOR FUTURE DESIGN

Specification-based prediction of the CFRP contribution to shear capacity varied widely among the different experimental approaches (Appendix F):

- ACI-440.2R-02 (2004) with the ACI-318-05 (2005);

- the Canadian Standards Association's CSA S806-02 (2002);

- the International Federation of Structural Concrete's FIB Bulletin 14 (2001) with the European standard, Eurocode 2, (British Standard, BS EN 2004);

- the Japan Society of Civil Engineer's (JSCE) Concrete Engineering Series #41, (2001); and

- the approach developed by Monti & Liotta in Italy (2005).

The methodology presented by Monti & Liotta provided the best agreement between the predicted and experimental results; however, the method is complex.

The ACI 440 methodology provided a reasonably simple approach for shear capacity prediction of RC girders with externally bonded CFRP shear reinforcing for T-beams and is recommended for design use.

The ACI 440 method was unconservative when the CFRP strips terminate in the flexural tension zone. To provide a consistent level of target reliability between T and IT conditions, the CFRP stress should be reduced by a factor of 2 for conditions when the CFRP strip is terminated in the flexural tension zone. These results are based on comparisons with just two T-beams (only one failing in shear), and further verification of these findings on other large-size specimens should be investigated.

Member shear strength can be increased using a targeted repair approach, applying CFRP material only to key critical sections rather than over the entire member. Thus, better economy

may be achieved by judiciously applying CFRP materials just to those sections that are understrength for shear.

Repair for shear using CFRP must recognize the impact of the increased shear capacity on the flexural demands to prevent anchorage failures at flexural bar cut-off and anchorage details.

Spacing between strips permits identification of concrete cracking and highlights locations for more detailed inspection. Debonding tends to occur at and around concrete cracking locations. Applications of FRP sheets do not permit such inspection. Discrete CFRP strips are recommended for future installations.

A CFRP strip spacing of $g = \frac{1}{2}\left(\frac{h_w}{\tan\theta} - 3w_f \right)$ ensures that at least one strip crosses the diagonal crack with an anchorage length of at least one-half the height of the web,

where

g (in.) is the gap spacing between FRP strips;
h_w (in.) is the height of the web;
θ is the crack angle; and
w_f (in.) is the FRP strip width.

This geometry provides a good basis for design of the CFRP strip layout.

Due to the importance of bond for the CFRP strips, particularly those terminating in the flexural tension zone, pull-off tests should be conducted to ensure the concrete bonding surfaces can achieve the manufacturer's minimum recommended bond strength, prior to material installation.

4.0 RECOMMENDATIONS

4.1 RECOMMENDATIONS FOR RETROFIT

CFRP strips applied vertically on the web can be used to provide increased shear capacity in reinforced concrete girders. Because ambient traffic-induced load effects will have minimal effect on performance, CFRP retrofits can be considered as longer-term repairs. The strips need only to be placed in the critical area that controls the shear capacity instead of across the entire length of the beam; however, at least one strip should be positioned across an existing or potential diagonal crack so that the anchorage length is at least one-half the height of the web.

The ACI 440 method should be used for designing CFRP retrofits because it provides a good balance between capacity prediction and ease of use. However, where a CFRP strip terminates in a flexural tension zone in negative bending moment areas, the permissible CFRP stress should be reduced by a factor of 2 in the ACI 440 method to maintain a level of conservatism consistent with the flexural compression regions.

To help assure expected performance, pull-off tests should be conducted on the concrete prior to installing the CFRP to verify that the concrete has adequate bond capacity. In-service inspections should focus on the terminating edges of the CFRP strips in flexural tension zones and on locations where strips cross cracks. Progressive debonding leading to large debonded areas should trigger remedial action.

4.2 RECOMMENDATIONS FOR FUTURE STUDY

Future studies on CFRP strengthening for shear could build on the work reported here by identifying optimal wrap configurations for strength including the combined effects of CFRP materials applied for shear and flexure, developing supplemental anchorage or bond enhancement at terminated edges in the flexural tension zone, and evaluation of combined structural loading and environmental exposures to better assess in-situ long-term durability. Additionally, evaluation of the different design approaches could be furthered by parametric study of different uniform stirrup spacing, member size, and CFRP materials.

APPENDICES

APPENDIX A: LITERATURE REVIEW

Literature Review for Long-Term Durability in CFRP Reinforced Concrete

CFRP has begun to gain widespread acceptance as an effective means to strengthen reinforced concrete structures. As the application and design criteria are established, research begins to focus on long-term performance issues with regards to material and member durability. FRP materials in general have been well researched by other industries, such as the aerospace industry, and found to be durable with high strength-to-weight ratios. However, additional research is needed specific to civil engineering applications. Specifically, the effect of exposure to long-term loading and harsh environments on the strength of the FRP-to-concrete bond are not known. A detailed review of the state-of-the-art knowledge regarding the durability of CFRP addresses some of these topics.

Fatigue

Flexural Applications

In the last ten years there have been numerous studies on the fatigue strength of FRP reinforced structures for flexure (Aidoo *et al.* 2004 and 2006, Shahawy and Beitelman 1999, Papakonstantinou *et al.* 2001, Brena *et al.* 2005, Barnes and Mays 1999, Quattlebaum *et al.* 2005). In summary, most of the research has shown that the addition of FRP for flexural applications to RC girders increases the fatigue life of the specimen. Composite materials such as FRP typically exhibit greater fatigue life than other typical reinforcing materials such as steel (Papakonstantinou *et al.* 2001). The fatigue failure mode for both FRP strengthened and non-strengthened beams in previous studies is rupture of the steel reinforcing, typically followed by FRP debonding. The addition of FRP reduces the steel stress, allowing for greater life in structures reinforced with FRP compared to those without FRP under the same load magnitude.

Aidoo *et al.* (2004) tested FRP-strengthened T-beams that were scaled to represent girders from a decommissioned bridge. Results showed the fatigue behavior of the retrofit beams was controlled by the fatigue of the steel but the FRP application reduced the magnitude of the steel stress and therefore, increased the fatigue life. The study cautions that the fatigue life is only increased if there is an adequate FRP-concrete bond. If there is not, and peeling of the FRP occurs, then the fatigue life is similar to that of an unretrofitted specimen. It was recommended that the retrofit be as stiff as possible to achieve maximum benefit from the FRP although it was cautioned that the increased stiffness also increases the FRP-concrete bond stress. The authors' study in 2006 tested eight girders from the decommissioned bridge under static and fatigue loads and compared the results to the capacity as predicted by the ACI (2002) design guide. The study concluded that the ACI design guidelines are appropriately conservative for static loading but a further reduction in FRP strain limits is required to account for damage induced by even small fatigue loads. This was because even though the ultimate static capacity was unaffected by the 2 million fatigue cycles, the ultimate deformation capacity was significantly reduced. It was hypothesized that the damage accumulation was in the bond of the CFRP to the concrete and may affect the ultimate performance of the girders under loading larger than those tested (service level loads).

Papakonstantinou *et al.* (2001) tested seventeen small-scale concrete specimens retrofitted with GFRP on the flexural tensile surface. The fatigue life of the reinforced beams was extended

beyond that of the control beams but the failure mode did not change. The failure mechanisms in both groups were due to fatigue of the steel reinforcing and therefore, existing fatigue models are deemed appropriate for use with FRP retrofitted beams as well. Barnes and May (1999) found the same results with concrete girders retrofitted with CFRP. Again, the tests were on small-scale specimens retrofitted in flexure and the results showed failure to be governed by the steel stress for both the control and non-control beams.

Brena *et al.* (2005) tested concrete specimens retrofitted with two different CFRP systems under varying load conditions. Various amplitudes and durations of fatigue loadings were applied to the specimens before static testing to failure. For load amplitudes corresponding to service loads, the fatigue damage was minimal in the FRP, even as the number of load cycles was increased, but amplitudes corresponding to extreme load conditions caused damage to the FRP and failures were dominated by debonding of the FRP. The damage caused failures to occur at stress values in the FRP far below the limit for FRP rupture stress recommended by ACI design guide. The limited number of test specimens and the wide scatter in test results suggests further examination of the results is needed to confirm these results.

Along with the overall impact of the FRP strengthening on fatigue life, other parameters are typically examined in testing. FRP application type is one such parameter. FRP can be applied in a number of different ways and new applications are still emerging. FRP sheets, either full wraps or strips are the predominant method for strengthening and, based on static tests, the full wraps outperform the strip application method (Shahawy and Beitelman 1999). The authors found that stiffness and fatigue life increased for retrofitted beams compared to the control specimens.

Quattlebaum *et al.* (2005) referred to the wrap and strip FRP method as the conventional adhesive application (CAA) and compared this method to two newer applications, near-surface mounted (NSM) FRP, and powder-actuated fastener-applied (PAF) FRP. NSM is an emerging application where FRP strips are inserted into grooves cut into the concrete. PAF is a new, experimental method of installing mechanical fasteners as a means to attach the FRP into the concrete substrate. This is accomplished by using a powder-actuated fastener gun that nails the FRP into place through pre-drilled holes in the FRP. The NSM method was the top performer under both high and low stress level fatigue loads with the CAA being the lowest performer. All fatigue specimens, whether tested under a low or high-stress range, were characterized by a large initial accumulation of damage followed by a smaller rate of damage accumulation.

Shear Applications

Fatigue studies of shear reinforced FRP concrete girders are limited compared to those for flexurally reinforced specimens. The few tests examining shear are limited in number and most are not narrowly focused for fatigue of FRP wraps. Lopez *et al.* (2003) tested two beams in shear, one monotonically and one cyclically under high amplitude loading. Both were tested under low temperature conditions. The limited test data indicated that the combination of factors reduced the interface bond strength but increased the stiffness of the beam. The fatigue specimen failed in a different mode than the static specimen. Failure was initiated in the steel reinforcing and was attributed to the cold temperature and not the fatigue.

Czaderski and Motavalli (2004) performed a single fatigue test on a shear deficient concrete structure repaired with FRP. Their work used bonded CFRP L-shaped plates and not the more common wrap application. Fatigue was shown to not damage the L-plates after 5 million cycles at a load range equal to 59% of the load at failure. The mode of failure was the same as those of non-fatigue specimens; crushing of concrete after yielding of internal flexural reinforcement.

All of the above cited research for flexural and shear reinforcement of deficient concrete structures have conducted experiments to investigate various parameters relating to durability and most of these tests have been conducted on reduced-scale specimens. One of the major concerns regarding the studies that have been conducted in regards to these smaller specimens is that there has been no verification that this adequately represents the results of tests on full-size concrete beams. Aidoo *et al.* (2006) addressed the issue of potential scale-effects in their research review. They previously tested full-size specimens from a decommissioned bridge and compared the results to those of their test specimens at 62% scale. Their findings indicated that there appears to be little effect on results due to specimen scale but the data is limited and their full-size test components were relatively small compared with many typical RCDG bridge members so further verification of this finding is necessary.

The current study employs full-scale girders, replicated to the existing conditions of typical 1950's vintage RCDG bridges. Furthermore, realistic loading conditions for the tests was assured through measurements of actual bridge response under ambient traffic conditions for 30+ days and actual CFRP strain data gathered. Service-level fatigue loading, accelerated to simulate extended service life, was found to not change the ultimate capacity of the specimens. The failure modes of the fatigued and non-fatigued specimens were similar.

A summary of the fatigue research for FRP reinforced concrete structures is summarized in Table 1.

Bond Fatigue

Local bond behavior under fatigue loads is another an important consideration for characterizing the response of FRP strengthened reinforced concrete members. Various test set-ups have been utilized to test the FRP-concrete bond. Ferrier *et al.* (2005) conducted single and double-lap FRP-concrete bond tests in fatigue to examine the suitability of the two test methods in determining the allowable bond shear strength and the tensile FRP strength as a function of the number of cycles of loading. The two tests were conducted at separate institutions and produced comparable results verifying both test methods as acceptable measures of the bond and FRP fatigue properties. Two authors of the study, Bizindavyi and Neale, developed the single lap test while the double-lap test was based on the Japanese Concrete Institute (1998) standard test. Each test used a constant amplitude sinusoidal fatigue load protocol. Design factors for the composite material and the adhesive joint are proposed based on S-N curves fitted to the experimental data using Wohler's law. The factors are expressed as a fraction of the material's ultimate strength and range in values from 0.46 to 0.54.

Yang and Nanni (submitted for publication) tested CFRP laminates to investigate the lap length necessary to develop the tensile capacity of the material as well as to investigate the fatigue behavior of the composite. They conducted tension tests of the lap splice in a symmetric configuration of two layers, as opposed to the traditional single layer, to avoid any eccentricities in the loading which has been found to cause peeling of the layers and misrepresenting actual bond conditions in RC members. It was found that the static failure load increased proportionately up to a fixed lap length (38.1 mm for their specimens). Additional length did not increase capacity. Fatigue tests showed a lap length of 2.67 times the static length (corresponding to 01.6 mm for their specimens) performed satisfactorily for up to 2.5 million cycles at 40% of ultimate static strength. The results confirmed the appropriateness of the ACI-440 Design guide in determining allowable stress for CFRP reinforced concrete subjected to fatigue.

Kobayashi *et al.* (2003) proposed an alternative to the tension test to evaluate bond. A beam bending type of apparatus was developed that places the FRP and concrete bond into shear by subjecting the specimen to a uniform moment at the center. This test set-up was used to investigate the effect of concrete strength and varying load ratios. Confirming other experimental data, bond strength under fatigue loading was greater with increased concrete strength and decreased load-ratios (defined as a fraction of the static strength).

SUMMARY of FATIGUE TESTS										
			sample							
Author	**Main affiliation**	**Year**	**Sample**	**Sample size, (mm), bxhxL**	**Frequency (Hz)**	**Test method**	**Test sample size**	**Fatigue Loading**	**Failure mode**	
Shahawy *et al.*	Florida DOT	1999	t-beams with CFRP partial and full wraps	b_w = 91, h = 445, L = 5790	1	4-pt bending	16	25 to 50% of static ultimate load	varies	**FLEXURAL TEST,** Fatigue life can be extended with CFRP and its strength is a function of # of layers, concrete strength, and wrap configuration
Papakon-stantinou *et al.*	U. of South Carolina	2001	square section with GFRP	152x152x1321	varied	3-pt bending	17	varied	fatigue of steel followed by FRP debond for fatigue and static tests	**FLEXURAL TEST,** Fatigue doesn't significantly affect ultimate capacity, GFRP reinforced specimens, ACI fatigue model is conservative
Lopez *et al.*	Clarkson	2003	square section, hollow core with CFRP full wrap	203x203x1982	3	4-pt bending	4	target = 10-80,90,100% of static ultimate load	all CFRP debond except shear fatigue yielding of flexural steel	**SHEAR TEST**, all tests at low temp (-29 deg C), fatigue did not affect ultimate load capacity
Czaderski & Motavalli	EMPA, Switzerland	2004	t-beams with CFRP L-straps	b_w = 150, h = 500, L = 3500	4.4	4-pt bending	1	39% to 59% of ultimate failure load	concrete crushing with yielding of flexural reinforcement	**SHEAR TEST**, test specimen compared to 5 other static tests from previous work, similar failure mode in all tests, steel controls fatigue design
Aidoo *et al.*	U. of South Carolina	2004	t-beam with CFRP strips and sheets	b_w = 209, h = 508, L = 5640, 62% scale of a interstate bridge girder	1	3-pt bending	8	high stress (~11.5 to 65%) low stress (varied to 52%) of ultimate	fatigue specimens failed by fracture of reinforcing steel followed by CFRP debond	**FLEXURAL TEST**, Fatigue of retrofit specimen is controlled by the fatigue of the reinforcing steel, future studies to be conducted on scale-effect
Brena *et al.*	U. of Mass.	2005	rectangular beam with a wet-layup CFRP and CFRP plates	A)203x356x2896 and B)203x406x3200	2	4-pt bending	10	35 to 57% of yield load	A) steel fracture B) FRP debond	**FLEXURAL TEST**, Fatigue of the composite was found for amplitudes corresponding to extreme load conditions (overload conditions).
Quattlebaum *et al.*	U. of Pitt., U. of Cyprus	2005	rectangular beam comparing CFRP types (CAA, NSM, and PAF)	152x254x4572	1.3	3-pt bending	12	35 to 56% of yield load	fatigue of steel followed by FRP debond for fatigue and tests	**FLEXURAL TEST**, NSM method performed well in all fatigue tests while CAA was the worst performer of the three
Aidoo *et al.*	U. of Pitt., U. of Cyprus	2006	decommissioned bridge girders with 3 types of CFRP: CAA, NSM, and PAF	b_w = 343, h = 825, L = 8025	1.3	3-pt bending	8	range from DL to DL+(LL(HS25)+IM)	intermediate crack-induced debonding of the CFRP	**FLEXURAL TEST**, ultimate capacity not affected by 2 million fatigue cycles but deformation capacity was, ACI guidelines may be unconservative in strain limits for fatigue design

Table 1. Summary details of previous fatigue tests with FRP applied to reinforced concrete beams.

Environmental Factors

The effect of the environment on the durability of FRP reinforced structures remains largely unknown due to the relatively recent development of the technology. Further complicating the issue is that results from many of the durability studies have conflicting conclusions. This is often attributed to the lack of standardized testing protocols and complexity of performing accelerated tests.

Temperature

Based on review of the literature, extreme temperatures, either low or high, typically do not greatly affect strength. Low temperature (-28° C) was not found to significantly effect bond between CFRP and concrete when tested on 1/3 scale beams (El-Hacha *et al.* 2004), although other studies found some deleterious effects in the form of matrix hardening and fiber-matrix bond degradation under subzero temperatures (Karbhari 2002). Karbhari *et al.* (2003) noted that high temperatures cause the resin or adhesive to soften excessively, creating a potential weakness. Remaining within the manufacturer's suggested service temperatures was recommended. Myers and Ekenel (2005) examined installation temperatures and established recommended limits based on strength and workability to be between 4°C and 32° C for the two FRP systems studied.

Extreme temperature fluctuations, or freeze/thaw cycling, is another parameter that has been investigated with conflicting findings for strength. A study by Bisby and Green (2002) reviewed the available literature and found some research indicating a decrease in overall strength as a result of exposure to freeze/thaw cycles while other studies showed no significant effect. Their research on 39 small-scale beam specimens supported the conclusion that the change in temperature extremes alone does not adversely affect the overall flexural strength of the specimen. An earlier study by Green *et al.* (2000) found similar results. Kong *et al.* (2005) recently showed that axial compressive strength of wrapped concrete cylinders was reduced only 3% as a result of cyclic thermal exposure. The bond of the FRP to the concrete was not affected by the cyclic exposure, but there was a change in the adhesive properties as evidenced by a change in failure modes.

In contrast, del Mar Lopez *et al.* (1999) tested 48 small-scale beam specimens and found that the moment capacity and the maximum deflection decreased as a function of freeze/thaw cycles. It was also noted that precracked beams exhibited a larger decrease than initially uncracked specimens. Saenz *et al.* (2004) found degradation of a range of FRP composite systems after 50 accelerated freeze/thaw cycles, although the thaw cycles were conducted in salt water.

Moisture

Exposure to moisture alone has not been as well-researched because it is commonly coupled with other environmental effects such as temperature or various solutions. Grace (2004) found that 87% of the effectiveness of the CFRP strengthening scheme can be lost if the specimen is exposed to long-term relative humidity of 100%. Karbhari *et al.* (2003) gap analysis confirmed this finding showing that exposure to moisture can have deleterious effects on the fiber-matrix bond due to wicking along the interphase.

Wu *et al.* (2004) studied the effect of water on the cure and mechanical properties of epoxy adhesives. They found that a small amount of water (+2%) improved the cure time and the modulus and strength properties but excess water (> +4%) had a negative impact on these same properties.

Alkalinity/Salt Water Solutions

Concrete bridge girders may come into contact with alkaline solutions by means of contact with soil or in the presence of concrete pore water. As with moisture, the effects of exposure to an alkaline solution are not well-researched and the effects cannot easily be isolated from the effects of the solution. Research by Grace (2004) showed that alkalinity did not reduce the effectiveness of bonded FRP plates and thus did not warrant a reduction factor. However, Karbhari *et al.* (2003) recommended reducing the FRP stress levels in the presence of alkaline solutions. Further recommendations to reduce the effects of alkaline solutions are to ensure the resin is properly cured and that there is an appropriate thickness to reduce the rate at which the alkaline solution moves through the composite.

Uomoto and Nishimura (1999) looked at the degradation of fibers alone subjected to alkaline solutions and found that carbon fiber had excellent resistance except at elevated temperatures (80°C) but glass fiber strength reduced quickly.

Salt water is present in the marine environment and from salt spray generated by traffic where deicing salts are used. The effect of the salt water on the strength of the FRP to concrete bond has been examined by Sen *et al.* (2001). They looked at the effect of wet/dry cycles with tidal water and found that the presence of the tidal water did degrade the bond in accelerated tests and this degradation was not readily detected by visual inspection. Furthermore, thermal conditions added to the cycles did not produce any further weakness in the bond strength.

Synergistic Effects

Karbhari *et al.* (2003) conducted a comprehensive durability gap analysis, and one of the main conclusions was the need for examination of combined effects. In-situ FRP installations do not have just one of these environmental conditions in isolation, so further studies under more realistic combined conditions was recommended.

Some durability studies have already examined the effects from combinations of environmental conditions. Malavar *et al.* (2003) found that the combination of high humidity and high temperature had a large impact on the bond strength as measured by pull-off tests. Maximum relative humidity during adhesive application was recommended to be 85%, which was later confirmed by research done by Myers and Ekenel (2005).

Mukhopadhyaya *et al.* (1998) found that bond transfer length, shear stress, and plate slip increased with freeze/thaw and wet/dry cycles using a chloride solution as well as with a combination of the two. However, ultimate strength did not appear to be affected, and this was attributed to the accelerated nature of the tests. Exposure duration was only for 9 months but it was predicted that these effects would become more significant over an extended period of time.

References

Aidoo, J., K.A. Harries, and M.F. Petrou, (2004). "Fatigue Behavior of Carbon Fiber Reinforced Polymer-Strengthened Concrete Bridge Girders." *Journal of Composites for Construction*, Vol. 8, No. 6, pp. 501-509.

Aidoo, J., K.A. Harries, and M.F. Petrou, (2006). "Full-scale Experimental Investigation of Repair of Reinforced Concrete Interstate Bridge using CFRP Materials." *ASCE Journal of Bridge Engineering,* Vol. 11, No. 3, pp (in press).

ACI 440.2R-02 (2002). "Guide for the Design and Construction of Externally Bonded FRP Systems for Strengthening Concrete Structures." American Concrete Institute. Farmington Hills, Michigan.

Barnes, R.A, and G.C. Mays, (1999). "Fatigue Performance of Concrete Plates Strengthened with CFRP Plates." *Journal of Composites for Construction*, Vol. 3, No. 2, pp. 63-72.

Bisby, L.A., and M. F. Green, (2002). "Resistance to Freezing and Thawing of Fiber-Reinforced Polymer-Concrete Bond." *ACI Structural Journal*, Vol. 99, No. 2, pp. 215-223.

Brena, S. F., M.A. Benouaich, M.E. Kreger, and S.L. Wood, (2005). "Fatigue Tests of Reinforced Concrete Beams Strengthened Using Carbon Fiber-Reinforced Polymer Composites." *ACI Structural Journal*, Vol. 102, No. 2, pp. 305-313.

Czaderski, C., and M. Motavalli, (2004). "Fatigue Behavior of CFRP L-shaped Plates for Shear Strengthening of RC T-beams." *Composites Part B: Engineering*, Vol. 35, No. 4, pp. 279-290.

del mar Lopez, M., A.E. Naaman, and R.D. Till, (1999). "Bending Behavior of Reinforced Concrete Beams Strengthened with Carbon Fiber Reinforced Polymer Laminates and Subjected to Freeze-Thaw Cycles." *Proceedings of the 4th International Symposium on Fiber-Reinforced Polymer Reinforcement for Reinforced Concrete Structures*, pp. 559-576.

El-Hacha, R., M.F. Green, and R.G. Wight, (2004). "Flexural Behaviour of Concrete Beams Strengthened with Prestressed Carbon Fibre Reinforced Polymer Sheets Subjected to Sustained Loading and Low Temperature." *Canadian Journal of Civil Engineering*, Vol. 31, No. 2, pp. 239-252.

Ferrier, E., D. Bigaud, P. Hamelin, L. Bizindavyi, and K. Neale, (2005). "Fatigue of CFRPs externally bonded to concrete." *Materials and Structures*, Vol. 38, No. 275, pp. 39-46.

Grace, N.F., (2004). "Concrete Repair with CFRP." *Concrete International*, Vol. 26, No. 5, pp. 45-52.

Green, M.F., L.A. Bisby, Y. Beaudoin, and P. Labossiere, (2000). "Effect of Freeze-Thaw Cycles on the Bond Durability Between Fibre Reinforced Polymer Plate Reinforcement and Concrete." *Canadian Journal of Civil Engineering*, Vol. 27, No. 5, pp. 949-959.

Japanese Concrete Institute (1998). "Report II of Research Committee on Continuous Fiber Reinforced Concrete." Japanese Concrete Institute. Tokyo, Japan.

Karbhari, V.M., J.W. Chin, D. Hunston, B. Benmokrane, T. Juska, R. Morgan, J.J. Lesko, U. Sorathia, and D. Reynaud, (2003). "Durability Gap Analysis for Fiber-Reinforced Polymer Composites in Civil Infrastructure." *Journal of Composites for Construction*, Vol. 7, No. 3, pp. 238-247.

Karbhari, V.M., (2002). "Response of Fiber Reinforced Polymer Confined Concrete Exposed to Freeze and Freeze-Thaw Regimes." *Journal of Composites for Construction*, Vol. 6, No. 1, pp. 35-40.

Kobayashi, A., S. Matsui, and M. Kishimoto, (2003). "Fatigue Bond of Carbon Fiber Sheets and Concrete in RC Slabs Strengthened by CFRP." *Proceedings of the 6th International Symposium on Fibre-Reinforced Polymer (FRP) Reinforcement for Concrete Structures*, pp. 865-874.

Kong, A., A. Fam, and M.F. Green, (2005). "Freeze-Thaw Behavior of FRP-Confined Concrete Under Sustained Load." *Proceedings of the 7th International Symposium on Fiber-Reinforced Polymer (FRP) Reinforcement for Concrete Structures*, Vol. 1, pp. 705-722.

Lopez, M.M., A.E. Naaman, and L. Pinkerton, (2003). "Behavior of RC Beams Strengthened with FRP Laminates and Tested Under Cyclic Loading at Low Temperature." *International Journal of Materials and Product Technology*, Vol. 19, No. 1-2, pp. 108-117.

Malavar, L.J., N.R. Joshi, J.A Beran, and T. Novinson, (2003). "Environmental Effects on the Short-Term Bond of Carbon Fiber-Reinforced Polymer (CFRP) Composites." *Journal of Composites for Construction*, Vol. 7, No. 1, pp. 58-63.

Meyers, J.J., and M. Ekenel, (2005). "Effect of Environmental Conditions on Bond Strength Between CFRP Laminate and Concrete Substrate." *Proceedings of the 7th International Symposium on Fiber-Reinforced Polymer (FRP) Reinforcement for Concrete Structures*, Vol. 2, pp. 1571-1592.

Mukhopadhyaya, P., R.N. Swamy, and C.J. Lynsdale, (1998). "Influence of Aggressive Exposure Conditions on the Behaviour of Adhesive Bonded Concrete-GFRP joints." *Construction and Building Materials*, Vol. 12, No. 8, pp. 427-446.

Papakonstantinou, C.G., M.F. Petrou, and K.A. Harries, (2001). "Fatigue Behavior of RC Beams Strengthened with GFRP Sheets." *Journal of Composites for Construction*, Vol. 5, No. 4, pp. 246-252.

Quattlebaum, J.B., K.A. Harries, and M.F. Petrou, (2005). "Comparison of Three Flexural Retrofit Systems under Monotonic and Fatigue Loads." *Journal of Bridge Engineering,* Vol. 10, No. 6, pp.731-740.

Saenz, N., C. P. Pantelides, and L.D Reaveley, (2004). "Long Term Durability of Strengthened Concrete with Externally Applied FRP Composites." *International SAMPE Symposium and Exhibition (Proceedings)*, Vol. 49, pp. 2953-2966.

Sen, R., G. Mullins, M. Shahawy, and J. Spain (2001). " Effect of Environment on the Integrity of CFRP/Concrete Bond." *Proceedings of the Eleventh International Offshore and Polar Engineering Conference,* Vol. 4, pp. 222-226.

Shahawy, M., and T.E. Beitelman, (1999). "Static and Fatigue Performance of RC Beams Strengthened with CFRP Laminates." *Journal of Structural Engineering*, Vol.125, No. 6, pp. 613-621.

Uomoto, T., and T. Nishimura, (1999). "Deterioration of Aramid, Glass, and Carbon Fibers Due to Alkali, Acid, and Water in Different Temperatures." *Proceedings of the 4th International Symposium on Fiber-Reinforced Polymer Reinforcement for Reinforced Concrete Structures*, pp. 551-522.

Wu, L., S.V. Hoa, M. Ton-That, (2004). " Effects of Water on the Curing and Properties of Epoxy Adhesive Used for Bonding FRP Composite Sheet to Concrete." *Journal of Applied Polymer Science*, Vol. 92, No. 4, pp. 2261-2268.

Yang, X., and A. Nanni, (submitted for publication). "Lap Splice Length and Fatigue Performance of FRP Laminates." *ACI Structural Journal*, 25 pp.

APPENDIX B: SUMMARY OF STATE TRANSPORTATION DEPARTMENT SURVEY AND RESPONSES

Summary of State Transportation Department Survey and Responses

As part of the investigation into the shear strengthening of bridges with FRP, a survey was distributed to all state DOT's in the United States and as well as the Canadian provinces to acquire information about experiences with this repair method. 48% of the US states responded, with 20% of the respondents having used FRP for shear strengthening RC bridges while 23% of the Canadian provinces responded and 2/3 confirmed having used the practice. The results of those that responded in the affirmative are summarized.

In general, respondents have repaired a small number of bridges with FRP in shear as all respondents reported the number of bridges repaired by this method was in the range of 1-5. The objective of the strengthening was more widely dispersed with several affirmative responses in each of the identified categories just under 70% having repaired at least one bridge with the objective to "repair damage".

The method for designing the FRP retrofit was split approximately evenly among the ACI-440 method, material supplier, or other miscellaneous methods. Three respondents, two of which were the Canadian provinces, used alternate methods other than the codified or material supplier approaches.

Carbon fiber was the predominant type of FRP used with only one respondent using another material, fiberglass. Furthermore, all installed the FRP in the same manner, using that of the wet lay-up. The majority of agencies used a proprietary FRP and adhesive system while 27% used a generic type.

The FRP material was most commonly applied to the bridges in a U-wrap scheme but over half used other wrapping methods such as a complete wrap and side application. Still others used completely different schemes than those commonly employed. Complete sheets were more often used than discrete strips. The orientation of the FRP fibers was split between vertically inclined or at multiple angles.

7 out of 10 respondents injected cracks with epoxy prior to installing the FRP and the same number applied some form of environmental protection post FRP application. 40% reported that no bond tests were conducted on the concrete and FRP. The majority has inspected the FRP retrofit of the bridge since the installation but the same number reports that no long-term monitoring of the repair has taken place. Of those agencies that have inspected the FRP, none have reported any issues related to the performance of the FRP. This may be misleading as over half of the bridges that were repaired were done less than 5 years ago and the rest were repaired less than ten years ago making any long-term durability results inconclusive.

In summary, FRP has seen limited applications and wide variability in the practice, installation methods, and post-installation inspection and monitoring for shear strengthening bridges. The in-service life has been relatively short, but to date, no performance issues have been identified.

States and provinces that responded to the survey:

Alaska
Arizona
Arkansas
Colorado
Connecticut
Delaware
Florida
Illinois
Indiana
Iowa
Maine
Maryland
Missouri
Montana
New Jersey
North Dakota
Oregon
Pennsylvania
South Dakota
Tennessee
Texas
Virginia
Washington
Wyoming
British Columbia
Ontario
Alberta

Of those that responded, the states and provinces that have used FRP for shear strengthening bridges:

Colorado
Connecticut
Delaware
Florida
Illinois
Missouri
Oregon
South Dakota
Texas
Washington
British Columbia
Ontario

OREGON STATE University
Department of Civil, Construction, and Environmental Engineering
220 Owen Hall, Corvallis, OR 97331

Experience with FRP for Shear Strengthening of Conventionally Reinforced Concrete Bridges

This survey inquires about your agency's experience with fiber reinforced polymer (FRP) materials used for **shear strengthening** of **conventionally reinforced concrete bridges (not prestressed)**. For this survey, the shear strengthening is directed toward **gravity loads only** (dead and live loads), not seismic, wind, or other load effects.
If the question does not apply to your experience, do not check any boxes for that question. When a question warrants, please check all answers that apply (click the box). Contact Chris Higgins at email: chris.higgins@orst.edu or phone 541-737-8869 with any questions. If possible, please fill out electronically and **email** to chris.higgins@orst.edu , **fax** manually filled out form to 541-737-3052, or **mail** to address above.

Name of Transportation Agency:

Has your agency used FRPs for shear strengthening of RC Bridges (not prestressed)? 11 Yes 0 No

Roughly how many of your agency bridges have been strengthened with FRP for shear? 11 1-5 0 6-10 0 11-20 0 >21

What was objective of the strengthening? 2 Permit higher loads (bridge not deficient) 4 Eliminate posting (bridge was deficient) 7 Repair damage 3 Other

What design approach(es) were used for the FRP strengthening? 4 ACI 440 0 International code 1 no response 0 Internal Agency 4 Material supplier 3 Other

What FRP materials were used for shear strengthening? 10 Carbon 1 Fiberglass 0 Aramid 0 Other

How were the fiber and adhesive paired? 7 Proprietary Fiber and Adhesive System 3 Generic Fiber and Adhesive

What installation type(s) have been employed? 10 Wet lay-up 0 Precured laminates 0 Near-surface mount 0 Other

What wrapping scheme(s) have been employed (see Fig. 1 for reference)? 7 U-wrap 3 Complete Wrap 2 Sides Only 0 Sides Overlapped 2 Other

What was the size of the FRP? 5 Discrete Strips 7 Complete Sheets

What fiber orientations were used across the girder web? 5 Vertical Only 0 Diagonal Only 2 no responses

1 Horizontal Only 4 Multiple Angles

Were diagonal cracks epoxy injected prior to FRP installation? 7 Yes 4 No

Were bond tests between FRP and concrete conducted? 4 Yes 6 No 1 no response

Was any environmental protection applied to the FRP after installation? 7 Yes 3 No 1 no response

What is the age of the oldest in-service FRP shear repair for your agency? 6 0-5 4 5-10 0 >10

Has any long-term monitoring been conducted on the FRP strengthened bridges? 3 Yes 8 No

Have bridges with FRP shear strengthening been inspected since installation of FRP? 8 Yes 2 No 1 no response

If yes, have issues been encountered with field performance? 0Yes 8 No

If yes, what problems have been identified? 0 Re-cracking of concrete 0 Debonding/peeling of FRP
0 Other

Is there an agency contact that can provide additional detail for any of the above items?
Name:
Phone Number:
Email Address:

Thank you for taking the time to respond to this survey.

Feel free to provide any additional comments here:

Fig. 1 - FRP Shear strengthening

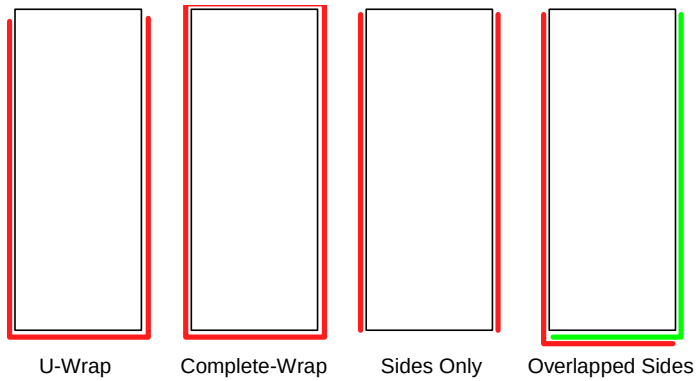

Table 2. Departments of Transportation FRP Survey Results

APPENDIX C: FULL-SCALE TESTS OF DIAGONALLY CRACKED CRC DECK–GIRDERS REPAIRED WITH CFRP

Full-Scale Tests of Diagonally Cracked CRC Deck–Girders Repaired with CFRP

Grahme T. Williams[1] and Christopher C. Higgins[2]

Biographical Sketch of Authors

[1] Design Engineer, Parsons Brinckerhoff, Melbourne, Australia (Former Graduate Research Assistant, Dept. of Civil, Construction and Environmental Engineering, Oregon State University, Corvallis, OR 97331)

[2]Associate Professor, Dept. of Civil, Construction and Environmental Engineering, Oregon State University, Corvallis, OR 97331

Keywords: bridges, carbon fiber, CFRP, full-scale testing, reinforced concrete, repair, shear

Abstract

The use of fiber reinforced polymers (FRP) is growing as a repair and strengthening technique for conventionally reinforced concrete (CRC) bridge elements. Much of the existing data regarding performance of members repaired with FRP has been gathered through testing of reduced-scale specimens. This investigation reports experimental results for five full-scale shear deficient reinforced concrete deck girders (RCDG) built to reflect 1950's vintage proportions, materials, and details. Specimens were loaded to produce diagonal cracks, repaired for shear with carbon fiber reinforced plastic (CFRP) u-wraps, and tested to failure. Results indicate the repaired members provide additional shear capacity and improve ductility even with large debonded regions prior to failure. The repairs also increased the member stiffness.

Introduction

Many 1950's CRC deck girder bridges remain in the national inventory and are reaching the end of their originally intended design lives. Field inspections in Oregon revealed that large numbers of these bridges exhibited significant diagonal cracks in the girders and bent caps (ODOT 2002). Over-estimation of the concrete contribution to shear resistance during design, reduced anchorage requirements for flexural steel, increasing service load magnitudes and volume, as well as shrinkage and temperature effects, may contribute to diagonal cracking of the bridge members. With the large population of cracked bridges and limited resources available for replacements, effective repair methods are needed. Many strengthening techniques for CRC elements have been introduced and studied, including the use of externally bonded steel plates, post-tensioning, and internal and external supplemental stirrups, among others. Externally bonded carbon fiber reinforced plastics (CFRP) are becoming more widely used and accepted for repair and strengthening of concrete members. CFRPs offer the potential for increased strength and stiffness, they have a relatively simple installation process, are resistant to corrosion from deicing chlorides, and contribute little additional weight to the member.

A significant amount of previous research exists on the behavior of CRC elements strengthened for shear with CFRP laminates (Chajes *et al*. 1995, Malvar *et al*. 1995, Sato 1996, Norris *et al*. 1997, Triantafillou 1998, Czaderski 2000, Kachlakev and McCurry 2000, Shehata *et al*. 2000, Al-Mahaidi *et al*. 2001, Li *et al*. 2001, Chen and Teng 2003). A very limited amount of this work has been done using full-scale specimens. Reduced-scale models may not adequately reflect realistic strain fields in large size members and limit the available development length for both reinforcing steel and FRP. The current design guide for FRP systems applied to structural concrete in the United States (ACI-440.2R-02 (2002)) recognizes the current lack of data on

large size elements in the introduction: “the design basis is the result of research primarily conducted on moderately sized and proportioned members” (ACI-440 2002). Other important factors for FRP applications to in-service members include incorporation of existing service level cracking as well as treatment of realistic reinforcement details such as flexural rebar cutoffs and variable stirrup spacing.

Research Significance

Large numbers of shear deficient CRC deck-girder bridges remain in service. A significant number exhibit diagonal cracking and there is concern regarding their ability to sustain the increasing volume and weight of modern truck traffic. Limited resources preclude wholesale replacements, and retrofit with CFRP offers the potential for extending their service life. Limited data is currently available and design approaches have not been fully validated regarding the performance of shear deficient full-size CRC girders repaired with CFRP. This paper provides details of an experimental program for five diagonally-cracked full-size CRC girders using realistic 1950’s stirrup and flexural details repaired with CFRP for shear.

Experimental Program

Test Specimens

Five specimens were tested monotonically to study the behavior of 1950’s vintage CRC deck bridge girders repaired for shear using CFRP u-wraps. Specimens were designed at full scale with considerations made for typical details and material properties. The behavior and capacity of the unrepaired specimens were well characterized based on previous work done by Higgins *et al*. (2004). Two designs were used to test both positive (T-beam) and negative moment bending regions (inverted-T (IT)) with various flexural bar cut-off, hook, and stirrup spacing details as seen in Fig. C1. Specimens were initially loaded to produce diagonal cracking representative of that observed from field inspections of existing Oregon highway bridges. They were then repaired with CFRP, and finally, tested to failure. The unrepaired shear strengths were predicted using the computer program *Response 2000* (Bentz 2000), which predicted the actual unrepaired member capacity to within 2% with a coefficient of variation of under 8% for a series of 44 similar full-size CRC specimens (Higgins *et al*. 2004). The estimated unrepaired shear capacities for the specimens are shown in Table C1.

All specimens were cast with the same cross-sectional geometry. Members had a height of 1219 mm (48 in.) with a stem width of 356 mm (14 in.) and a deck portion 914 mm (36 in.) wide by 152 mm (6 in.) thick as depicted in Fig. C1. Reinforcing bars for all of the specimens were from the same heats and tension tests were conducted to determine material properties, as summarized in Table C2. ASTM A615 Grade 420 (60 ksi) steel was used for the longitudinal reinforcing, with Grade 300 (40 ksi) steel for the stirrups. The stirrup grade is representative of intermediate grade steel used in the 1950’s. A concrete mix design was used which produced compressive strengths similar to core samples obtained from ODOT bridges of around 24 MPa (3500 psi). The 28-day and day-of-test compressive strengths are shown in Table C3.

All repairs were done using unidirectional high strength carbon fiber fabric applied in a wet lay-up procedure. Two different fibers were used with individual component and composite properties shown in Table C4. Composite properties were determined from unidirectional tension tests performed for each fiber thickness as per ASTM 3039 (2001) recommendations.

Pull-off tests of the CFRP were performed to determine bond strength for each specimen. Test results are shown in Table C3 and exhibited wide scatter.

Specimen Variables

All tests were conducted using a three-point loading configuration as shown in Fig. C2. Inverted-T (IT) specimens were tested at a span length of 6280 mm (20.6 ft) between centerline of supports for both initial and failure loading schemes and the T-beam was tested at 7315 mm (24 ft) span. Force was applied through a 3560 kN (800 kip) capacity hydraulic cylinder operating on a 69 MPa (10,000 psi) system. The applied force was measured with a 2670 kN (600 kip) capacity load cell and was distributed through a 25 mm (1 in.) thick, 305 mm (12 in.) square steel plate. End reactions were provided through 102 mm (4 in.) wide steel plates resting on 51 mm (2 in.) diameter steel rollers, supported on steel beams attached to the strong-floor. High-strength grout was applied to the interface between the steel plates and concrete beams to ensure uniform bearing areas.

Instrumentation was installed to capture local and global behaviors. Strain gages were used to monitor internal steel reinforcing and external CFRP strains, displacement transducers were used to measure diagonal deformations, local crack motions, and support displacements at each corner of the reaction plates, and string potentiometers were used to measure centerline displacement. Typical instrumentation is illustrated in Fig. C3.

Testing Method

An initial loading protocol was performed to induce diagonal cracking representative of in-service CRC girders, based on field measured values from previous research (Higgins *et al*. 2004). Maximum diagonal crack sizes after loading of each beam are shown in Table C3, and ranged from 0.635 – 1.27 mm (0.025 – 0.05 in.). After reaching the desired level of cracking, the applied load was removed from all but one specimen. The subsequent crack patterns are shown in Fig. C4. Specimen 1IT01 was held at an applied load of 356 kN (80 kips) after reaching the desired level of diagonal cracking to study the influence of superstructure dead load during repair. The dead load magnitude is representative of the service-level dead load shear near an interior support location for a typical 1950's vintage three-span continuous CRC deck-girder bridge having 15.2 m (50 ft) spans and a uniform dead load of 23.3 kN/m/girder (1.6 kip/ft/girder). The applied laboratory dead load moment was somewhat higher than the service-level bridge dead load moment due to the span geometry.

Once girders were diagonally cracked, a commercially available CFRP unidirectional high strength carbon fiber fabric laminate system was applied to the specimens in a pattern based on typical ODOT application methods and according to the manufacturer's recommended specifications. The entire repair procedure was performed by a qualified contractor with experienced personnel. Cracks were inspected and all significant diagonal cracks were injected with a high-strength epoxy resin and allowed to cure. It should be noted that not all visible cracks were injected, just those of sufficient width necessary to allow material to flow between the crack surfaces. The beams were then surfaced with a diamond bit grinder to remove loose concrete and expose surface voids. A primer was applied to the concrete surface. Once the primer was dry, putty and then saturant were applied to the surface. While both of these were wet, the carbon fiber was cut and applied to the specified locations, being worked into place with a soft trowel until the fibers were saturated. A final layer of saturant was then applied.

Upon reaching the manufacturer recommended curing time, the specimens were instrumented and tested to failure. U-wrap laminate locations on each specimen are shown in Fig. C5. A 406 mm (16 in.) gap was used between CFRP strips at midspan of each IT specimen to simulate the transverse bent cap location in a bridge structure, where CFRP could not be applied. Specimens 1IT01 and 1IT02 were repaired with a single layer of 305 mm (12 in.) wide CF130 laminate spaced 356 mm (14 in.) on-center. This allows a 51 mm (2 in.) gap between strips to permit visual identification of cracking in the concrete stem and is representative of what is done in the field. Specimen 1IT01 was loaded in 188 kN (40 kip) increments, followed by unloading to a minimum of 222 kN (50 kips) until failure. All other specimens were loaded in 222 kN (50 kip) increments followed by unloading to a minimum of 22 kN (5 kips) until failure. The overall load-deflection responses for all specimens are shown in Fig. C6.

Specimen 2T04 was repaired with a single layer of 254 mm (10 in.) wide CF160 laminate. For specimen 2T04, support locations were initially placed at 7315 mm (24 ft) and loaded to 2000 kN (450 kips). Member response did not exhibit signs of shear failure even as the flexible capacity was approached. The supports were moved to 6280 mm (20.6 ft) and the specimen was loaded to 2000 kN (450 kips), again without evidence of shear failure. Thus, the support spacing was again shortened to 5334 mm (17.5 ft) and the specimen was loaded to failure.

A targeted repair approach was used on specimen 4IT07 to attempt to produce a different failure mode or location than observed for specimens 1IT01 and 1IT02. The CFRP material was applied to a finite area (high shear and high moment region) rather than over the entire span. Laminate strips were a single layer of 305 mm (12 in.) wide CF160 spaced 356 mm (14 in.) on-center. The same unidirectional CF160 laminate was used to retrofit specimen 4IT08, but was applied with the fibers oriented horizontally rather than vertically. Four 254 mm (10 in.) wide strips were applied to each face of the web as shown in Fig. C5 and two 203 mm (8 in.) wide strips were applied in the center of the top surface of the deck flange on each side of the web. A gap between the longitudinal strips was again used to simulate the bent cap location whereby the strips cannot be continuous.

Experimental Results

The performance of each of the repaired specimens was evaluated through load-deflection response, internal stirrup and external CFRP strains, flexural reinforcement demands, and crack width growth. Global and local demands were compared before and after the specimens were repaired to assess the effect of CFRP on the internal stress distribution. Upon reloading after repair, cracking was observed along the previously epoxy injected diagonal cracks and occurred at approximately the same load levels as the original diagonal cracks. Debonding of the CFRP u-wraps was monitored in areas of terminations and at diagonal crack locations. As the applied load increased on all specimens, loud popping and snapping was heard as the strips progressively debonded from the web along the strip termination in the flexural tension zone and along the edges of the diagonal cracks. In all specimens partial debonding was observed to occur progressively. Even portions of the span that did not contain the failure crack had debonded strips and peeling from the surface of the concrete web. The progressive debonding of the multiple strips over the loading history provided a quasi-ductile response. Debonded areas were easily detectable by infrared thermography, by visual inspection, and sounding the CFRP strips.

Compared with adequately bonded strip areas, the debonded areas tended to have a lower, hollow sound when the surface was tapped, similar to that from the commonly used "chain-drag" technique used to identify delaminations in concrete decks. All specimens exhibited significant CFRP debonding, and a single remaining CFRP strip crossed the diagonal crack prior to failure (upon debonding of that strip). The debonding and peeling away of the CFRP strips at failure was a noticeable indicator of imminent failure. This progressive debonding provided a quasi-ductile response in that some amount of deformation was achieved as the maximum load remained constant. Further, the progressive debonding of the CFRP strips provides some of the philosophical intent behind the designer's desire for ductile response: warning of impending collapse.

The diagonal failure crack for the CFRP repaired specimens was generally observed to be at a steeper angle than those observed previously in similar unrepaired CRC girders (Higgins *et al*. 2004). None of the specimens exhibited fiber rupture. As fiber rupture did not occur at failure, the bond strength controlled the strength of the CFRP u-wraps. The condition of the single u-wrap remaining across the diagonal failure crack for each specimen prior to failure is shown in Fig. C7. The average bond stress (determined from the bonded area shown in Fig. C7) necessary to develop the measured CFRP strains at mid height of the u-wrap are shown in Table C1.

Specimens 1IT01 and 1IT02 were used to study the effect of dead load during repair procedures. Both specimens were repaired with identical material size, ply, layout, and procedure. The applied shear force at failure for specimen 1IT01 and 1IT02 were 1145 kN (258 kips) and 1112 kN (250 kips), respectively. The difference of 33 kN (8 kips) in applied shear force at failure showed little overall difference between the specimens. For the sufficiently ductile stirrup reinforcement and flexural details, the level of dead load did not significantly impact overall member capacity. Strain gage readings for the internal stirrups and the external CFRP u-wraps at nearly the same location, mid-height along the diagonal failure cracks, for Specimen 1IT01 exhibited strain compatibility over much of the loading history, as shown in Fig. C8(a). The strains in the stirrup and the CFRP were similar until a load of approximately 2060 kN (463 kips). Afterward the CFRP strain increased at a higher rate than the proximate stirrups. In contrast, specimen 1IT02 showed a lack of strain compatibility between the internal stirrup and the CFRP. As seen in Fig. C8(a), the strain in the CFRP was higher than that of the stirrup at each particular load step. A difference in performance between these two specimens was also seen from the diagonal deformations across the failure crack as shown in Fig. C8(b). Specimen 1IT01 exhibited less deformation, and was stiffer, than specimen 1IT02. This was also seen in the midspan displacement of the two specimens in Fig. C6.

Specimen 2T04 was the only test performed with the CFRP material applied to the positive bending region. During the load test to failure using the original span configuration, minimal CFRP debonding was observed and the flexural capacity was approached. To investigate the behavior of the CFRP in a shear dominated failure mode, the span length was shortened to preclude flexural failure. In Fig. C6, three different midspan displacement response curves show the behavior of the specimen during the precrack and at the two different span lengths subsequent to repair. A much stiffer response was observed by the addition of the CFRP laminate repair and by the shortened span length as shown in the midspan displacement behavior and also in the individual CFRP strains. In the different support configurations, the CFRP strains were smaller at corresponding load steps when the specimen had smaller moment for the same

shear magnitude. This indicates CFRP repaired members exhibit shear-moment interaction that may lend itself to sectional analysis methods such as modified compression field theory.

Example measured stirrup and CFRP strains across the failure diagonal crack show an uneven distribution in Fig. C8(a). The strains were larger in the CFRP than the stirrup at each load step. Also of interest, the diagonal deformation of the specimen across the failure crack in Fig. C8(b) showed larger values than any of the other specimens, but the deformations decreased upon unloading. Large regions of the CFRP material were observed to be debonded from the concrete surface, although the specimen continued to carry additional load. Upon reaching the peak load, the applied force was held as the CFRP u-wraps were observed to debond initiating from the strip termination located at the deck/stem interface and peeling away from the stem. After several strips had debonded, a single remaining CFRP strip crossing (one side of the web only) the diagonal crack debonded, resulting in sudden failure. The diagonal crack angle was approximately at 40^{o} from horizontal and initially would have crossed three of the CFRP u-wraps.

Specimen 4IT07 used a targeted repair scheme based on the observed response of specimen 1IT02. The goal of the repair was to achieve similar capacity or a different failure mode using CFRP material applied to only a portion of the specimen. The applied shear at failure was 1110 kN (250 kips) and similar to specimen 1IT02 although failure initiated by anchorage loss at the flexural bar cut-off location. The diagonal failure crack was 44^{o} from horizontal. Splitting cracks were observed at the deck edge and large sections of concrete spalled off the bottom of the deck near the cutoff location. Strain behavior of the stirrups and CFRP, as well as the diagonal deformation across the failure crack, were similar to those observed for specimen 1IT02. The flexural anchorage failure indicates that designers must recognize and address the increased demands placed on the often poor flexural details when shear capacity of existing structures is increased using FRP.

The strain behavior of the thicker CFRP material on specimen 4IT07 compared with specimen 1IT01 was significant even though the CFRP strip strength was not fully realized due to flexural anchorage failure. Prior to failure, specimen 4IT07 showed much less debonding and less cracking and popping of the CFRP was heard as the applied load increased compared with specimen 1IT02 (having the thinner CFRP). At failure, a smaller portion of the remaining load carrying strip was bonded in specimen 4IT07 than in 1IT02 (Fig. C7), yet it was carrying similar force. It is evident that the thicker material (CF160) requires a higher bond stress than does the thinner (CF130) CFRP to develop the force in the strip of similar width (even if the CFRP strains are smaller) as seen in Table 1. The thicker CFRP material also exhibited the lowest pull-off strengths (Table C3), indicating the thicker material may permit higher bond strengths (in shear) due to the higher stiffness which reduces strains at the bond interface. Additional work is required to further validate this observation for shear dominated response.

Specimen 4IT08 was repaired using only longitudinal CFRP strips in the flexural tension zone. Strain readings of the continuous flexural bars at the flexural cut-off detail are shown along with the strain in the CFRP applied to the deck soffit directly above the end of the cut-off bar in Fig. C8(a). As seen in this figure, the CFRP exhibited higher strains than the adjacent flexural reinforcing bars. At an applied load of 1334 kN (300 kips), the strains in the flexural bars were only slightly less than that observed during the precrack phase (unrepaired). Considering the

diagonal deformation response shown in Fig. C8(b), the addition of the CFRP strips did reduce the amount of diagonal cracking compared to the unrepaired specimen at precracking, although there was no increase in shear capacity. The final failure crack on specimen 4IT08 was observed to develop slowly. As the applied shear increased, the crack continued to open further causing debonding and bending of the fibers in the CFRP strips at the diagonal crack locations. Addition of longitudinal CFRP alone was not effective in increasing shear capacity due to debonding and fiber bending at diagonal crack locations. This finding was confirmed by the predicted value for the unrepaired capacity of 4IT08 from *Response 2000*. The predicted value matched the experimental value very closely, within 2%, indicating there was little to no contribution from the FRP. Addition of transverse CFRP strips may improve the response for the longitudinal strips and enable the longitudinal strips to better reduce flexural demands at cutoff locations. Additional study is required to validate this concept.

Conclusions

Laboratory tests were performed on five CRC deck girders built to reflect 1950's vintage proportions, materials, and details at near static conditions. Specimens were precracked, repaired with CFRP strips, and tested to failure while monitoring global and local member responses. Factors considered included flexural cut-off details, variable stirrup spacing, dead load, positive and negative moment bending, and different repair configurations. Based on the experimental observations, the following conclusions are presented:

- Superimposed dead load of the magnitude considered (typical for moderate span vintage RCDG bridges) and with ductile stirrups did not impact the ultimate strength of the specimens. For longer span bridges with higher dead to live load ratios or different material properties, the impact of dead load could be significant.
- Repair schemes for shear using discrete CFRP strips provided a significant increase in ultimate strength capacity compared to unrepaired members.
- Specimen response after repair was noticeably stiffer in terms of midspan displacement and diagonal deformations.
- The repaired members exhibited strain compatibility between external CFRP strips and internal stirrups. Addition of the CFRP strips reduced the live-load demand in the internal stirrups at similar load levels.
- Repair for shear using CFRP must recognize the impact of the increased shear capacity on the flexural demands to prevent anchorage failures at flexural bar cut-off and anchorage details.
- Failure was controlled by debonding of CFRP strips initiating near the deck/stem interface.
- Thicker CFRP material exhibited reduced amounts of debonding and cracking and achieved higher bond stress than the thinner material.
- It was possible to increase the member shear strength using a targeted repair approach applying CFRP material only to a critical section rather than over the entire member.
- The CFRP repaired members tended to exhibit steeper crack angles than similar unrepaired specimens. At the point of failure, only one u-wrap was still acting across the failure crack.
- Prior to failure, significant areas of debonded CFRP material were observed. Progressive debonding of the multiple strips over the loading history provided a visual indication of distress prior to failure.

- Addition of longitudinal CFRP strips did not increase capacity due to debonding and bending of fibers at the poorly constrained diagonal cracks. The combined effect of longitudinal and transverse strips was not investigated, although some synergistic benefits are anticipated.

Acknowledgments

This research was funded by the Oregon Department of Transportation and Federal Highway Administration and overseen by research coordinator Mr. Steven Soltesz. All repair materials and procedures were donated by MBrace of Cleveland, Ohio and Pioneer Waterproofing of Portland, Oregon with the help of Mr. Neil Antonini. The help of both of these individuals is greatly appreciated. Reinforcing steel and fabrication were donated by Cascade Steel Rolling Mills of McMinnville, Oregon and Farwest Steel of Eugene, Oregon, respectively. The authors would also like to thank Dr. Tanarat Potisuk, Mr. Richard Forrest, Mr. Thomas Schumacher, Ms. Michelle Chavez, and Ms. Angela Rogge for their assistance in experimental testing and data reduction. The findings and conclusions are those of the authors and do not necessarily reflect those of the project sponsors or the individuals acknowledged.

Notation

The following symbols are used in this paper:

f_{bond} = bond strength demand of CFRP on concrete surface (MPa);
f'_c = compressive strength of concrete (MPa);
f_{ult} = ultimate stress of internal reinforcing steel (MPa);
f_y = yield stress of internal reinforcing steel (MPa);
St Dev = standard deviation of measured CFRP properties;
V_{APP} = applied shear from actuator (kN);
V_{Pred} = predicted shear capacity using *Response 2000*™ (kN);
$\mu\varepsilon_{max}$ = maximum measured CFRP strain at mid height of u-wrap με); and
θ_{ck} = angle of diagonal failure crack (degrees).

References

1. ODOT, "Oregon's Bridges 2002." Oregon Department of Transportation, <http://www.odot.state.or.us/tsbbridgepub/PDFs/Senate_05_16_02.pdf> (May 16, 2002), Salem, Oregon.
2. Chajes, M. J., Januszka, T.F., Mertz, D.R., Thomson, T.A., Finch, W.W., "Shear Strengthening of Reinforced Concrete Beams Using Externally Applied Composite Fabrics," ACI Structural Journal, v. 92, No. 3, May-June 1995, pp. 295-303.
3. Malvar, L.J., Warren, G.E., Inaba, C., "Rehabilitation of Navy Pier Beams with Composite Sheets," Proceedings of the Second International RILEM Symposium, August 23-25, 1995, pp. 533-540.
4. Sato, Y., Ueda, T., Kakuta, Y., Tanaka, T., "Shear Reinforcing Effect of Carbon Fiber Sheet Attached to Side of Reinforced Concrete Beams," Advanced Composite Materials in Bridges and Structures, 1996, pp. 621-627.
5. Norris, T., Saadatmanesh, H., Ehsani, M.R., "Shear and Flexural Strengthening of R/C Beams with Carbon Fiber Sheets," ASCE Journal of Structural Engineering, v. 123, No. 7, July 1997, pp. 903-911.
6. Triantafillou, T.C., "Shear Strengthening of Reinforced Concrete Beams Using Epoxy-Bonded FRP Composites," ACI Structural Journal, v. 95, No.2, March-April 1998, pp. 107-115.
7. Czaderski, C., EMPA, Swiss Federal Laboratories for Materials Testing and Research, "Shear Strengthening of Reinforced Concrete with CFRP," 45th International SAMPE Symposium, May 21-25, 2000, pp. 880-894.
8. Kachlakev, D., McCurry, D.D., "Behavior of Full-Scale Reinforced Concrete Beams Retrofitted for Shear and Flexural with FRP Laminates," Composites Part B: Engineering, v. 31, no. 6-7, 2000, pp. 445-452.
9. Shehata, E., Morphy, R., Rizkalla, S., "Fibre Reinforced Polymer Shear Reinforcement for Concrete Members: Behaviour and Design Guidelines," Canadian Journal of Civil Engineering, v. 27, no. 5, October 2004.
10. Al-Mahaidi, R., Lee, K., Taplin, G., "Behavior and Analysis of RC T-Beams Partially Damaged in Shear and Repaired with CFRP Laminates," Structures Congress, ASCE, Washington DC, May 2001.
11. Li, A., Assih, J., Delmas, Y., "*Shear* Strengthening of RC Beams with Externally Bonded CFRP Sheets," ASCE Journal of Structural Engineering, v. 127, No. 4, April 2001, pp. 374-380.
12. Chen, J.F., Teng, J.G., "Shear Capacity of Fiber-Reinforced Polymer-Strengthened Reinforced Concrete Beams: Fiber Reinforced Polymer Rupture," ASCE Journal of Structural Engineering, v. 129, No. 5, May 2003, pp. 615-625.
13. ACI 440.2R-02, American Concrete Institute, "Guide for the Design and Construction of Externally Bonded FRP Systems for Strengthening Concrete Structures." Farmington Hills, Michigan, 2002.
14. Higgins, C., Miller, T.H., Rosowsky, D.V., Yim, S.C., Potisuk, T., Daniels, T.K., Nicholas, B.S., Robelo, M.J., Lee, A-Y, and R.W. Forrest, "Research Project SPR 350 SR 500-91: Assessment Methodology for Diagonally Cracked Reinforced Concrete Deck Girders," Oregon Department of Transportation, Salem, OR, October 2004.
15. Bentz, E., (2000), Response 2000, University of Toronto, <http://www.ecf.utoronto.ca/~bentz/r2k.htm>.
16. Master Builders, Inc., "MBrace Composite Strengthening System Material Specifications," Cleveland, OH, 2001.

17. ASTM D 3039/D 3039M-00, American Society of Testing and Materials, “Standard Test Method for Tensile Properties of Polymer Matrix Composite Materials,” ASTM, West Conshohocken, PA, 2001.

Specimen	Failure Mode	V_n (kN)**	V_{APP} (kN)	V_d (kN)	V_{EXP} (kN)	θ_{ck} (deg)	$\mu\varepsilon_{max}$	f_{bond} (Mpa)
1IT01	Shear / Compression	934	1145	12	1157	37	4930	0.70
1IT02	Shear / Compression	907	1112	14	1126	37	8708	1.23
2T04	Shear / Compression	677	1225	19	1244	40	4424	1.46
4IT07	Shear / Tension	909	1110	8	1118	44	4073	1.57
4IT08	Shear / Compression	899	865	20	884	23	3812	-
** Nominal shear capacity of specimen without CFRP predicted with Response 2000 (Bentz 2000).								

Table C1: Experimental summary.

Description	Bar Size	Grade	f_y (MPa)	f_{ult} (MPa)
Stirrups	# 13	300	350	559
Deck	# 13	420	443	724
Skin	# 19	420	461	648
Flexure	# 36	420	481	717
Hooks	# 36	420	481	717

Table C2: Internal steel reinforcing properties.

Specimen	f_c' (MPa)		Initial Max Crack Size (mm)	CFRP Pull-off Bond Strength (MPa)
	28-Day	Failure		
1IT01	28.06	29.30	0.635	3.50
1IT02	26.27	26.34	1.016	2.02
2T04	26.27	29.37	0.762	1.82
4IT07	23.51	26.27	1.016	0.74
4IT08	22.89	23.10	1.270	1.23

Table C3: Concrete and CFRP bond properties and maximum initial diagonal crack size.

Property	Individual Component*			Composite†			
	Saturant	Carbon Fiber		CF130		CF160	
		CF130	CF160	Mean	St Dev	Mean	St Dev
Thickness, t (mm/ply)	-	0.165	0.33	0.975	0.134	1.47	0.16
Ultimate Tensile Strength (MPa)	55.2	3800	3800	717	94	846	151
Ultimate Tensile Strength per Unit Width (kN/mm/ply)	-	0.625	1.25	0.692	0.042	1.22	0.13
Tensile Modulus (MPa)	3034	227000	227000	38750	4530	54400	7020
Ultimate Rupture Strain, %	3.5	1.67	1.67	1.85	0.11	1.55	0.18

*Master Builders, Inc. 2001 material vendor specifications.

†Average and standard deviation values obtained from 20 composite samples of each fiber type tested in accordance with ASTM D 3039/D 3039M.

Table C4: Composite material properties: Reported and experimental.

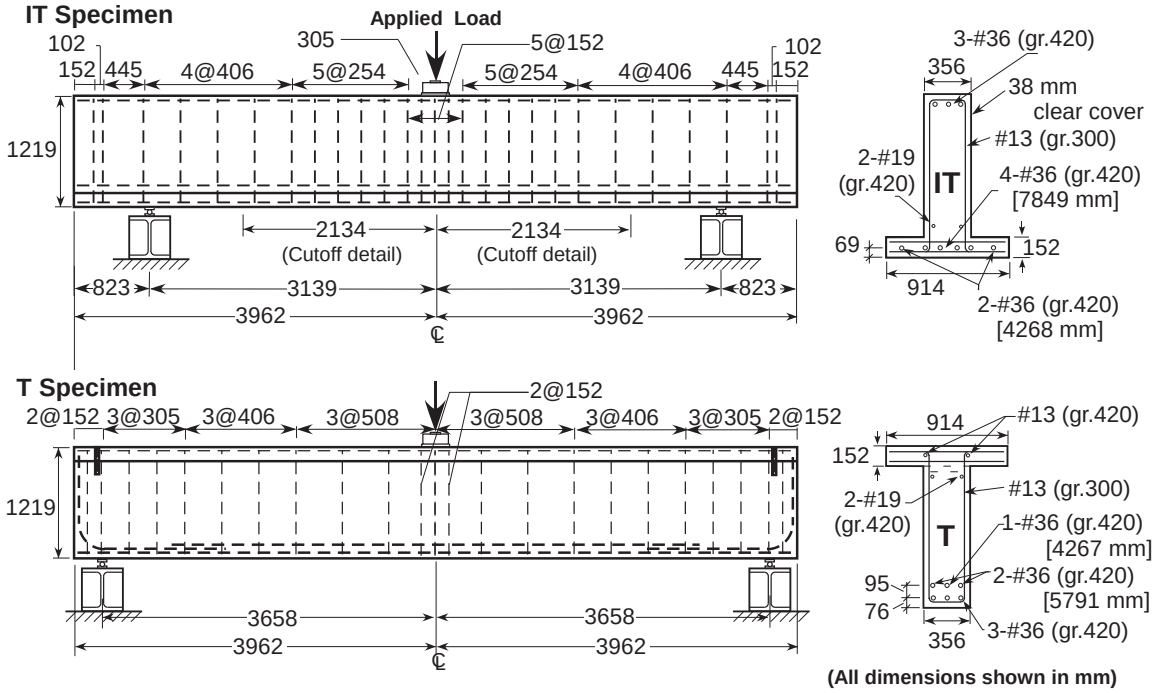

Fig. C1: Specimen configurations

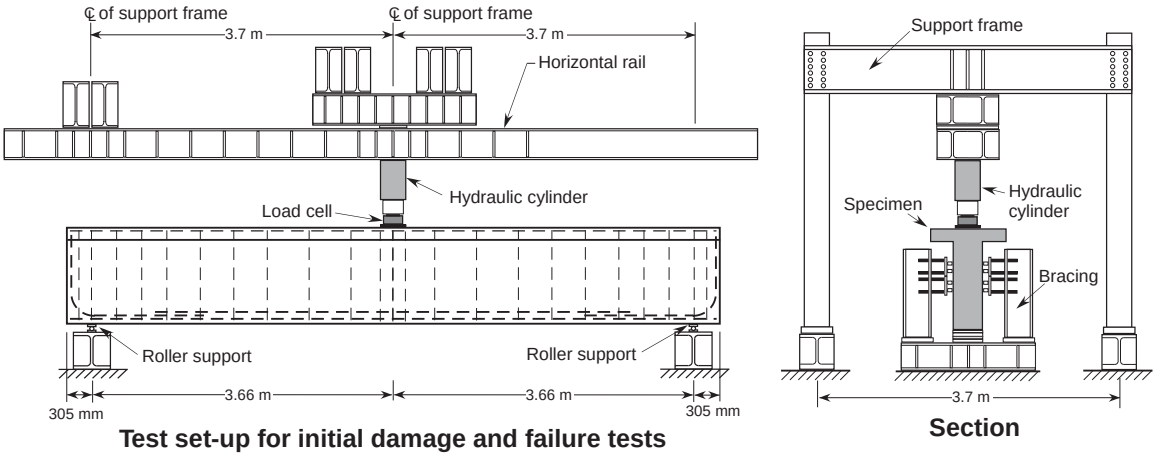

Fig. C2: Test setup

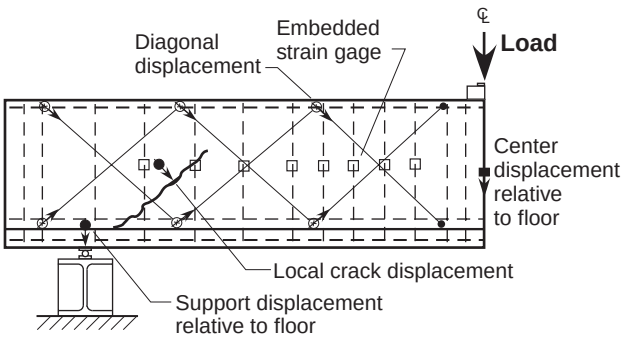

Fig. C3: Instrumentation

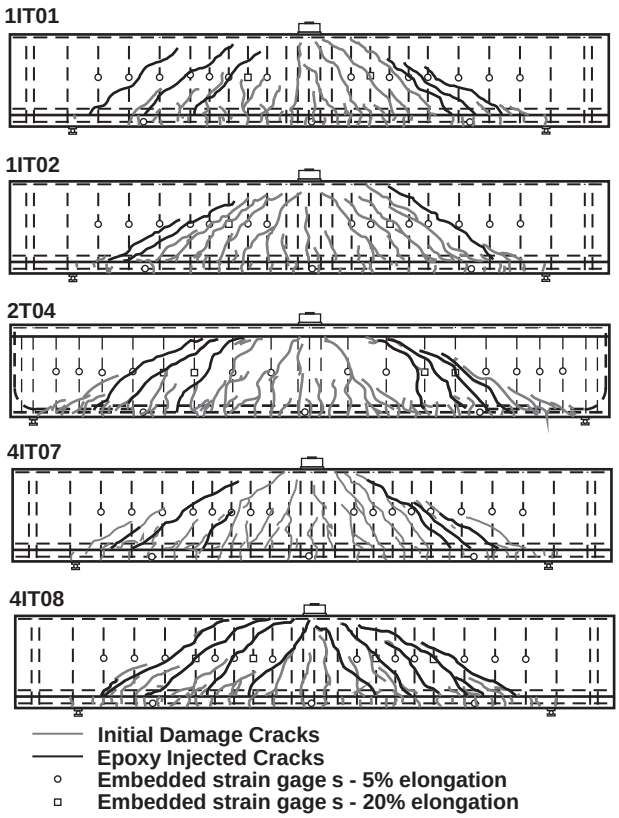

Fig. C4: Cracked specimens and internal steel strain gages

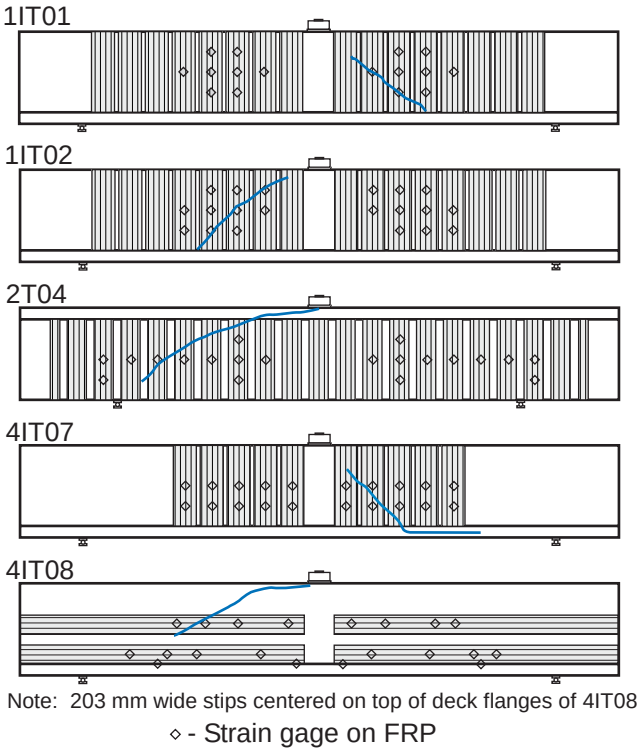

Fig. C5: Repaired specimen configuration and corresponding failure crack

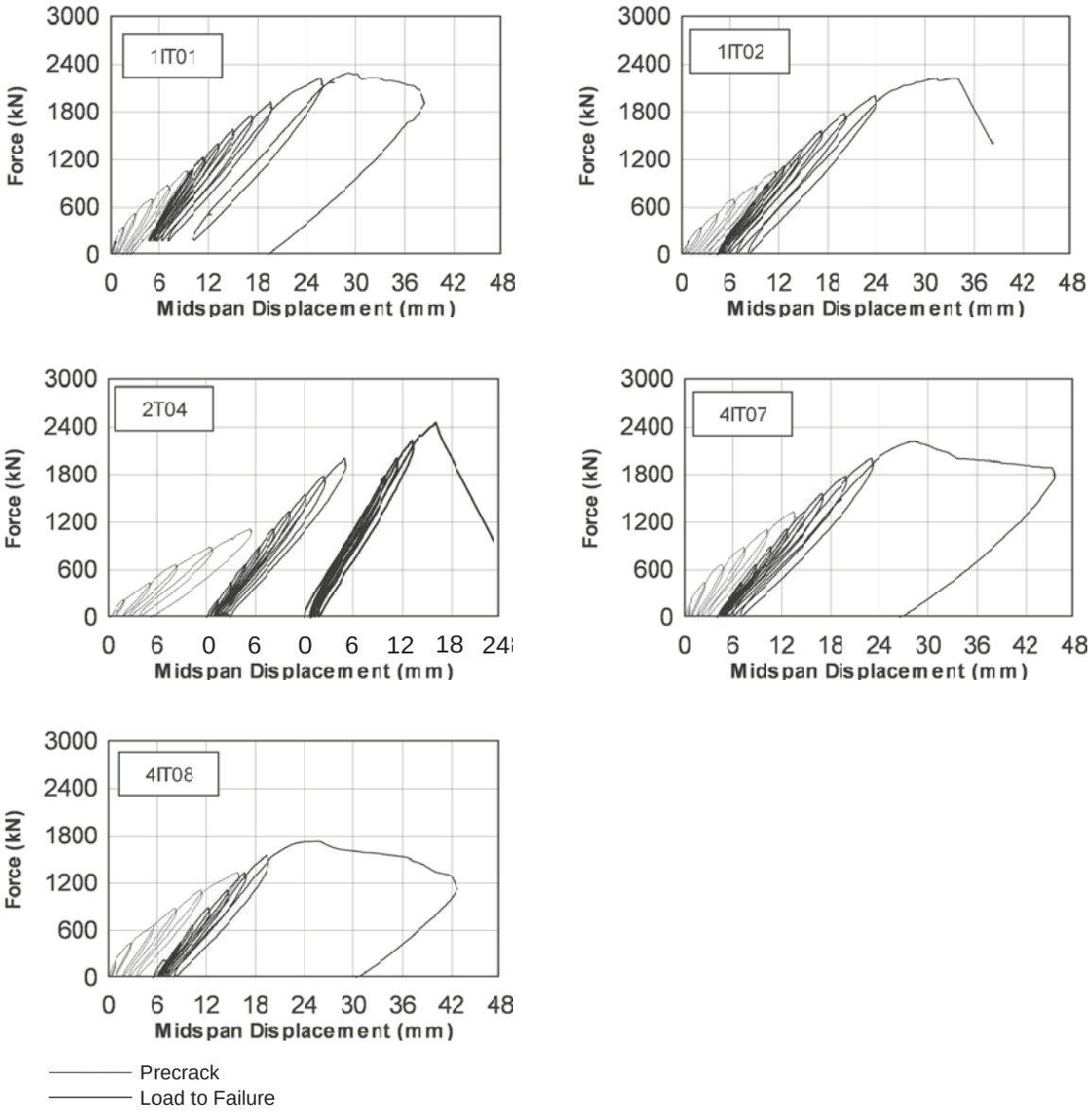

Fig. C6: Midspan deformation response

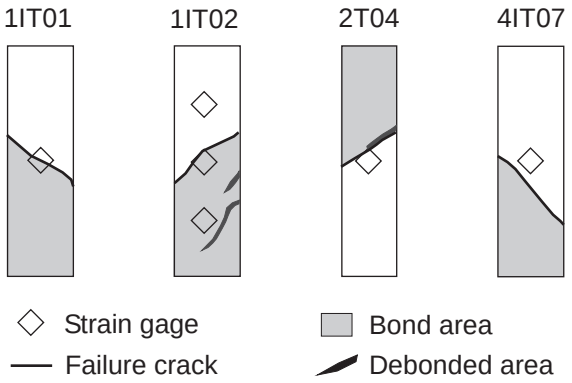

Fig. C7: Bond regions of primary load carrying CFRP u-wraps across failure cracks

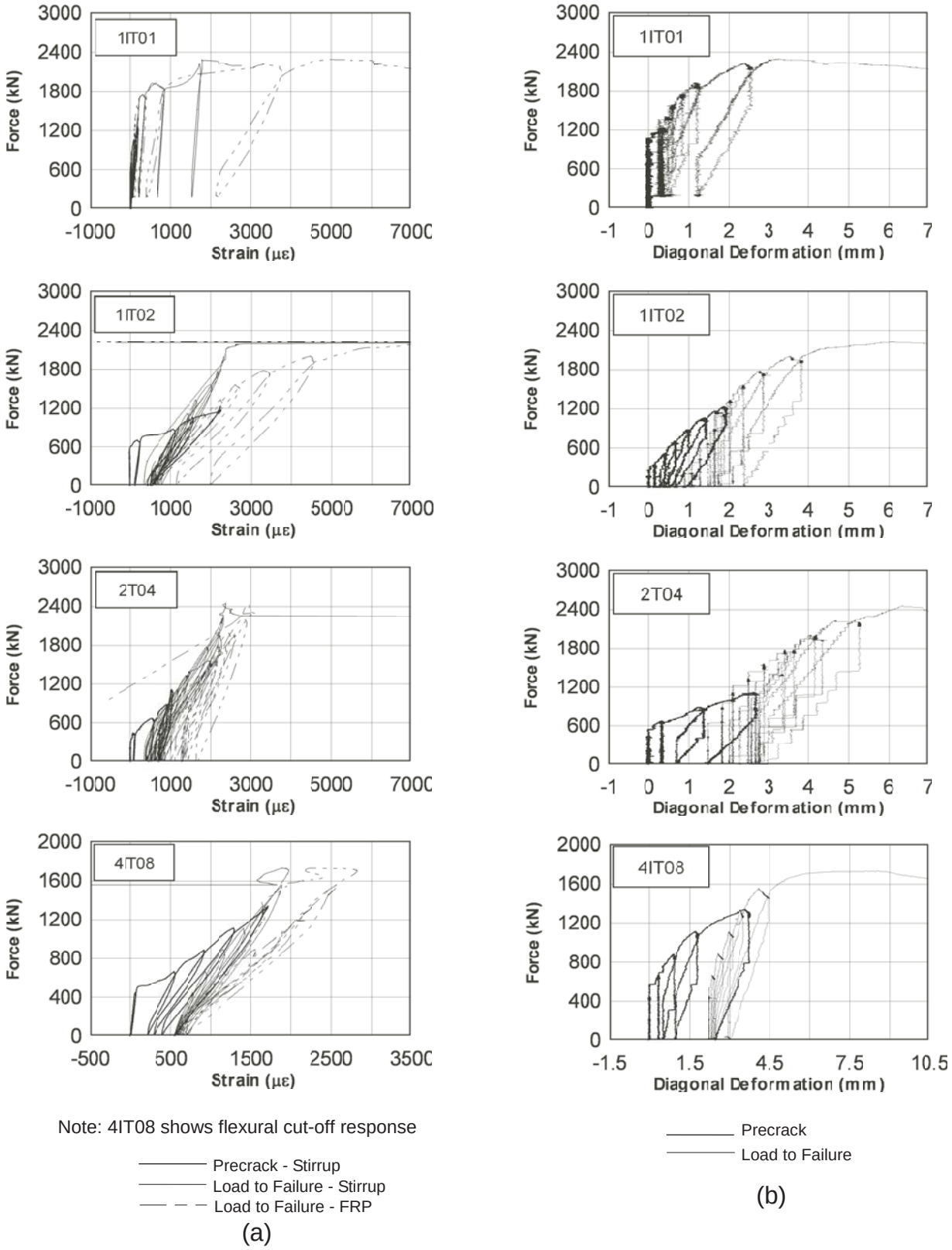

Fig. C8: (a) Strain Measurements, (b) Diagonal deformation of failure crack region

APPENDIX D: FATIGUE OF DIAGONALLY-CRACKED RC GIRDERS REPAIRED WITH CFRP

Fatigue of Diagonally-Cracked RC Girders Repaired with CFRP

By Grahme Williams[1] and Christopher Higgins, P.E., M. ASCE[2]

Abstract: Fiber reinforced polymers (FRP) are becoming more widely used for repair and strengthening of conventionally reinforced concrete (RC) bridge members. Once repaired, the member may be exposed to millions of load cycles during its service life. The anticipated life of FRP repairs for shear strengthening of bridge members under repeated service loads is uncertain. Field and laboratory tests of FRP repaired RC deck-girders were performed to evaluate high-cycle fatigue behavior. An in-service 1950's vintage RC deck-girder bridge repaired with externally bonded carbon fiber laminates for shear strengthening was inspected and instrumented. FRP strain data were collected under ambient traffic conditions. In addition, three full-size girder specimens repaired with bonded carbon fiber laminate for shear strengthening were tested in the laboratory under repeated loads and compared with two unfatigued specimens. Results indicated relatively small in-situ FRP strains, laboratory fatigue loading produced localized debonding along the FRP termination locations at the stem-deck interface, and the fatigue loading did not significantly alter the ultimate shear capacity of the specimens.

CE Database subject headings: Reinforced concrete, bridges, shear, field testing, fatigue, fiber reinforced polymer

Introduction

The national bridge inventory contains large numbers of RC bridges that are lightly reinforced for shear. One of the most common types of RC bridges is the deck-girder bridge (RCDG) used widely during the highway expansion of the late 1940's through the early 1960's. Many RCDG bridges are reaching the end of their originally intended design lives and the combined effects of over-estimation of allowable concrete shear stress at design, reduced anchorage requirements for flexural steel, increasing service load magnitudes and volume, as well as shrinkage and temperature effects, may contribute to diagonal tension cracking in these bridges. Due to the relatively light shear reinforcement, diagonal cracks may not be well constrained and therefore become quite wide. Repeated loading may further cause cracks to widen. Inspections of approximately 1,800 vintage RCDG bridges in Oregon by Oregon Department of Transportation (ODOT) personnel revealed over 500 with varying levels of diagonal cracking. As a result, a repair program was initiated to extend the service lives of these bridges. One type of repair material being used is externally bonded carbon fiber reinforced polymer (CFRP) laminates. The anticipated life of these CFRP repairs under repeated service loads is uncertain and research was undertaken to investigate the life of diagonally-cracked RCDG bridges repaired with CFRP.

Background

High-cycle fatigue behavior of RC beams in shear is influenced by the concrete, reinforcing steel, and the interaction between the concrete and reinforcing steel. Previous research on high-cycle fatigue of concrete structures has focused on plain concrete, fatigue of beams, and reinforcing steel (ACI SP-41, 1974; ACI SP-75, 1982; ACI Committee 215, 1992). Fatigue tests of concrete beams without shear reinforcement were conducted by Chang and Kesler (1958). Shear fatigue of concrete beams with stirrups was investigated by Hawkins (1974), Ueda and Okamura (1981, 1983), as well as Kwak and Park (2001). Fatigue tests of deep beams were performed by Teng *et al*. (1998). Bond fatigue (between rebar and concrete) was studied by Rehm and Eligehausen (1979) and Balazs (1998). High-cycle fatigue of reinforcing steel was studied by Hanson *et al*. (1968), Hanson *et al*. (1974), Helgason and Hanson (1974), Jhamb and MacGregor (1974), Corley *et al*. (1978), and Kreger *et al*. (1989). Fatigue cracks tend to initiate at the transverse rib along the surface of the bar and the fatigue behavior depends on the stress conditions, reinforcing bar geometry including deformation height, base radius, width and bar diameter, as well as material properties (Hanson *et al*., 1974; ACI-215, 1992). Fatigue life has generally been expressed in terms of the stress range (Hanson *et al*., 1974). The current ACI specification (ACI-318, 2002) does not address fatigue of reinforcing steel, although ACI Committee 215 (1992) recommends a maximum service-level stress range, σ_r (MPa), for straight deformed reinforcing bars of:

$$\sigma_r = 161 - 0.33\sigma_{min} \quad (1)$$

where σ_{min} (MPa) is the minimum stress with tension taken as positive and compression taken as negative. The σ_r need not be taken as less than 138 MPa (20 ksi). The current AASHTO provisions (2002) specify a maximum stress range at service loads with impact be calculated as:

$$\sigma_r = 145 - 0.33\sigma_{min} + 55\frac{r}{h} \quad (2)$$

where σ_{min} (MPa) is the minimum stress as defined previously, and r/h is the ratio of the base radius to transverse deformation height. When the r/h ratio is not known, a value of 0.3 is recommended.

Previous laboratory investigation involving fatigue response of externally bonded FRP laminates has focused primarily on flexural conditions (Muszynski and Sierakowski 1996, Papakonstantinou *et al*. 2001, Lopez *et al*. 2003, Breña *et al*. 2005). Some research has also been done on in-situ FRP repaired bridges (Tedesco *et al*. 1996) with monitoring conditions both before and after repair showing stiffer member response and decreased stress of the reinforcing steel.

The fatigue behavior of full-sized RC bridge girders repaired with FRP for shear under realistic service-level stress ranges has not previously been investigated. Strain ranges in the CFRP of repaired in-service RC deck-girder bridges are not known and the susceptibility of these repairs to damage under high-cycle fatigue is uncertain (ACI-440 2002).

Field Study

A RCDG bridge designed in 1954 was investigated in the field testing portion of this research program. The Willamette River bridge *(ODOT Bridge Inventory Number 08156)* is located on Oregon Highway 219, near Newberg, OR. Inspection of the bridge in late summer of 2001 indicated significant diagonal cracking in the high-shear regions near the supports. The bridge consists of ten spans: four steel plate girder spans over water and three conventionally reinforced concrete approach spans at each end. Concrete approach spans exhibited significant diagonal cracks and were repaired using externally bonded carbon fiber-reinforced polymer materials after completion of the initial inspection. The bridge has a regular layout with rectangular prismatic girders and the south approach spans were selected for instrumentation. The approach spans have three equal span lengths, 16.8 m (55 ft) each, and have a total width of 10.7 m (35 ft) as illustrated in Fig. D1. The spans are comprised of one simple span having five girders 368x1346 mm (14.5x53 in.) and two continuous spans having four girders 330x1346 mm (13x53 in.). Reinforced concrete diaphragms 229x1219 mm (9x48 in.) are located at quarter points of each span. The approach spans have three simple supports and are continuous over one interior support with a transverse bent cap 419x1803 mm (16.5x71 in.) supported by two columns. The specified concrete compression strength was 22.75 MPa (3300 psi) and reinforcing steel consisted of ASTM A305 intermediate grade deformed square and round bars with nominal yield stress of 276 MPa (40 ksi). The bridge was repaired primarily for shear with CFRP in the fall of 2001. The material used was CF130 unidirectional high-strength carbon fiber fabric, manufactured by MBrace. Prior to application of the CFRP, the surface was prepared by diamond grinding and the diagonal and flexural cracks were epoxy injected. An epoxy primer was then applied followed by a high viscosity epoxy paste. Individual (12 in.) wide strips of CFRP laminate were applied in a U-shape to the prepared surface around the girder webs and soffit in varying plies with an epoxy encapsulated resin saturant. An open space of approximately 51 mm (2 in.) was left between strips. Additionally, CFRP strips were placed along the web soffit and along the top of the web to provide supplemental flexural reinforcing. Typical CFRP repair of the main girders and bent caps is shown in Figs. D2a and D2b, respectively.

In October 2004, three years after installation of the CFRP repairs, the bridge was re-inspected, instrumented, and monitored under ambient traffic conditions to measure in-situ CFRP strain ranges at high shear locations. The bent caps and longitudinal deck girders were re-inspected to determine if cracking re-occurred and to identify the as-built locations of the CFRP strips. A hand-held laser distance meter was used to rapidly locate cracks and CFRP strips relative to support locations. Examples of stirrup locations, original cracks, and CFRP strips, on the exterior girder, are shown in Fig. D3. During the post-repair inspection, no new diagonal cracks were observed in the bent caps or girders. Flexural cracking was observed at only one location near midspan of the exterior girder.

After inspection, strain gages were installed on individual CFRP strips at selected high-shear locations. Strain gages were bonded to the surface of the CFRP at mid-depth of the girder and oriented in the vertical (fiber) direction. The chosen strain gage length was 51 mm (2 in.), permitting strain averaging over several transverse weave fibers that were spaced approximately 8 mm (0.31 in.). Instrumented locations are illustrated schematically in Fig. D4. The strain gages were connected to a high-speed, multi-channel, 16-bit digital data logger. To reduce noise and prevent aliasing in the data, both analog and digital filters were employed. During the ambient

monitoring period, data were sampled at 100 Hz. The system recorded sensor readings and converted signals into corresponding CFRP strains. Data from sensors were archived for retrieval and post-processing.

Ambient Traffic Induced CFRP Strains

Ambient traffic induced CFRP strains at mid-depth of the girders and bent cap were monitored over a period of 32.6 days. The strain ranges and numbers of cycles recorded at the instrumented locations are shown in Fig. D5. The largest single strain range was measured at approximately 34 με for location #2 on the bent cap. Miner's Rule (Miner, 1945), was used to express the variable amplitude strains as an equivalent constant amplitude strain range for each of the instrumented locations:

$$SR_{eqv} = \sqrt[k]{\sum \frac{n_i}{N_{tot}} SR_i^k} \qquad \textbf{(3)}$$

where SR_i is the i^{th} strain range, n_i is the number of cycles observed for the i^{th} strain range, N_{tot} is the total number of cycles at all strain ranges, and k is the fatigue exponent or slope of the S-N curve. Steel is generally regarded as having a relatively low fatigue exponent of 3 compared with composite materials having higher fatigue exponents of 10 or above (Mandell *et al*. 1993). For materials with higher fatigue exponents, fatigue damage is not particularly sensitive to the low strain-range cycles, however the few cycles that occur at higher strain ranges contribute disproportionately to fatigue damage as compared with low fatigue exponent materials. Thus, there is a higher degree of uncertainty related to events that occur in the upper tails of the distribution when using short data collection windows. Considering a high fatigue exponent of 10 and using the field data collected over the relatively long time frame relative to the in-service life of the CFRP installation, equivalent constant amplitude strain ranges were computed at all instrumented locations as shown in Fig. D6. The single highest equivalent constant amplitude strain range was 15 με for location 2.

Field-measured strain ranges and numbers of cycles for each instrumented location were used to determine an equivalent strain range for laboratory fatigue specimens. To simulate the effects of high-cycle fatigue in laboratory specimens, 1,000,000 cycles of repeated loading was selected to produce equivalent damage in a reasonably short period of time. The strain range required to produce equivalent damage in laboratory specimens at 1,000,000 cycles, as that measured in the field over a projected period of 10, 20, and 50 years, was estimated by computing an equivalent strain range per Eqn. 3 with k=10, using the location exhibiting the highest strain ranges (location #2). It was assumed that the field measured CFRP strain ranges and numbers of cycles remain constant over the extended life of the bridge. Based on the field-measured rainflow counts, the CFRP strain ranges required to approximate in-situ fatigue damage for the laboratory specimens were 19, 20.5, and 22.5 με for 10, 20, and 50 year service lives, respectively. Laboratory tests of full-size girder specimens with 1950's vintage proportions were initially loaded until cracked, repaired with CFRP, and subjected to high-cycle service-level loads approximating those observed in the field to produce equivalent fatigue damage. These laboratory tests and results are reported subsequently.

Laboratory Tests

Test Specimens

Five specimens were tested as part of the experimental investigation. Two control specimens were tested monotonically and three under fatigue loading. Specimens were designed to reflect 1950's vintage proportions, materials, and details at full scale based on previous work done by Higgins *et al*. (2004). Two designs were used to test both positive (T-beam) and negative moment bending regions (inverted-T (IT)) with various flexural bar cut-off, hook, and stirrup spacing details as seen in Fig. D7. Specimens were initially loaded to produce diagonal cracking representative of that observed in field inspections of existing Oregon highway bridges. They were then repaired with CFRP, fatigued for 1 million cycles (except the control specimens), and then tested to failure.

All specimens were cast with the same cross-sectional geometry. Members had a height of 1219 mm (48 in.) with a stem width of 356 mm (14 in.) and a deck portion 914 mm (36 in.) wide by 152 mm (6 in.) thick as depicted in Fig. D7. Reinforcing bars for all of the specimens were from the same heats and tension tests were conducted to determine material properties as summarized in Table D1. ASTM A615 Grade 420 (60 ksi) steel was used for the longitudinal reinforcing, with Grade 300 (40 ksi) steel for the stirrups. The stirrup grade is representative of intermediate grade steel used in the 1950's. A concrete mix design was used which produced compressive strengths similar to ODOT specified compressive strengths of around 24 MPa (3500 psi). The 28-day and day-of-test cylinder strengths are shown in Table D2.

All repairs were done using unidirectional high strength carbon fiber fabric applied in a wet lay-up procedure. Two different fibers were used with individual component and composite properties shown in Table D3. Composite properties were determined from unidirectional tension tests performed for each fiber thickness per ASTM 3039 recommendations. The same materials were used on the laboratory specimens as were used in the repair of the field study bridge, and both were done by the same ODOT approved applicator.

Test Variables

All tests were conducted using a three-point loading configuration. Precrack and failure tests were done in a setup as shown in Fig. D8. Load was applied through a 3560 kN (800 kip) capacity hydraulic cylinder. The applied force was measured with a 2670 kN (600 kip) capacity load cell. Fatigue loading was performed using load-control in a setup shown in Fig. D9. Force was applied through a 980 kN (220 kip) capacity hydraulic actuator. Applied force was measured with a 1330 kN (300 kip) load cell. Load was distributed through a 25 mm (1 in.) thick 305 mm (12 in.) square steel plate in both setups. End reactions were applied through 102 mm (4 in.) wide steel plates resting on 51 mm (2 in.) diameter steel rollers, fastened to steel spreader beams attached to the laboratory strong-floor. High-strength grout was applied to the contact surfaces between the steel plates and specimens to ensure level and even bearing areas. Inverted-T (IT) specimens were tested at a span length of 6280 mm (20.6 ft) between centerline of supports for both precrack and failure loading schemes and at 7315 mm (24 ft) span for fatigue. T-beams were tested at 7315 mm (24 ft) spans for all three loading phases.

Instrumentation was applied to each specimen to capture local and global behaviors. Strain gages were used to monitor internal steel reinforcing and external CFRP strains, displacement transducers were used to measure diagonal deformations, local crack motions, and support

displacements at each corner of the reaction plates, and string potentiometers to measure centerline displacement. Typical instrumentation is shown in Fig. D10.

Testing Method

The initial loading protocol was performed to induce diagonal cracking representative of in-service RC girders. Load was applied incrementally at 222 kN (50 kips) to a level of 1112 kN (250 kips) for T specimens and 1334 kN (300 kips) for IT specimens with removal of load between each step. Maximum crack sizes after loading of each beam are shown in Table D2, and ranged from 0.08 – 1.0 mm (0.03 – 0.04 in.). After reaching the desired level of diagonal cracking, the applied load was removed.

Once girders were diagonally cracked, a commercially available CFRP unidirectional high strength carbon fiber fabric laminate system was applied to the specimens. The entire repair procedure was performed by a qualified contractor with experienced personnel. Cracks were inspected and all significant diagonal cracks were injected with a high strength epoxy resin and allowed to cure. Not all visible cracks were injected, just those of sufficient width to permit the epoxy to flow between the crack surfaces. The beams were then surfaced with a diamond bit grinder to remove loose concrete and expose voids. A primer was spread over areas to be applied with CFRP and once dry, a putty and saturant were applied. While both were wet, the carbon fiber was cut and applied to the specified locations, being worked into place with a soft trowel until the saturant made its way through the fibers. A final layer of saturant was then applied.

Upon reaching the manufacturers recommended curing times, the specimens were instrumented, fatigued (except 1IT02 and 2T04), and tested to failure. U-wrap laminate locations on each specimen are shown in Fig. D11. A 406 mm (16 in.) space in the center of each IT specimen was included to simulate the bent cap location in a bridge structure where it is not possible to apply the CFRP. Specimens 1IT02, 3IT05, and 3IT06 were repaired with a single layer of 305 mm (12 in.) wide CF130 laminate spaced 256 mm (14 in.) on center. Specimens 2T03 and 2T04 were repaired with a single layer of 254 mm (10 in.) wide CF160 laminate spaced 256 mm (14 in.) on center.

After repair, the specimens were subjected to an initial overload prior to beginning high-cycle fatigue loading. An incremental load program was conducted from zero to 890 kN (200 kips) at 222 kN (50 kips) steps with unloading. Reaching the peak overload condition resulted in diagonal cracking visible between individual u-wraps. This creates a worst-case scenario for damage sequencing (though diagonal cracking was not observed in the field study bridge) as the significant initial load sufficient to cause cracking creates higher stresses in the embedded rebar (both flexural and stirrups) as well as in the CFRP and facilitates bond fatigue.

Fatigue loading was conducted using a sinusoidal loading function with unique load ranges for each specimen to obtain target damage for one million cycles. The T specimen 2T03 was fatigued at a load range of 445 kN (100 kips) with a mean of 267 kN (60 kips) at a frequency of 1.25 Hz. Specimen 3IT05 was fatigued at a load range of 800 kN (180 kips) at 1.0 Hz and 3IT06 at 489 kN (110 kips) and 1.25 Hz, with means of 445 kN (100 kips) and 334 kN (75 kips), respectively. Consideration was taken to limit measured strains of the internal steel reinforcing to ensure levels were below the fatigue limit of 165 MPa (24 ksi) at one million cycles. This was done to preclude rebar metal fatigue, and only incorporate effects of rebar bond fatigue and

CFRP material and bond fatigue that can reasonably occur at service-level conditions based on field measured bridge response described previously and further detailed by Higgins *et al*. (2004).

All specimens were loaded in 222 kN (50 kip) increments from zero to failure with removal of load to 22 kN (5 kips) each cycle. Peak applied shear force at failure is shown in Table D4 as V_{APP} for each specimen. Also shown, is the amount of member self-weight contributing to shear at the failure location labeled as V_d because specimen sizes for these tests have a significant self-weight contribution. The summation of the applied shear and the self-weight shear forces yields the total failure shear force, V_{EXP}.

Experimental Results

The performance of the repairs was evaluated through load-deflection response, internal rebar and external CFRP strains, flexural reinforcement demand, and diagonal crack growth. Global and local demands were compared before and after the specimens were fatigued to determine changes over one million cycles of repeated load. Debonding of the CFRP u-wraps and crack propagation were also monitored during tests.

Ultimate strength capacity of fatigue specimens with comparable unfatigued specimens showed that the fatigue loading did not significantly affect capacity, as shown in Table 4. There were observed differences between specimens and changes were noted for local and global deformations and strains during fatigue testing.

IT specimens produced additional overall displacement under fatigue loading as progressive debonding of the CFRP strips and internal stirrups occurred. The T specimen did not exhibit changes in overall displacement as shown in Fig. D12. The higher load range produced softening in specimen 3IT05, comparing the start and end of fatigue testing. Changes in local diagonal crack widths were observed during fatigue as shown in Fig. D13. It was evident that the higher load range produced larger diagonal crack opening after one million cycles than the lower load range. Diagonal deformation response within a section of the shear span of the IT specimens also showed similar results. The deformation responses of a section 1067 mm (42 in.) wide by 991 mm (39 in.) high in the same location on the stem for the control and two fatigue IT specimens are shown in Fig. D14. The control specimen 1IT02 was much stiffer with negligible deformation up to 1000 kN (225 kips) of applied force. Specimens 3IT06 and 3IT05 experienced greater deformations, respectively, than the control at corresponding loads. This trend continued through most of the load-deformation response until the load began to approach ultimate. At ultimate, all of the diagonal deformation magnitudes were similar, and all failed at approximately the same applied shear force as shown in Table D4.

In the fatigue specimens, diagonal cracks had already developed during the initial reload after repair and been worked during the fatigue loading. This allowed greater deformations to occur at corresponding loads due to local CFRP debonding and stirrup bond fatigue (between concrete and stirrup legs) associated with the diagonal crack locations. The IT fatigue specimens also contained regions of debonded CFRP material at the strip termination at the flexural tension region along the deck/stem interface. These locally debonded areas were sufficiently small so that as higher loads were reached during failure tests the member capacity was not impacted. Indeed, there was no marked change in the visual condition at the onset of failure between

fatigued and unfatigued specimens. Failure was controlled for all specimens by bond failure as the CFRP u-wraps peeled away from the web, allowing diagonal cracks to propagate. The exception was specimen 2T03, which failed in flexure without CFRP debonding. No fiber rupture was observed for any of the specimens.

The intent of a CFRP retrofit for shear is to extend the service life of the member by providing additional capacity and/or reducing demand on the internal reinforcing steel. Comparison of the stirrup and flexural rebar strains before application of CFRP and during failure testing after fatigue showed that the CFRP tended to decrease the stirrup demands, particularly when the initial stirrup strain was large (those that would control performance), as shown in Fig. D15. Application of the CFRP strips for shear did not significantly change the flexural steel demands at the cut-off locations.

Representative strain behavior of the stirrups at mid-height of an IT member and of CFRP u-wraps at mid-height and in the flexural tension zone are shown in Fig. D16. The stirrup strain near mid-height is shown at a location near the eventual failure crack region. The stirrup strain range was far below the threshold of 830 με based on Eqn. B1 for inducing metal fatigue over one million cycles. In the T-beam specimen, shear demand was sufficiently low so that the stirrups showed very little change in strain throughout fatigue loading, and several showed a slight decreasing trend. The stirrup strain ranges were all well below the threshold required for long life.

Strain response in the CFRP under fatigue varied depending on the instrument location relative to diagonal cracks and strip termination locations along the deck/stem interface. CFRP strain ranges near diagonal cracks tended to exhibit a nonlinear response, with strains increasing at a higher rate during initial fatigue cycles and then gradually increasing at a lower rate, as shown in Fig. D16. CFRP strains measured closer to the flexural tension zone near the terminated edge of the u-wraps trended upwards at a higher rate in early cycles and gradually moved towards a steady-state. For the CFRP strain gage near the edge shown in Fig. D16, strain ranges during the initial cycles were unchanged because no cracks or CFRP debonding had yet propagated near the gage location. Once a crack propagated or debonding progressed (typically early in the fatigue history), the CFRP strain range increased at an initially high rate and then began to slow as stresses were redistributed, cracking does not continue to propagate, and debonding slows. The observed initial plateau does not necessarily exist, if the u-wrap bond to the surface of the specimen is near initial cracks or debonded prior to fatigue cycling. The representative strain at mid-height of the CFRP u-wraps exhibited a different behavior. The CFRP strain gage location shown was near a diagonal crack visible on both sides of the u-wrap. Strain range in the CFRP increased at the onset of fatigue cycling and then reached a near stationery value. During fatigue loading, diagonal cracks opened and closed. The crack surfaces wear against each other and small pieces of concrete at the crack interface may ravel and fall into the crack. This debris does not allow the crack to fully close and produced some small additional strain observed as an increase in the mean strain value. At the same time, the CFRP u-wraps gradually and locally debonded from the concrete surface at cracks and the terminated edge in the flexural tension zone while the stirrup legs undergo bond fatigue whereby the stirrup provides less constraint across the diagonal crack. Eventually near steady-state conditions were reached, and the strain ranges became almost constant. However, the observed strain ranges did not reach true steady-state conditions, and it may be projected that the CFRP debonding and stirrup bond fatigue

continue to occur. Based on the level of CFRP debonding observed prior to failure in the control specimens, very substantial debonding must occur before it significantly impacts ultimate capacity. It would be anticipated that this substantial and visually apparent debonding would be identified during routine and regular bridge inspections, when inspectors focus on the tell-tale locations.

Progressive debonding of the CFRP strips produced a very fine concrete powder along the deck/stem interface in the flexural tension zone of the IT specimens. Accumulation of the gray powdery material was visible on the deck and developed more rapidly during early fatigue cycles and then slowly decreased. This was not the case with the T-beam specimen as the terminated edges of the u-wraps were located near the flexural compression zone, and thus the demand at the strip termination edges was sufficiently low so that debonding did not occur. Identification of debonding of the CFRP u-wraps from the concrete surface was relatively easy using infrared thermography and also by sounding or tapping the CFRP surface. Compared with an adequately bonded area, the debonded areas tended to have a lower, hollow sound when tapped. Also observed during fatigue loading were vertical splitting cracks between the individual fibers of the CFRP u-wraps over diagonal cracks. These cracks were occasionally accompanied with local debonding, and often extended only a few centimeters vertically, as shown in Fig. D11. It should be noted that the observed fatigue-induced CFRP cracking and debonding did not significantly affect the capacity of the members as seen in Table D4.

Conclusions

Field tests were performed on an in-service RCDG bridge that had exhibited diagonal cracking and was retrofitted with CFRP shear reinforcing. The bridge was inspected and CFRP u-wraps were instrumented. Strain ranges in CFRP strips were measured under ambient traffic conditions and equivalent constant amplitude strain ranges were determined. The field data provided a baseline for laboratory tests to determine the impact of repeated loading on strength and behavior of RCDG bridge members repaired with CFRP for shear. Positive and negative bending moment regions were investigated and the effect of different fatigue load ranges were considered. Based on the field inspections and tests and subsequent laboratory investigation, the following conclusions are presented:

- Under ambient traffic loading, the single largest field measured strain range for an instrumented CFRP strip on an in-service bridge was approximately 34 με.
- Based on ambient traffic induced strain ranges, an equivalent strain range was determined for each of the instrumented CFRP strip locations. The equivalent constant amplitude strain range was below 15 με for all locations.
- Based on the highest field measured strain location, a CFRP strain range required to produce an estimated equivalence of 50 years of service-life damage in 1,000,000 cycles for laboratory specimens was determined as approximately 22.5 με.
- Service-level fatigue loading histories, higher than those observed in the field, did not produce significant changes in ultimate shear capacity.
- Vertical CFRP strips reduced service-level stirrup stresses but did not reduce flexural steel stresses.
- Under repeated loading, small areas of the CFRP strips debonded along diagonal cracks and at the terminating edges of the strips in the flexural tension zone at the deck/stem interface. Field inspections for debonded regions should focus on these regions.

- An open space between adjacent CFRP strips permitted identification of diagonal cracking in the girder after repair and is recommended for future installations to facilitate inspection and identification of debonded locations.
- Debonded areas of CFRP material were easily identified by infrared thermography or by sounding the CFRP material and listening for a change in sound frequency.
- Failure was controlled by debonding of CFRP strips initiating in the flexural tension zone near the deck/stem interface for both fatigued and unfatigued IT specimens. No substantial visual differences between fatigued and unfatigued specimens prior to failure were observed.
- Terminating edges of the CFRP strips located near the compression zone did not exhibit debonding under fatigue load.
- Diagonal crack motions increased under repeated fatigue loading and the higher fatigue load range produced larger crack motions, although for the applied load history, the shear capacity was not significantly affected.

Acknowledgements

This research was funded by the Oregon Department of Transportation and Federal Highway Administration and overseen by research coordinator Mr. Steven Soltesz. All CFRP materials and installation were donated by MBrace of Cleveland, OH and Pioneer Waterproofing of Portland, OR with the help of Mr. Neil Antonini. Reinforcing steel and fabrication were donated by Cascade Steel Rolling Mills of McMinnville, OR and Farwest Steel of Eugene, OR, respectively. The authors would also like to thank Dr. Tanarat Potisuk, Mr. Richard Forrest, Mr. Thomas Schumacher, Ms. Michelle Chavez, and Ms. Angela Rogge for their assistance in experimental testing and data reduction. The findings and conclusions are those of the authors and do not necessarily reflect those of the project sponsors or the individuals acknowledged.

Notation

The following symbols are used in this paper:

f_{bond} = bond strength demand of CFRP on concrete surface (MPa);
f'_c = compressive strength of concrete (MPa);
f_{ult} = ultimate stress of internal reinforcing steel (MPa);
f_y = yield stress of internal reinforcing steel (MPa);
h = height of reinforcing deformation lug (mm);
k = fatigue exponent;
n_i = number of cycles observed for the i^{th} strain range;
N_{tot} = total number of cycles at all strain ranges;
r = radius of reinforcing deformation lug (mm);
Sr_i = the i^{th} strain range (με);
S_{r_rep} = strain range of internal stirrup after CFRP repair (με);
S_{r_unr} = strain range of internal stirrup before CFRP repair (με);
SR_{eqv} = equivalent constant amplitude strain range (με);
St Dev = standard deviation of measured CFRP properties;
V_{APP} = applied shear from actuator (kN);
V_{Pred} = predicted shear capacity using *Response 2000*™ (kN);
Δ = change in displacement magnitude (mm);
$\mu\varepsilon_{max}$ = maximum measured CFRP strain at mid height of u-wrap (με);

θ_{ck} = angle of diagonal failure crack (degrees);
σ_{min} = minimum stress in reinforcing bar (MPa); and
σ_r = stress range (MPa).

REFERENCES

AASHO (American Association of State Highway Officials), (1941, 1944, 1949, 1953, 1957, 1961, 1965). "Standard Specifications for Highway Bridges." 3rd to 9th Editions, AASHO, Washington, D.C.

AASHTO, (2002) "Standard Specification for Highway Bridges." 17th Edition." AASHTO, Washington, D. C.

ACI 318-63, (1963). "Building Code Requirements for Structural Concrete." American Concrete Institute, Detroit, Michigan.

ACI 318-02, (2002). "Building Code Requirements for Structural Concrete." American Concrete Institute, Farmington Hills, Michigan.

ACI Committee 215R-92 (1992). "Considerations for Design of Concrete Structures Subjected to Fatigue Loading." American Concrete Institute, Detroit, Michigan.

ACI SP-41 (1974). *Abeles Symposium - Fatigue of Concrete*. American Concrete Institute, Detroit, Michigan.

ACI SP-75 (1982). *Fatigue of Concrete Structures*. S.P. Shah (editor), American Concrete Institute, Detroit, Michigan.

ACI 440.2R-02, (2002). "Guide for the Design and Construction of Externally Bonded FRP Systems for Strengthening Concrete Structures." American Concrete Institute, Farmington Hills, Michigan.

ASTM A305-50T, (1950). "Tentative Specifications for Minimum Requirements for the Deformations of Deformed Steel Bars Concrete Reinforcement." ASTM, Philadelphia, PA.

ASTM D 3039/D 3039M-00, (2001). "Standard Test Method for Tensile Properties of Polymer Matrix Composite Materials." ASTM, West Conshohocken, PA.

Balazs, G.L., (1998). "Bond Under Repeated Loading." SP 180-6: Bond under Repeated Loading, A Tribute to Dr. Peter Gergely, Leon, R. (Editor), American Concrete Institute, Farmington Hills, Michigan, pp. 125-143.

Breña, S.F., Benouaich, M.A., Kreger, M.E., and Wood, S.L., (2005). "Fatigue Tests of Reinforced Concrete Beams Strengthened Using Carbon Fiber-Reinforced Polymer Composites." *ACI Structural Journal*, v. 102, No. 2, March-April, pp. 305-313.

Chang, T.S. and C.E. Kesler, (1958). "Static and Fatigue Strength in Shear of Beams with Tensile Reinforcement." *Journal of the American Concrete Institute*, Vol. 29, No. 12, pp. 1033-1053.

Corley, W.G., Hanson, J.M., and T. Helgason, (1978). "Design of Reinforced Concrete for Fatigue." *Journal of the Structural Division,* ASCE, Vol. 104, No. ST6, pp. 921-932.

Hanson, J.M., Burton, K.T., and E. Hognestad, (1968). "Fatigue Tests of Reinforcing Bars – Effect of Deformation Pattern." Journal of the PCA Research and Development Laboratories, Vol. 10, No. 3, pp.2-13.

Hanson, J.M. and Hulsbos, C.L. and D.A. VanHorn, (1970). "Fatigue Tests of Prestressed Concrete I-Beams." *Journal of the Structural Division,* ASCE, Vol. 96, No. ST11, pp. 2443-2464.

Hanson, J.M., Somes, M.F. and T. Helgason, (1974). "Investigation of Design Factors Affecting Fatigue Strength of Reinforcing Steel – Test Program." *SP-41: Abeles Symposium - Fatigue of Concrete*, American Concrete Institute, Detroit, Michigan, pp. 71-106.

Hawkins, N.M. (1974). "Fatigue Characteristics in Bond and Shear of Reinforced Concrete Beams." *SP-41: Abeles Symposium - Fatigue of Concrete*, American Concrete Institute, Detroit, Michigan, pp. 203-236.

Helgason, T. and J.M. Hanson, (1974). "Investigation of Design Factors Affecting Fatigue Strength of Reinforcing Steel – Statistical Analysis." *SP-41: Abeles Symposium - Fatigue of Concrete*, American Concrete Institute, Detroit, Michigan, pp. 107-138.

Higgins, C., Miller, T.H., Rosowsky, D.V., Yim, S.C., Potisuk, T., Daniels, T.K., Nicholas, B.S., Robelo, M.J., Lee, A-Y, and R.W. Forrest, (2004). "Assessment Methodology for Diagonally Cracked Reinforced Concrete Deck Girders." *Report No. FHWA-OR-RD-05-04*, Federal Highway Administration, Washington, D. C.

Jhamb I.C. and J.G. MacGregor, (1974). "Effects of Surface Characteristics on Fatigue Strength of Reinforcing Steel." *SP-41: Abeles Symposium - Fatigue of Concrete*, American Concrete Institute, Detroit, Michigan, pp. 139-168.

Kreger, M.E., Bachman, P.M., and J.E. Breen, (1989). "An Exploratory Study of Shear Fatigue Behavior of Prestressed Concrete Girders." *PCI Journal,* July/August pp. 104-125.

Kwak, K-H. and J-G. Park, (2001). "Shear-Fatigue Behavior of High-Strength Concrete Under Repeated Loading." *Structural Engineering and Mechanics,* Vol. 11, No. 3, pp. 301-314.

Kwak, K-H., Suh, J., and C-Z., T. Hsu, (1991). "Shear-Fatigue Behavior of Steel Fiber Reinforced Concrete Beams." *ACI Structural Journal,* Vol. 88, No. 2, pp. 155-160.

Lopez, M.M., Naaman, A.E., Pinkerton, L., Till, R.D., (2003). "Behavior of RC Beams Strengthened with FRP Laminates and Tested Under Cyclic Loading at Low Temperatures." *International Journal of Materials and Product Technology*, v. 19, Nos. 1-2, pp. 108-117.

Mandell, J.F., Reed, R.M., Samborsky, D.D., and Pan, Q., (1993). "Fatigue Performance of Wind Turbine Blade Composite Materials." *Wind Energy – 1993*, S.M. Hock, editor, SED-Vol. 14, ASME.

Master Builders, Inc., (2001). “MBrace Composite Strengthening System Material Specifications.” Cleveland, OH.

Miner, M. A., (1945) "Cumulative Damage in Fatigue.” *Journal of Applied Mechanics*, Vol. 12, Trans. ASME Vol. 67, pp. A159-A164.

Muszynski, L.C. and Sierakowski, R.L., (1996). “Fatigue Strength of Externally Reinforced Concrete Beams.” *Proceedings of the Materials Engineering Conference*, v. 1, pp. 648-656.

Papakonstantinou, C.G., Petrou, M.F., Harries, K.A., (2001). “Fatigue Behavior of RC Beams Strengthened with GFRP Sheets.” *Journal of Composites for Construction*, v. 5, No. 4, November, pp. 246-253.

Price, K.M. and A.D. Edwards, (1971). “Fatigue Strength in Shear of Prestressed Concrete I-Beams.” *ACI Journal,* ACI, Vol. 68, April, pp. 282-292.

Rehm, G. and R. Eligehausen, (1979). “Bond of Ribbed Bars Under High-Cycle Repeated Loads.” *ACI Journal,* Vol. 76, Feb., pp. 297-309.

Siess, C.P. (1960). “Research, Building Codes, and Engineering Practice.” *ACI Journal*, May, ACI, pp. 1105-1122.

Tedesco, J.W., Stallings, J.M., El-Mihilmy, M., McCauley, M.W., (1996). “Rehabilitation of a Concrete Bridge Using FRP Laminates.” *Proceedings of the Materials Engineering Conference*, v. 1, pp. 631-637.

Teng, S., Ma, W., Tan, K.H., and F.K. Kong, (1998). “Fatigue Tests of Reinforced Concrete Deep Beams.” *The Structural Engineer*, Vol. 76, No. 18, pp. 347-352.

Ueda, T. and H. Okamura, (1983). “Behavior in Shear of Reinforced Concrete Beams under Fatigue Loading.” *Journal of the Faculty of Engineering,* The University of Tokyo, Vol. 37, No. 1, pp. 17-48.

Ueda, T. and H. Okamura, (1981). “Behavior of Stirrup Under Fatigue Loading.” *Transactions of the Japan Concrete Institute,* JCI, Vol. 3, pp. 305-318.

Table D1: Steel reinforcing property description.

Description	Bar Size	Grade	f_y (MPa)	f_{ult} (MPa)
Stirrups	# 13	300	350	559
Deck	# 13	420	443	724
Skin	# 19	420	461	648
Flexure	# 36	420	481	717
Hooks	# 36	420	481	717

Table D2: Concrete and CFRP bond properties and maximum initial diagonal crack size.

Specimen	f_c' (MPa)		Initial Max Crack Size (mm)	CFRP Bond Strength (MPa)
	28-Day	Failure		
2T04	26.27	29.37	0.762	1.82
2T03	23.17	25.40	0.762	2.83
1IT02	26.27	26.34	1.016	2.02
3IT05	23.48	25.39	1.016	2.15
3IT06	22.70	23.33	0.762	1.81

Table D3: Composite material properties: Reported and experimental.

Property	Individual Component*			Composite†			
	Saturant	Carbon Fiber		CF130		CF160	
		CF130	CF160	Mean	St Dev	Mean	St Dev
Thickness, t (mm/ply)	-	0.165	0.33	0.975	0.134	1.47	0.16
Ultimate Tensile Strength (MPa)	55.2	3800	3800	717	94	846	151
Ultimate Tensile Strength per Unit Width (kN/mm/ply)	-	0.625	1.25	0.692	0.042	1.22	0.13
Tensile Modulus (MPa)	3034	227000	227000	38750	4530	54400	7020
Ultimate Rupture Strain, %	3.5	1.67	1.67	1.85	0.11	1.55	0.18

*Master Builders, Inc. 2001 material vendor specifications.

†Average and standard deviation values obtained from 20 composite samples of each fiber type tested in accordance with ASTM D 3039/D 3039M.

Table D4: Experimental summary.

Specimen	Fatigue Load Range (kN)	Failure Mode	V_n (kN)**	V_{APP} (kN)	V_d (kN)	V_{EXP} (kN)	θ_{ck} (deg)
2T04	-	Shear / Compression	677	1228	18.3	1246	40
2T03	445	Flexure	681	956	0.0	956	90
1IT02	-	Shear / Compression	934	1112	12.7	1125	37
3IT05	800	Shear / Compression	906	1134	13.0	1147	45
3IT06	490	Shear / Tension	899	1116	9.3	1126	39

** Nominal shear capacity of specimen without CFRP predicted with Response 2000 (Bentz 2000).

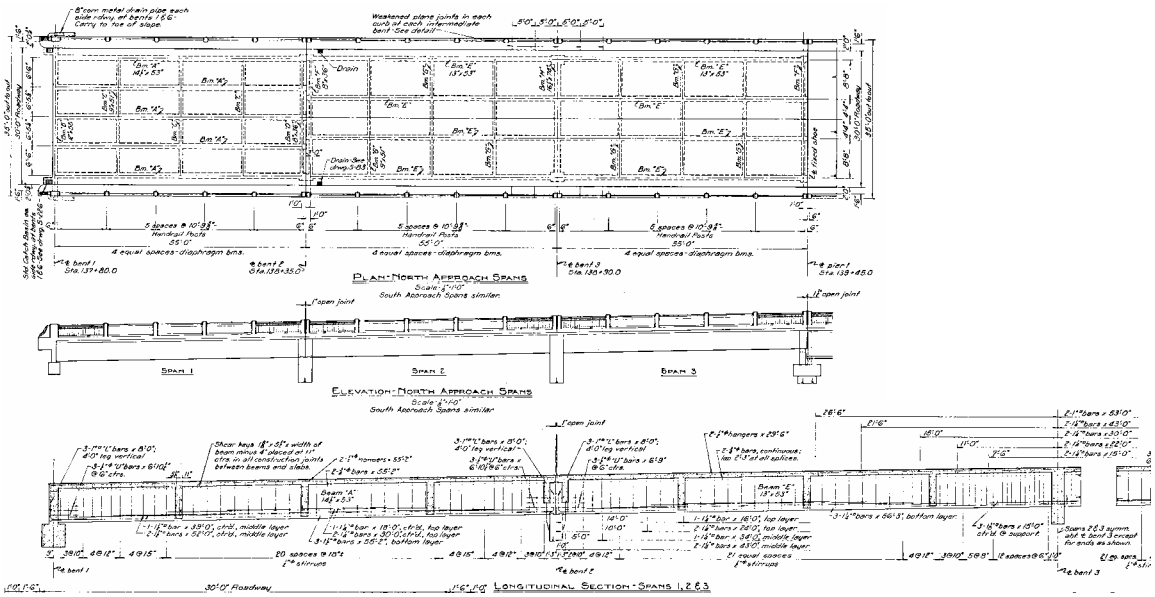

Fig. D1- Willamette River Bridge overall plan and elevation and main girder details.

a)

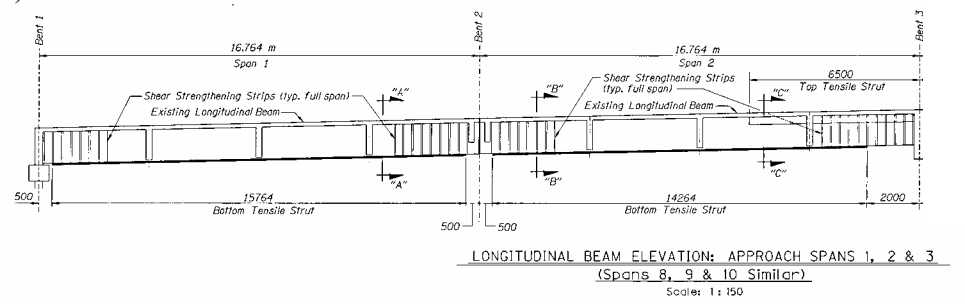

b)

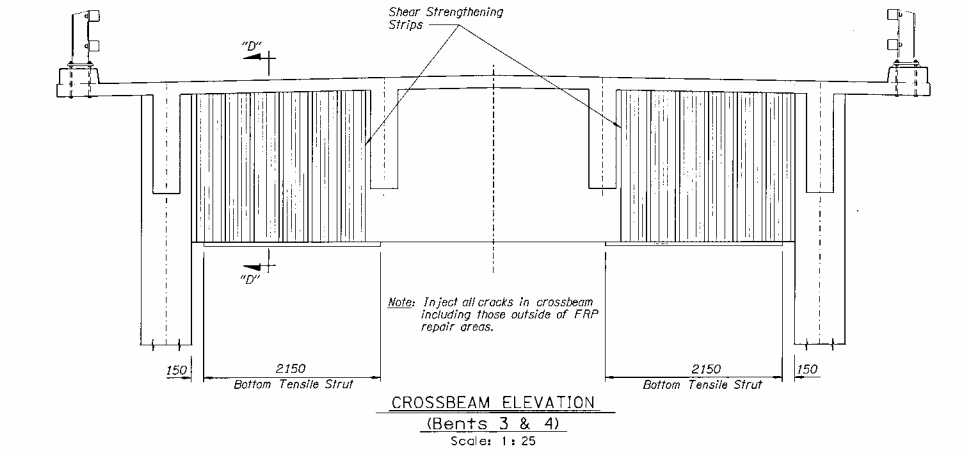

Fig. D2- CFRP repairs to a) main girders and b) bent caps.

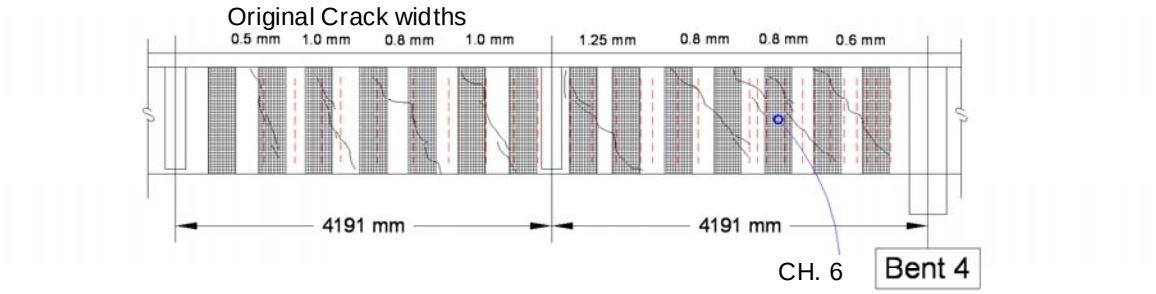

Fig. D3- Field measured cracking, embedded stirrups, and externally bonded CFRP on exterior girder.

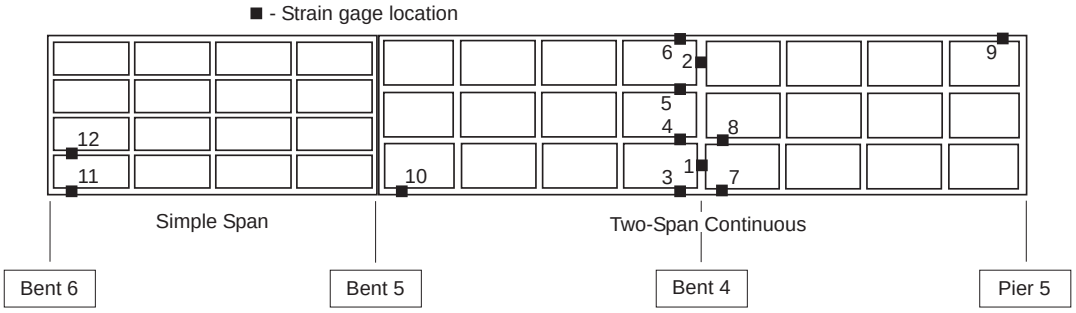

Fig. D4- Schematic of instrumentation locations.

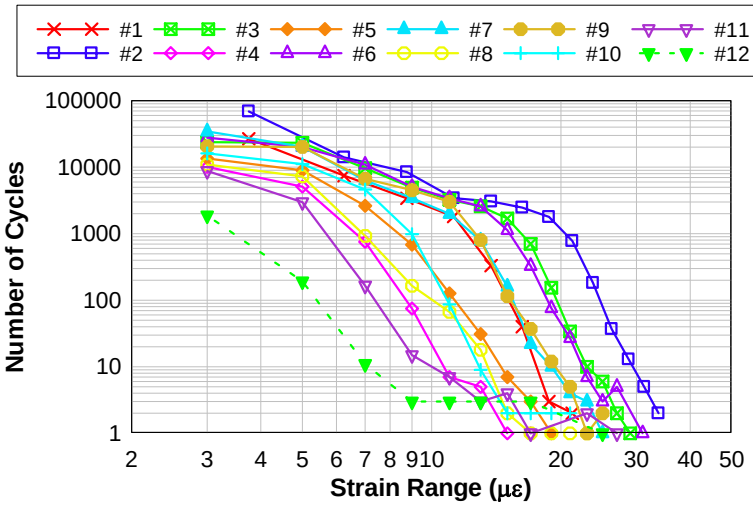

Fig. D5- Strain range-number of cycles measured under ambient traffic conditions at all CFRP instrumented locations.

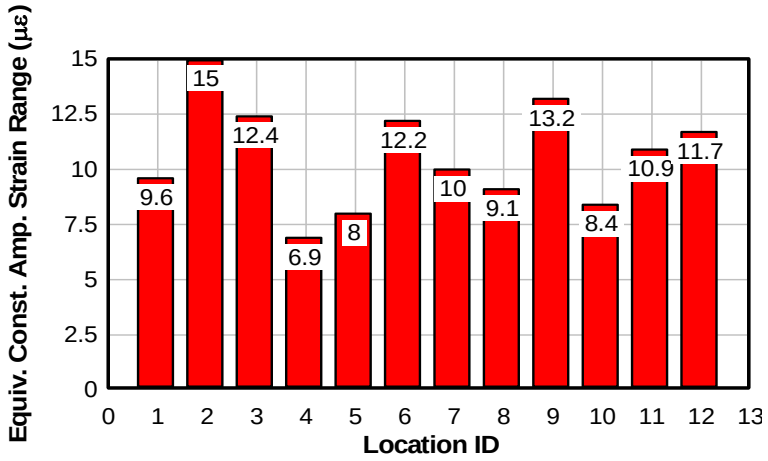

Fig. D6- Equivalent constant amplitude strain ranges for all instrumented locations.

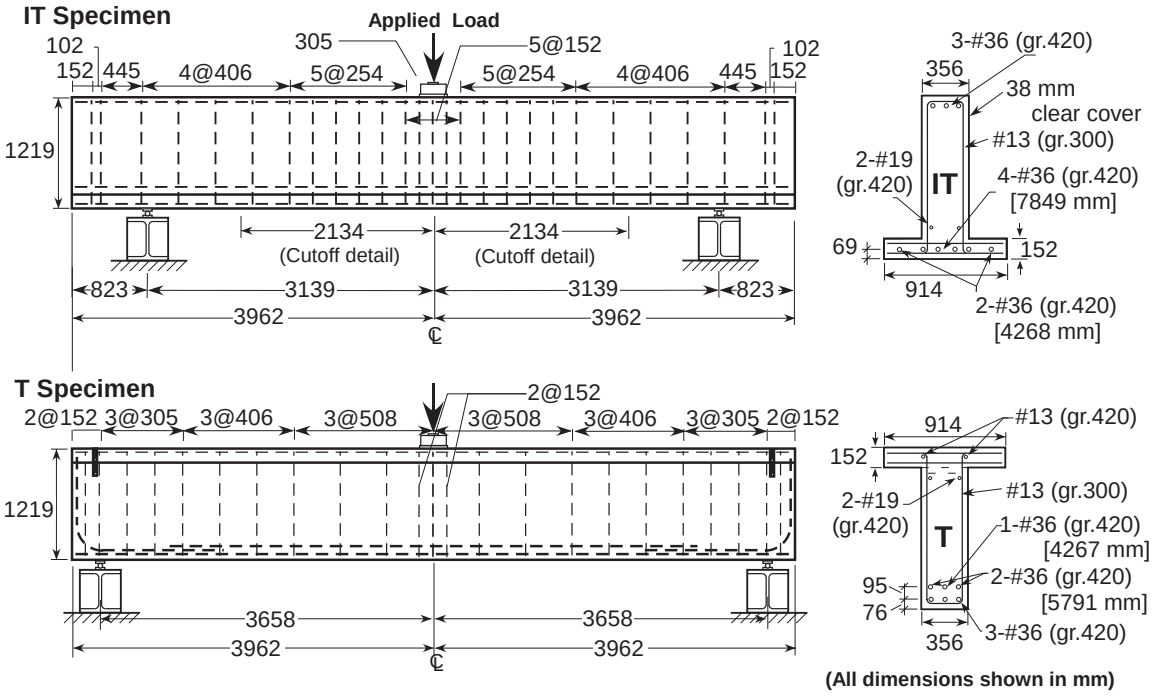

Fig. D7- Typical specimen details.

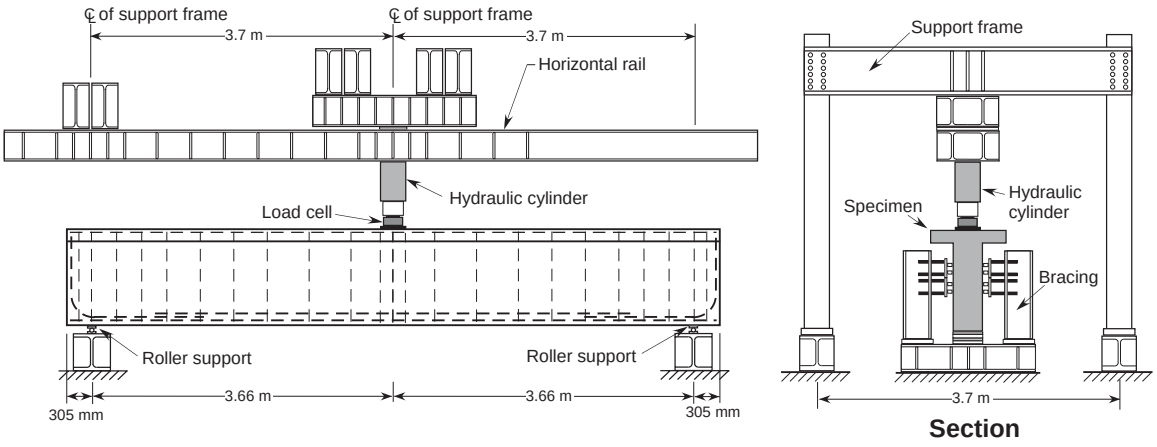

Fig. D8- Schematic of precracking and failure test setup.

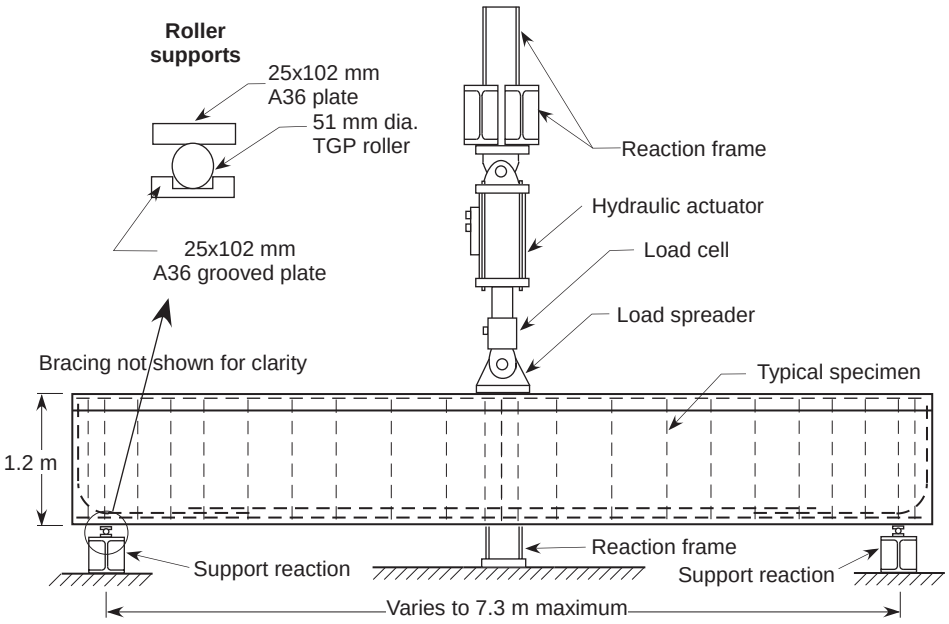

Fig. D9- Schematic of fatigue test setup.

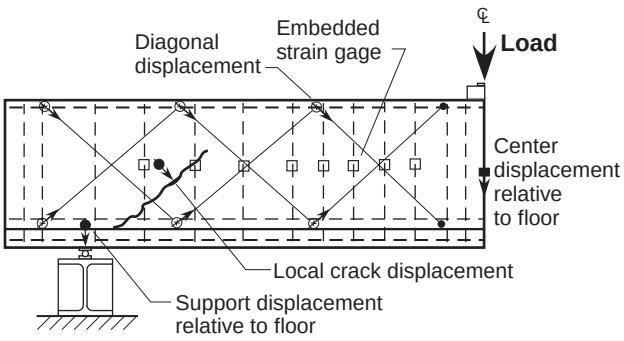

Fig. D10- Typical instrumentation layout.

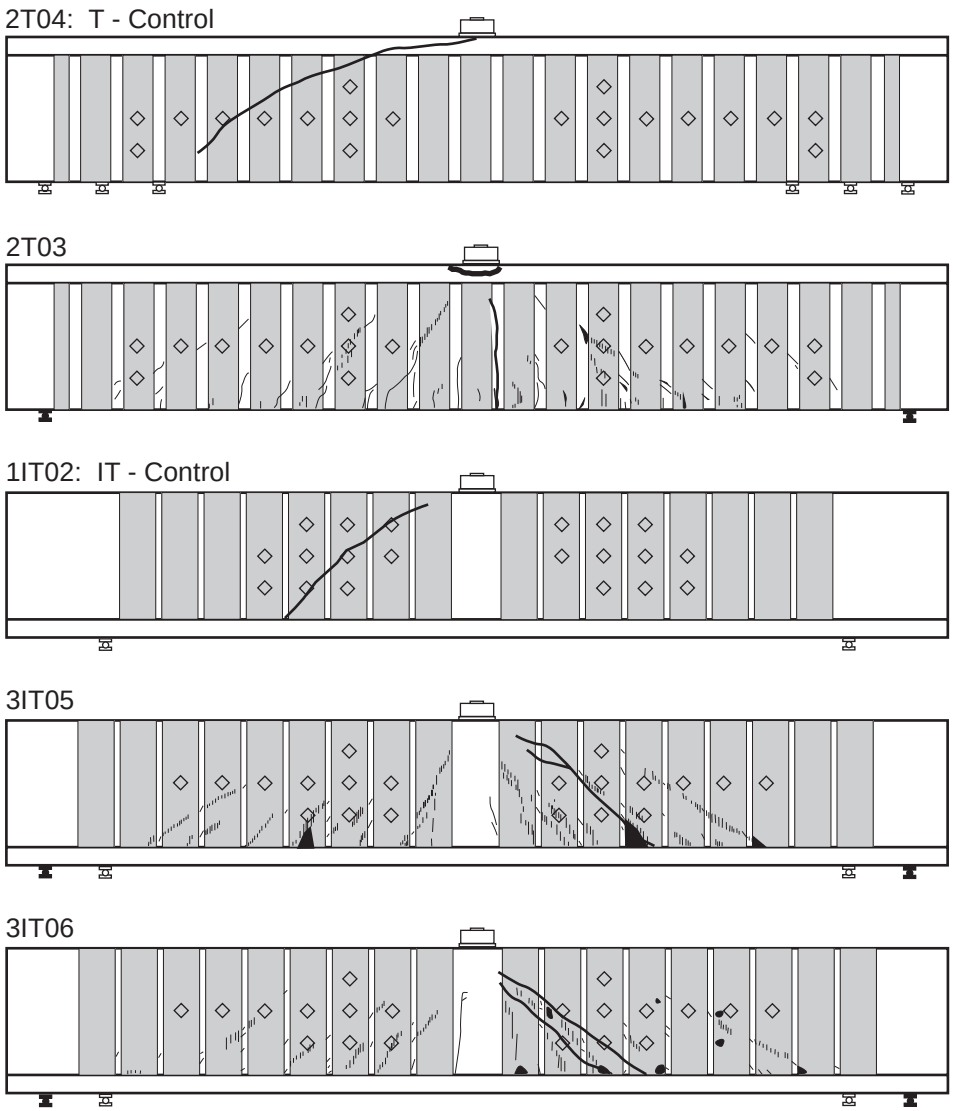

◇ - Strain gages on FRP — Failure cracks

⫴ - Cracking between fibers - Fatigue ⊟ - Precrack and Failure support locations

● - Debonded CFRP - Fatigue ▮ - Fatigue support locations

Fig. D11- FRP repair layout, fatigue damage, failure cracks, and debonding.

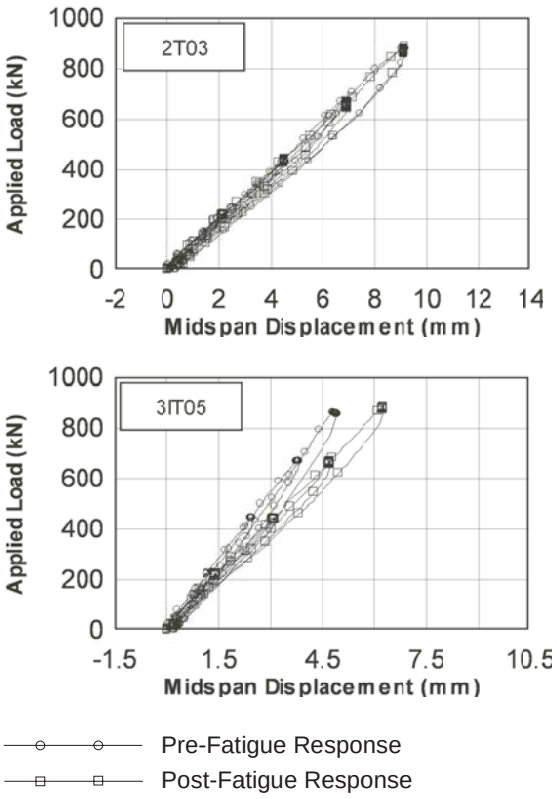

Fig. D12: Midspan displacement responses of T and IT specimens prior to and after fatigue loading.

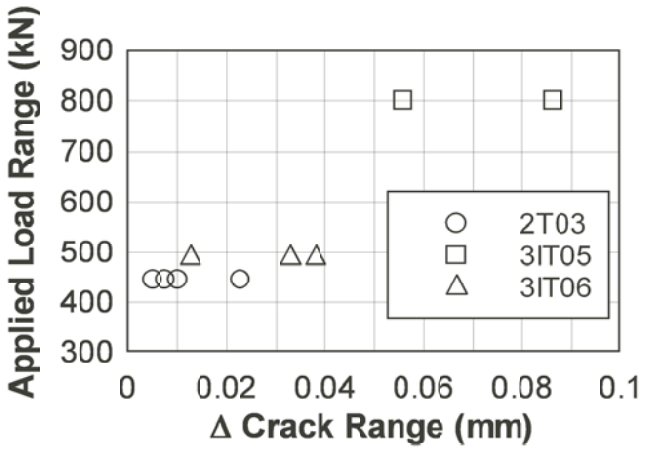

Fig. D13: Change in diagonal crack opening displacement ranges.

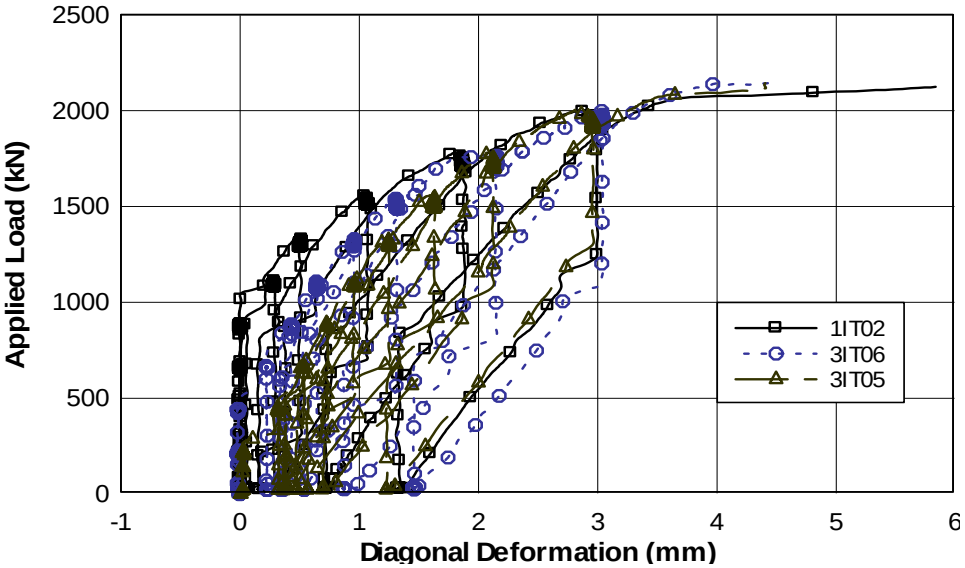

Fig. D14: Diagonal deformation response of IT specimens.

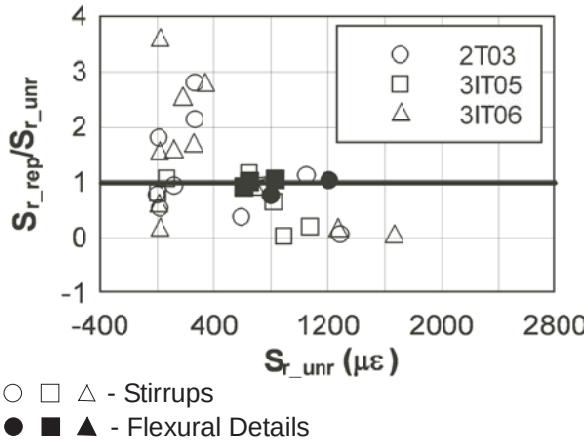

Fig. D15: Internal reinforcing steel strain changes due to application of CFRP strips (S_{r_rep} = rebar range after installation of CFRP, S_{r_unr} = rebar strain range before installation of CFRP).

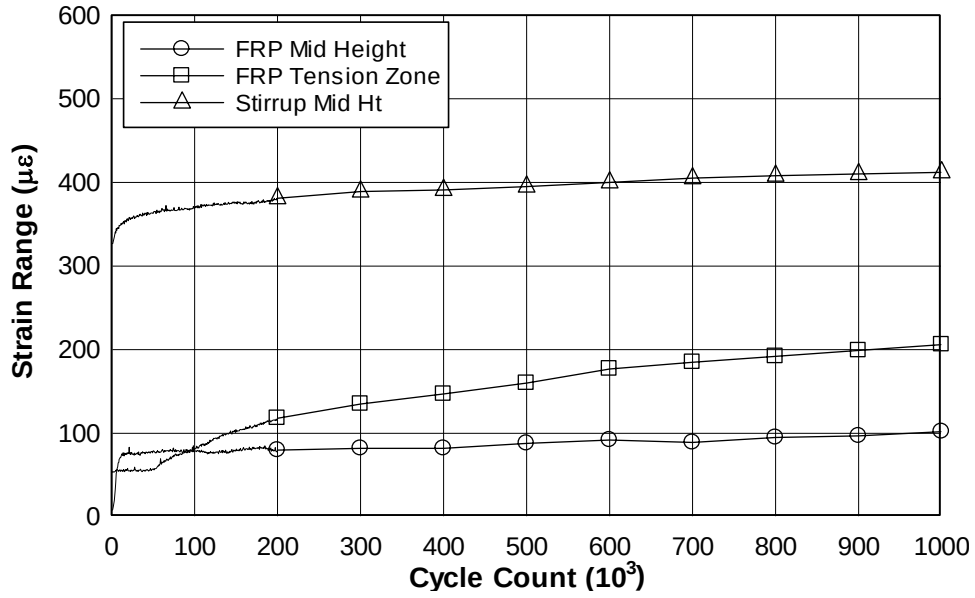

Fig. D16: Representative strains measured during fatigue loading (specimen 3IT05).

APPENDIX E: LABORATORY INVESTIGATION DATA

CAST 1 – SPECIMEN 1IT01

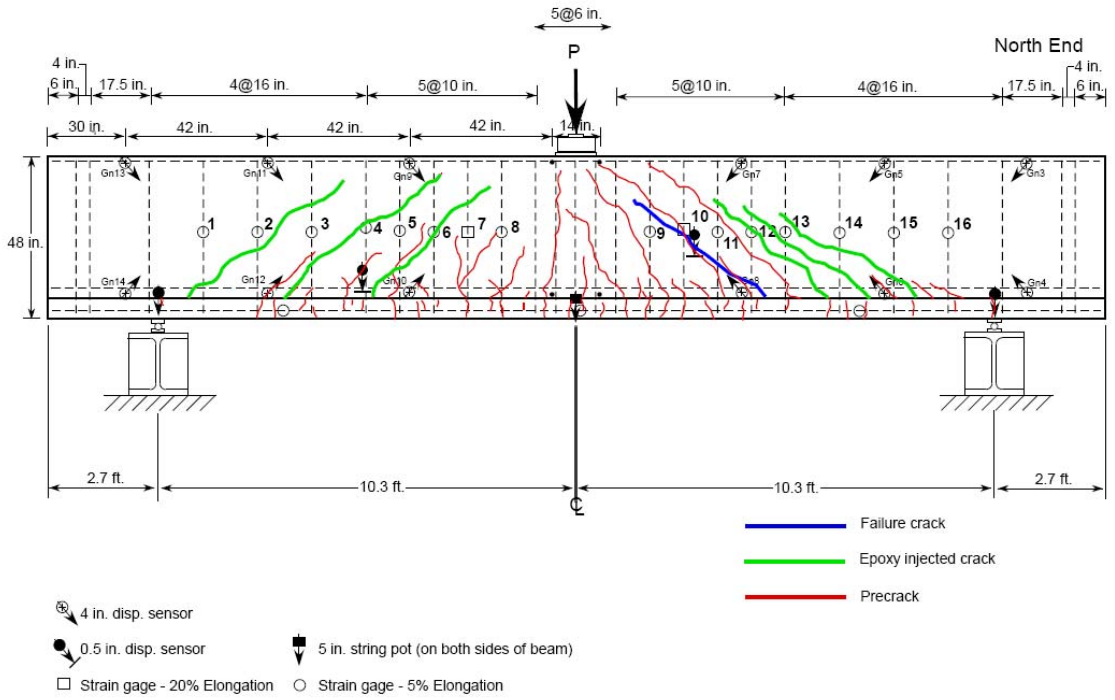

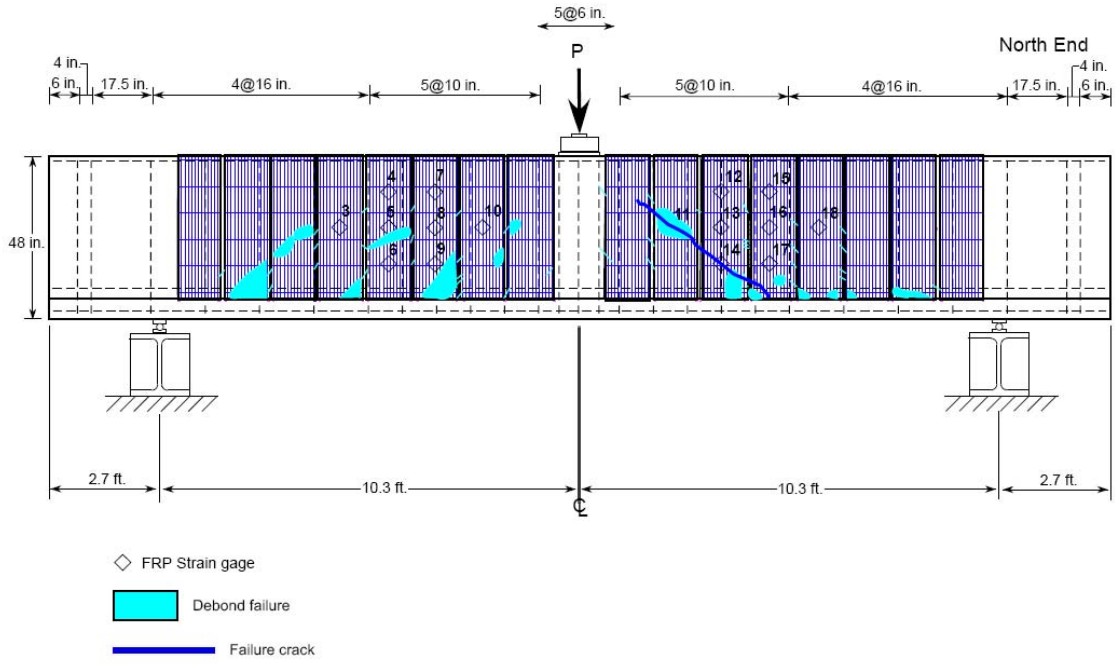

Cast 1 - Specimen 1
Negative Bending (IT-beam)
East Face of Specimen

SPECIMEN 1IT01 – PRECRACK LOAD PLOTS

Force - Midspan Displacement
1IT01 - Precrack

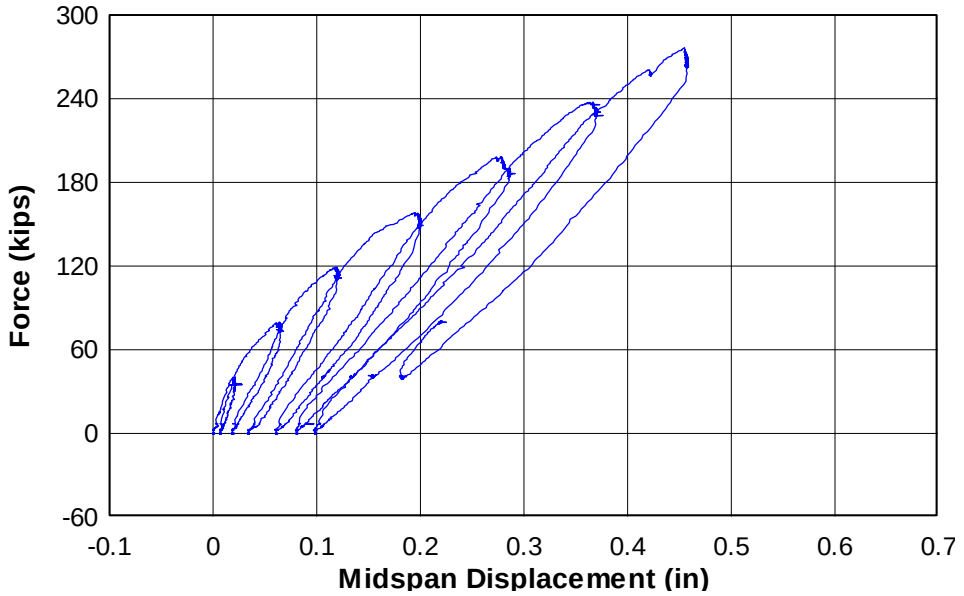

Force - Flexural Reinforcement Strain
1IT01
Detail Locations

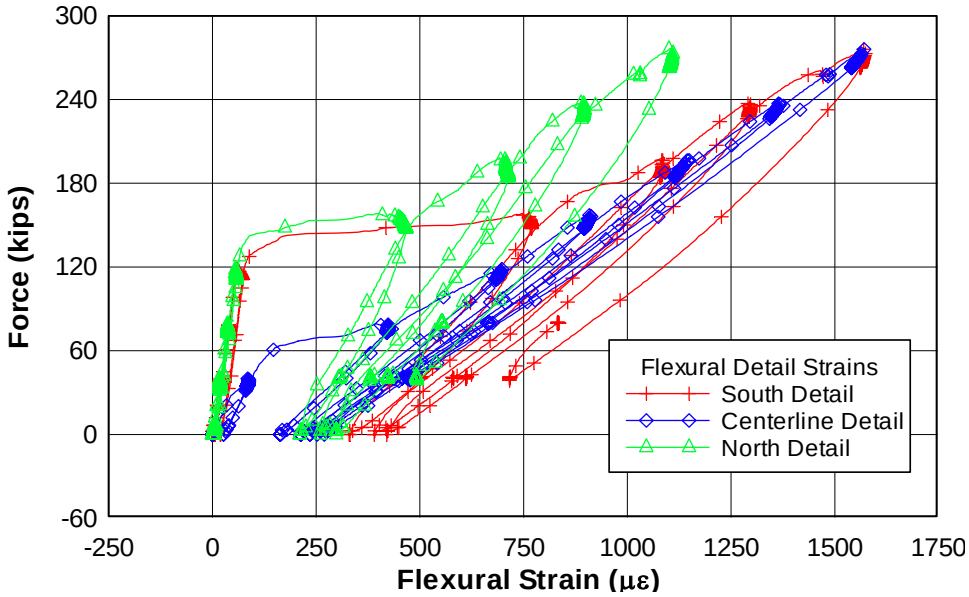

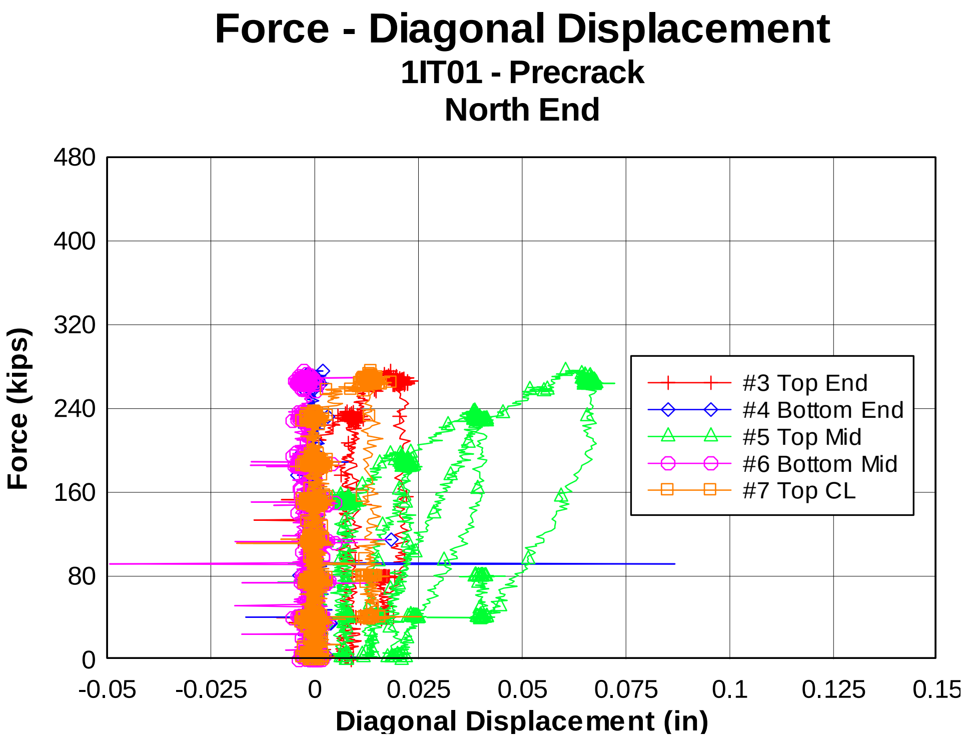
Force - Diagonal Displacement
1IT01 - Precrack
North End
480
400
320
240
160
80
0
-0.05
-0.025
0
0.025
0.05
0.075
0.1
0.125
0.15
Force (kips)
Diagonal Displacement (in)
#3 Top End
#4 Bottom End
#5 Top Mid
#6 Bottom Mid
#7 Top CL

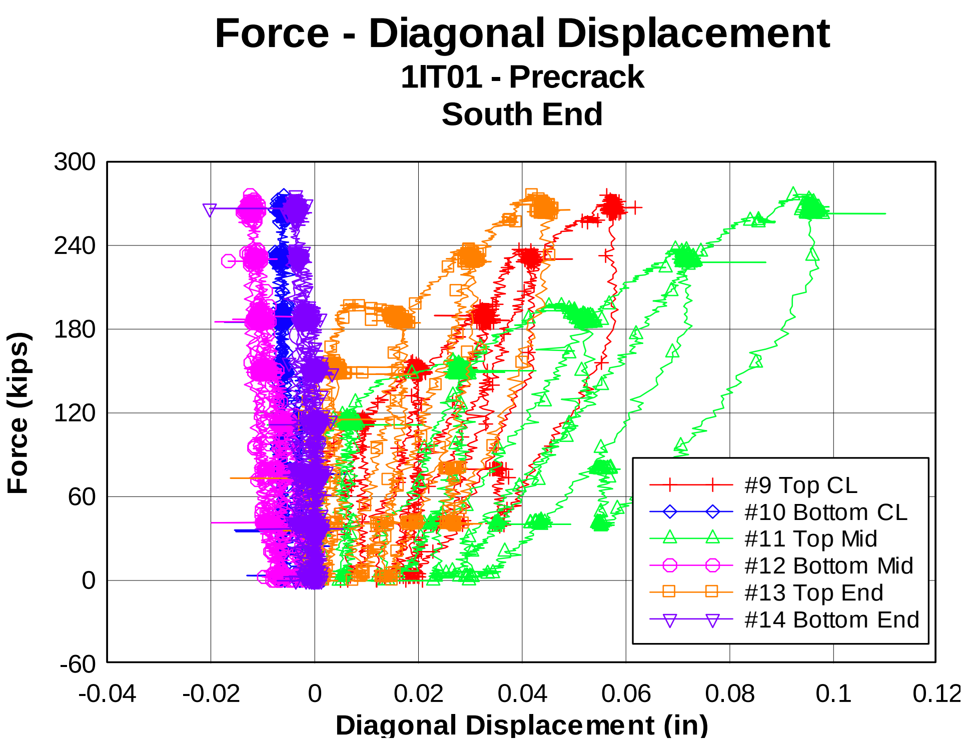
Force - Diagonal Displacement
1IT01 - Precrack
South End
300
240
180
120
60
0
-60
-0.04
-0.02
0
0.02
0.04
0.06
0.08
0.1
0.12
Force (kips)
Diagonal Displacement (in)
#9 Top CL
#10 Bottom CL
#11 Top Mid
#12 Bottom Mid
#13 Top End
#14 Bottom End

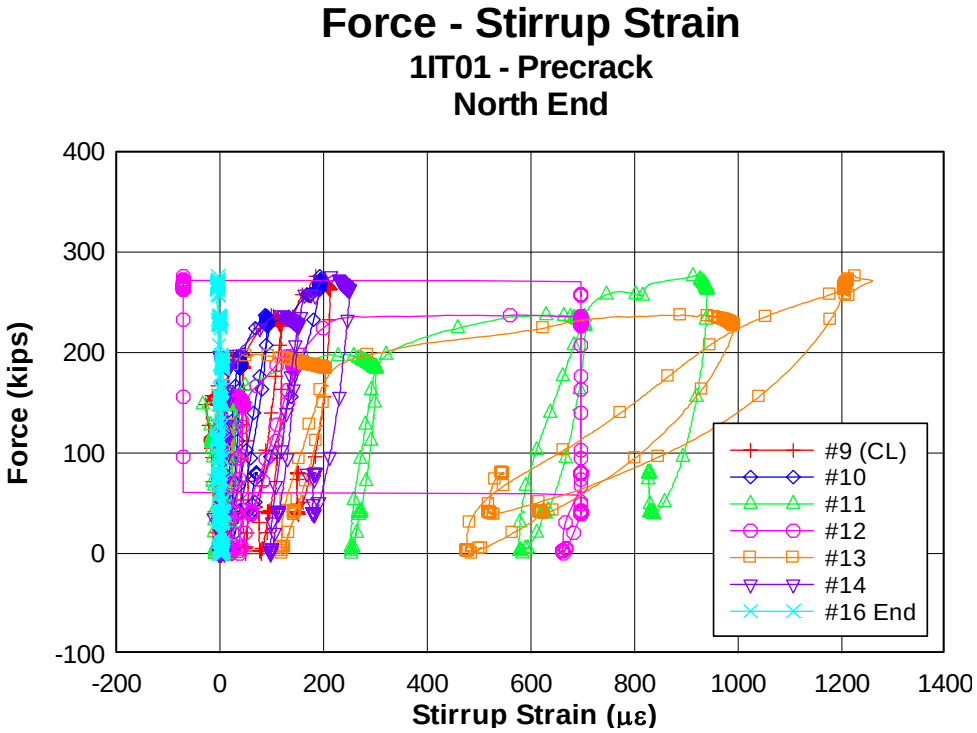
Force - Stirrup Strain
1IT01 - Precrack
North End
Force (kips)
Stirrup Strain (με)
400
300
200
100
0
-100
-200
0
200
400
600
800
1000
1200
1400
#9 (CL)
#10
#11
#12
#13
#14
#16 End

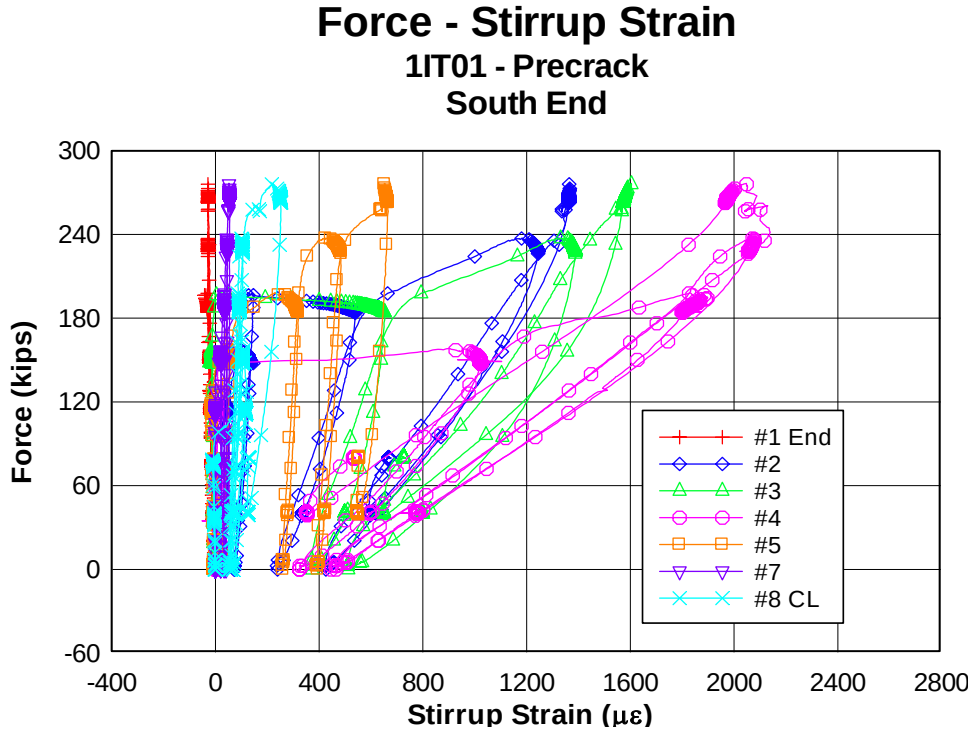
Force - Stirrup Strain
1IT01 - Precrack
South End
Force (kips)
Stirrup Strain (με)
300
240
180
120
60
0
-60
-400
0
400
800
1200
1600
2000
2400
2800
#1 End
#2
#3
#4
#5
#7
#8 CL

SPECIMEN 1IT01 – FAILURE LOAD PLOTS

Force - Midspan Displacement

1IT01 - Test to Failure

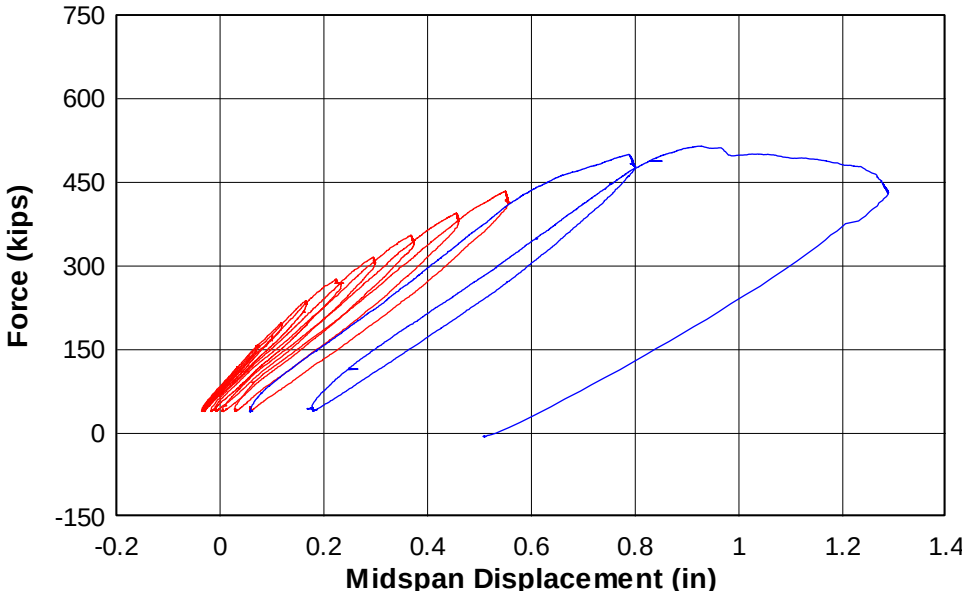

Force - Crack Width

1IT01 - Load to Failure

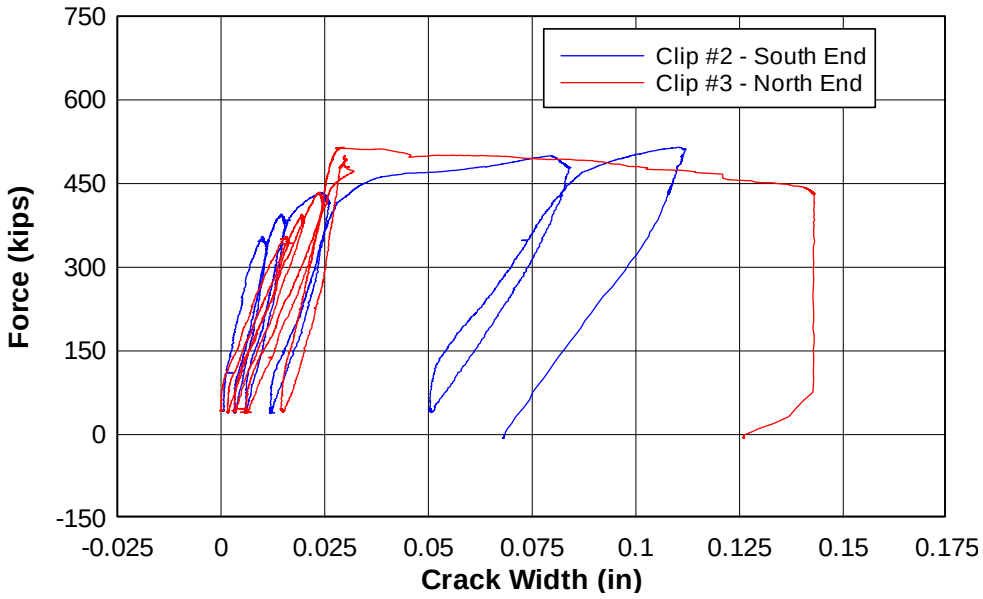

Force - Flexural Reinforcement Strain
1IT01 - Load to Failure
Detail Locations

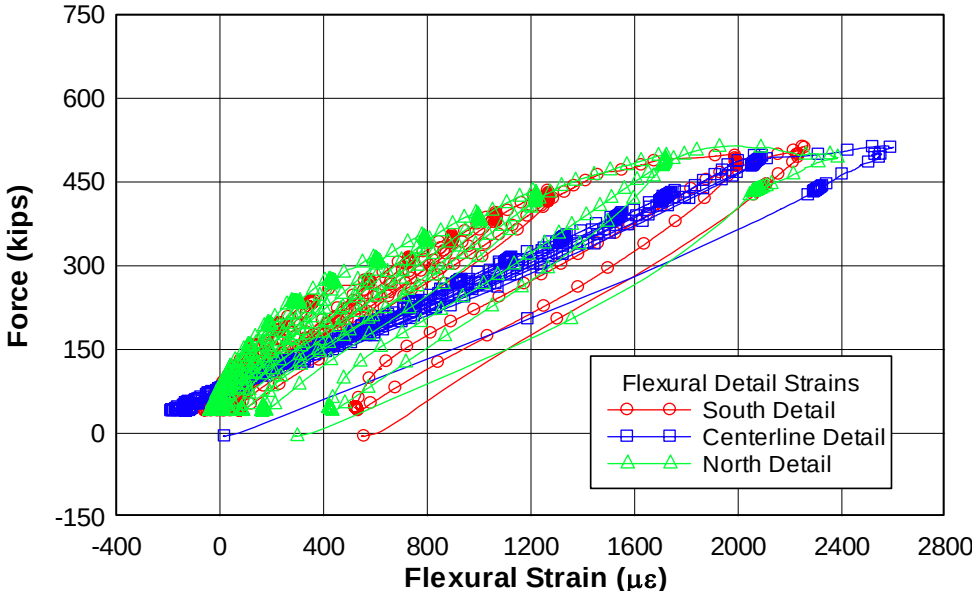

Force - Diagonal Displacement
1IT01 - Load to Failure
North End

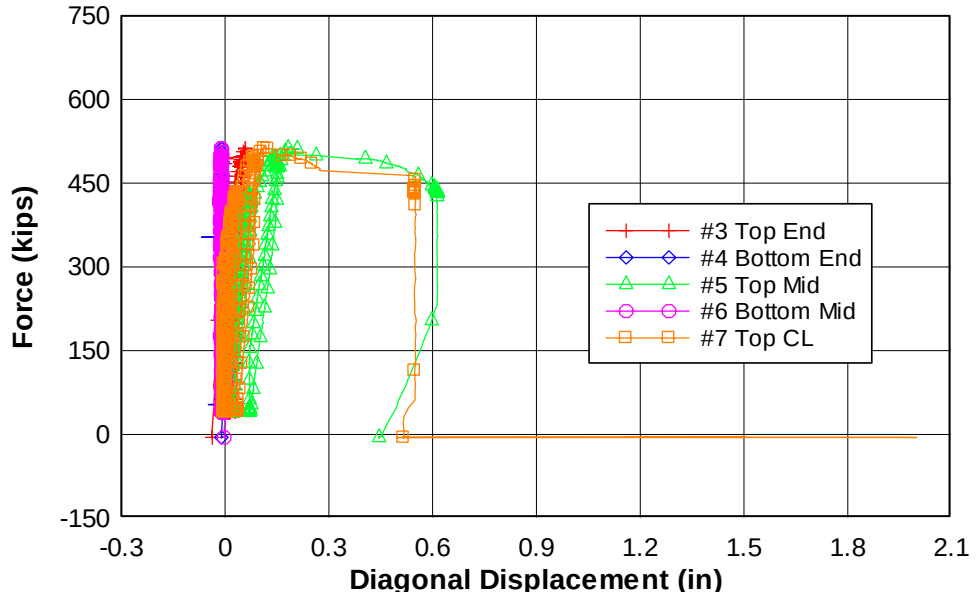

Force - Diagonal Displacement

1IT01 - Load to Failure
South End

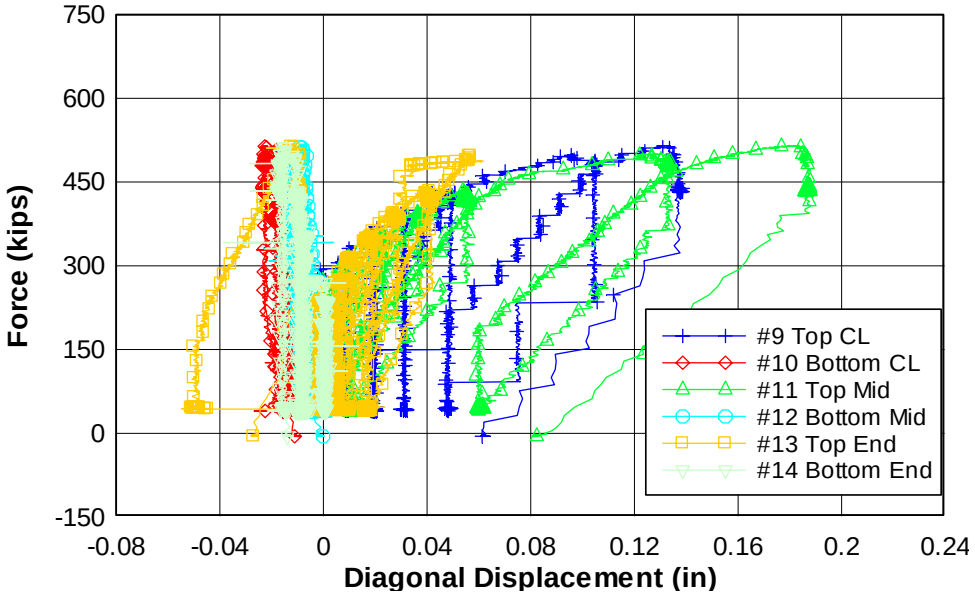

Force - Stirrup Strain

1IT01 - Load to Failure
North End

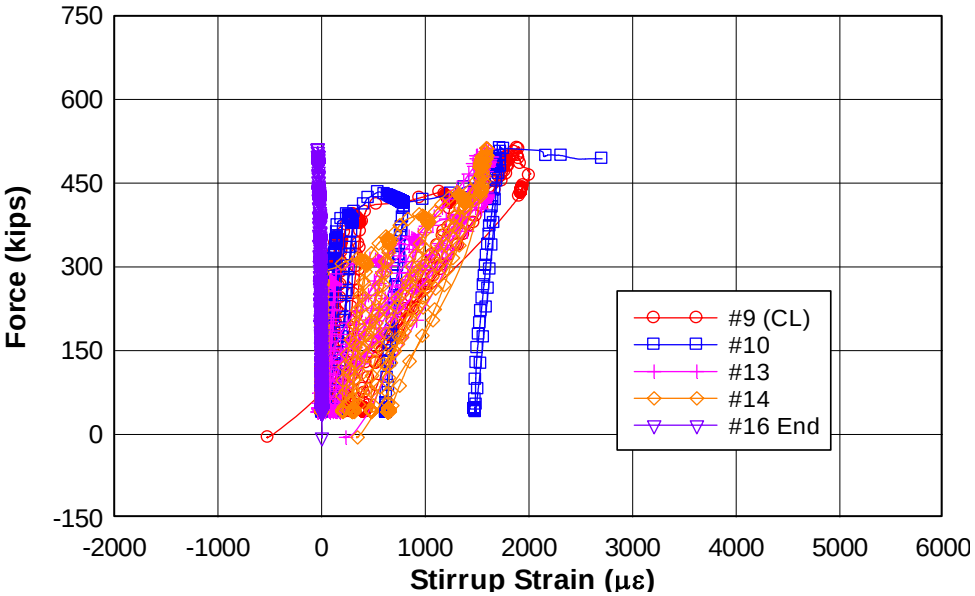

Force - Stirrup Strain

1IT01 - Load to Failure
South End

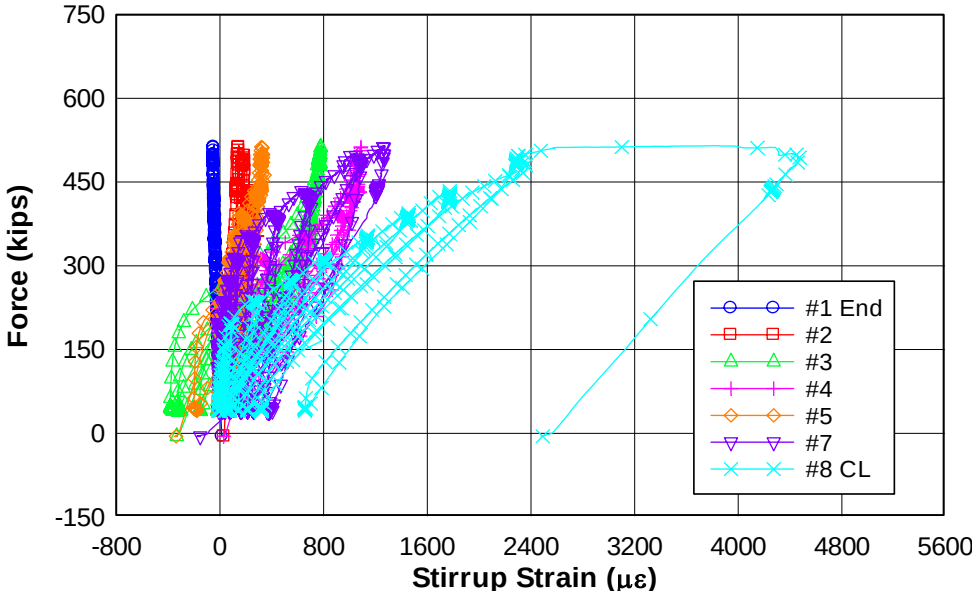

Force - CFRP Strain

1IT01 - Load to Failure
North End

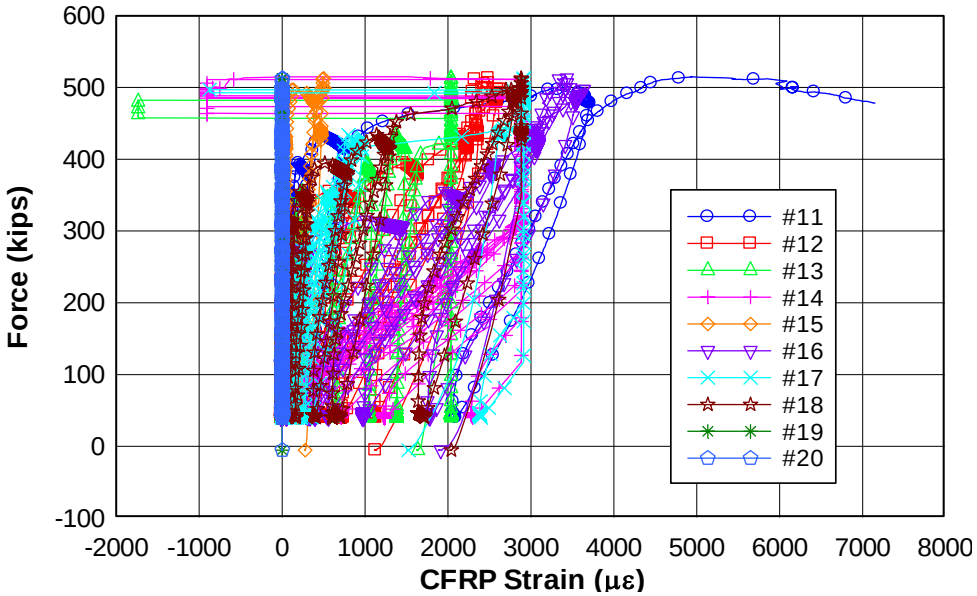

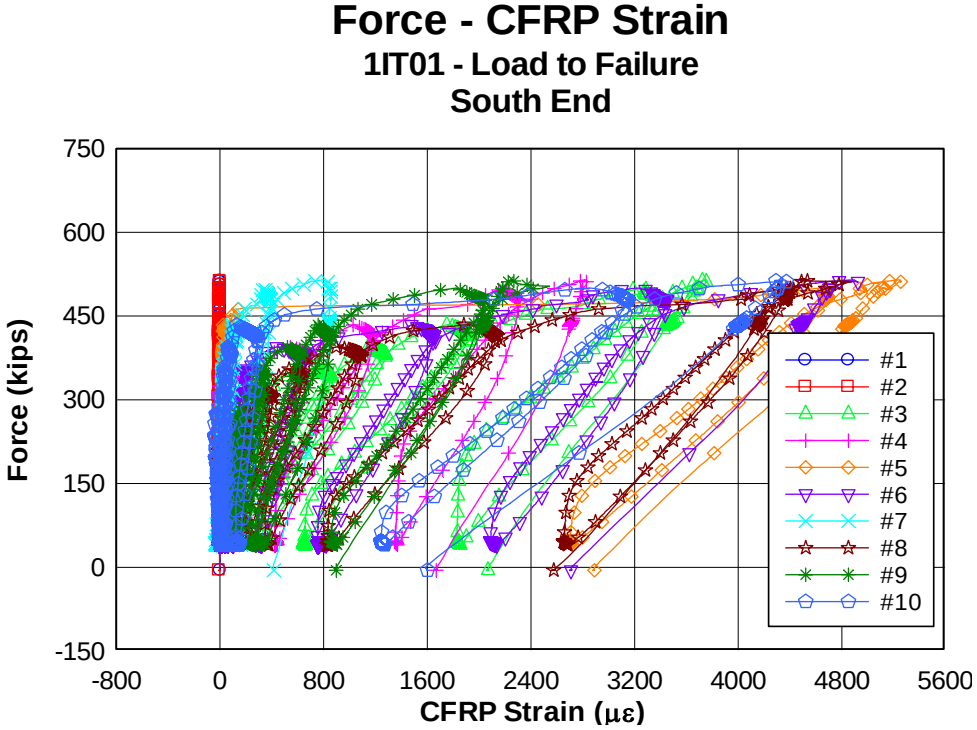
Force - CFRP Strain
1IT01 - Load to Failure
South End
750
600
450
300
150
0
-150
Force (kips)
-800
0
800
1600
2400
3200
4000
4800
5600
CFRP Strain (με)
#1
#2
#3
#4
#5
#6
#7
#8
#9
#10

CAST 1 – SPECIMEN 1IT02

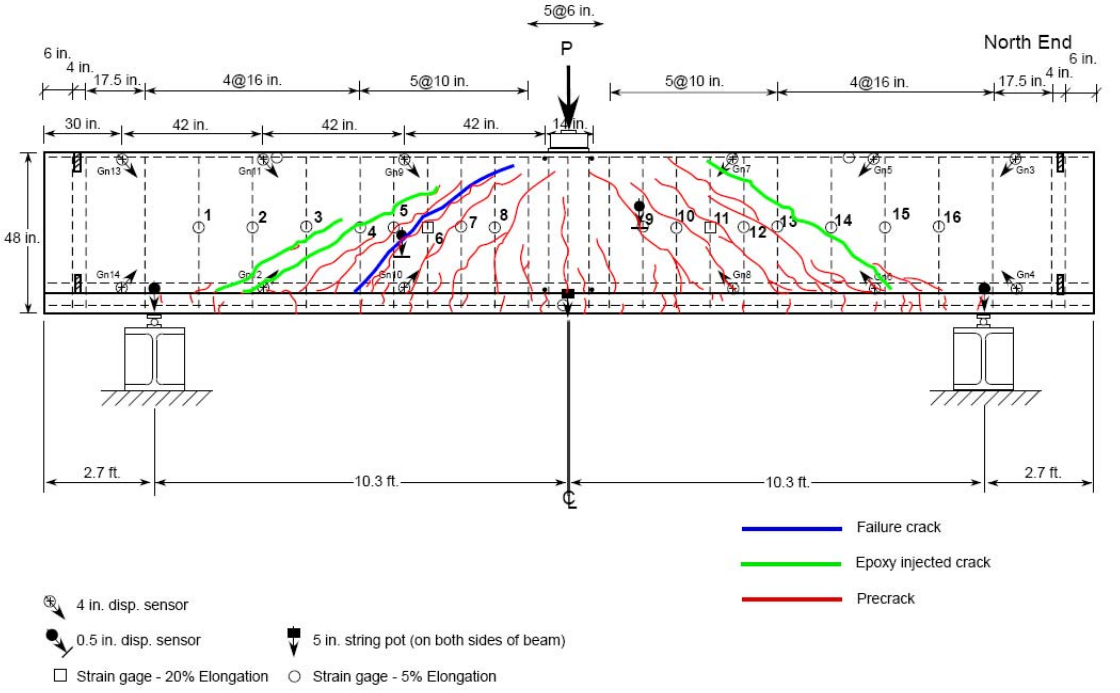

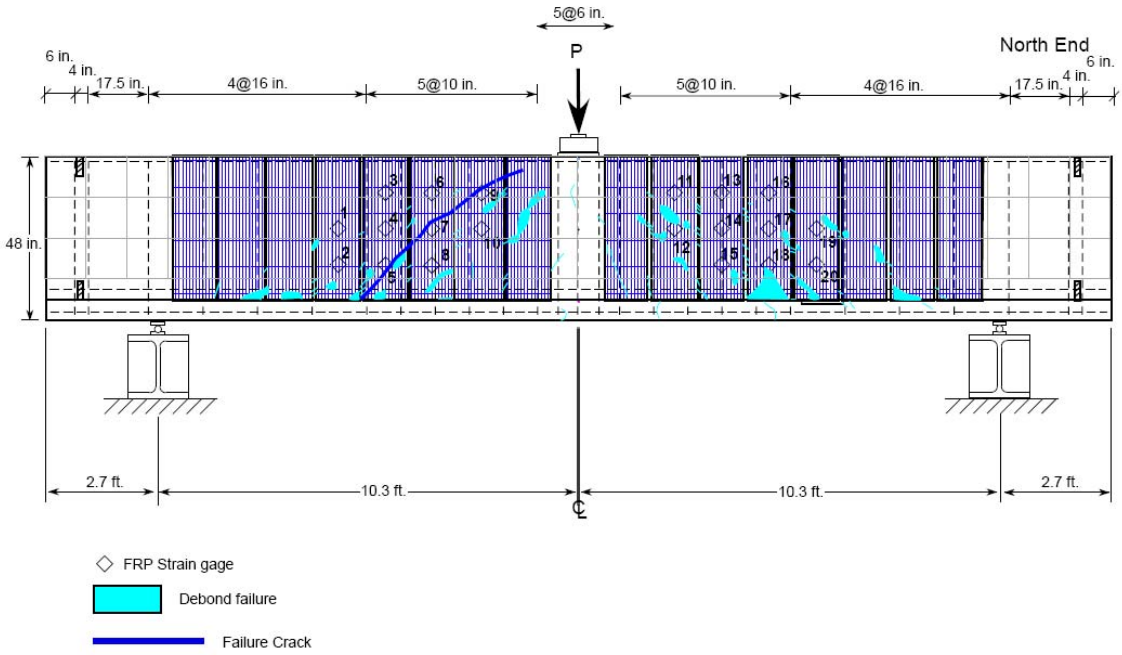

Cast 1 - Specimen 2
Negative Bending (IT-Beam)
East Face of Specimen

SPECIMEN 1IT02 – PRECRACK LOAD PLOTS

Force - Midspan Displacement
1IT02 - Precrack

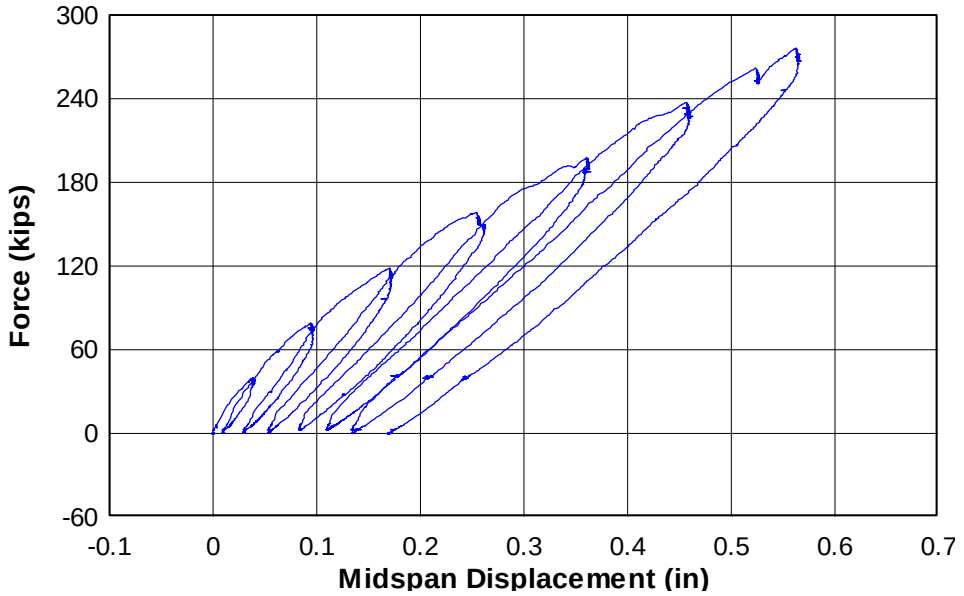

Force - Flexural Reinforcement Strain
1IT02 - Precrack
Detail Locations

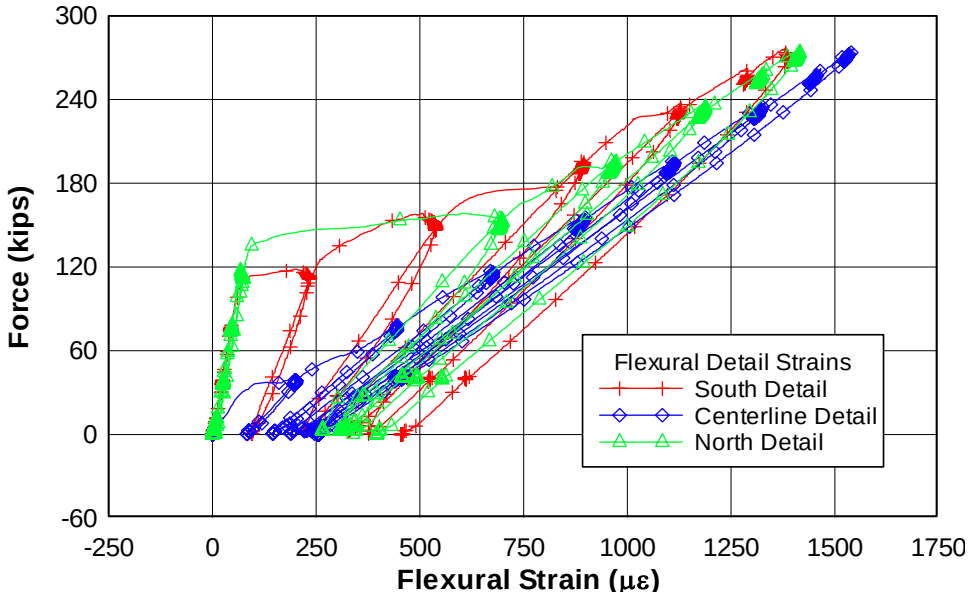

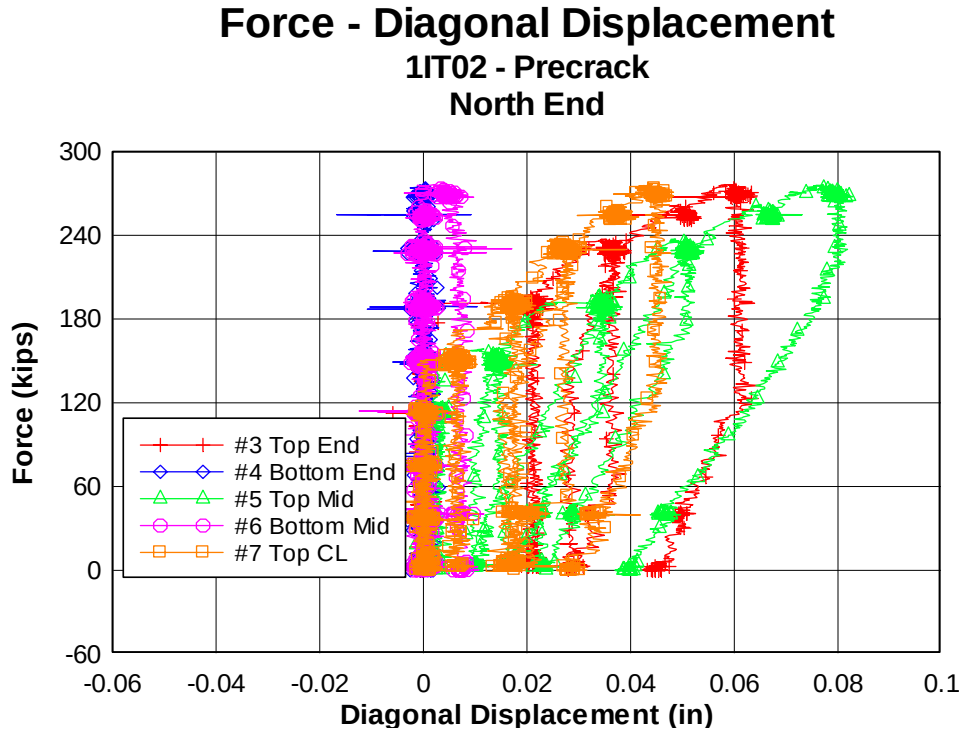
Force - Diagonal Displacement
1IT02 - Precrack
North End
Force (kips)
Diagonal Displacement (in)
300
240
180
120
60
0
-60
-0.06
-0.04
-0.02
0
0.02
0.04
0.06
0.08
0.1
#3 Top End
#4 Bottom End
#5 Top Mid
#6 Bottom Mid
#7 Top CL

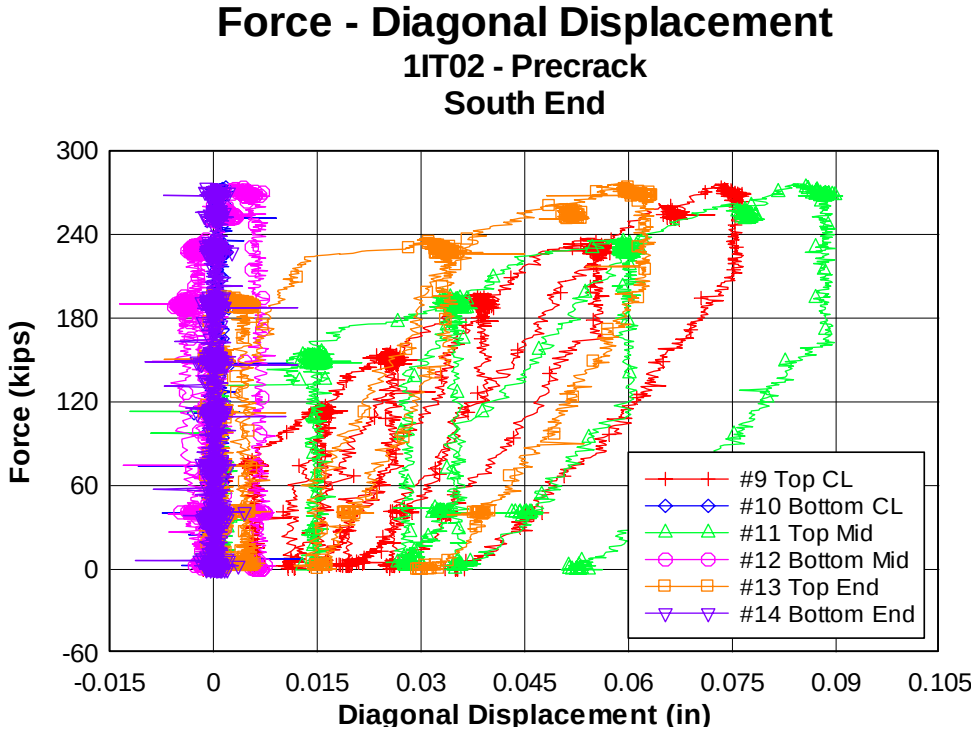
Force - Diagonal Displacement
1IT02 - Precrack
South End
Force (kips)
Diagonal Displacement (in)
300
240
180
120
60
0
-60
-0.015
0
0.015
0.03
0.045
0.06
0.075
0.09
0.105
#9 Top CL
#10 Bottom CL
#11 Top Mid
#12 Bottom Mid
#13 Top End
#14 Bottom End

Force - Stirrup Strain Precrack

1IT02 - Precrack
North End

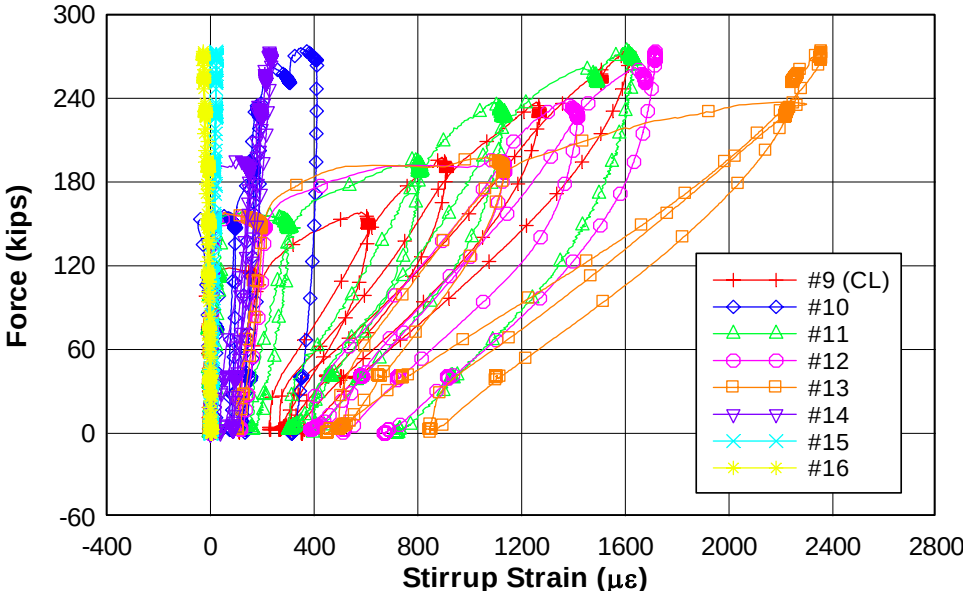

Force - Stirrup Strain

1IT02 - Precrack
South End

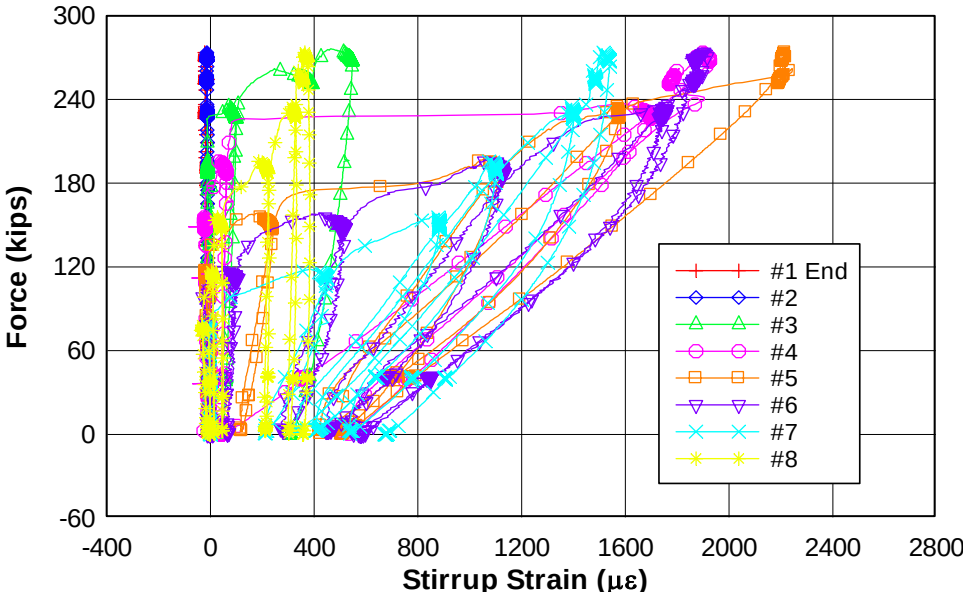

SPECIMEN 1IT02 – FAILURE LOAD PLOTS

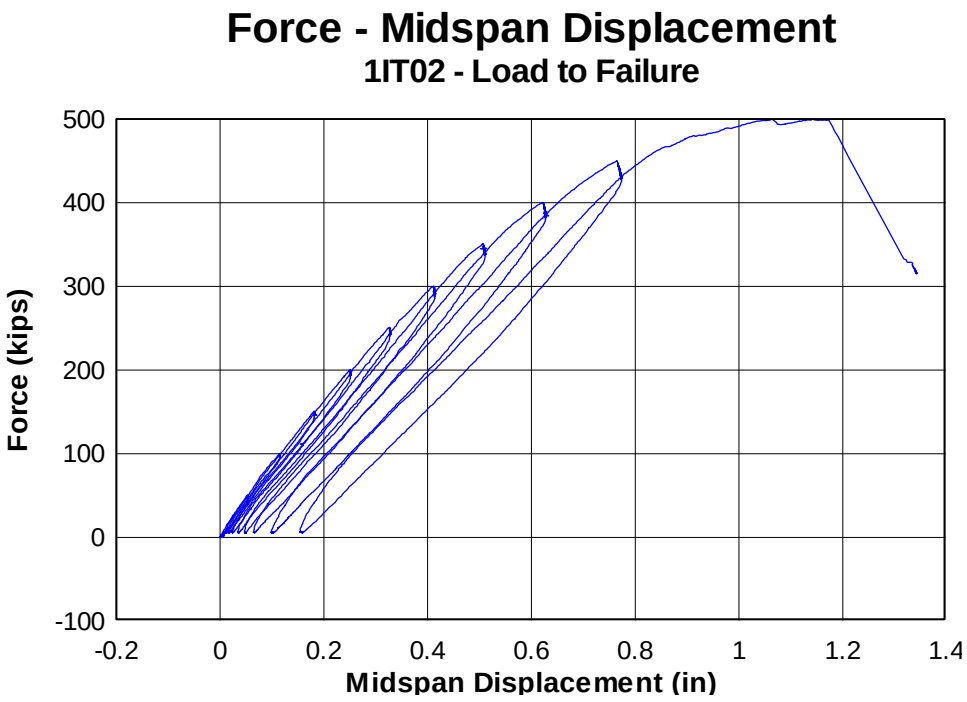
Force - Midspan Displacement
1IT02 - Load to Failure
Force (kips)
500
400
300
200
100
0
-100
-0.2
0
0.2
0.4
0.6
0.8
1
1.2
1.4
Midspan Displacement (in)

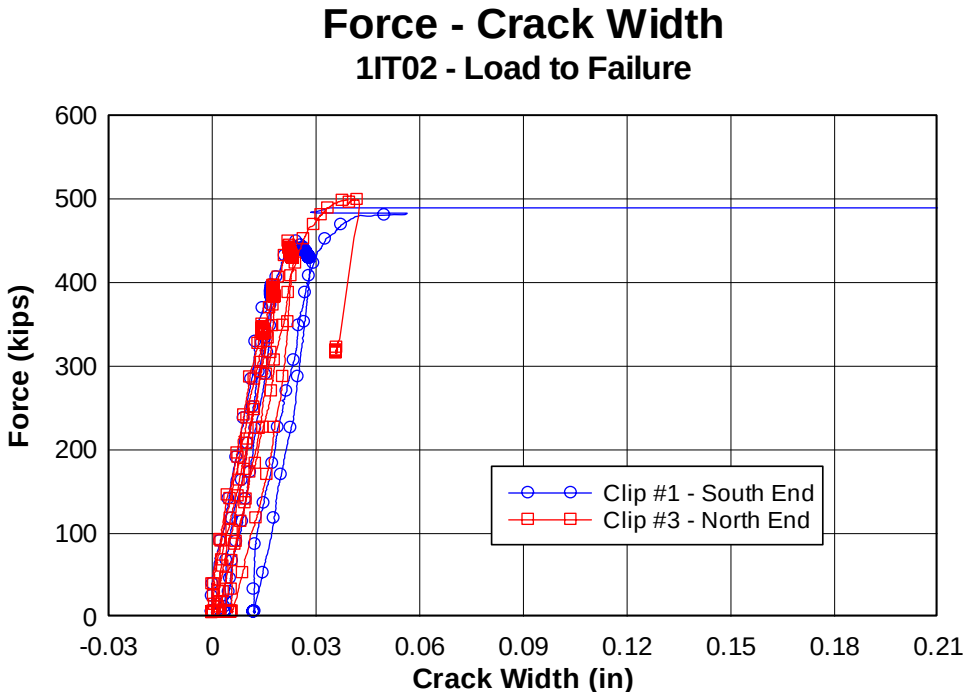
Force - Crack Width
1IT02 - Load to Failure
Force (kips)
600
500
400
300
200
100
0
-0.03
0
0.03
0.06
0.09
0.12
0.15
0.18
0.21
Crack Width (in)
Clip #1 - South End
Clip #3 - North End

Force - Flexural Reinforcement Strain

1IT02 - Load to Failure
Detail Locations

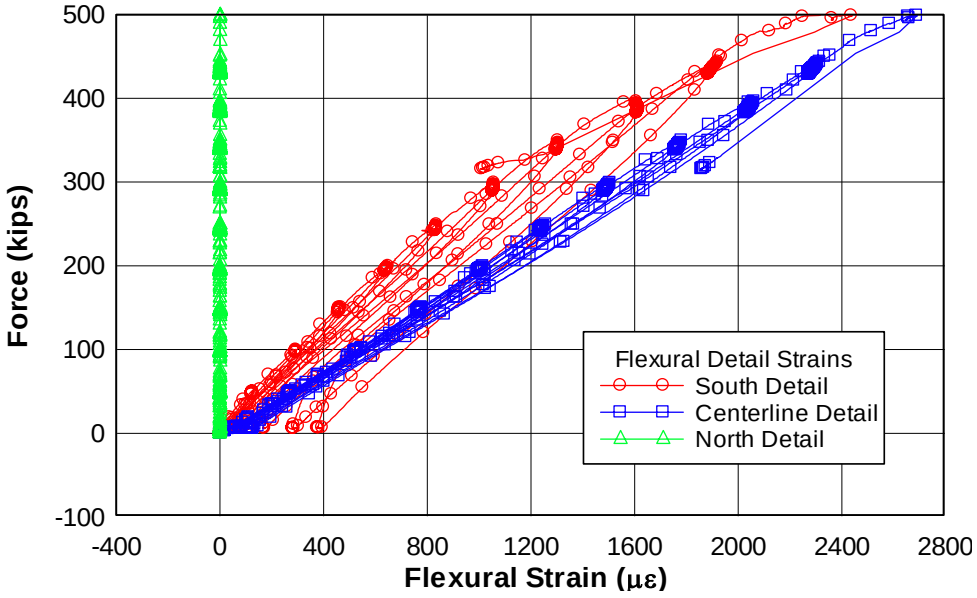

Force - Diagonal Displacement

1IT02 - Load to Failure
North End

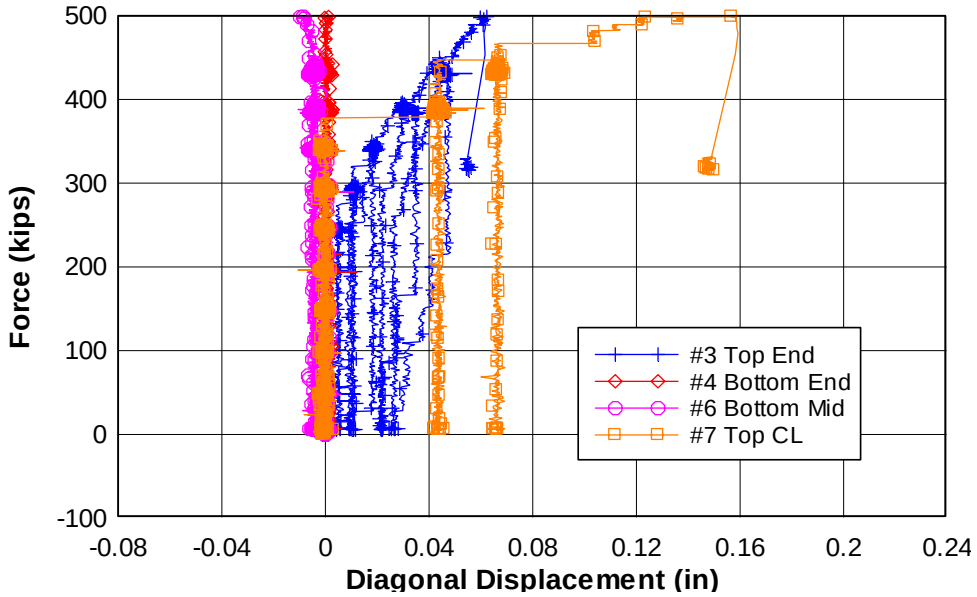

Force - Diagonal Displacement
1IT02 - Load to Failure
South End

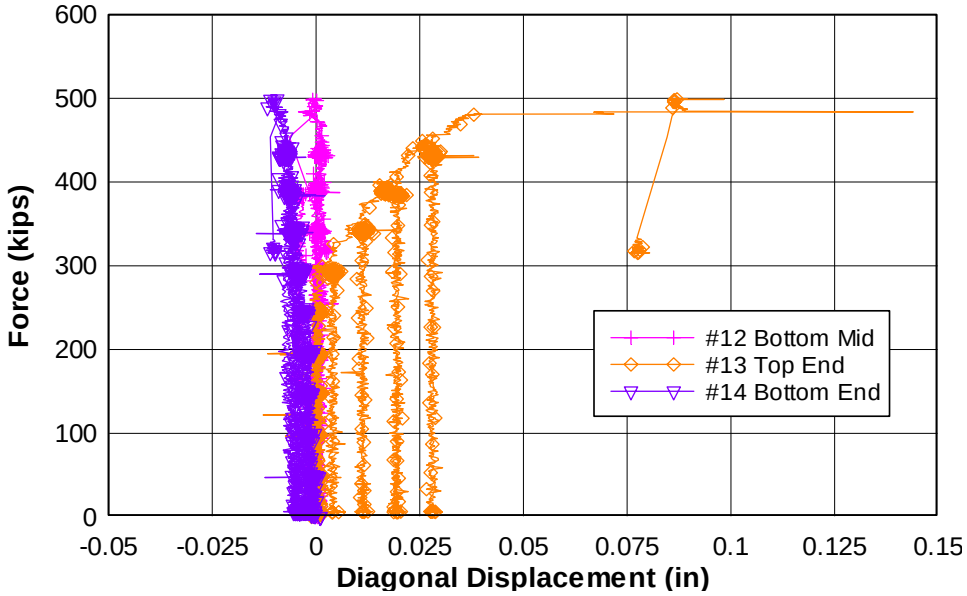

Force - Stirrup Strain
1IT02 - Load to Failure
North End

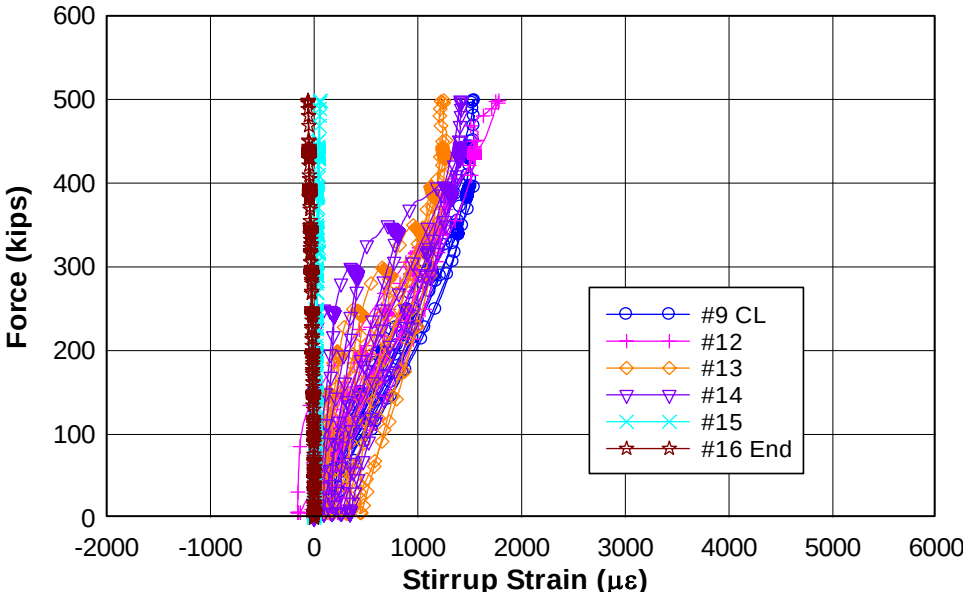

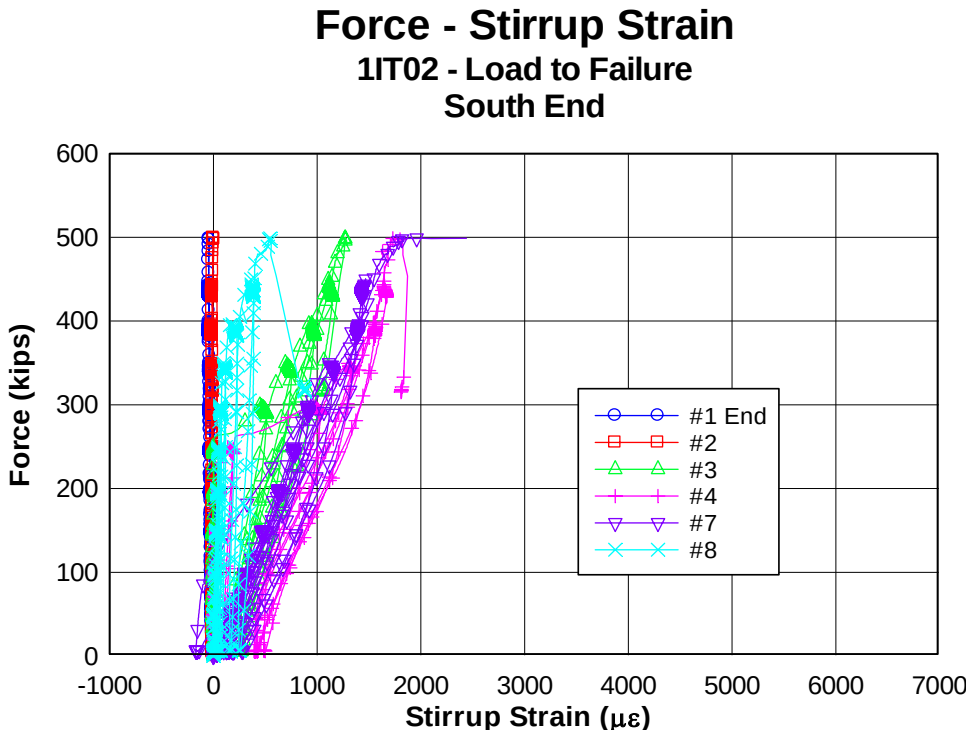
Force - Stirrup Strain
1IT02 - Load to Failure
South End
Force (kips)
Stirrup Strain (με)
600
500
400
300
200
100
0
-1000
0
1000
2000
3000
4000
5000
6000
7000
#1 End
#2
#3
#4
#7
#8

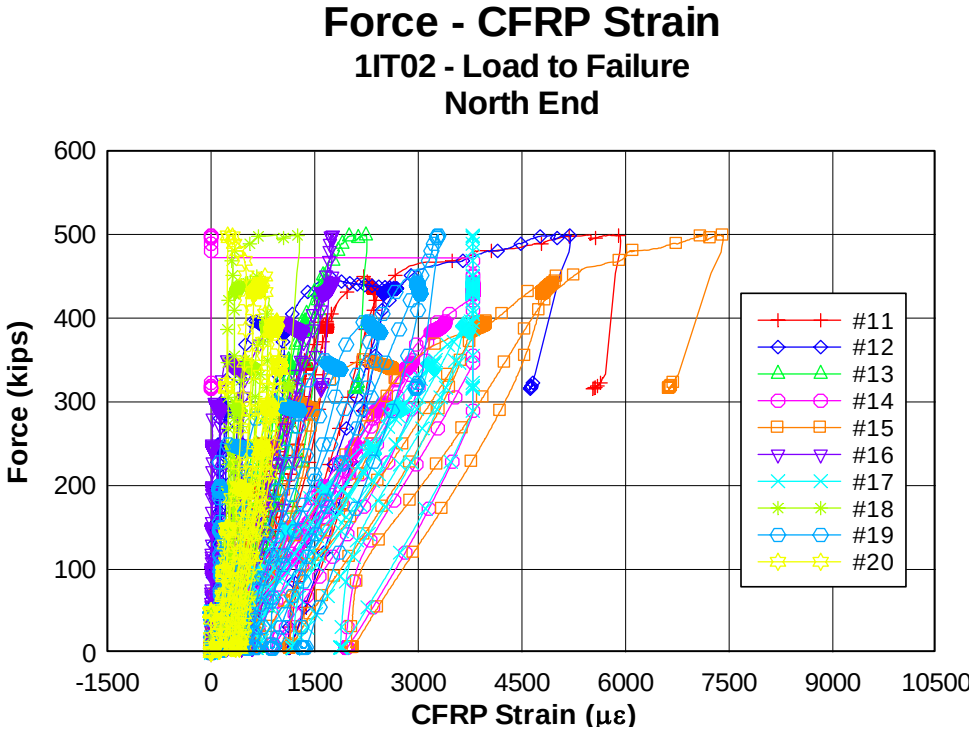
Force - CFRP Strain
1IT02 - Load to Failure
North End
Force (kips)
CFRP Strain (με)
600
500
400
300
200
100
0
-1500
0
1500
3000
4500
6000
7500
9000
10500
#11
#12
#13
#14
#15
#16
#17
#18
#19
#20

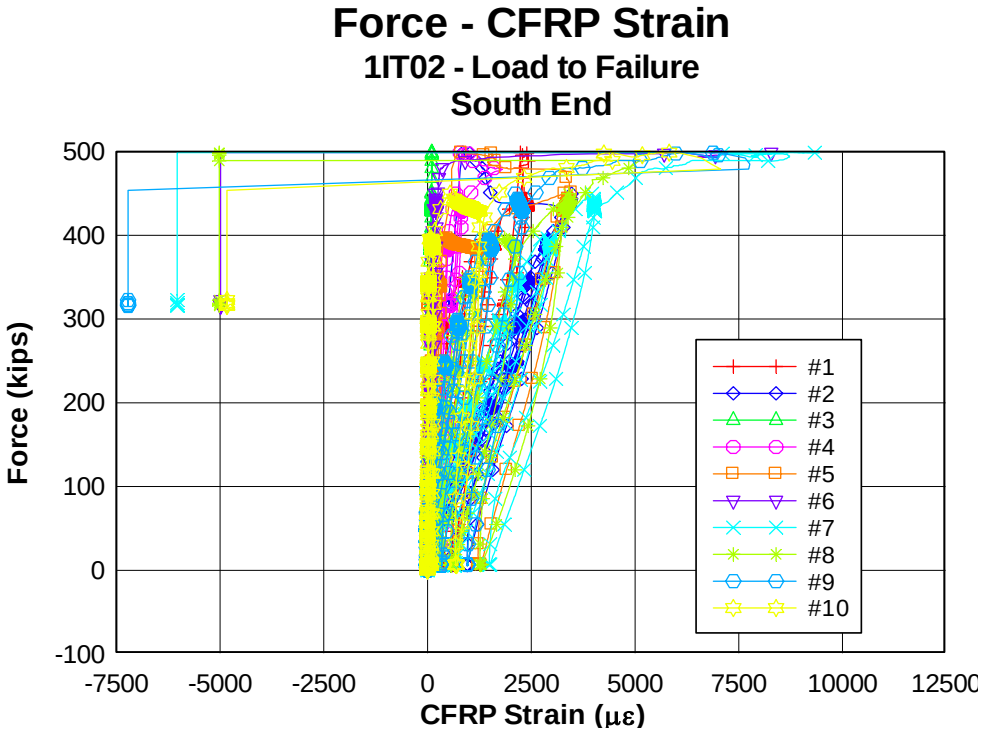
Force - CFRP Strain
1IT02 - Load to Failure
South End
Force (kips)
500
400
300
200
100
0
-100
-7500
-5000
-2500
0
2500
5000
7500
10000
12500
CFRP Strain (με)
#1
#2
#3
#4
#5
#6
#7
#8
#9
#10

CAST 2 – SPECIMEN 2T03

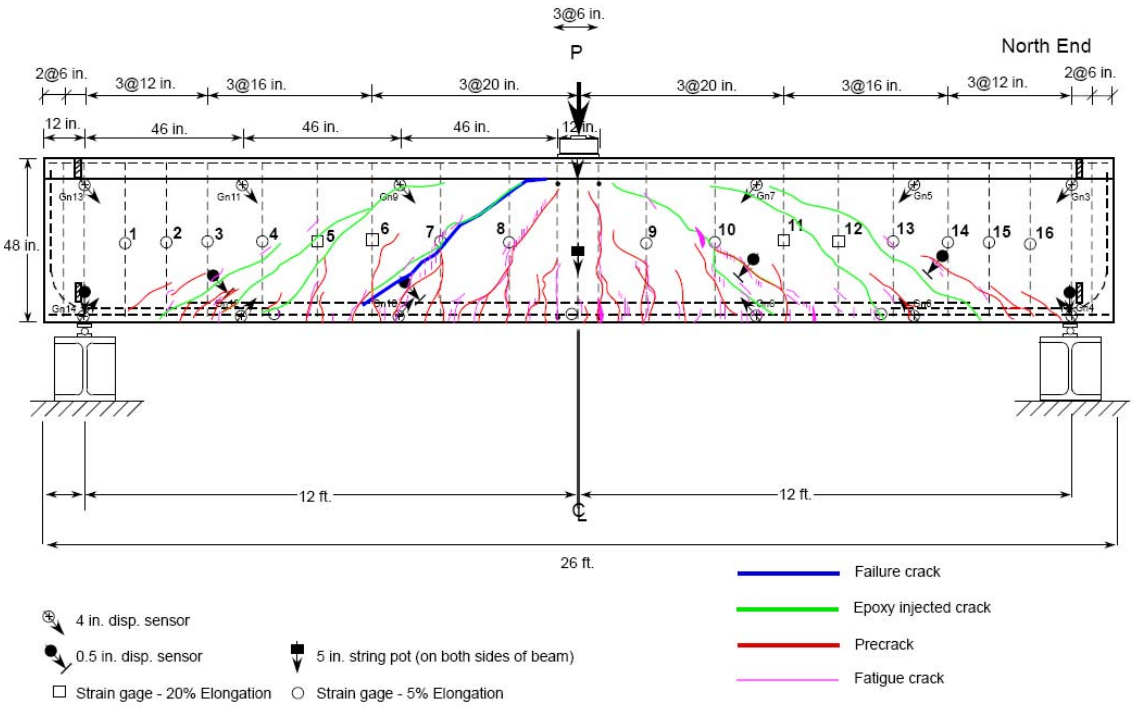

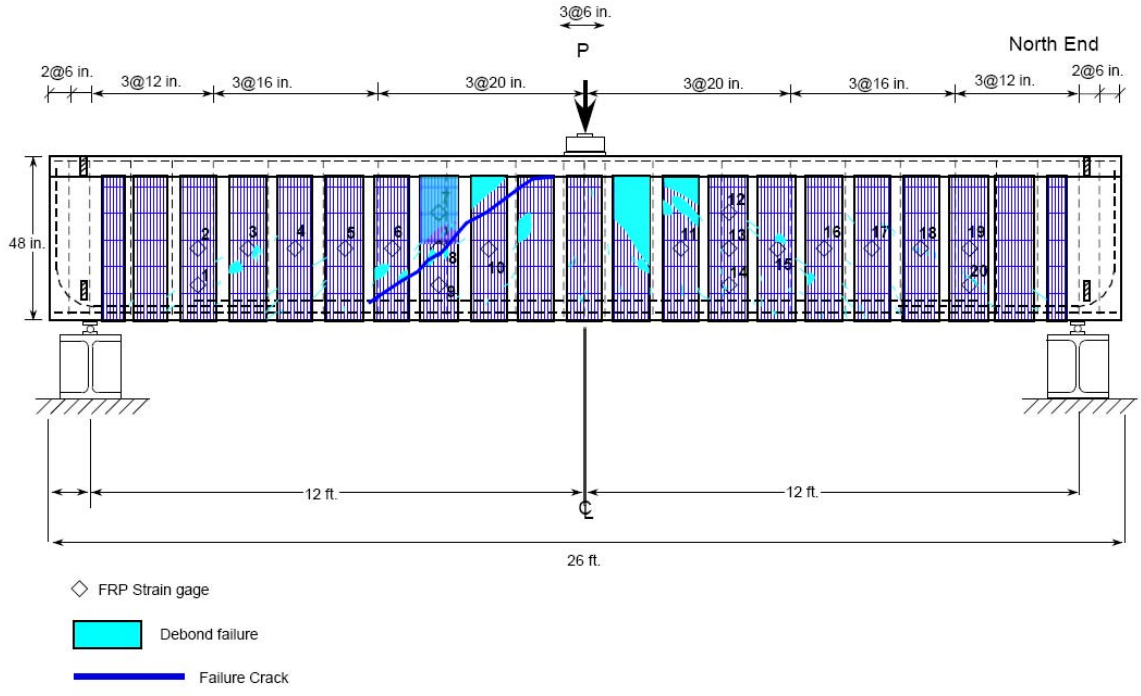

Cast 2 - Specimen 3
Positive Bending (T-Beam)
East Face of Specimen

SPECIMEN 2T03 – PRECRACK LOAD PLOTS

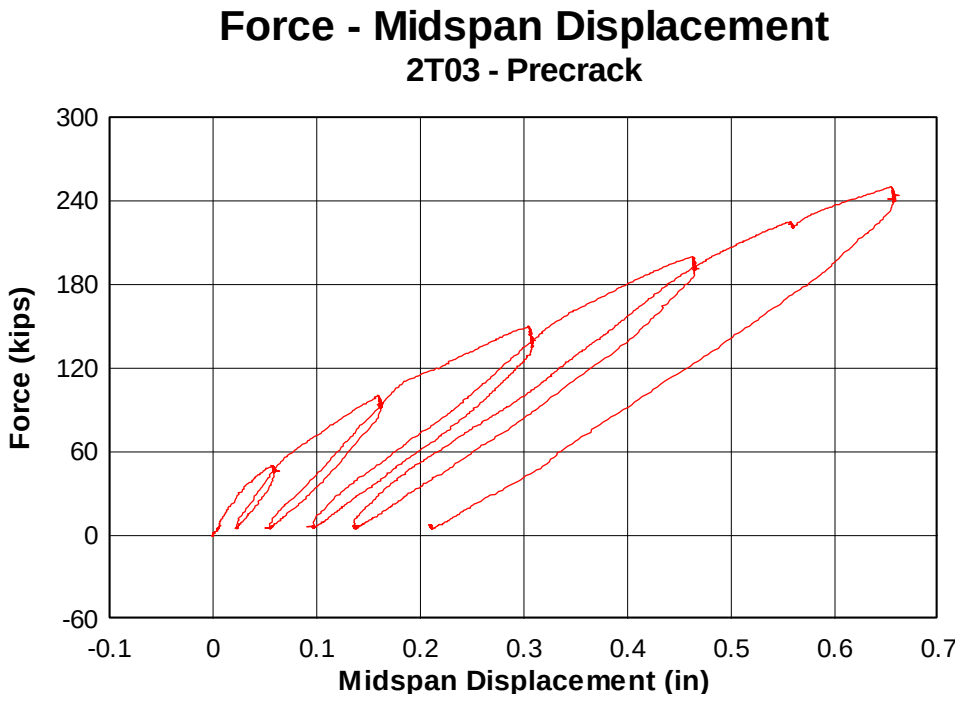
Force - Midspan Displacement
2T03 - Precrack
Force (kips)
300
240
180
120
60
0
-60
-0.1
0
0.1
0.2
0.3
0.4
0.5
0.6
0.7
Midspan Displacement (in)

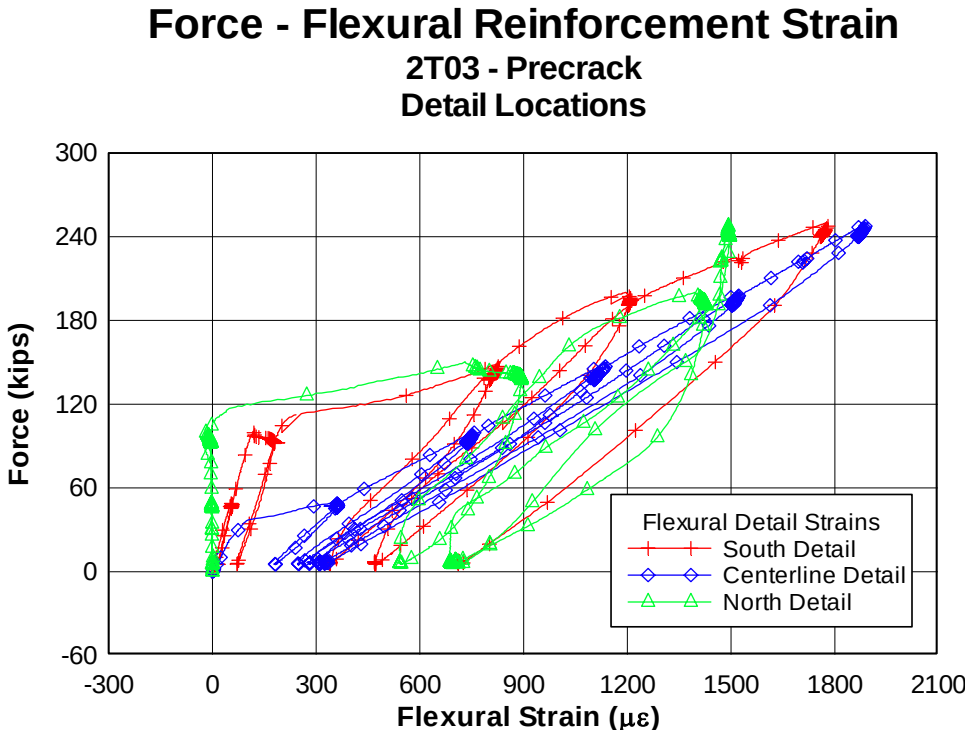
Force - Flexural Reinforcement Strain
2T03 - Precrack
Detail Locations
Force (kips)
300
240
180
120
60
0
-60
-300
0
300
600
900
1200
1500
1800
2100
Flexural Strain (με)
Flexural Detail Strains
South Detail
Centerline Detail
North Detail

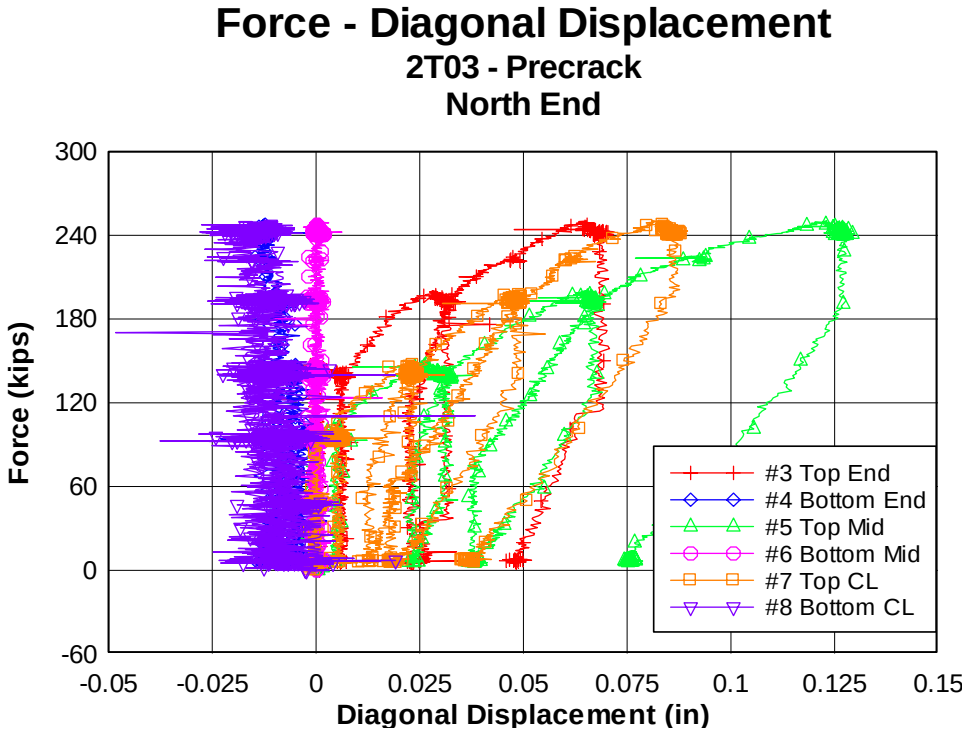
Force - Diagonal Displacement
2T03 - Precrack
North End
Force (kips)
Diagonal Displacement (in)
300
240
180
120
60
0
-60
-0.05
-0.025
0
0.025
0.05
0.075
0.1
0.125
0.15
#3 Top End
#4 Bottom End
#5 Top Mid
#6 Bottom Mid
#7 Top CL
#8 Bottom CL

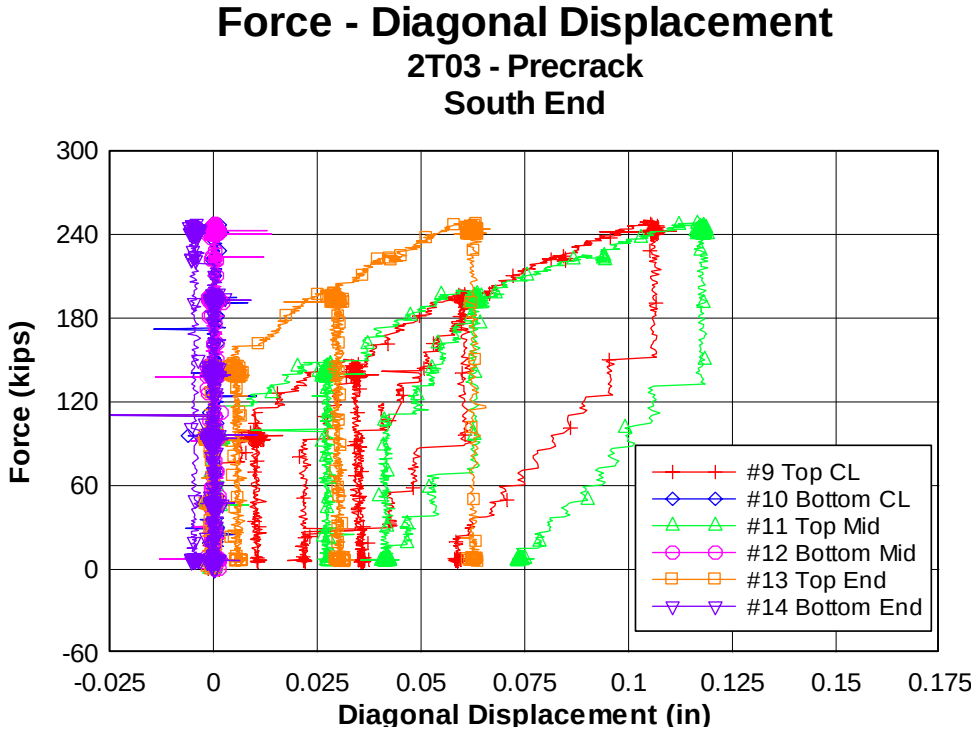
Force - Diagonal Displacement
2T03 - Precrack
South End
Force (kips)
Diagonal Displacement (in)
300
240
180
120
60
0
-60
-0.025
0
0.025
0.05
0.075
0.1
0.125
0.15
0.175
#9 Top CL
#10 Bottom CL
#11 Top Mid
#12 Bottom Mid
#13 Top End
#14 Bottom End

Force - Stirrup Strain
2T03 - Precrack
North End

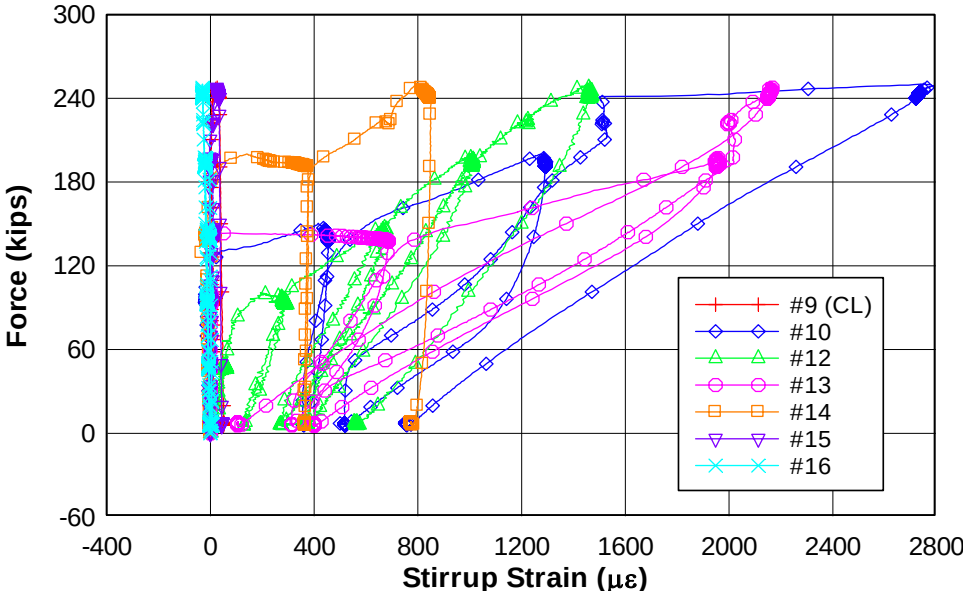

Force - Stirrup Strain
2T03 - Precrack
South End

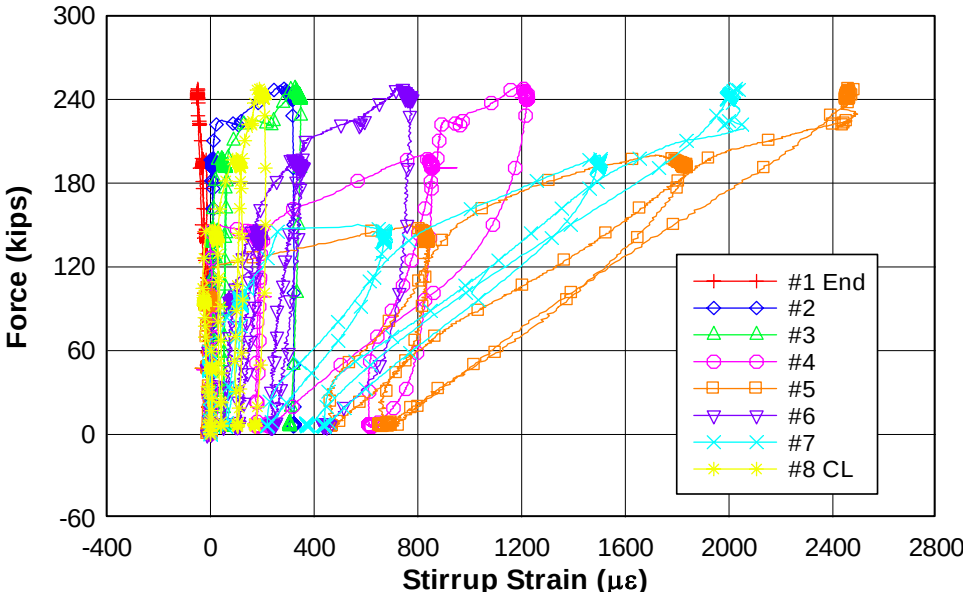

SPECIMEN 2T03 – FAILURE LOAD PLOTS

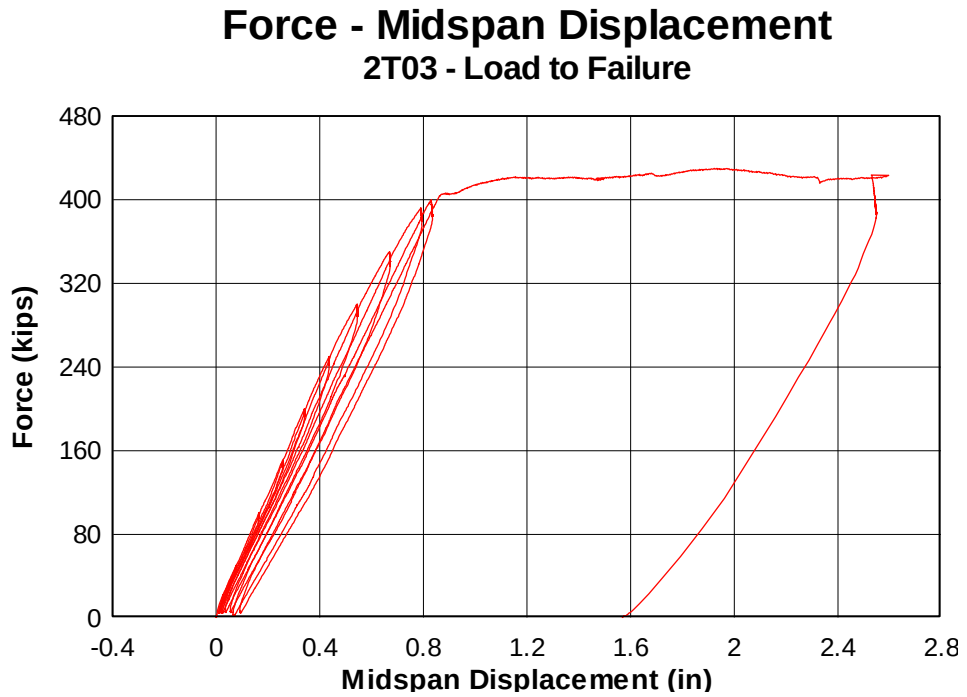
Force - Midspan Displacement
2T03 - Load to Failure
Force (kips)
480
400
320
240
160
80
0
-0.4
0
0.4
0.8
1.2
1.6
2
2.4
2.8
Midspan Displacement (in)

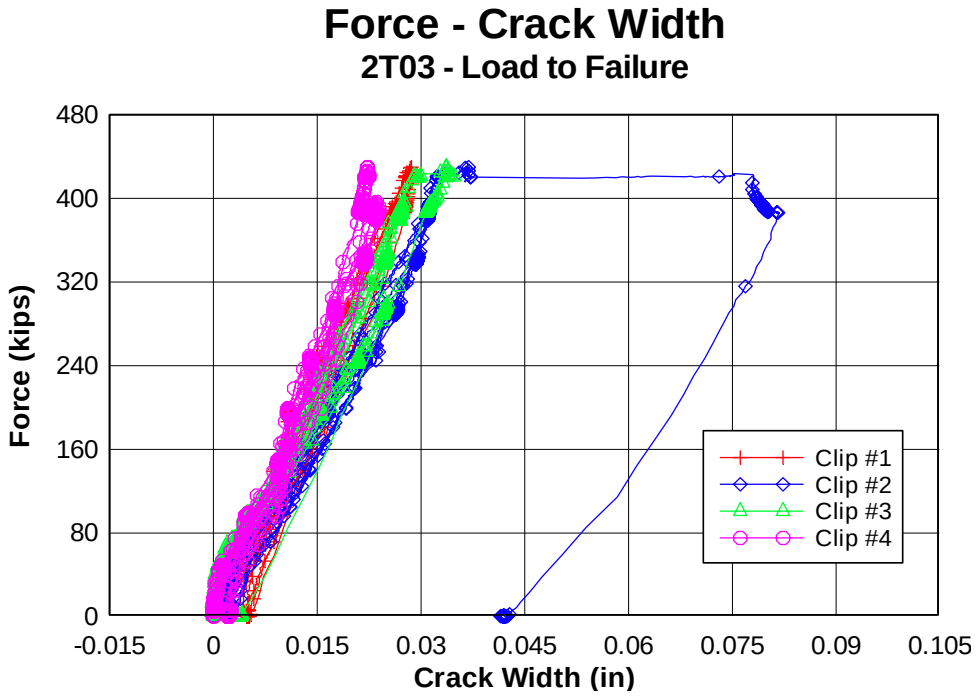
Force - Crack Width
2T03 - Load to Failure
Force (kips)
480
400
320
240
160
80
0
-0.015
0
0.015
0.03
0.045
0.06
0.075
0.09
0.105
Crack Width (in)
Clip #1
Clip #2
Clip #3
Clip #4

Force - Flexural Reinforcement Strain
2T03 - Load to Failure
Detail Locations

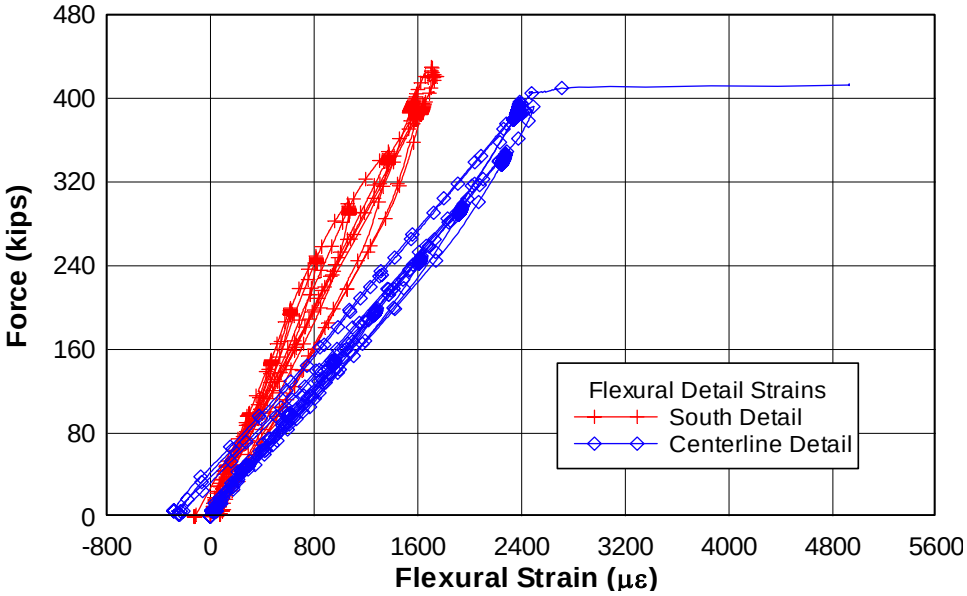

Force - Diagonal Displacement
2T03 - Load to Failure
North End

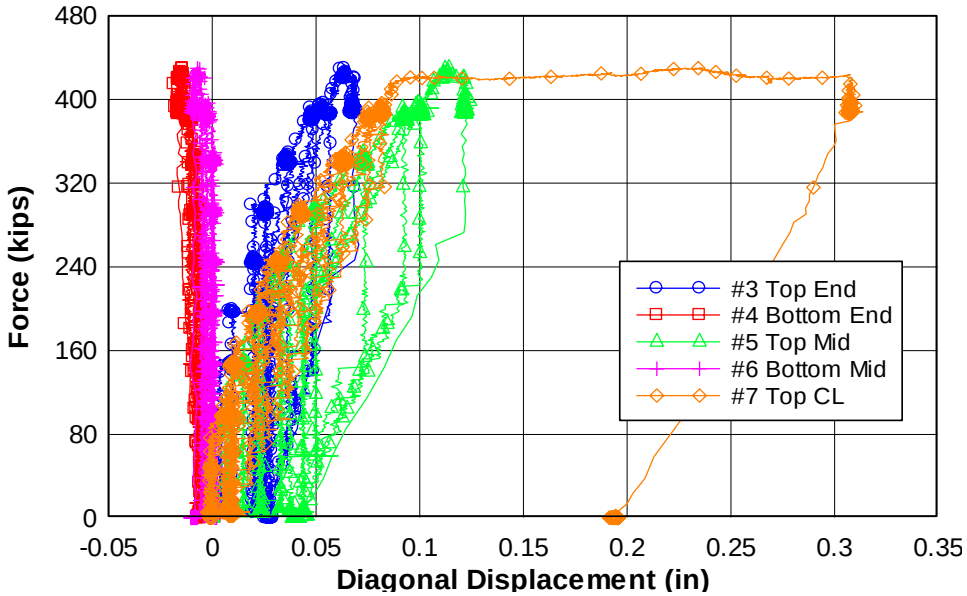

Force - Diagonal Displacement
2T03 - Load to Failure
South End

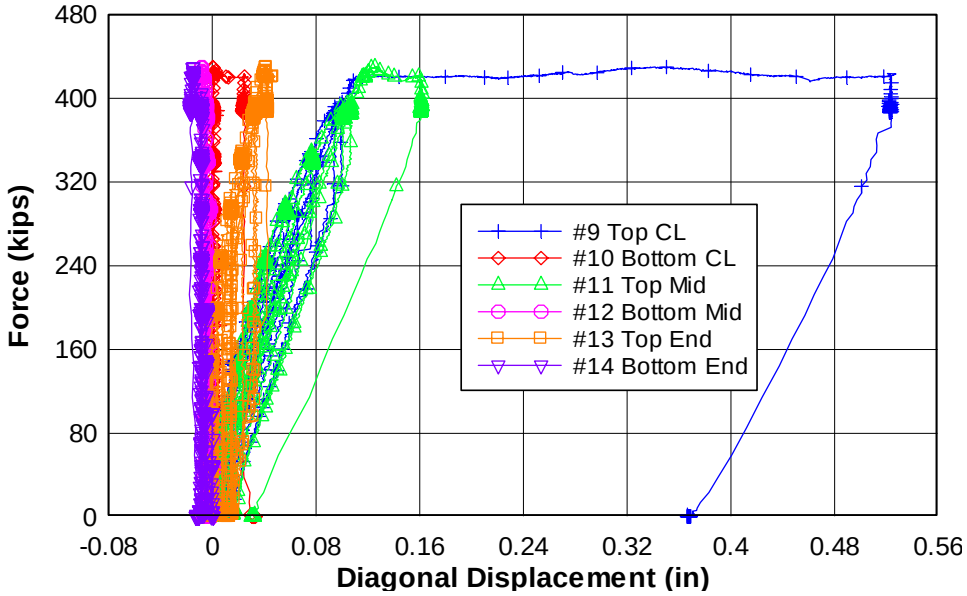

Force - Stirrup Strain
2T03 - Load to Failure
North End

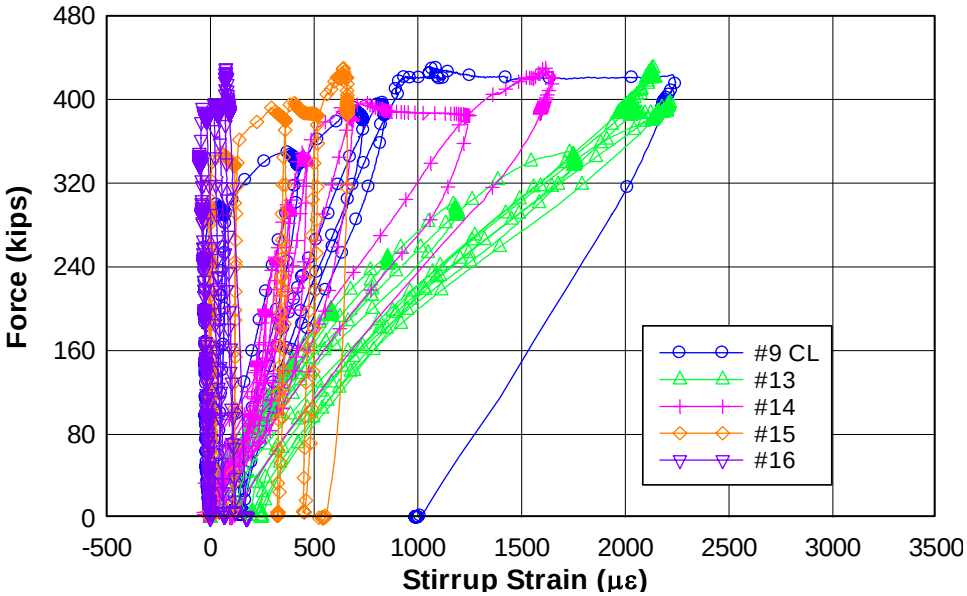

Force - Stirrup Strain
2T03 - Load to Failure
South End

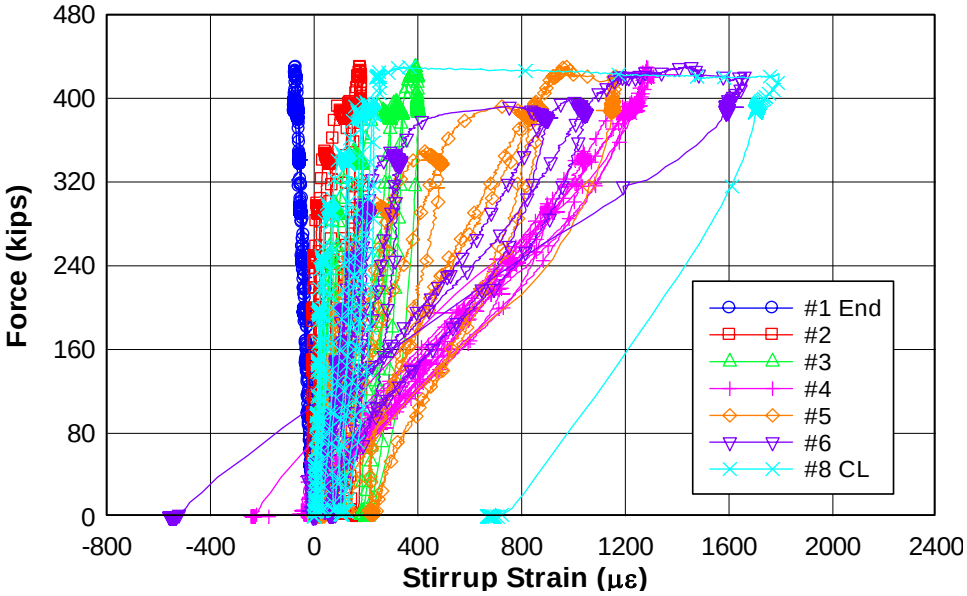

Force - CFRP Strain
2T03 - Load to Failure
North End

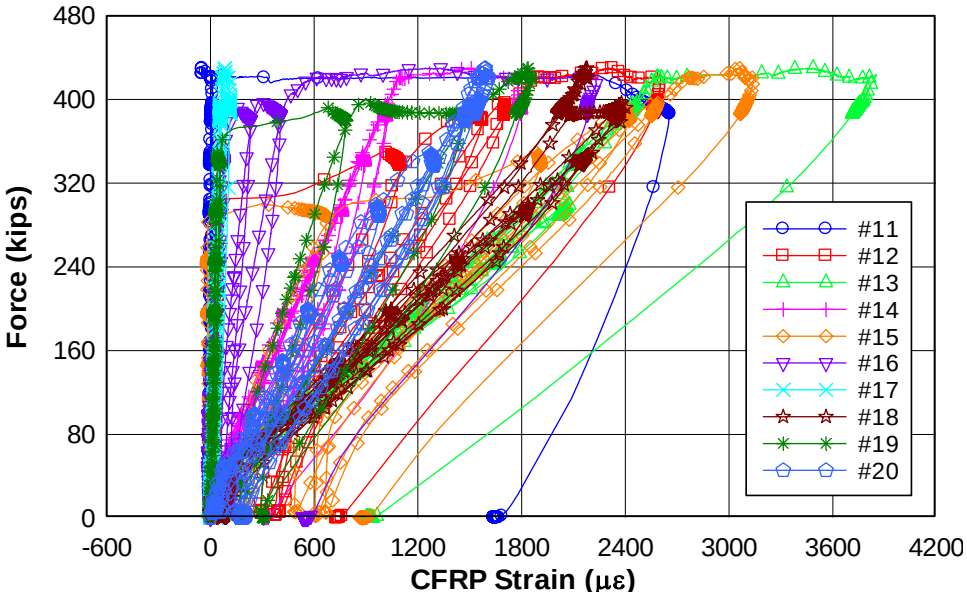

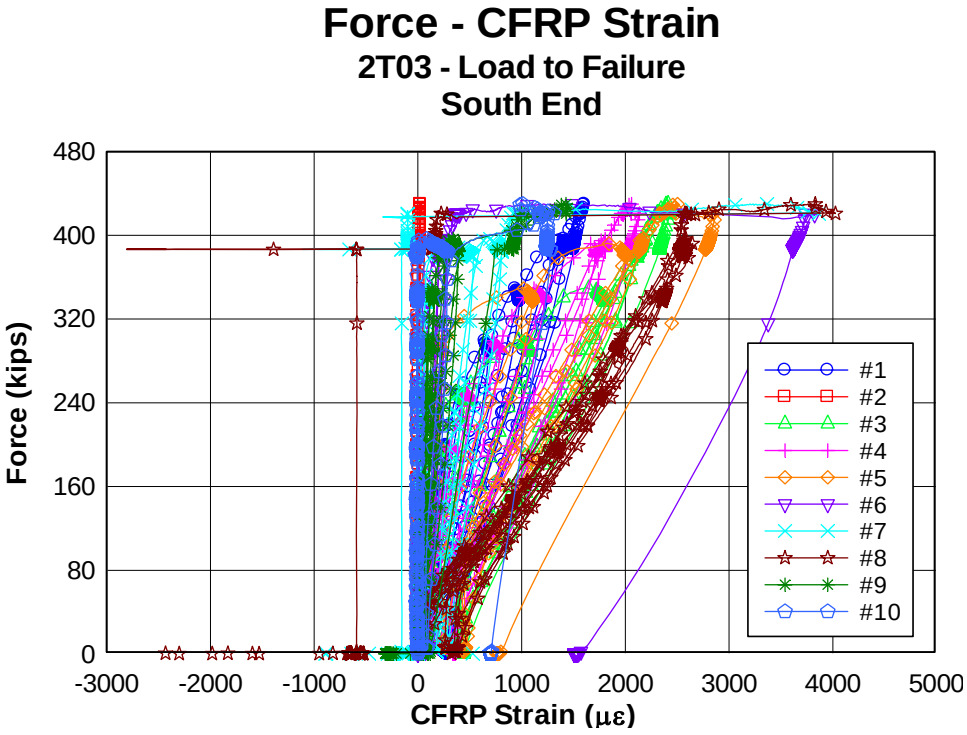
Force - CFRP Strain
2T03 - Load to Failure
South End
Force (kips)
480
400
320
240
160
80
0
-3000
-2000
-1000
0
1000
2000
3000
4000
5000
CFRP Strain (με)
#1
#2
#3
#4
#5
#6
#7
#8
#9
#10

SPECIMEN 2T03 – FATIGUE LOAD PLOTS

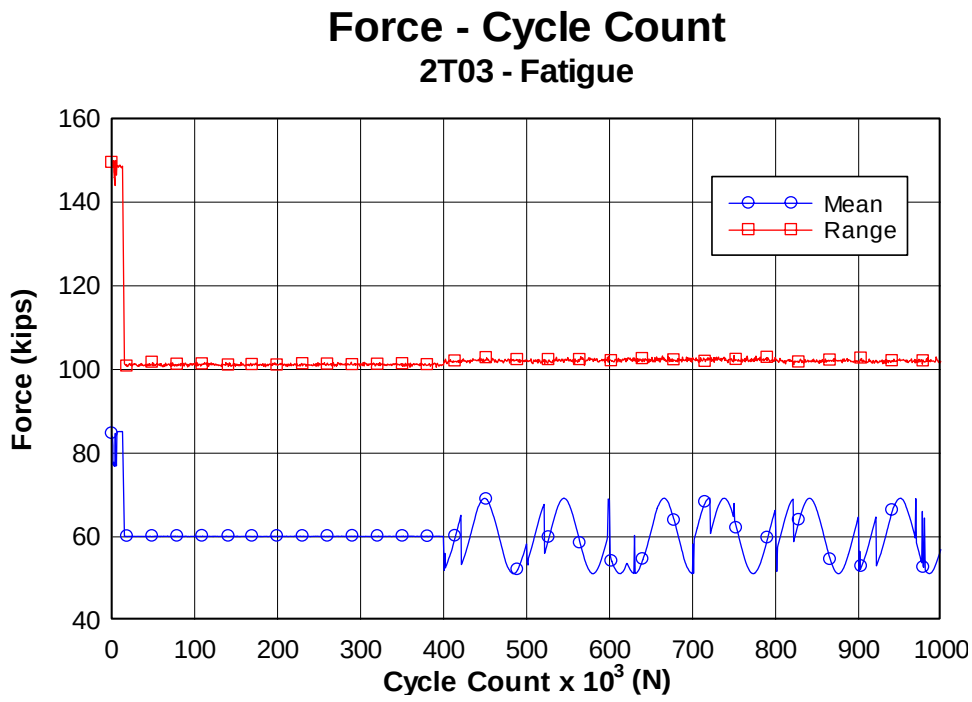
Force - Cycle Count
2T03 - Fatigue
Force (kips)
160
140
120
100
80
60
40
0
100
200
300
400
500
600
700
800
900
1000
Cycle Count x 10^3 (N)
Mean
Range

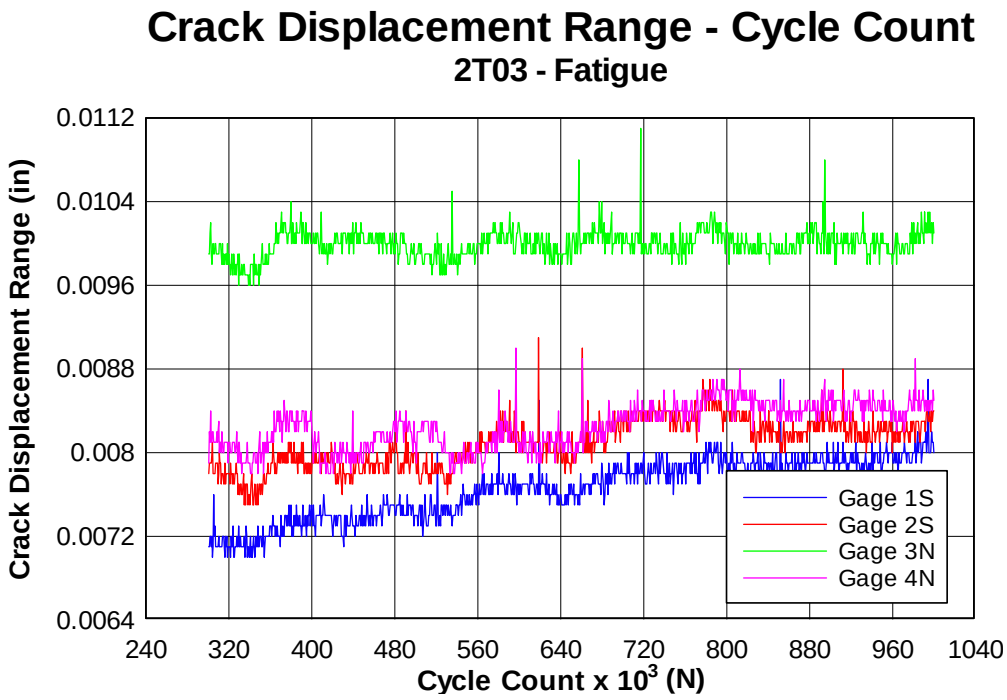
Crack Displacement Range - Cycle Count
2T03 - Fatigue
Crack Displacement Range (in)
0.0112
0.0104
0.0096
0.0088
0.008
0.0072
0.0064
240
320
400
480
560
640
720
800
880
960
1040
Cycle Count x 10^3 (N)
Gage 1S
Gage 2S
Gage 3N
Gage 4N

Flexural Strain Range - Cycle Count
2T03 - Fatigue
Detail Locations

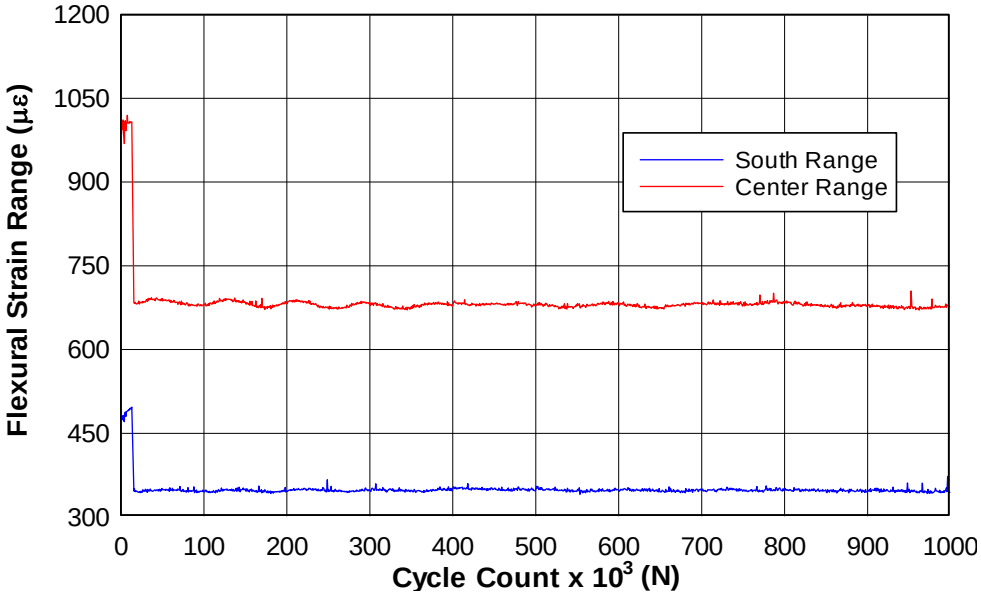

Stirrup Strain Range - Cycle Count
2T03 - Fatigue
North End

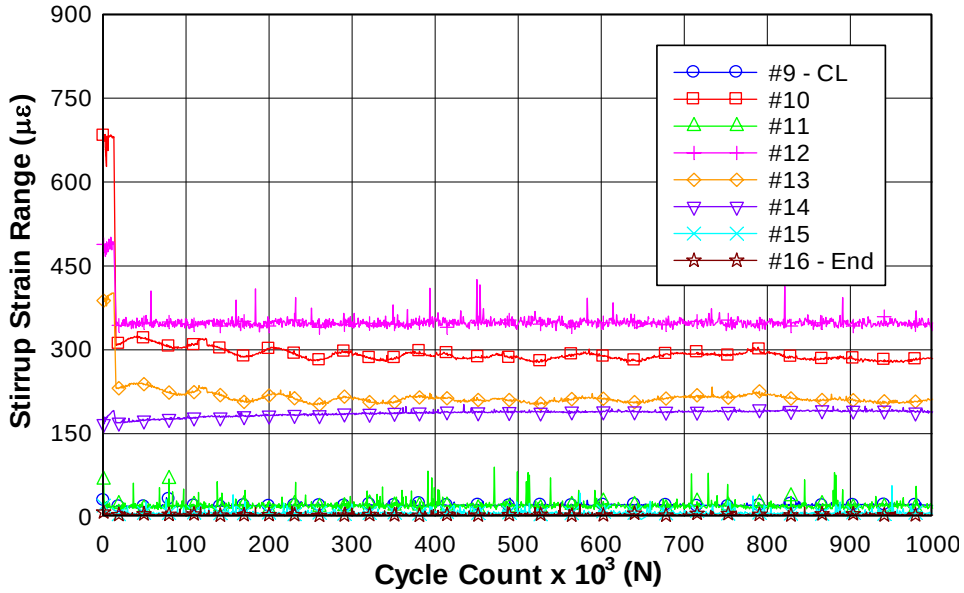

Stirrup Strain Range - Cycle Count
2T03 - Fatigue
South End

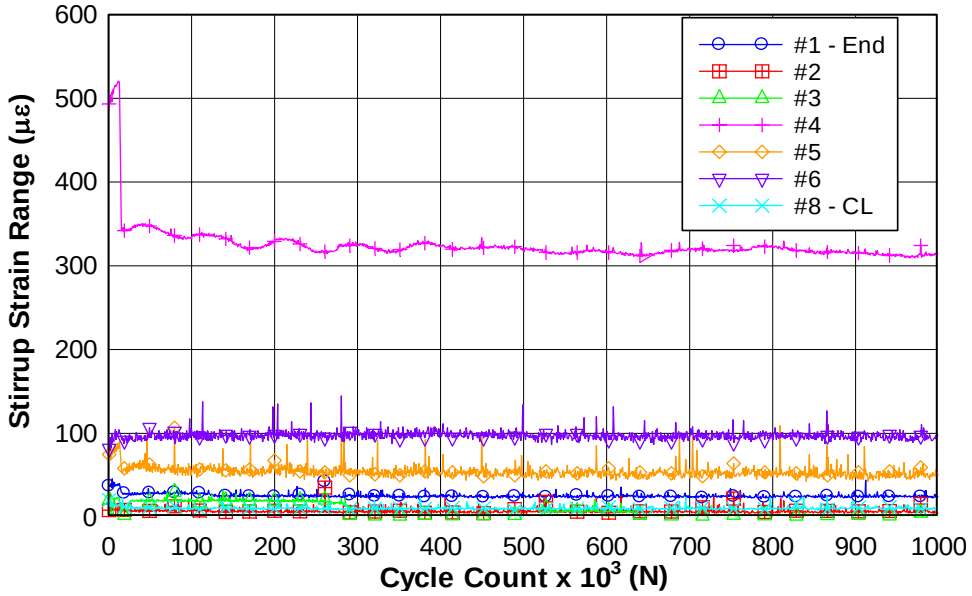

CFRP Strain Range - Cycle Count
2T03 - Fatigue
North End

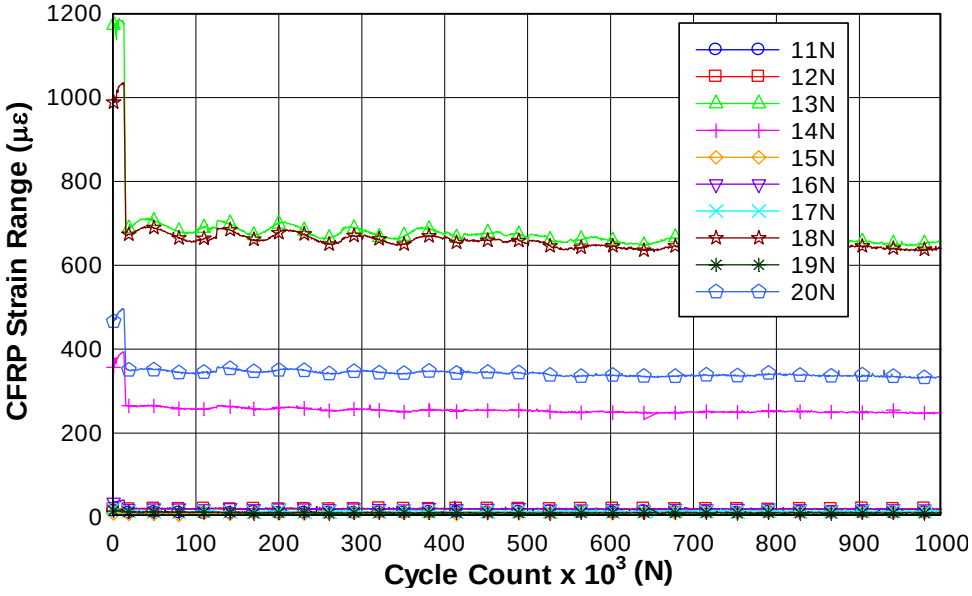

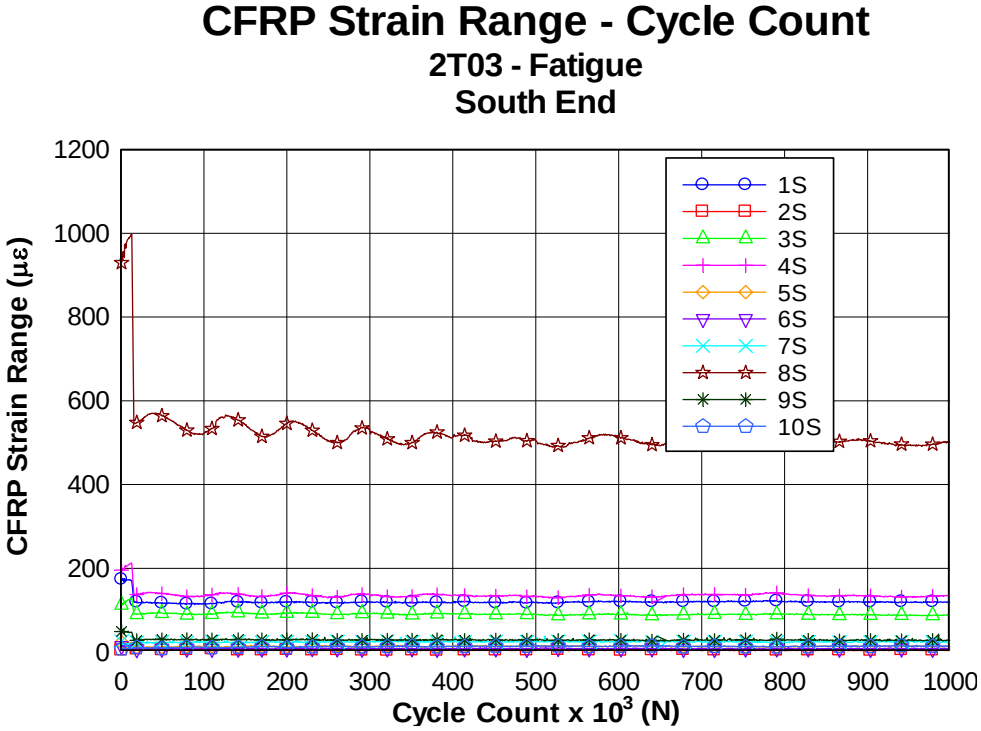
CFRP Strain Range - Cycle Count
2T03 - Fatigue
South End
CFRP Strain Range (με)
Cycle Count x 10^3 (N)
1S
2S
3S
4S
5S
6S
7S
8S
9S
10S
0
200
400
600
800
1000
1200
0
100
200
300
400
500
600
700
800
900
1000

CAST 2 – SPECIMEN 2T04

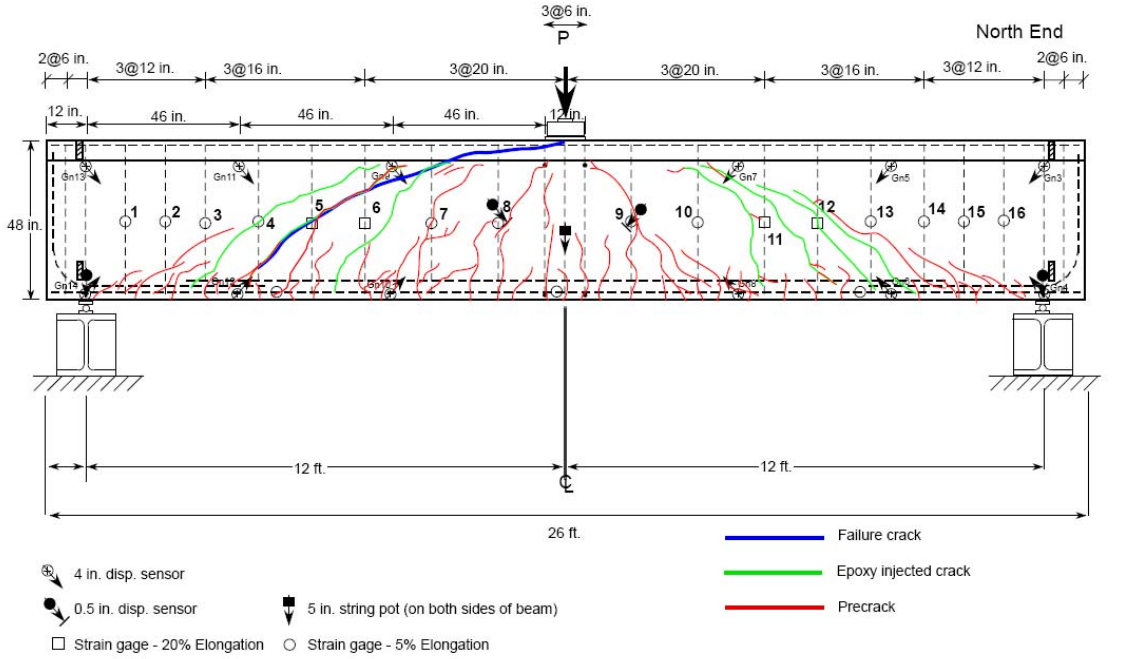

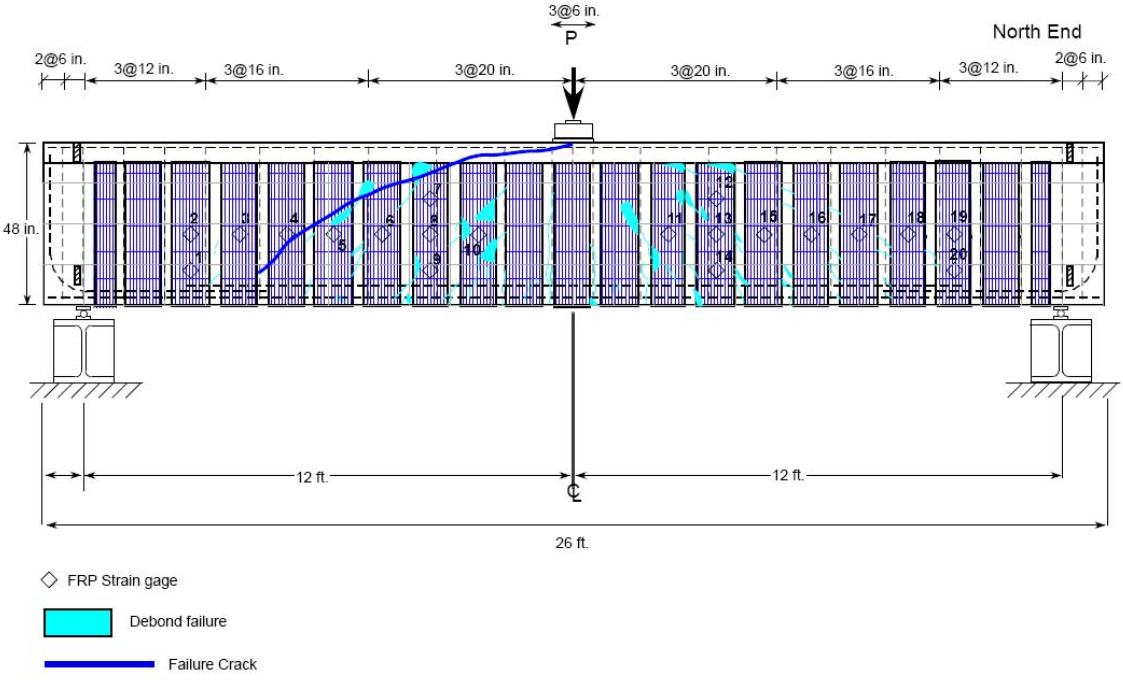

Cast 2 - Specimen 4
Positive Bending (T-Beam)
East Face of Specimen

SPECIMEN 2T04 – PRECRACK LOAD PLOTS

Force - Midspan Displacement
2T04 - Precrack

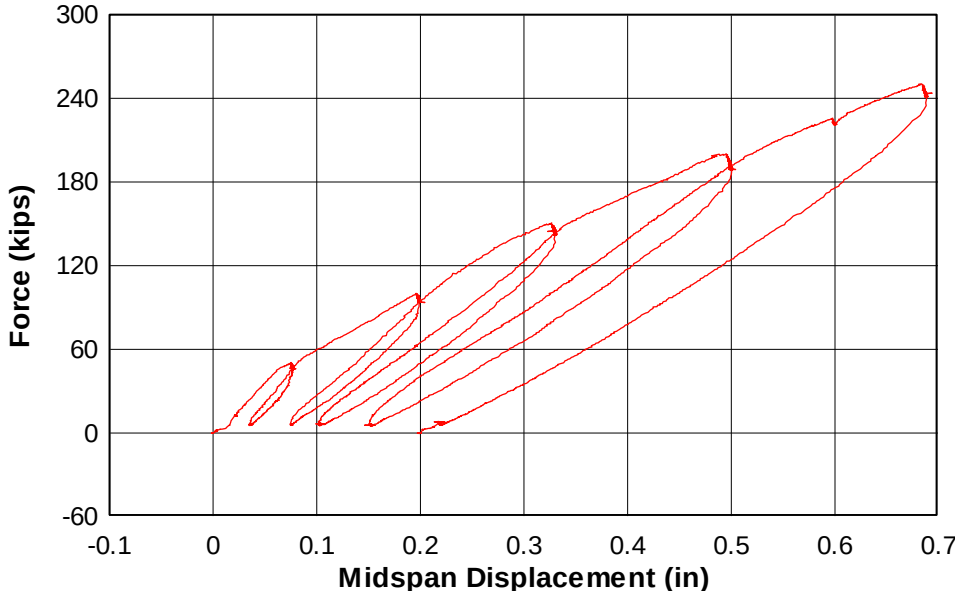

Force - Flexural Reinforcement Strain
2T04 - Precrack
Detail Locations

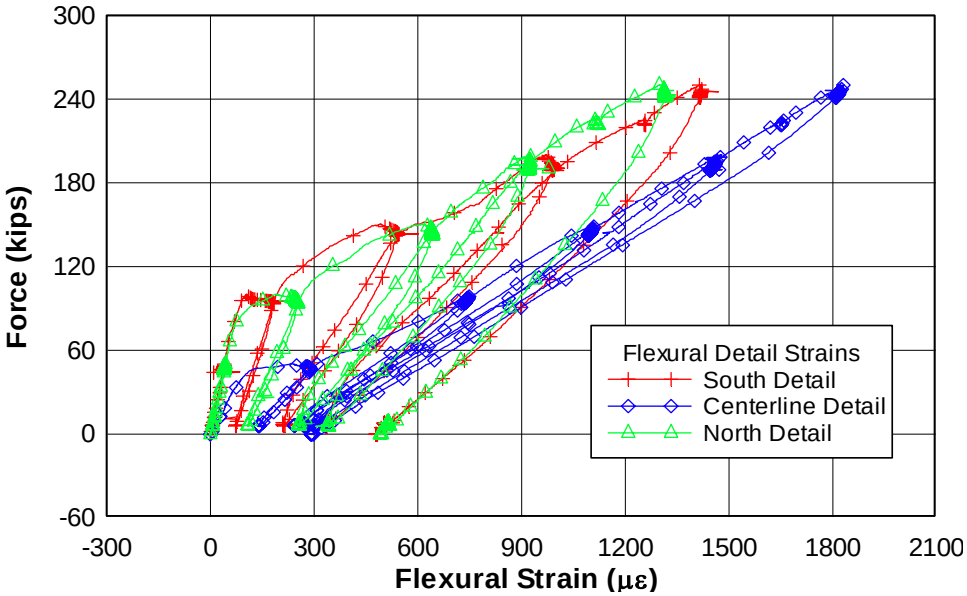

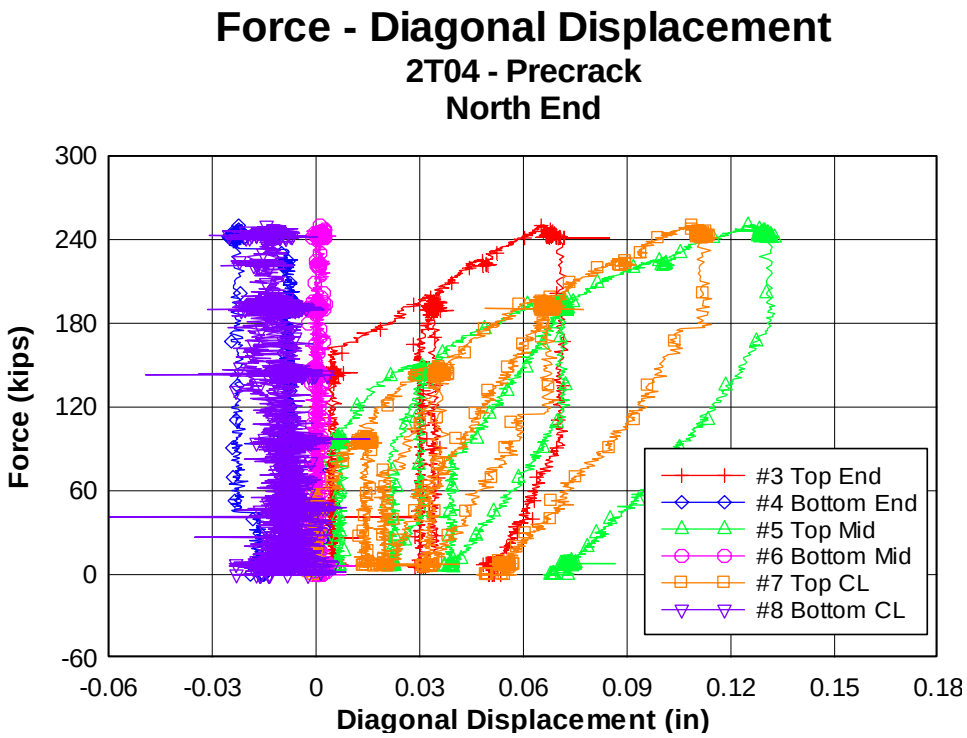
Force - Diagonal Displacement
2T04 - Precrack
North End
Force (kips)
Diagonal Displacement (in)
300
240
180
120
60
0
-60
-0.06
-0.03
0
0.03
0.06
0.09
0.12
0.15
0.18
#3 Top End
#4 Bottom End
#5 Top Mid
#6 Bottom Mid
#7 Top CL
#8 Bottom CL

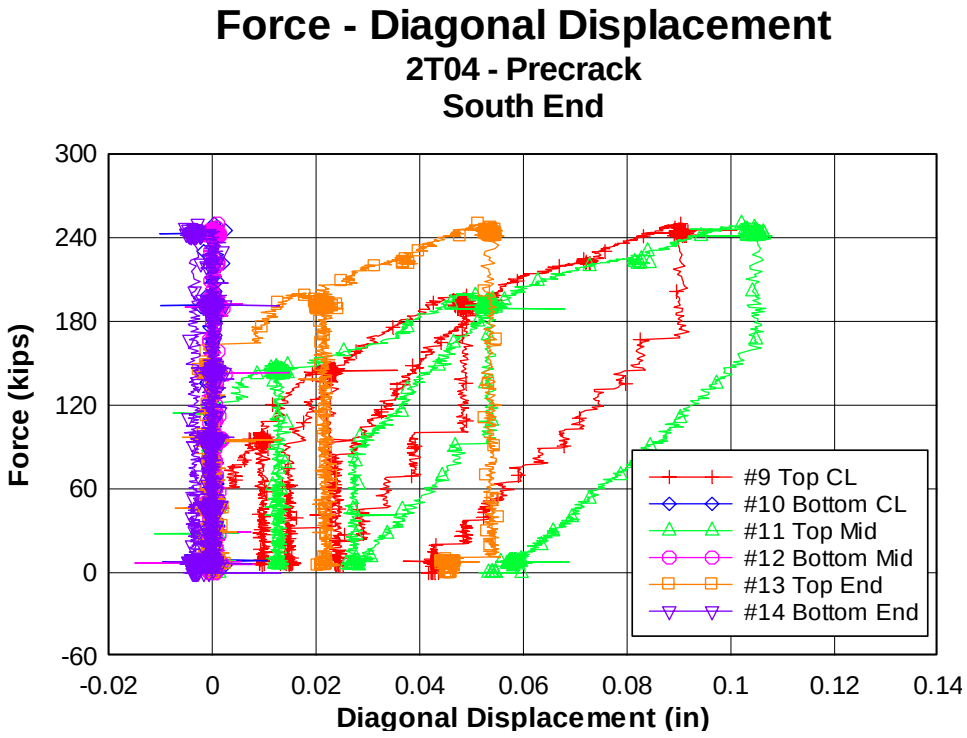
Force - Diagonal Displacement
2T04 - Precrack
South End
Force (kips)
Diagonal Displacement (in)
300
240
180
120
60
0
-60
-0.02
0
0.02
0.04
0.06
0.08
0.1
0.12
0.14
#9 Top CL
#10 Bottom CL
#11 Top Mid
#12 Bottom Mid
#13 Top End
#14 Bottom End

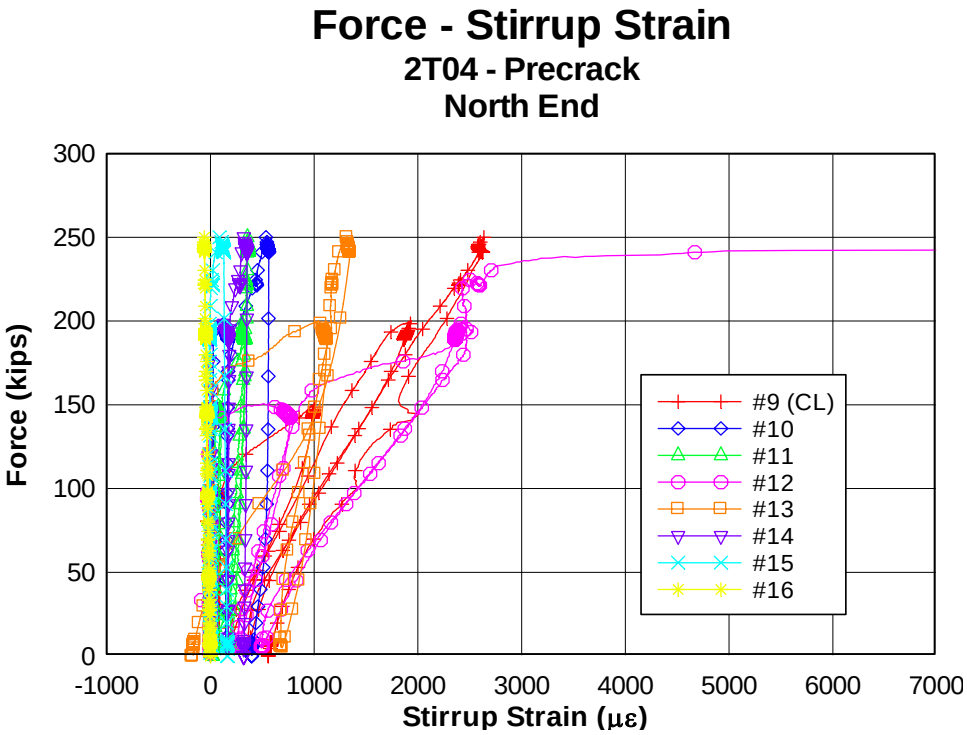
Force - Stirrup Strain
2T04 - Precrack
North End
Force (kips)
Stirrup Strain (με)
300
250
200
150
100
50
0
-1000
0
1000
2000
3000
4000
5000
6000
7000
#9 (CL)
#10
#11
#12
#13
#14
#15
#16

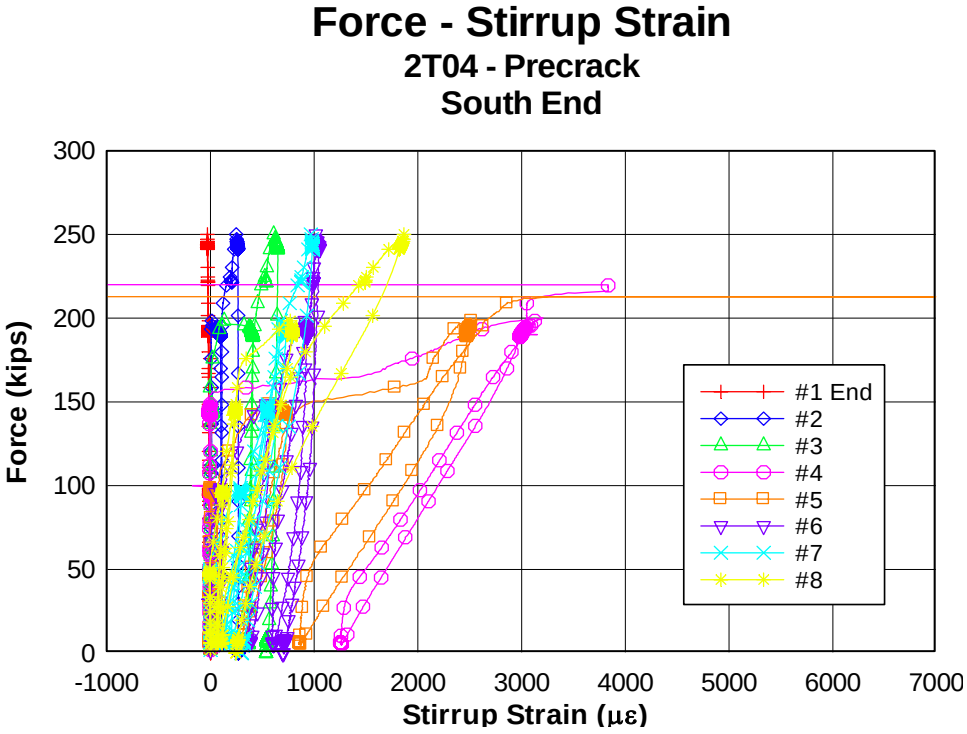
Force - Stirrup Strain
2T04 - Precrack
South End
Force (kips)
Stirrup Strain (με)
300
250
200
150
100
50
0
-1000
0
1000
2000
3000
4000
5000
6000
7000
#1 End
#2
#3
#4
#5
#6
#7
#8

SPECIMEN 2T04 – FAILURE LOAD PLOTS

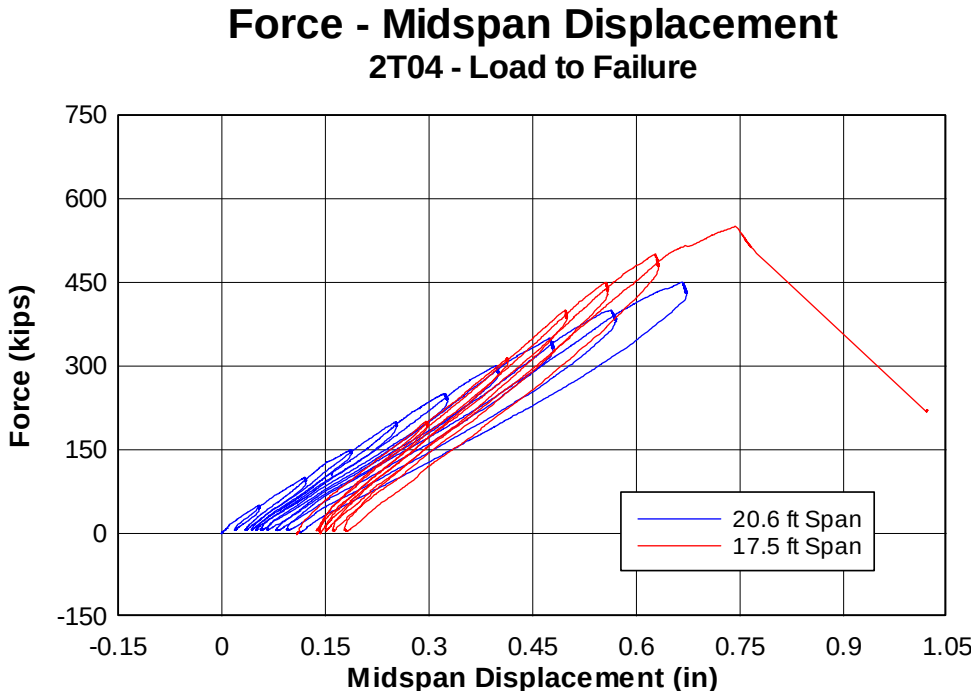
Force - Midspan Displacement
2T04 - Load to Failure
Force (kips)
750
600
450
300
150
0
-150
-0.15
0
0.15
0.3
0.45
0.6
0.75
0.9
1.05
Midspan Displacement (in)
20.6 ft Span
17.5 ft Span

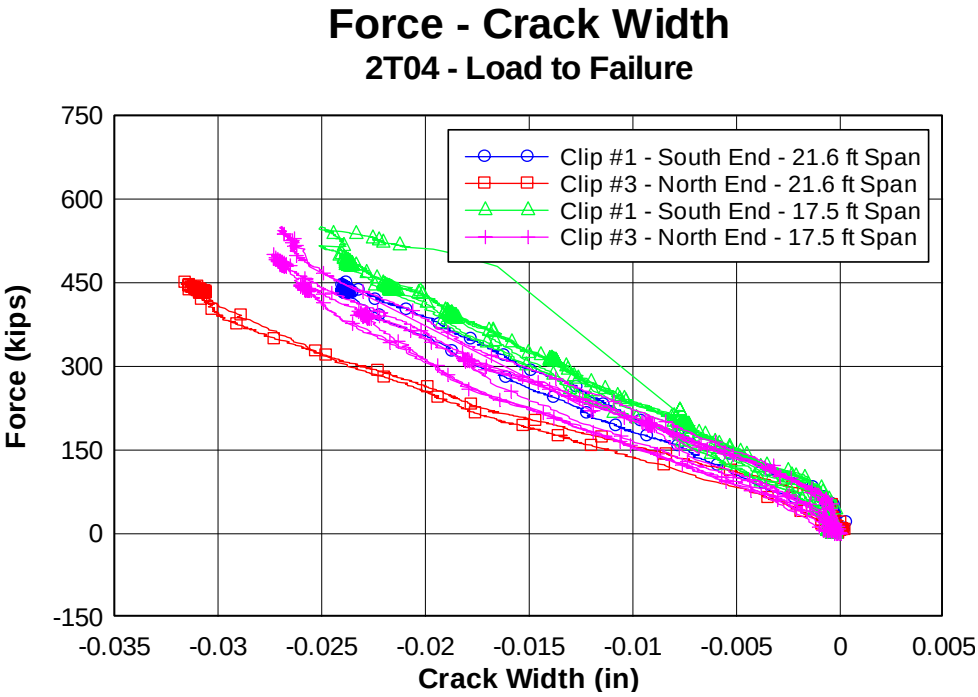
Force - Crack Width
2T04 - Load to Failure
Force (kips)
750
600
450
300
150
0
-150
-0.035
-0.03
-0.025
-0.02
-0.015
-0.01
-0.005
0
0.005
Crack Width (in)
Clip #1 - South End - 21.6 ft Span
Clip #3 - North End - 21.6 ft Span
Clip #1 - South End - 17.5 ft Span
Clip #3 - North End - 17.5 ft Span

Force - Flexural Reinforcement Strain
2T04 - Load to Failure
Detail Locations

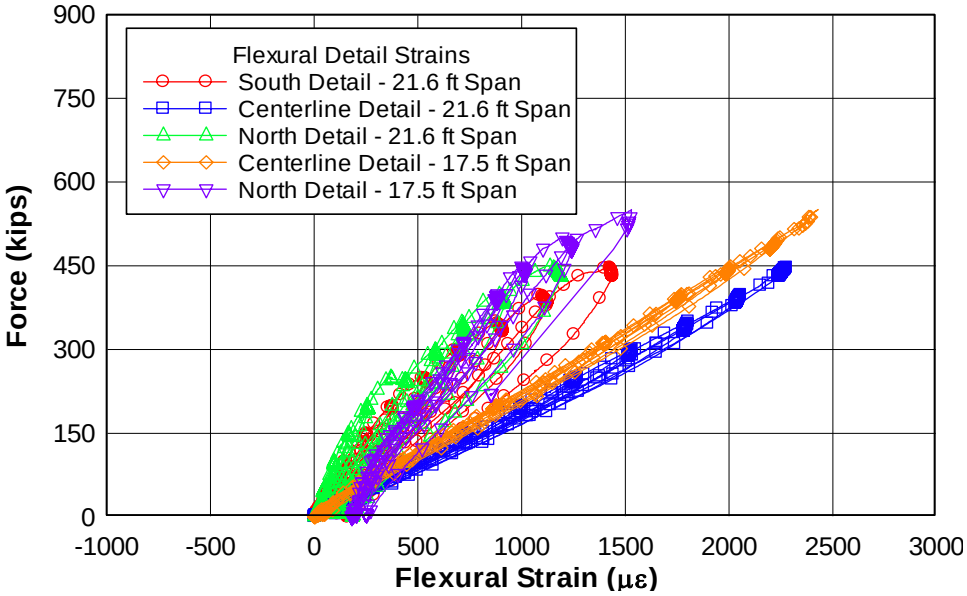

Force - Diagonal Displacement
2T04 - Load to Failure
South End

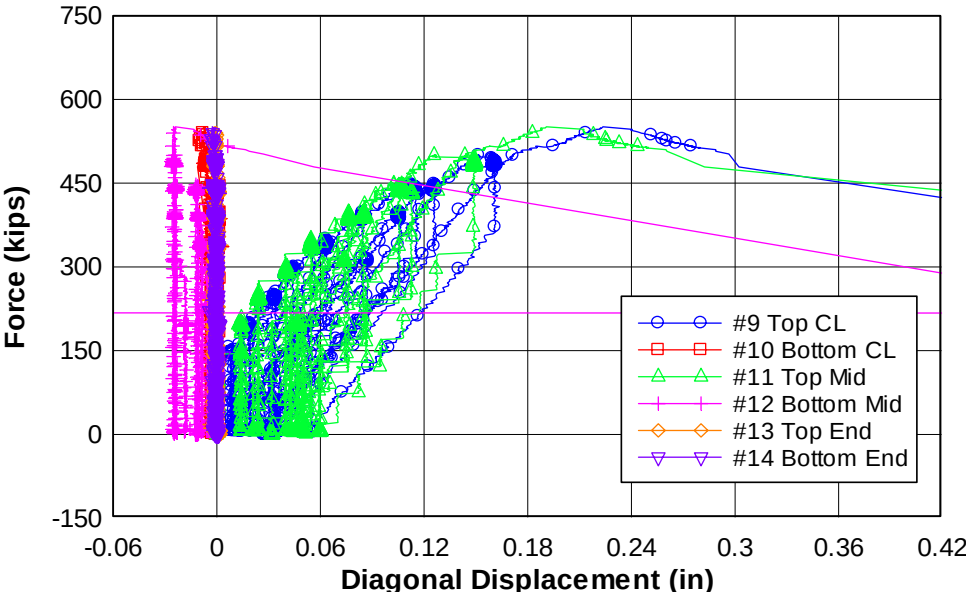

Force - Stirrup Strain
2T04 - Load to Failure
South End

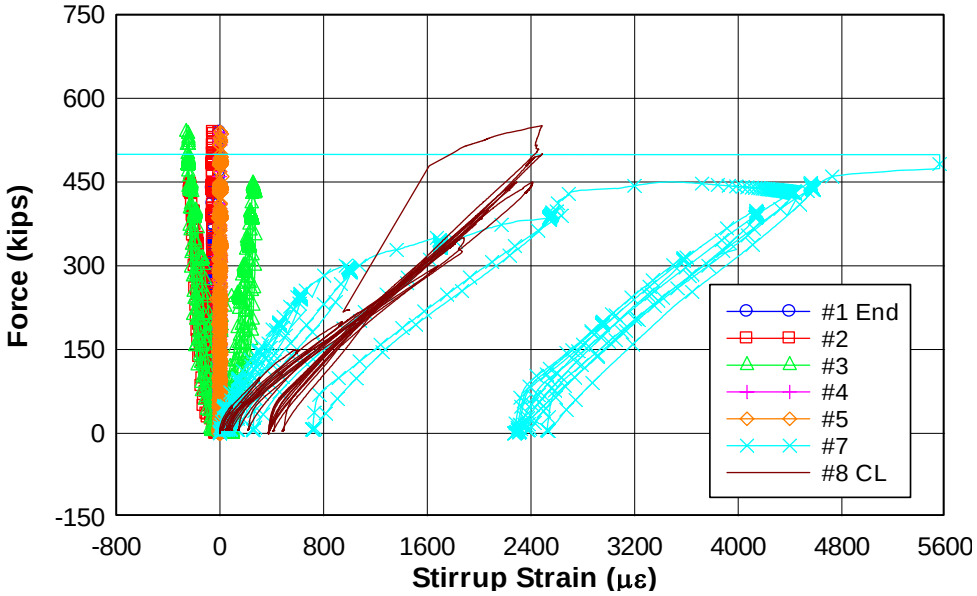

Force - CFRP Strain
2T04 - Failure
South End

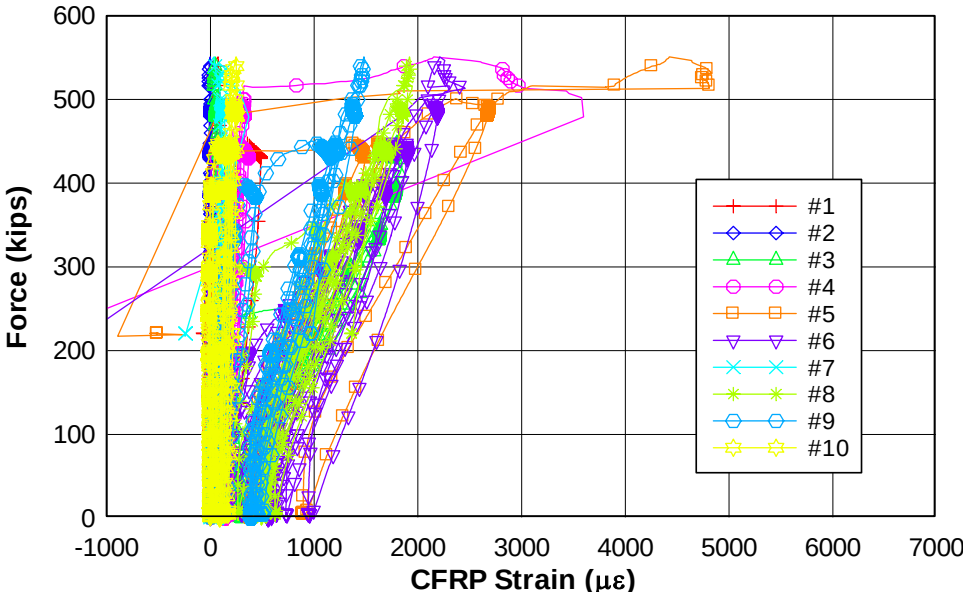

CAST 3 – SPECIMEN 3IT05

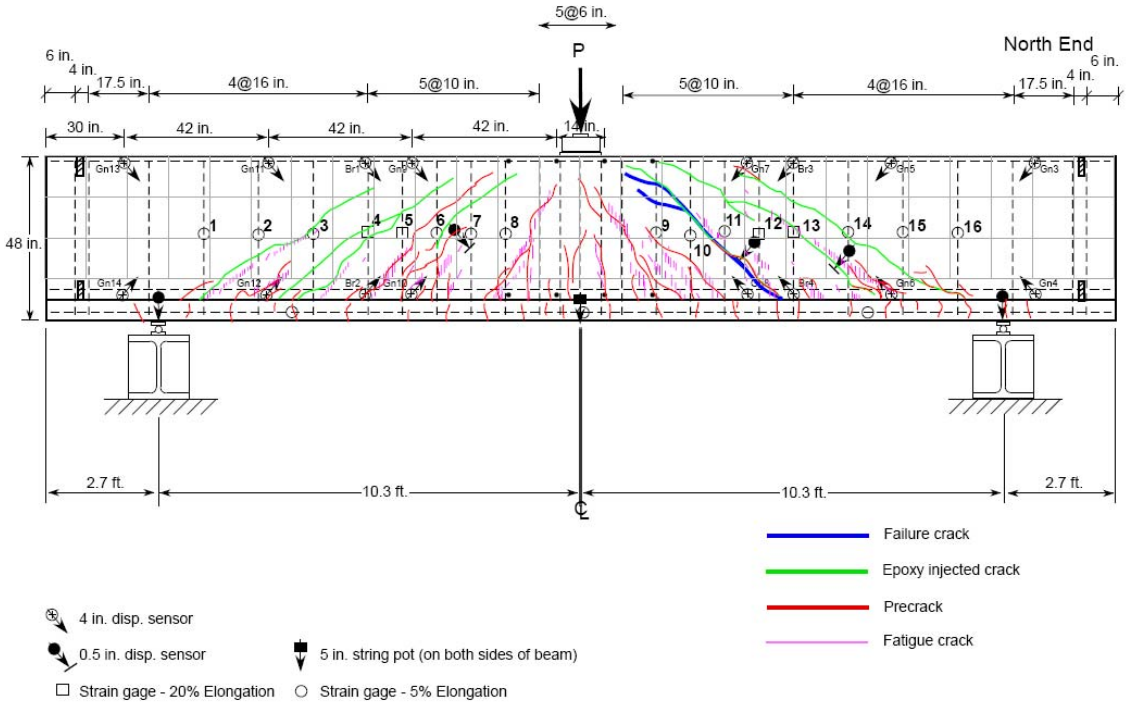

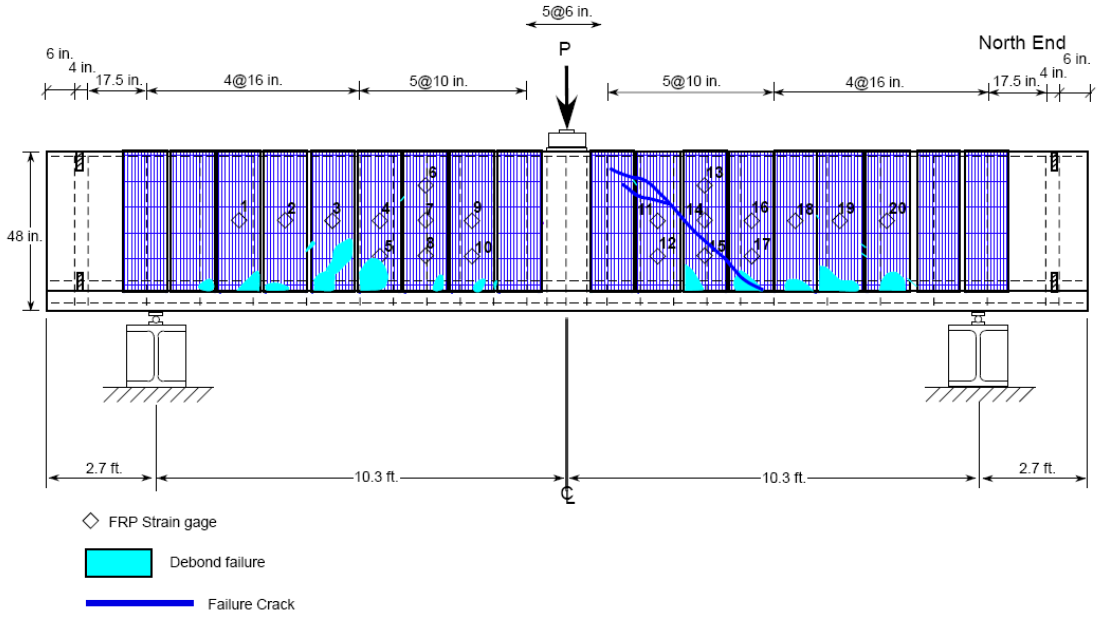

Cast 3 - Specimen 5
Negative Bending (IT-Beam)
East Face of Specimen

SPECIMEN 3IT05 – PRECRACK LOAD PLOTS

Force - Midspan Displacement

3IT05 - Precrack

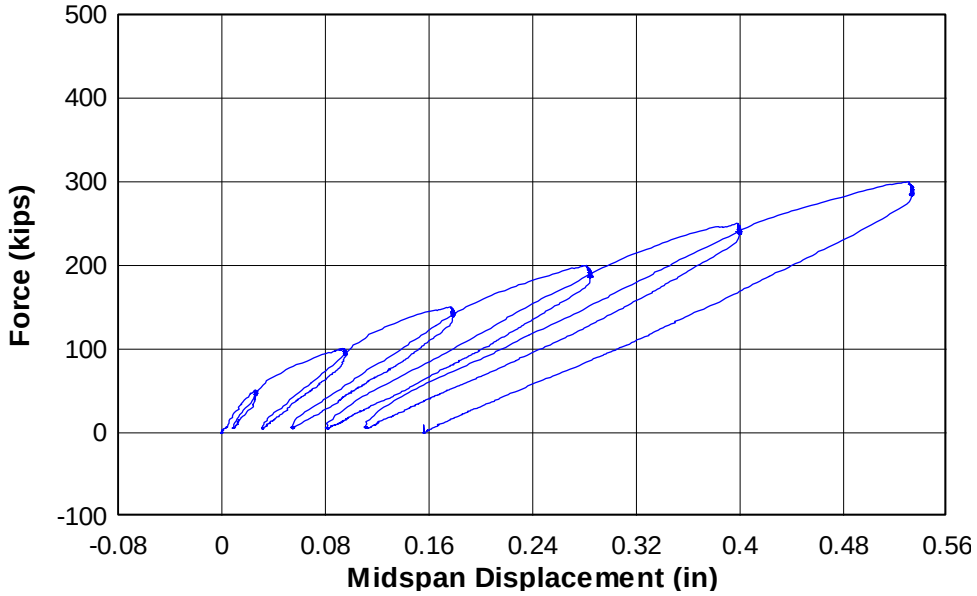

Force - Flexural Reinforcement Strain

3IT05 - Precrack
Detail Locations

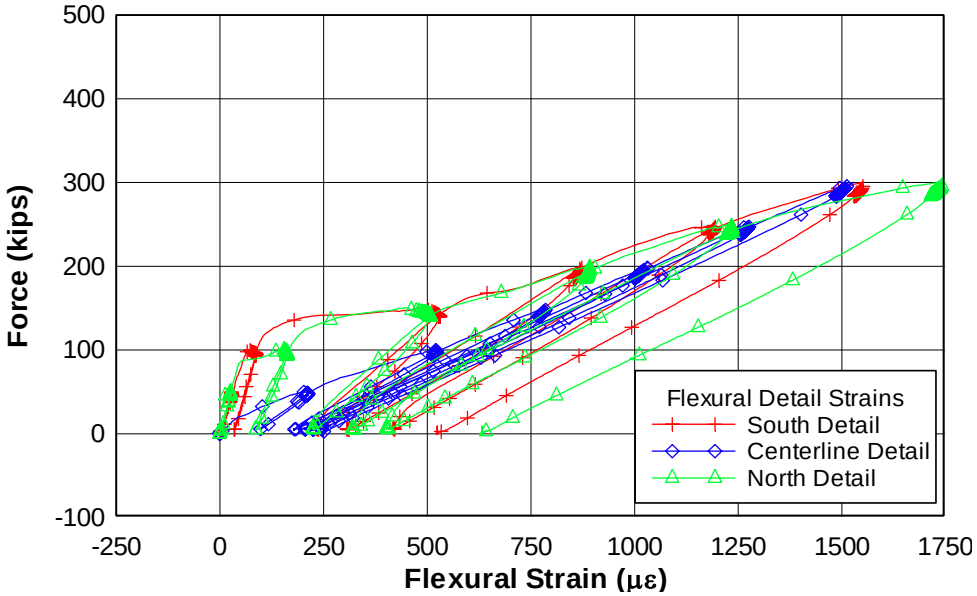

Force - Diagonal Displacement
3IT05 - Precrack
North End

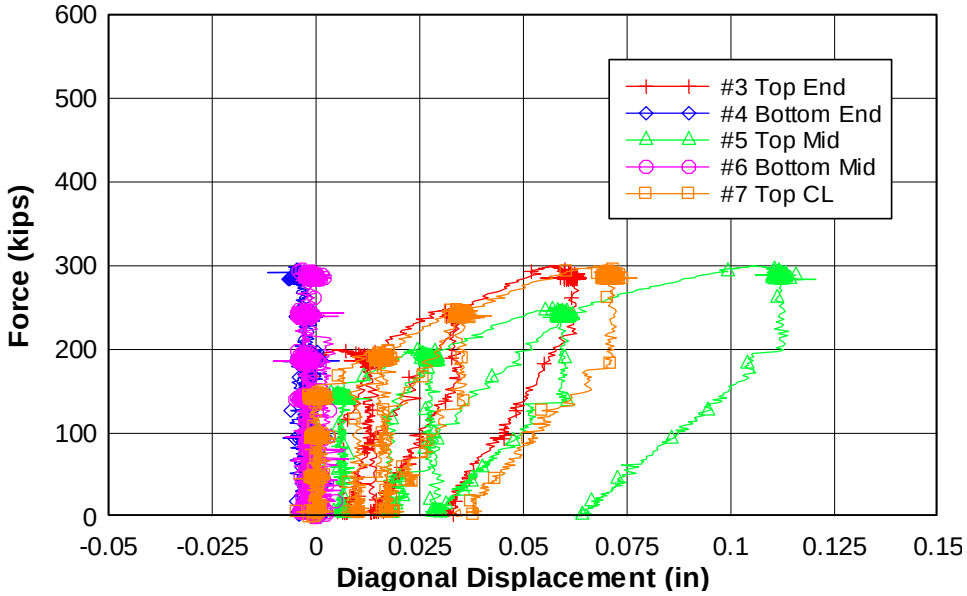

Force - Diagonal Displacement
3IT05 - Precrack
South End

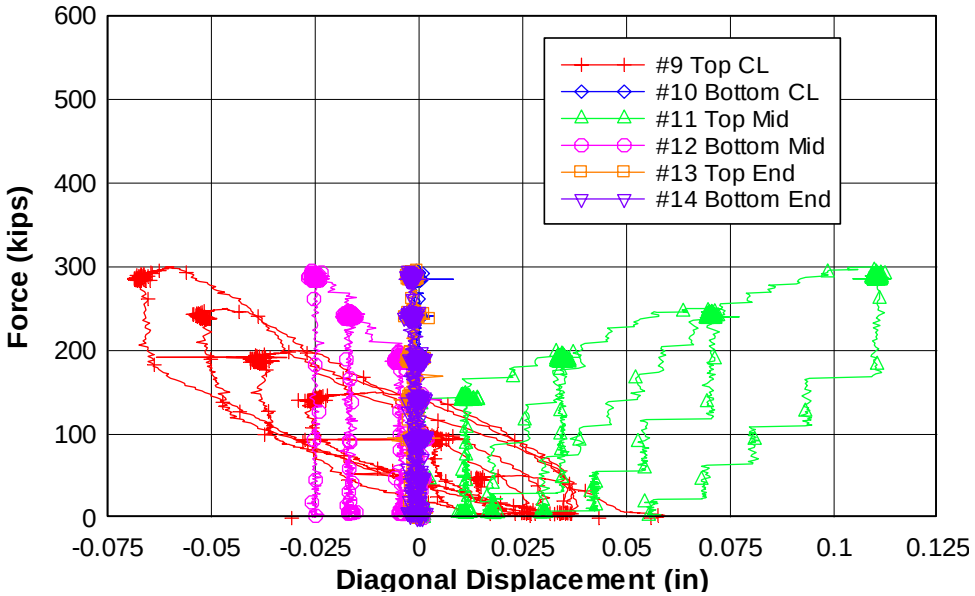

Force - Stirrup Strain Precrack

3IT05 - Precrack
North End

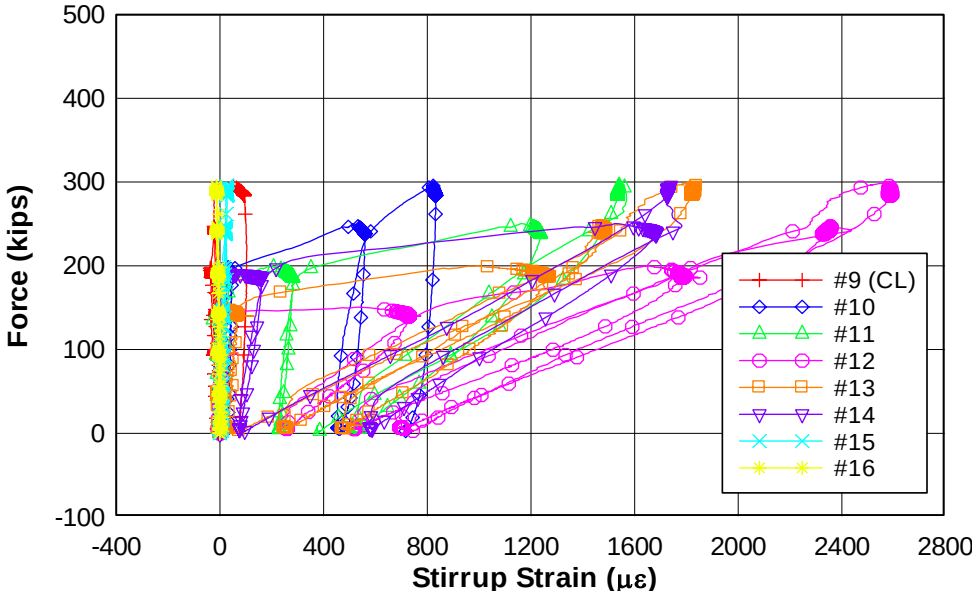

Force - Stirrup Strain

3IT05 - Precrack
South End

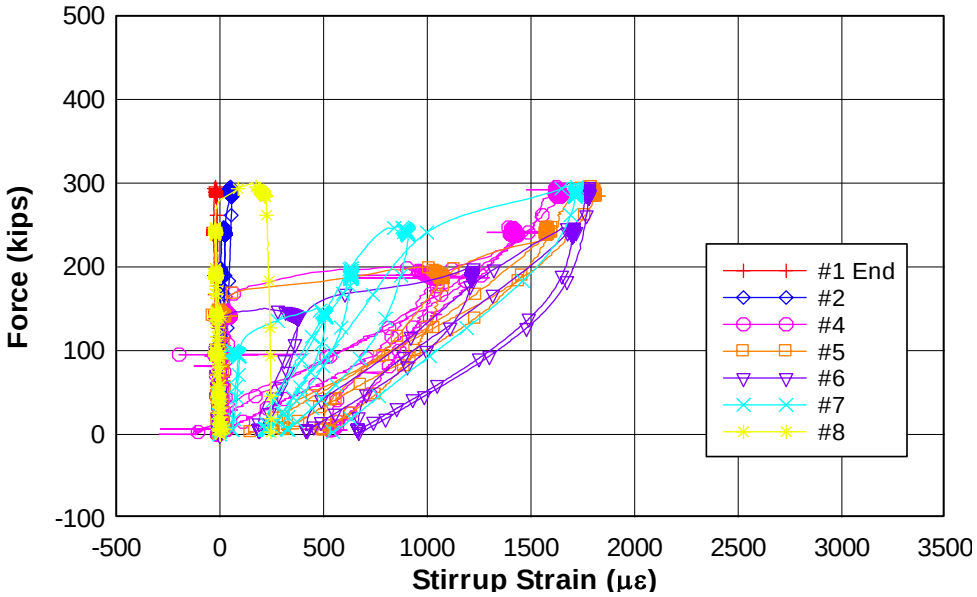

SPECIMEN 3IT05 – FAILURE LOAD PLOTS

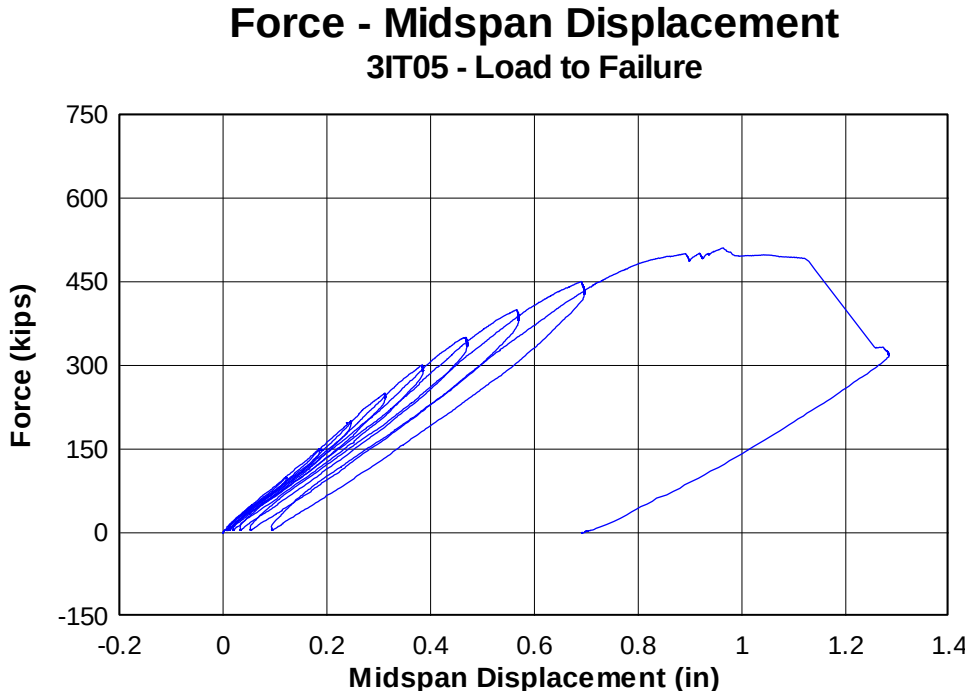
Force - Midspan Displacement
3IT05 - Load to Failure
Force (kips)
750
600
450
300
150
0
-150
-0.2
0
0.2
0.4
0.6
0.8
1
1.2
1.4
Midspan Displacement (in)

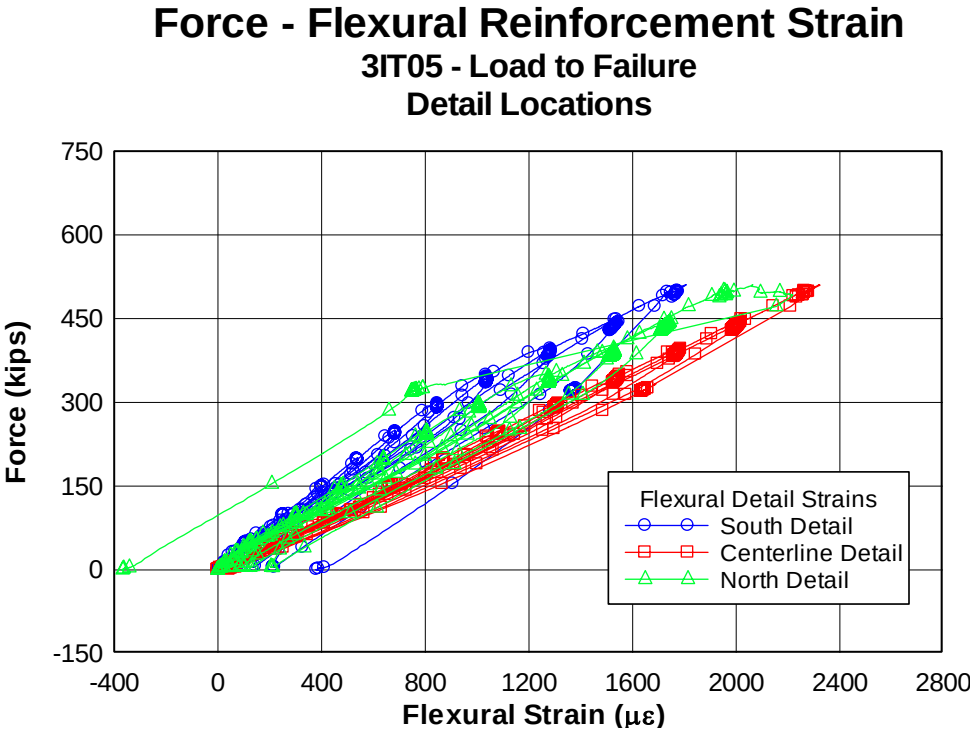
Force - Flexural Reinforcement Strain
3IT05 - Load to Failure
Detail Locations
Force (kips)
750
600
450
300
150
0
-150
-400
0
400
800
1200
1600
2000
2400
2800
Flexural Strain (με)
Flexural Detail Strains
South Detail
Centerline Detail
North Detail

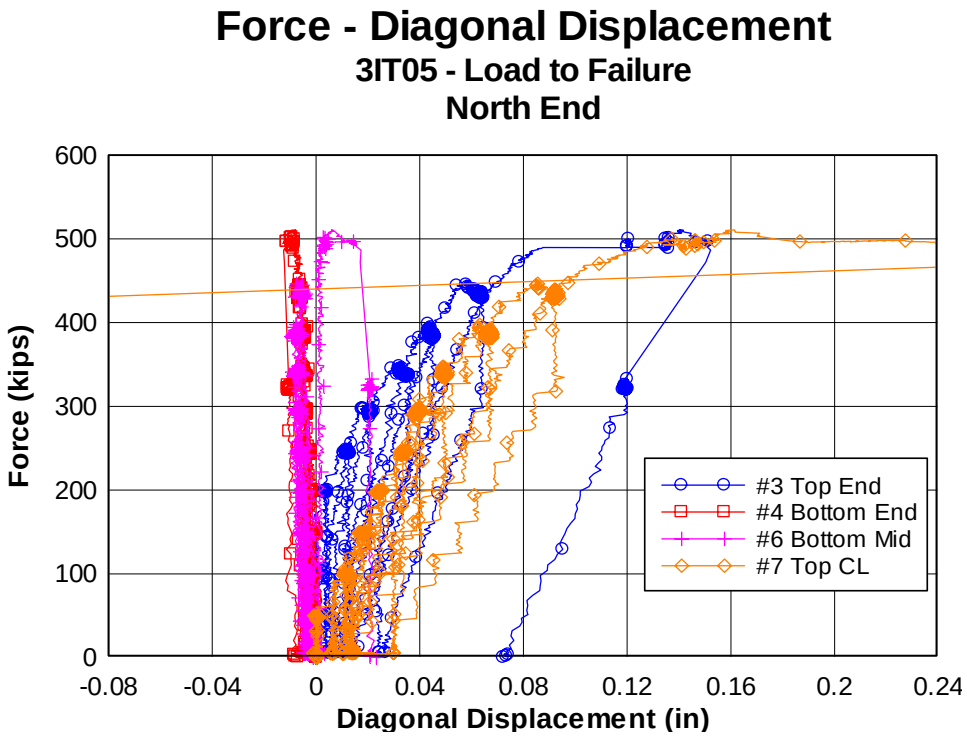
Force - Diagonal Displacement
3IT05 - Load to Failure
North End
Force (kips)
Diagonal Displacement (in)
600
500
400
300
200
100
0
-0.08
-0.04
0
0.04
0.08
0.12
0.16
0.2
0.24
#3 Top End
#4 Bottom End
#6 Bottom Mid
#7 Top CL

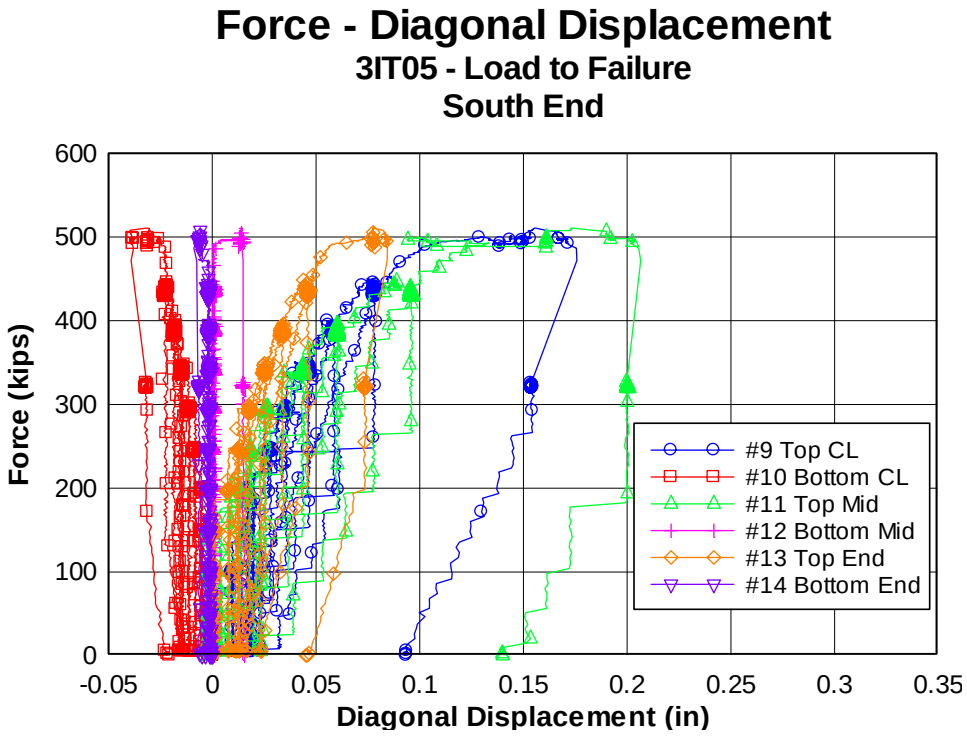
Force - Diagonal Displacement
3IT05 - Load to Failure
South End
Force (kips)
Diagonal Displacement (in)
600
500
400
300
200
100
0
-0.05
0
0.05
0.1
0.15
0.2
0.25
0.3
0.35
#9 Top CL
#10 Bottom CL
#11 Top Mid
#12 Bottom Mid
#13 Top End
#14 Bottom End

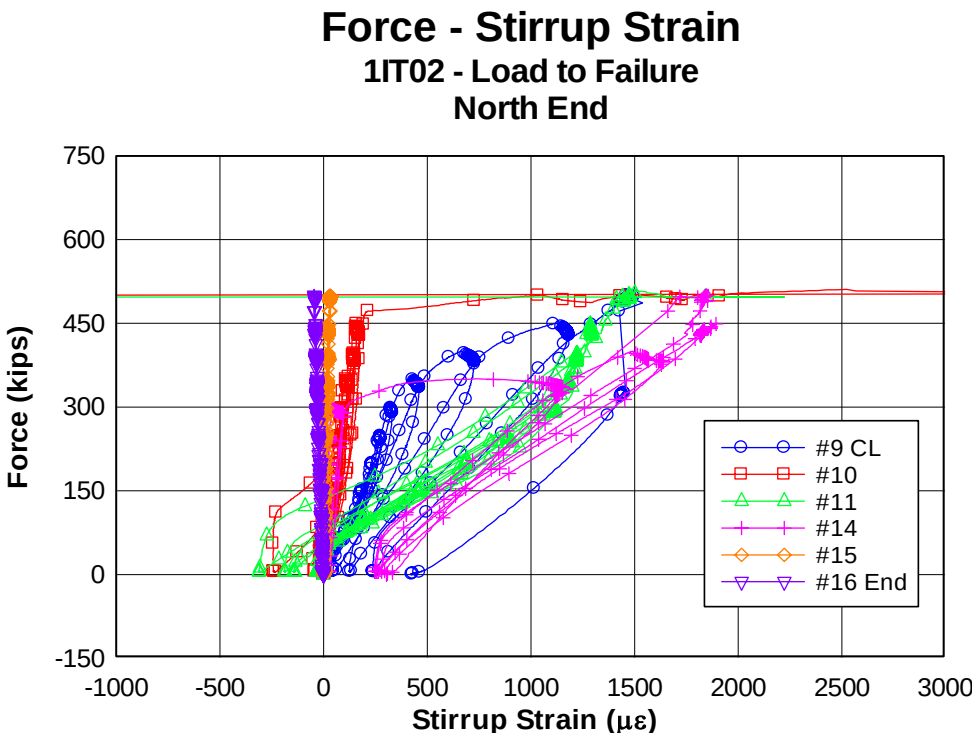
Force - Stirrup Strain
1IT02 - Load to Failure
North End
Force (kips)
Stirrup Strain (με)
750
600
450
300
150
0
-150
-1000
-500
0
500
1000
1500
2000
2500
3000
#9 CL
#10
#11
#14
#15
#16 End

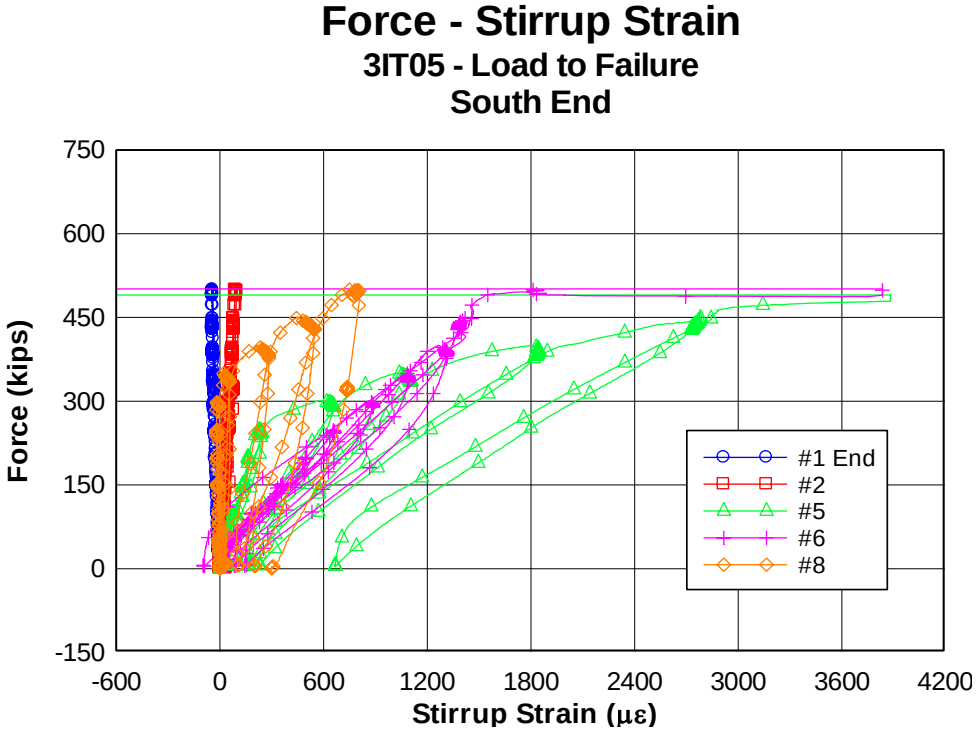
Force - Stirrup Strain
3IT05 - Load to Failure
South End
Force (kips)
Stirrup Strain (με)
750
600
450
300
150
0
-150
-600
0
600
1200
1800
2400
3000
3600
4200
#1 End
#2
#5
#6
#8

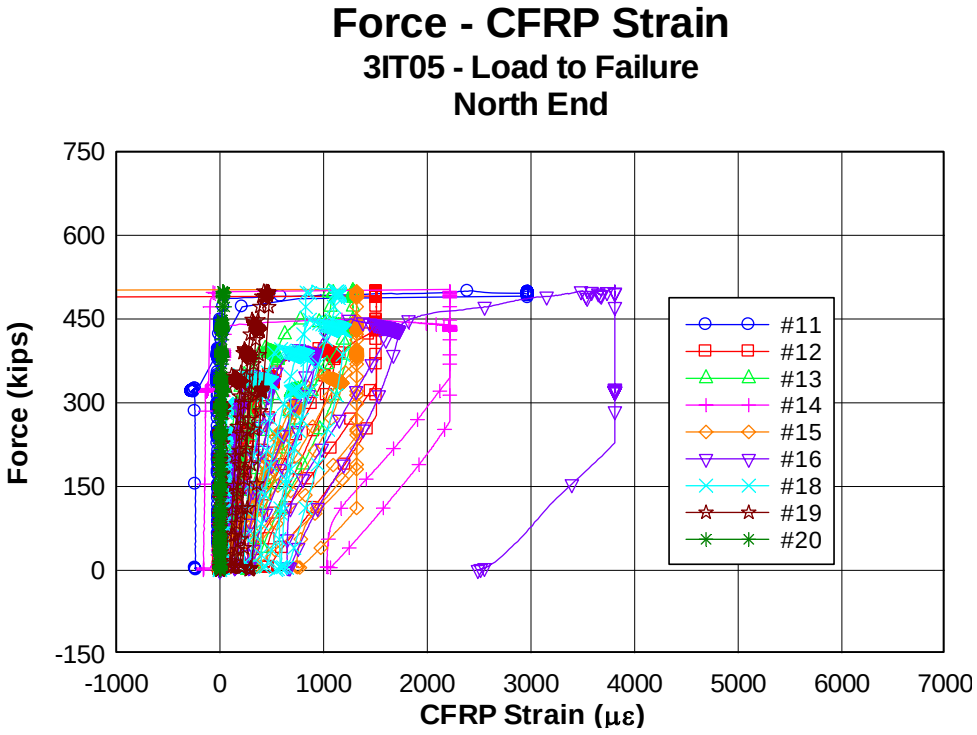
Force - CFRP Strain
3IT05 - Load to Failure
North End
Force (kips)
CFRP Strain (με)
750
600
450
300
150
0
-150
-1000
0
1000
2000
3000
4000
5000
6000
7000
#11
#12
#13
#14
#15
#16
#18
#19
#20

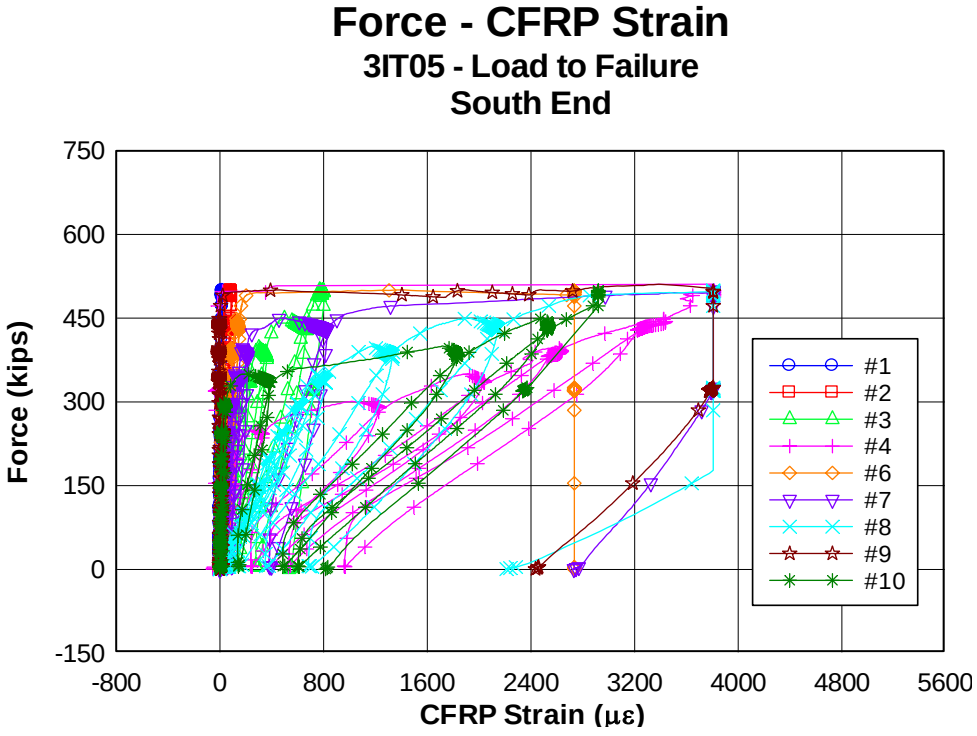
Force - CFRP Strain
3IT05 - Load to Failure
South End
Force (kips)
CFRP Strain (με)
750
600
450
300
150
0
-150
-800
0
800
1600
2400
3200
4000
4800
5600
#1
#2
#3
#4
#6
#7
#8
#9
#10

SPECIMEN 3IT05 – FATIGUE LOAD PLOTS

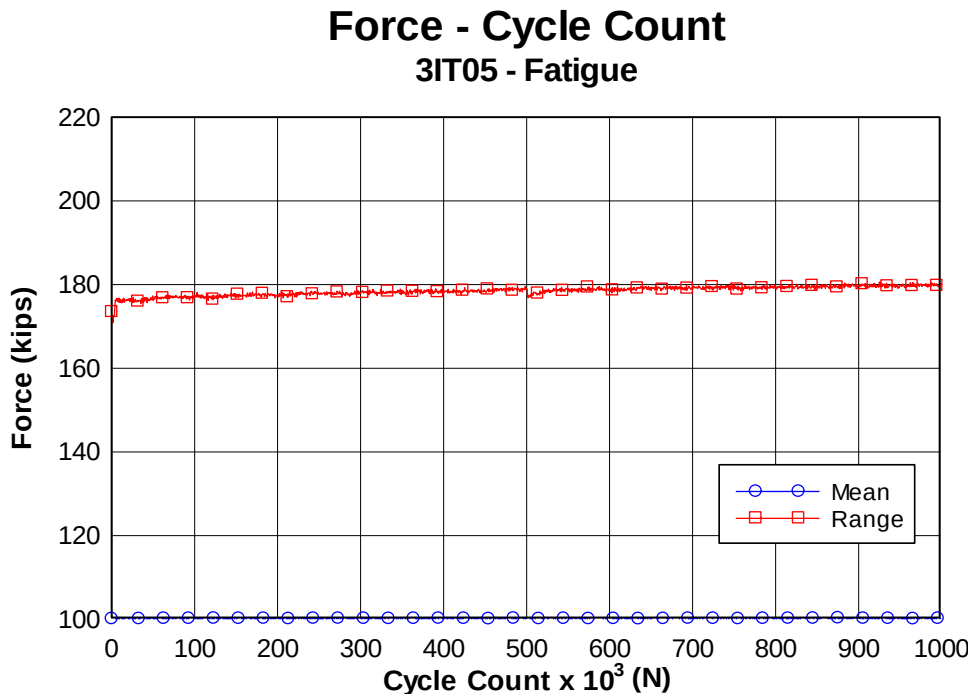
Force - Cycle Count
3IT05 - Fatigue
Force (kips)
220
200
180
160
140
120
100
0
100
200
300
400
500
600
700
800
900
1000
Cycle Count x 10^3 (N)
Mean
Range

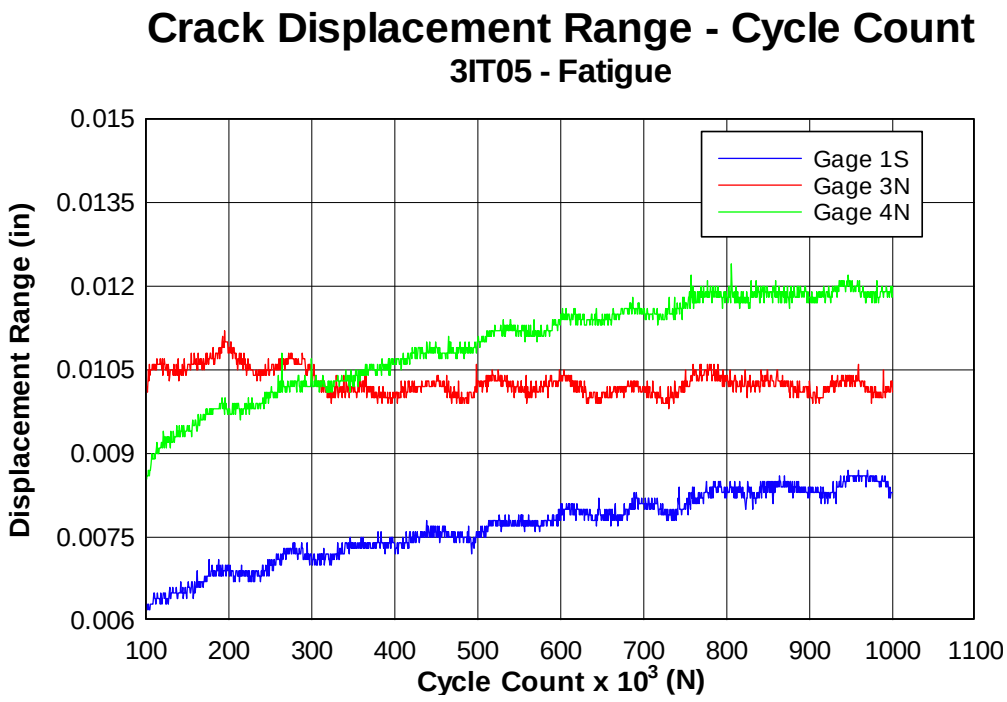
Crack Displacement Range - Cycle Count
3IT05 - Fatigue
Displacement Range (in)
0.015
0.0135
0.012
0.0105
0.009
0.0075
0.006
100
200
300
400
500
600
700
800
900
1000
1100
Cycle Count x 10^3 (N)
Gage 1S
Gage 3N
Gage 4N

Flexural Strain - Cycle Count
3IT05 - Fatigue
Flexural Detail Locations

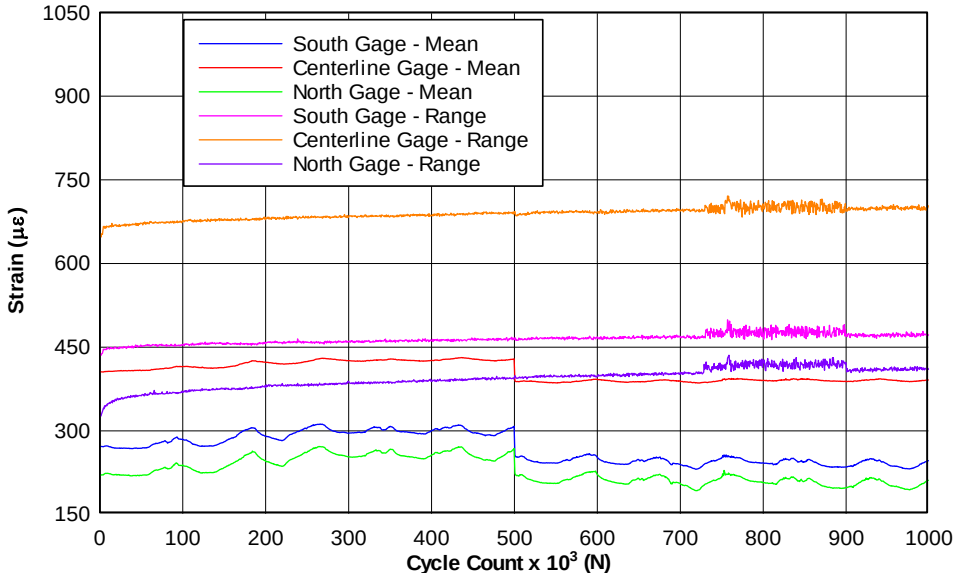

Stirrup Strain Range - Cycle Count
3IT05 - Fatigue
North End

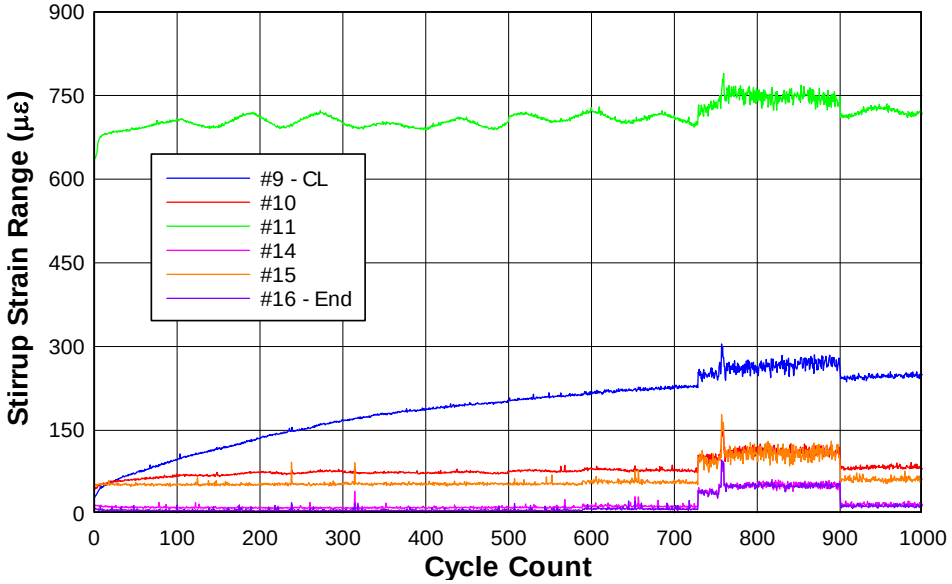

Stirrup Strain Range - Cycle Count
3IT05 - Fatigue
South End

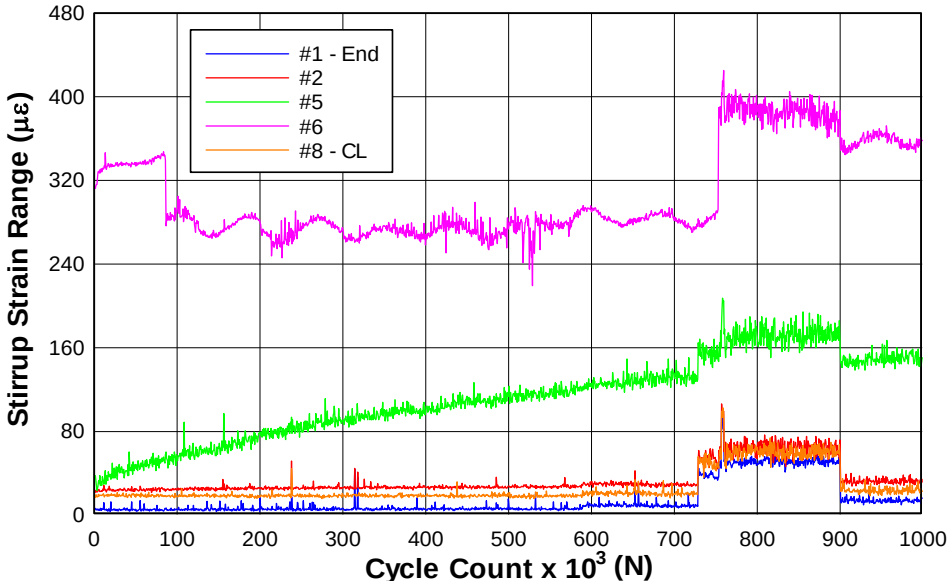

CFRP Strain Range - Cycle Count
3IT05 - Fatigue
North End

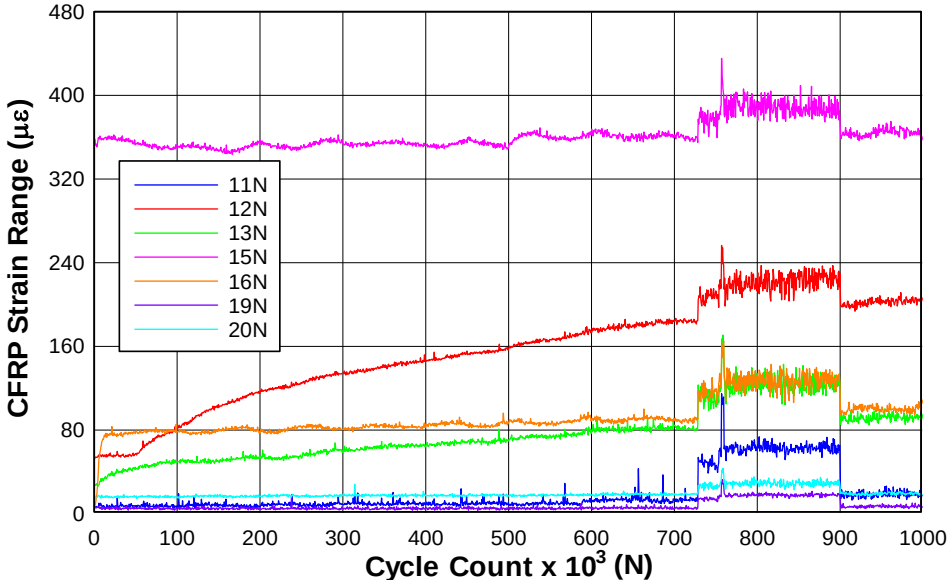

CFRP Strain Range - Cycle Count

3IT05 - Fatigue

South End

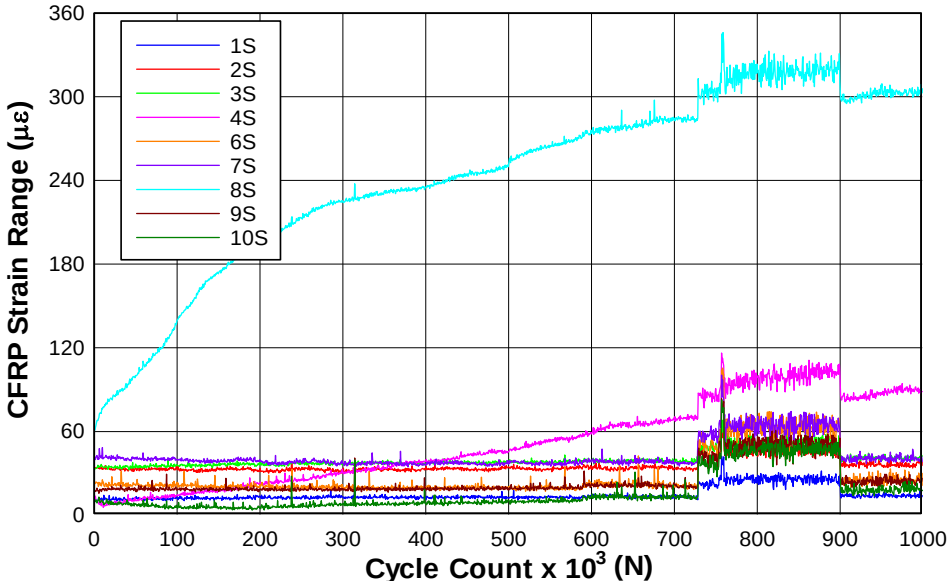

CAST 3 – SPECIMEN 3IT06

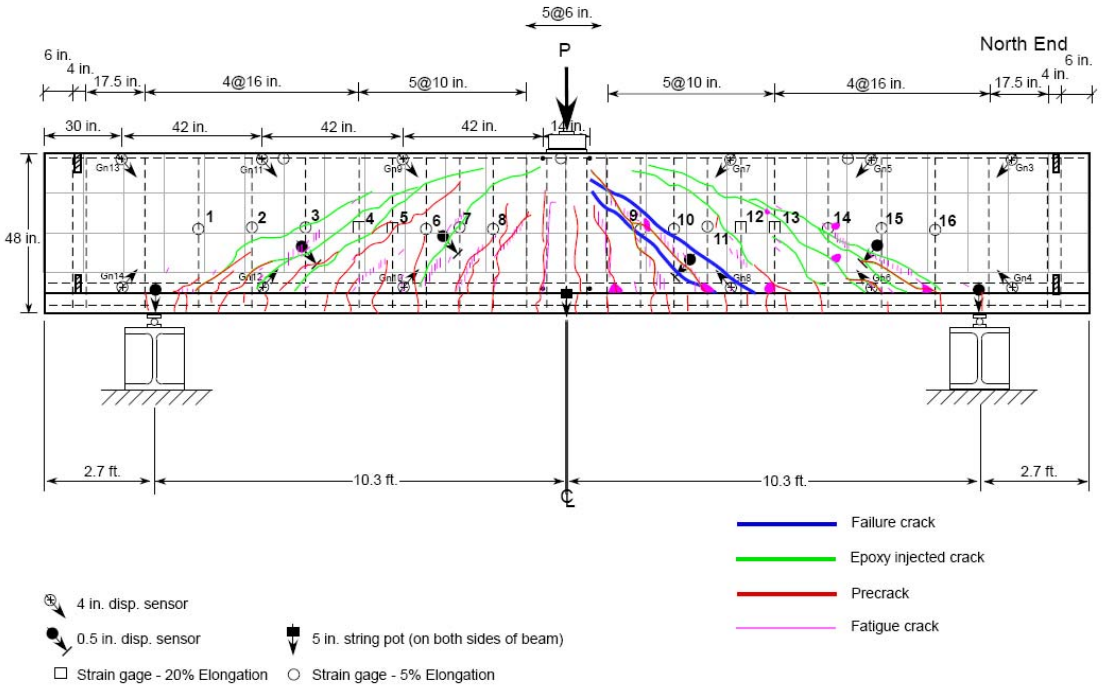

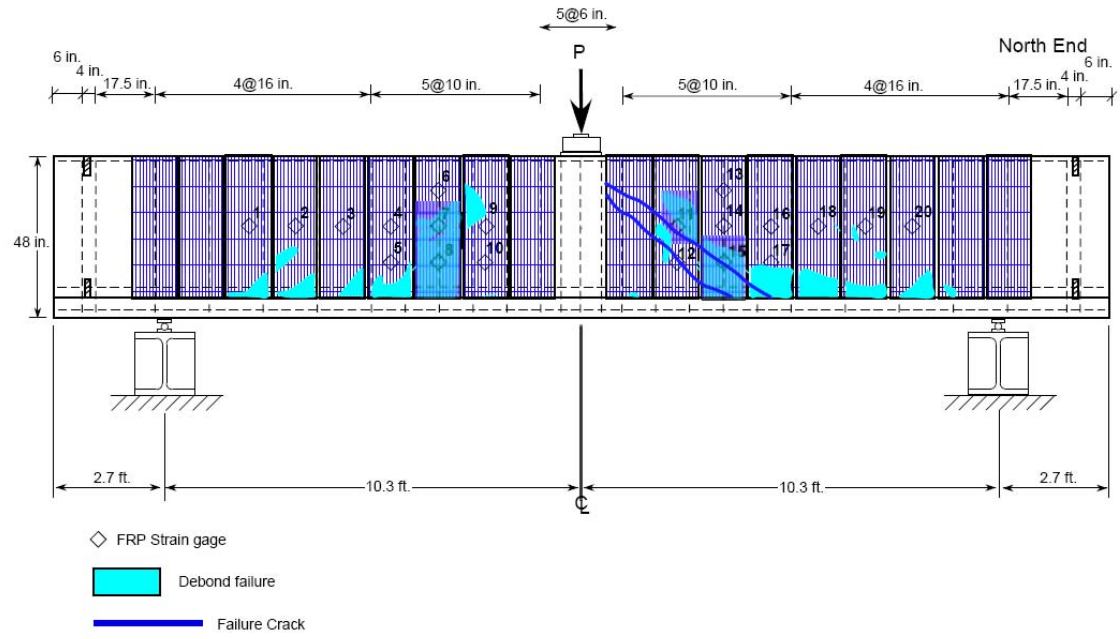

Cast 3 - Specimen 6
Negative Bending (IT-Beam)
East Face of Specimen

SPECIMEN 3IT06 – PRECRACK LOAD PLOTS

Force - Midspan Displacement

3IT06 - Precrack

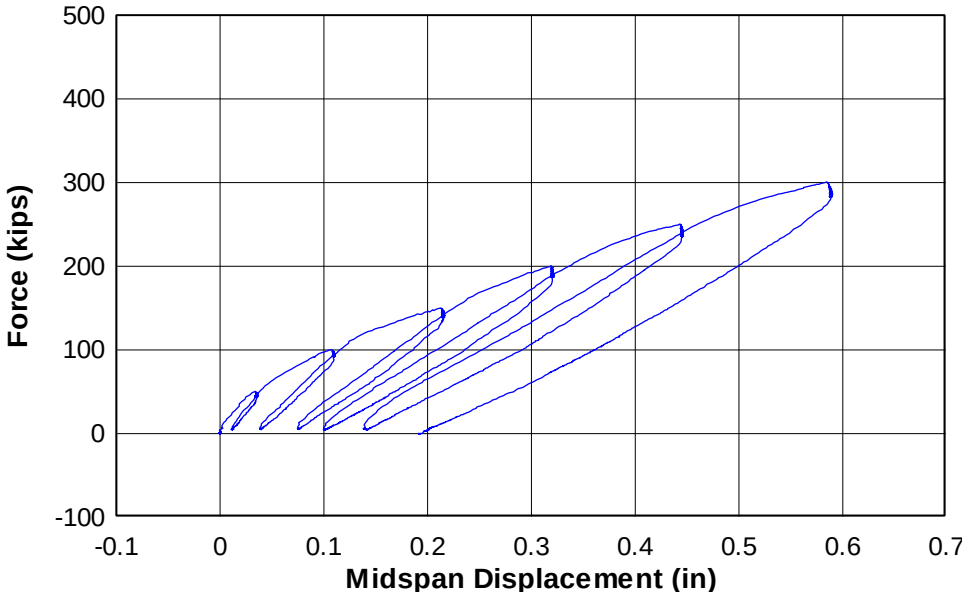

Force - Flexural Reinforcement Strain

3IT06 - Precrack
Detail Locations

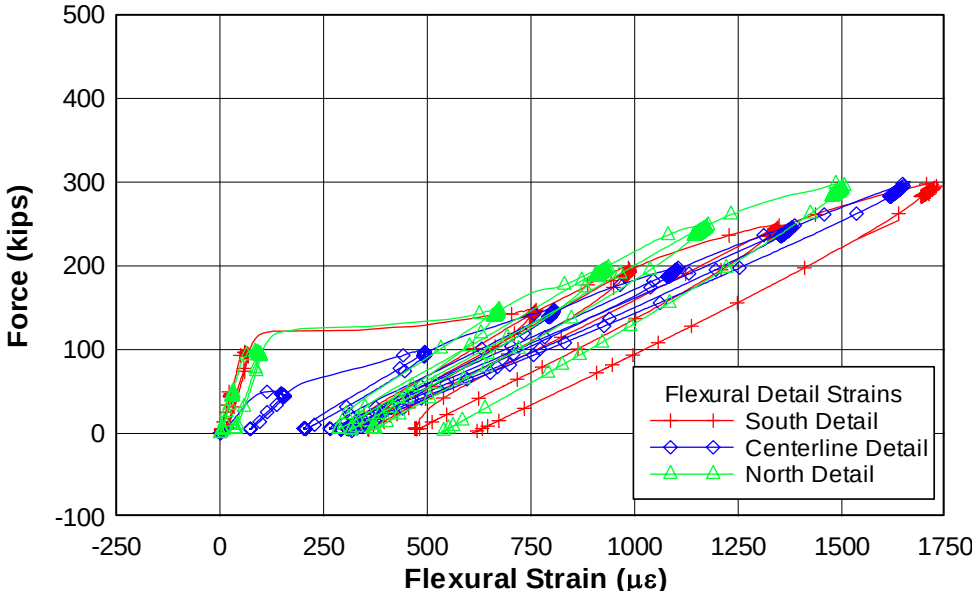

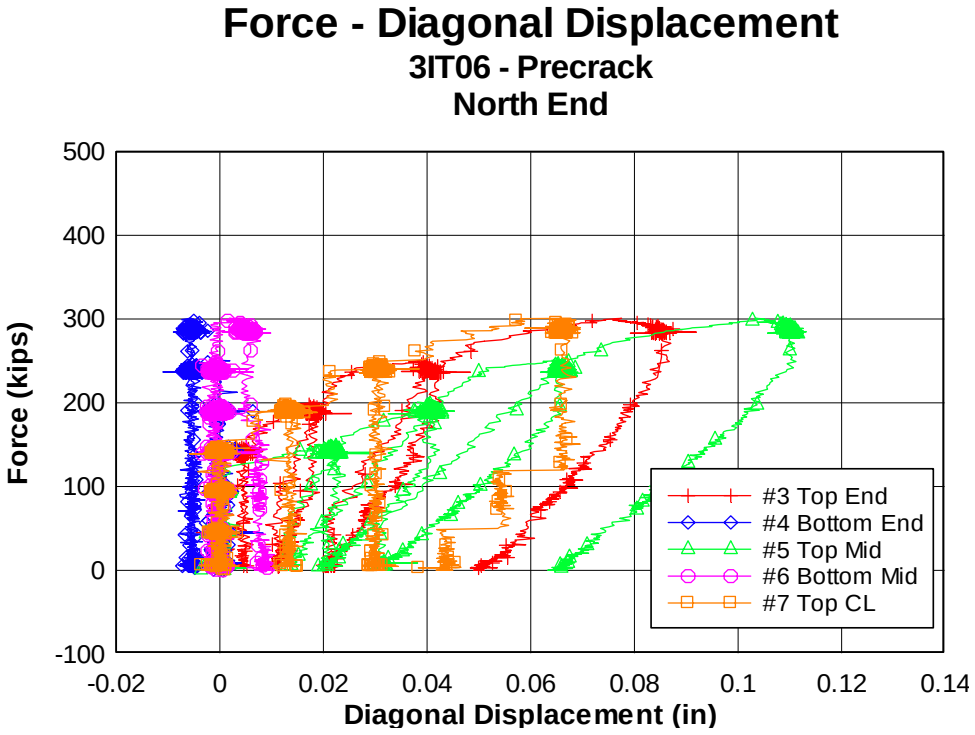
Force - Diagonal Displacement
3IT06 - Precrack
North End
Force (kips)
Diagonal Displacement (in)
500
400
300
200
100
0
-100
-0.02
0
0.02
0.04
0.06
0.08
0.1
0.12
0.14
#3 Top End
#4 Bottom End
#5 Top Mid
#6 Bottom Mid
#7 Top CL

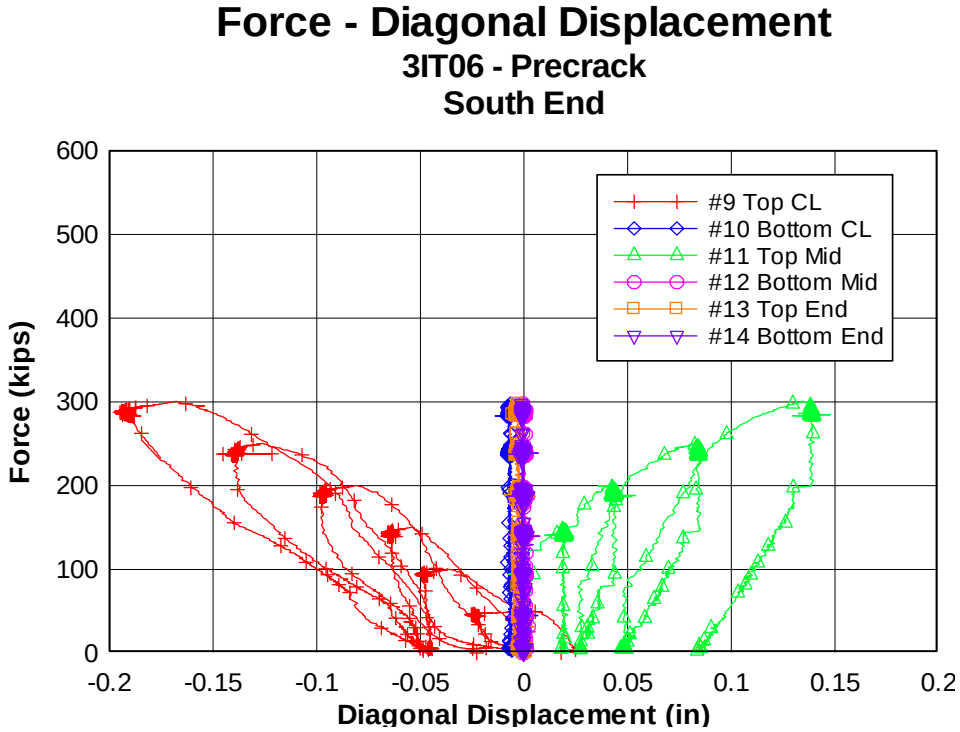
Force - Diagonal Displacement
3IT06 - Precrack
South End
Force (kips)
Diagonal Displacement (in)
600
500
400
300
200
100
0
-0.2
-0.15
-0.1
-0.05
0
0.05
0.1
0.15
0.2
#9 Top CL
#10 Bottom CL
#11 Top Mid
#12 Bottom Mid
#13 Top End
#14 Bottom End

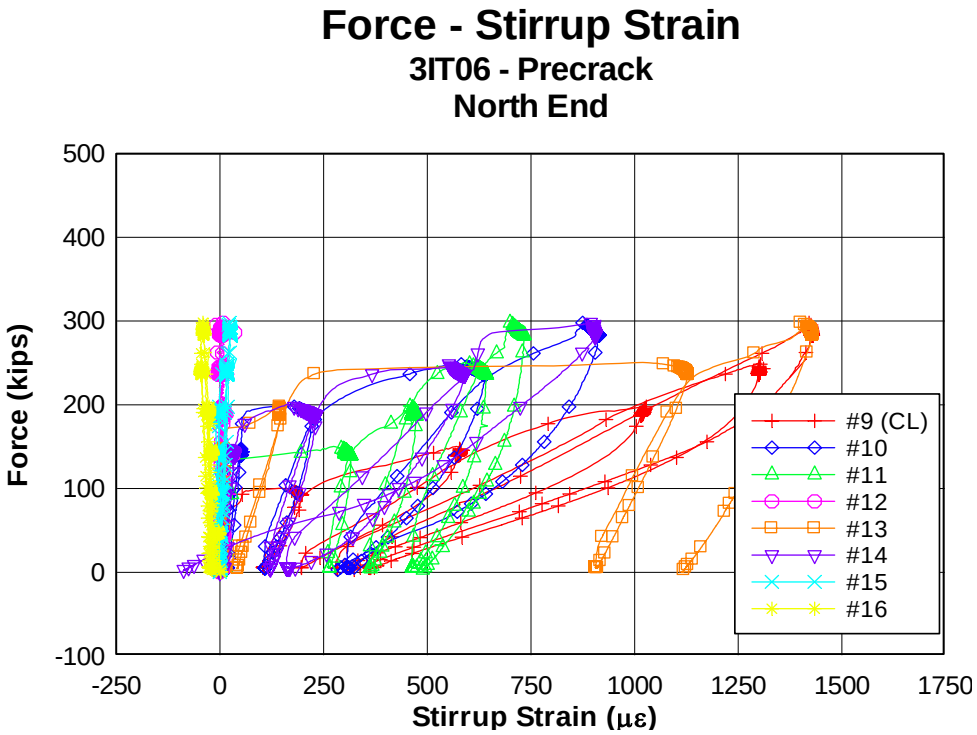
Force - Stirrup Strain
3IT06 - Precrack
North End
Force (kips)
Stirrup Strain (με)
500
400
300
200
100
0
-100
-250
0
250
500
750
1000
1250
1500
1750
#9 (CL)
#10
#11
#12
#13
#14
#15
#16

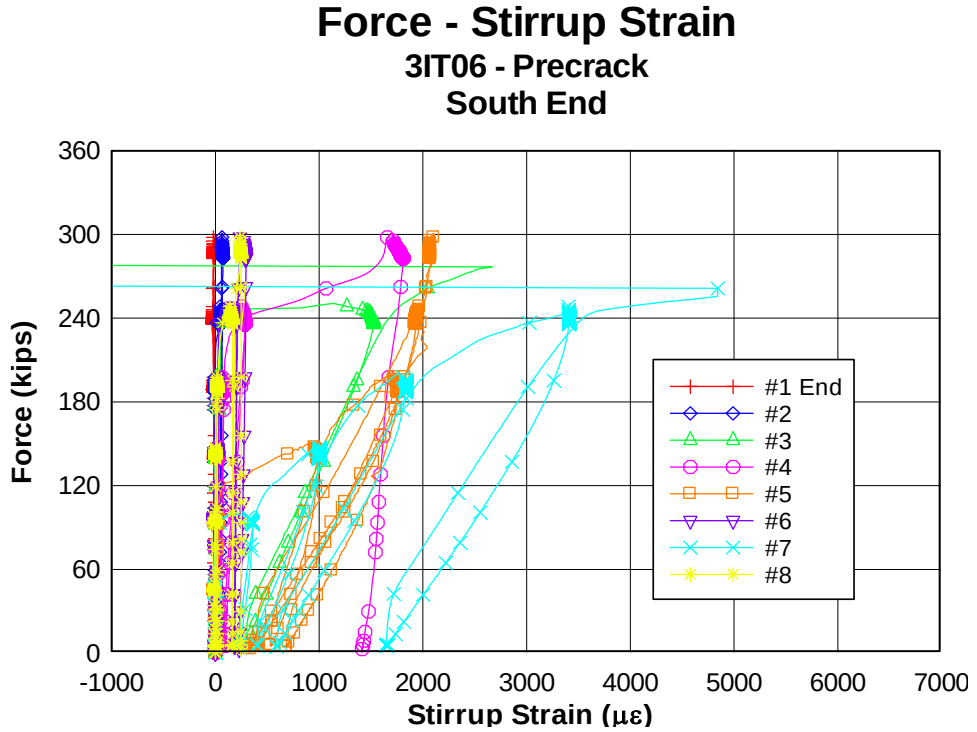
Force - Stirrup Strain
3IT06 - Precrack
South End
Force (kips)
Stirrup Strain (με)
360
300
240
180
120
60
0
-1000
0
1000
2000
3000
4000
5000
6000
7000
#1 End
#2
#3
#4
#5
#6
#7
#8

SPECIMEN 3IT06 – FAILURE LOAD PLOTS

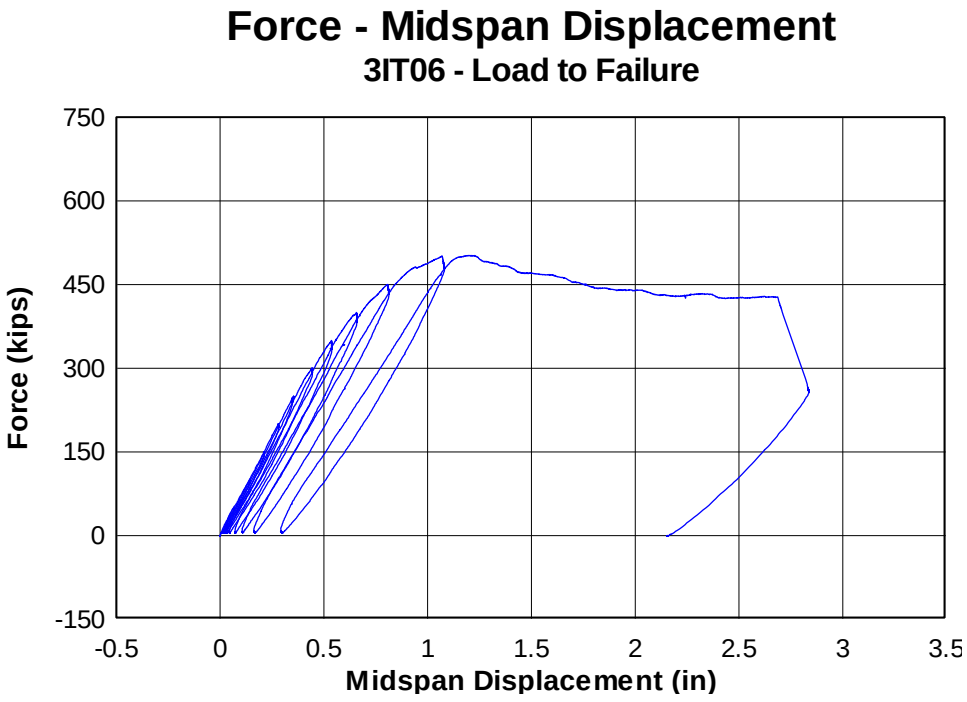
Force - Midspan Displacement
3IT06 - Load to Failure
750
600
450
300
150
0
-150
Force (kips)
-0.5
0
0.5
1
1.5
2
2.5
3
3.5
Midspan Displacement (in)

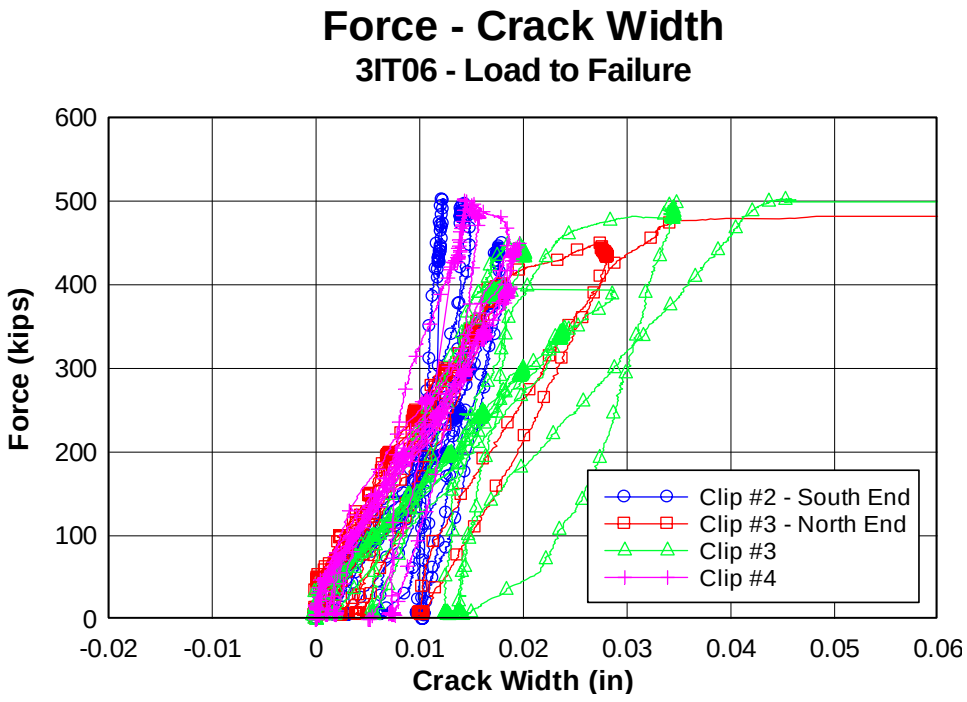
Force - Crack Width
3IT06 - Load to Failure
600
500
400
300
200
100
0
Force (kips)
-0.02
-0.01
0
0.01
0.02
0.03
0.04
0.05
0.06
Crack Width (in)
Clip #2 - South End
Clip #3 - North End
Clip #3
Clip #4

Force - Flexural Reinforcement Strain
3IT06 - Load to Failure
Detail Locations

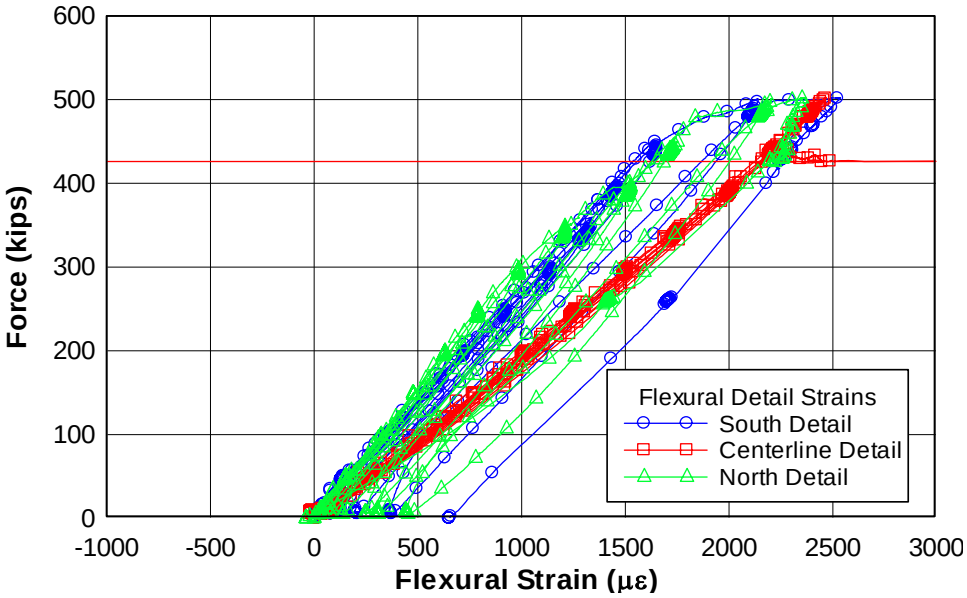

Force - Diagonal Displacement
3IT06 - Load to Failure
North End

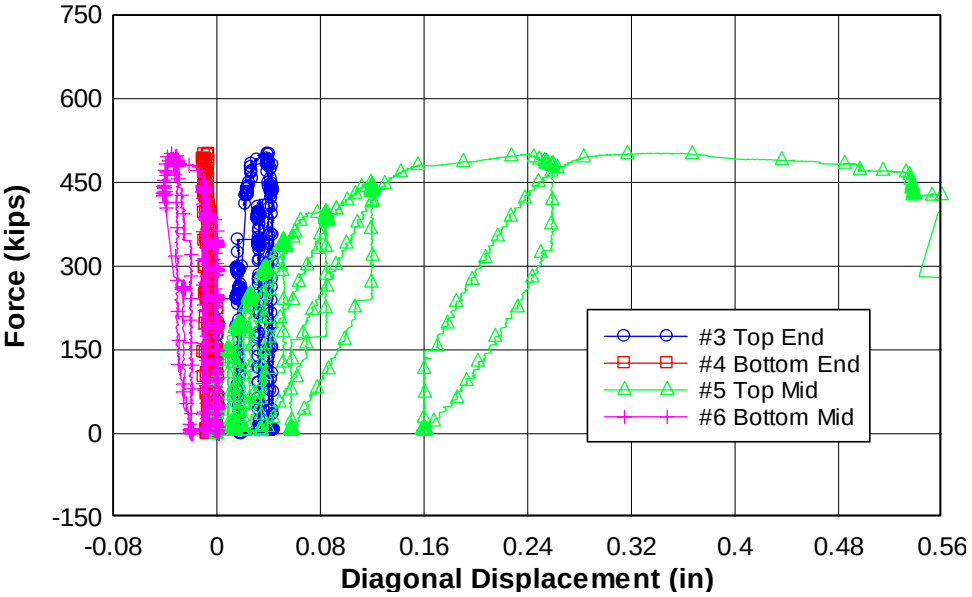

Force - Diagonal Displacement
3IT06 - Load to Failure
South End

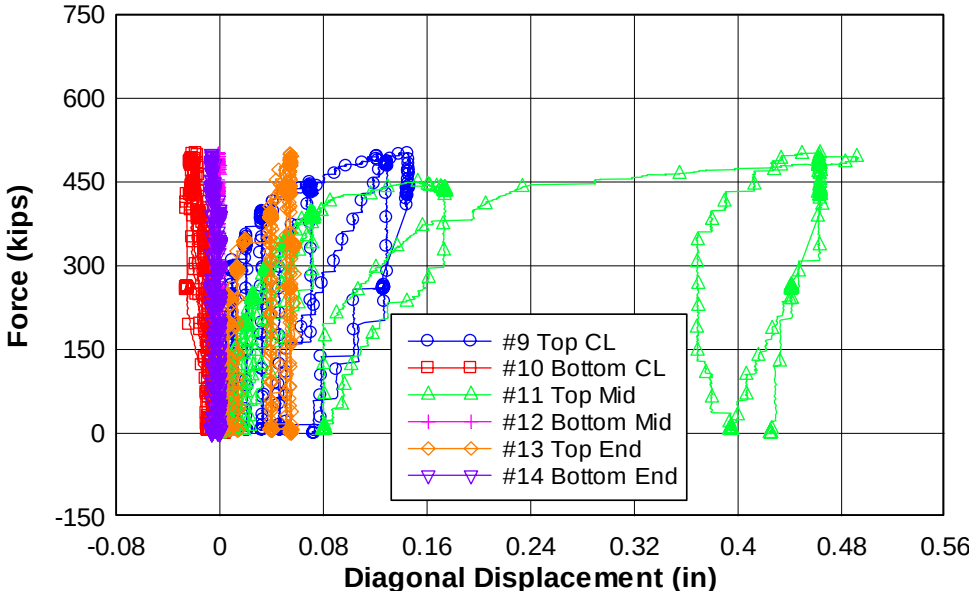

Force - Stirrup Strain
3IT06 - Load to Failure
North End

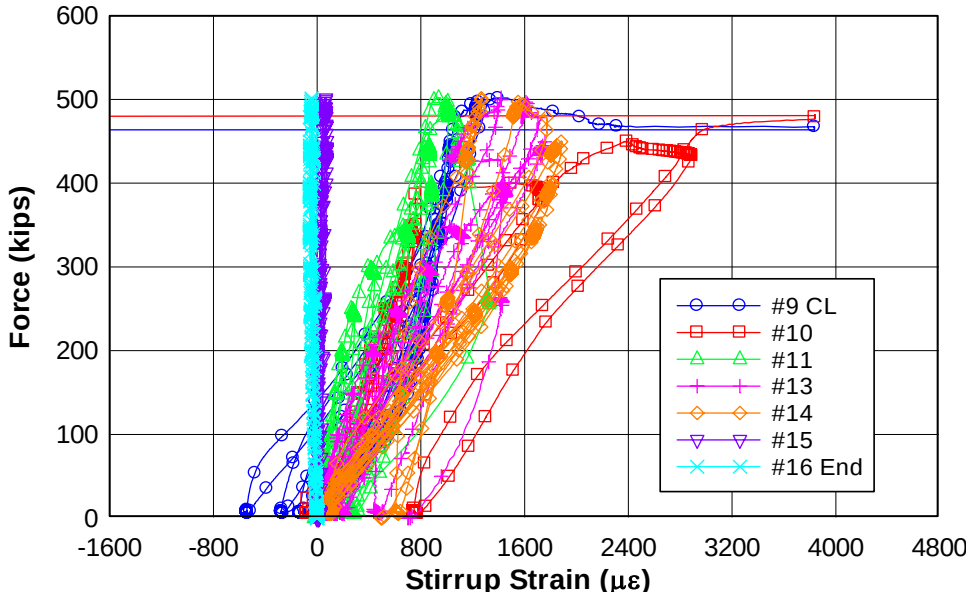

Force - Stirrup Strain
3IT06 - Load to Failure
South End

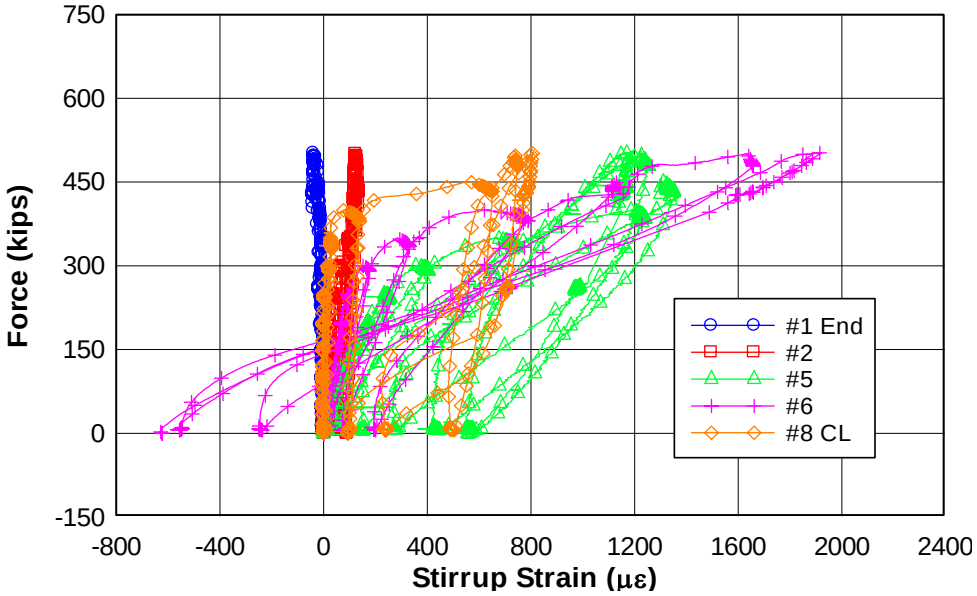

Force - CFRP Strain
3IT06 - Load to Failure
North End

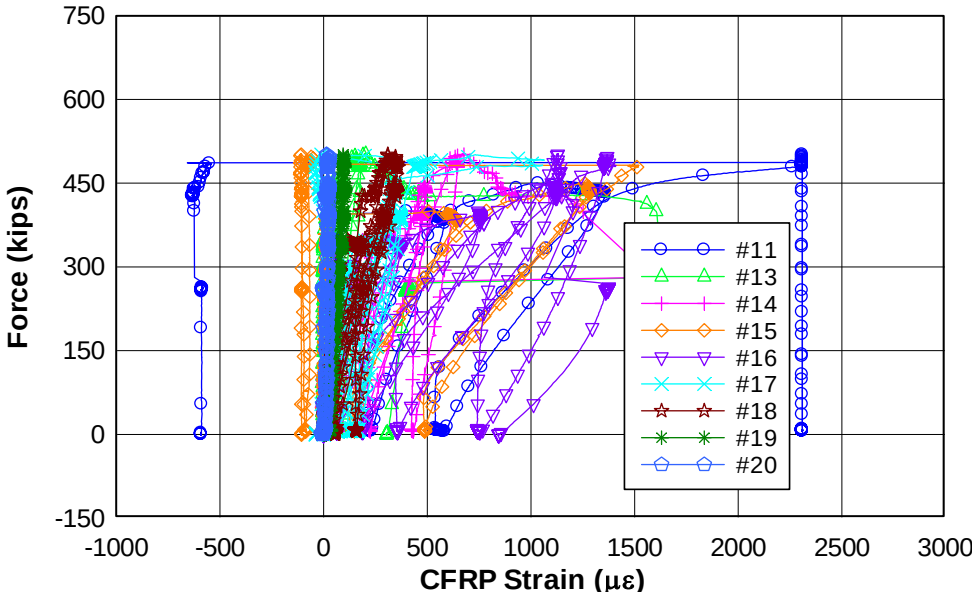

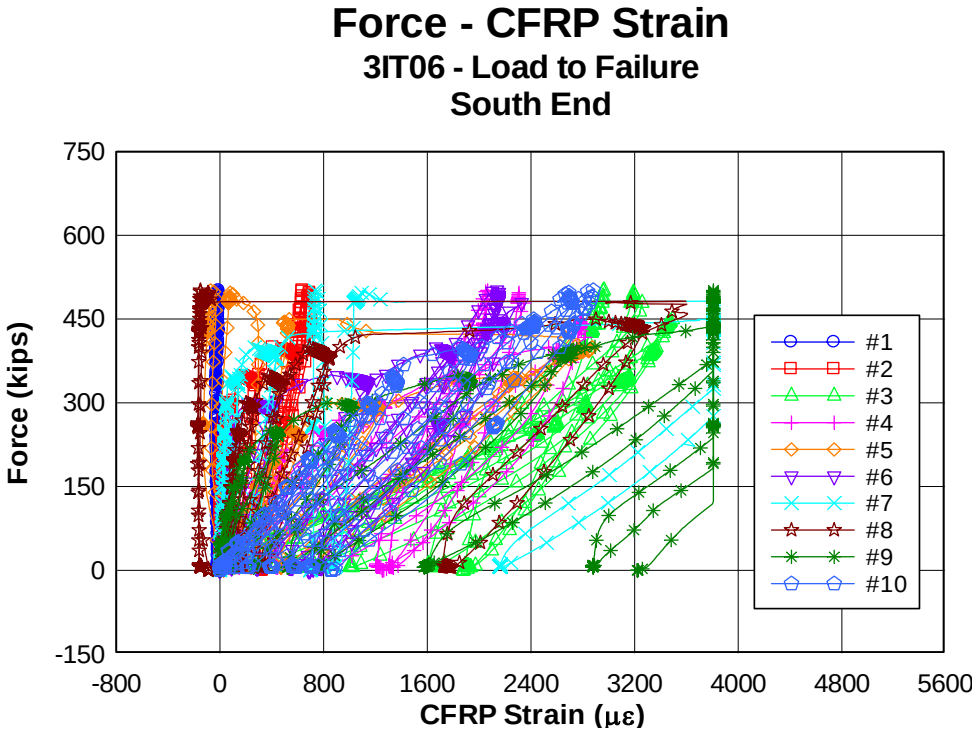
Force - CFRP Strain
3IT06 - Load to Failure
South End
Force (kips)
750
600
450
300
150
0
-150
-800
0
800
1600
2400
3200
4000
4800
5600
CFRP Strain (με)
#1
#2
#3
#4
#5
#6
#7
#8
#9
#10

SPECIMEN 3IT06 – FATIGUE LOAD PLOTS

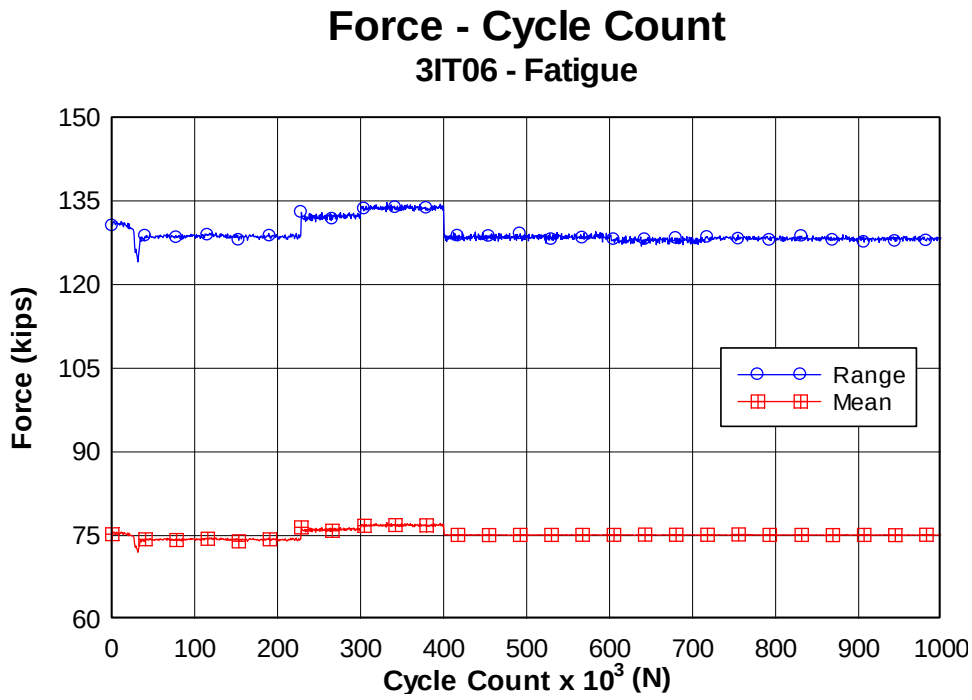
Force - Cycle Count
3IT06 - Fatigue
Force (kips)
150
135
120
105
90
75
60
0
100
200
300
400
500
600
700
800
900
1000
Cycle Count x 10^3 (N)
Range
Mean

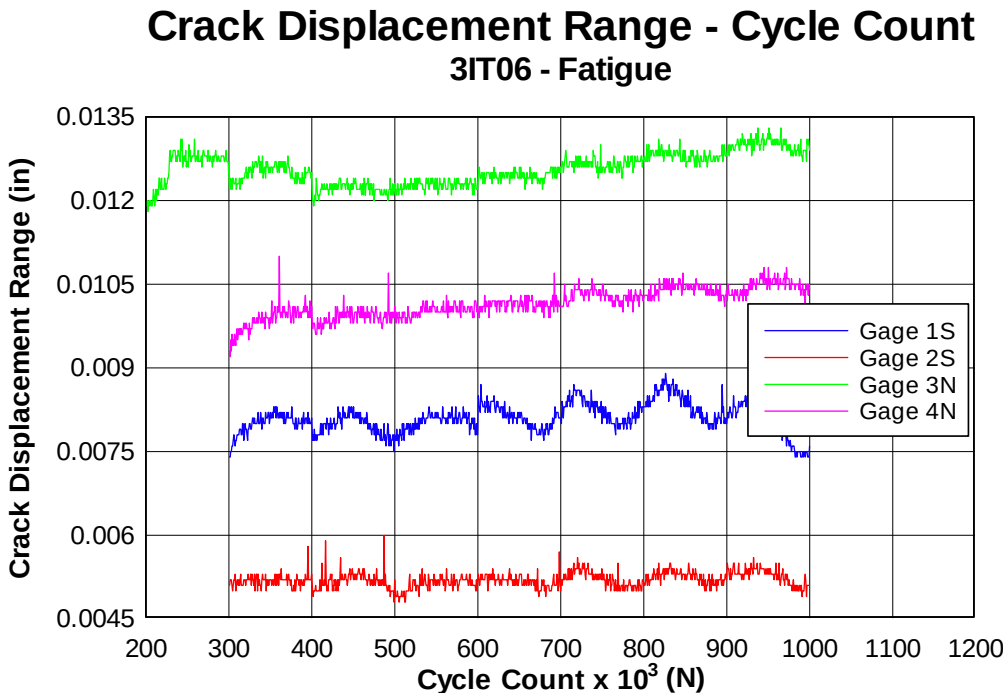
Crack Displacement Range - Cycle Count
3IT06 - Fatigue
Crack Displacement Range (in)
0.0135
0.012
0.0105
0.009
0.0075
0.006
0.0045
200
300
400
500
600
700
800
900
1000
1100
1200
Cycle Count x 10^3 (N)
Gage 1S
Gage 2S
Gage 3N
Gage 4N

Flexural Strains - Cycle count
3IT06 - Fatigue
Detail Locations

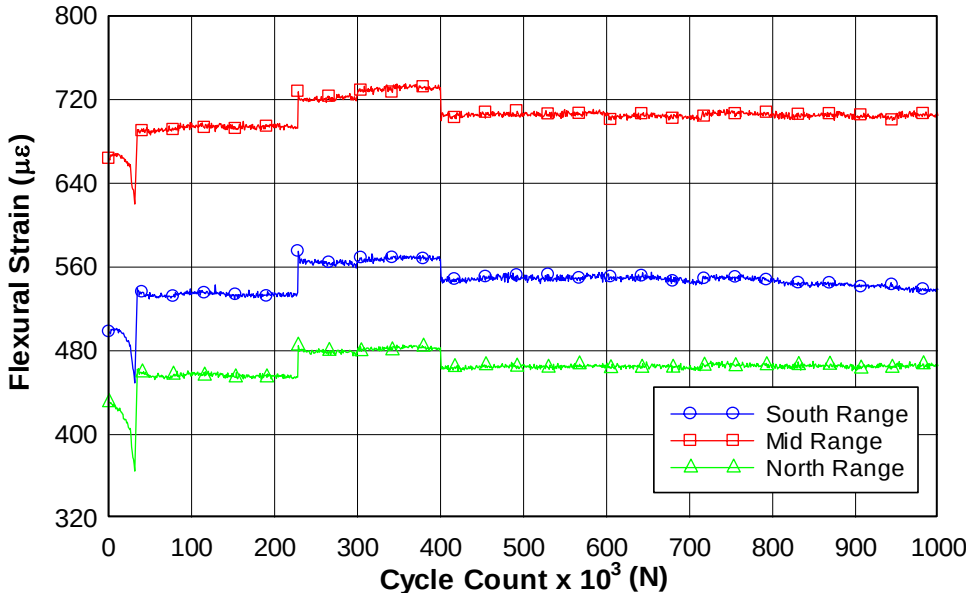

Stirrup Strain Range - Cycle Count
3IT06 - Fatigue
North End

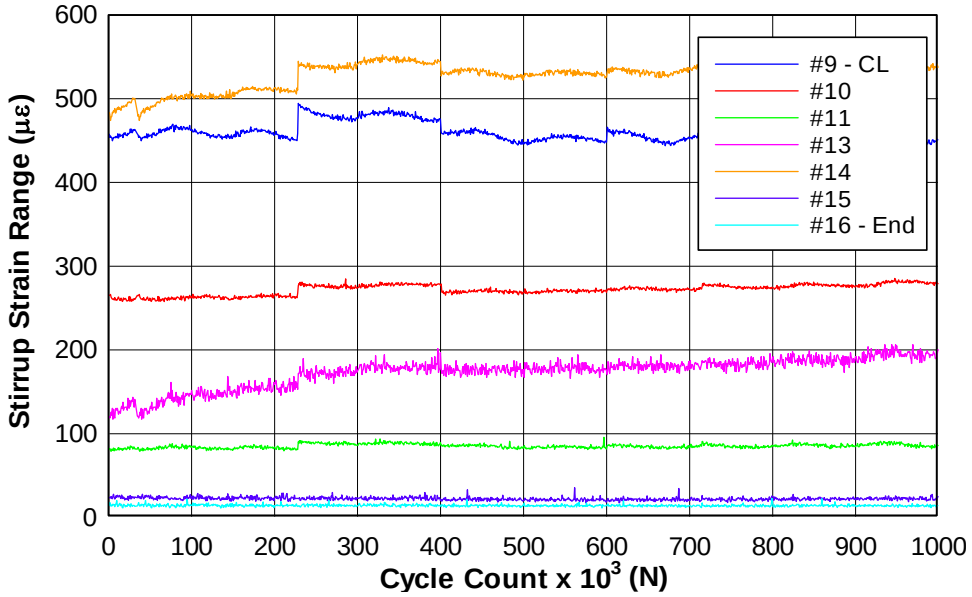

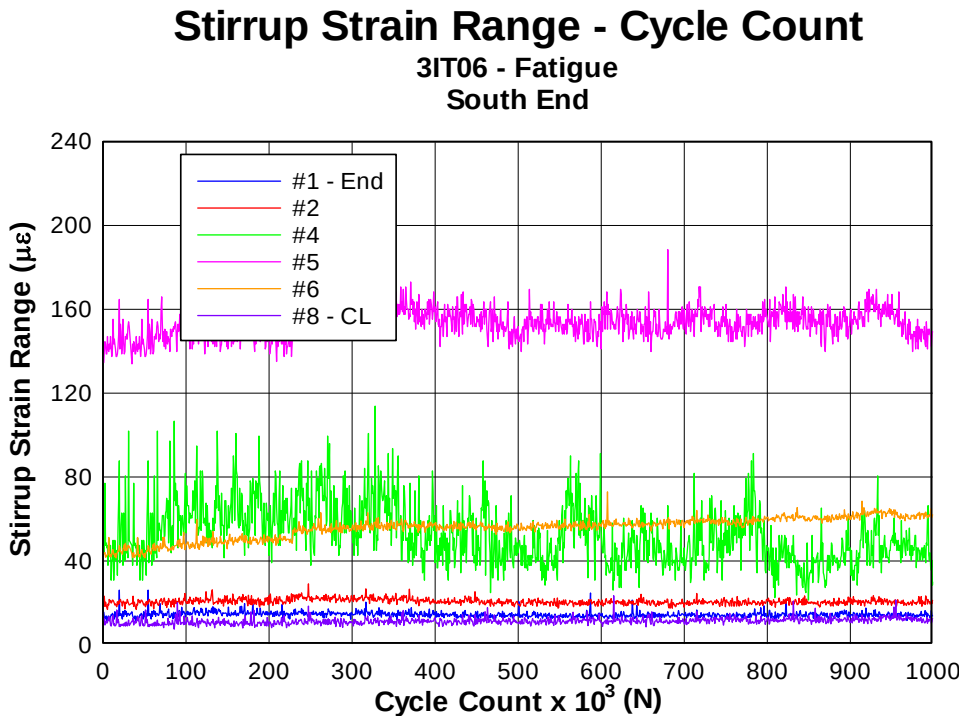
Stirrup Strain Range - Cycle Count
3IT06 - Fatigue
South End
Stirrup Strain Range (με)
Cycle Count x 10^3 (N)
#1 - End
#2
#4
#5
#6
#8 - CL
0
40
80
120
160
200
240
0
100
200
300
400
500
600
700
800
900
1000

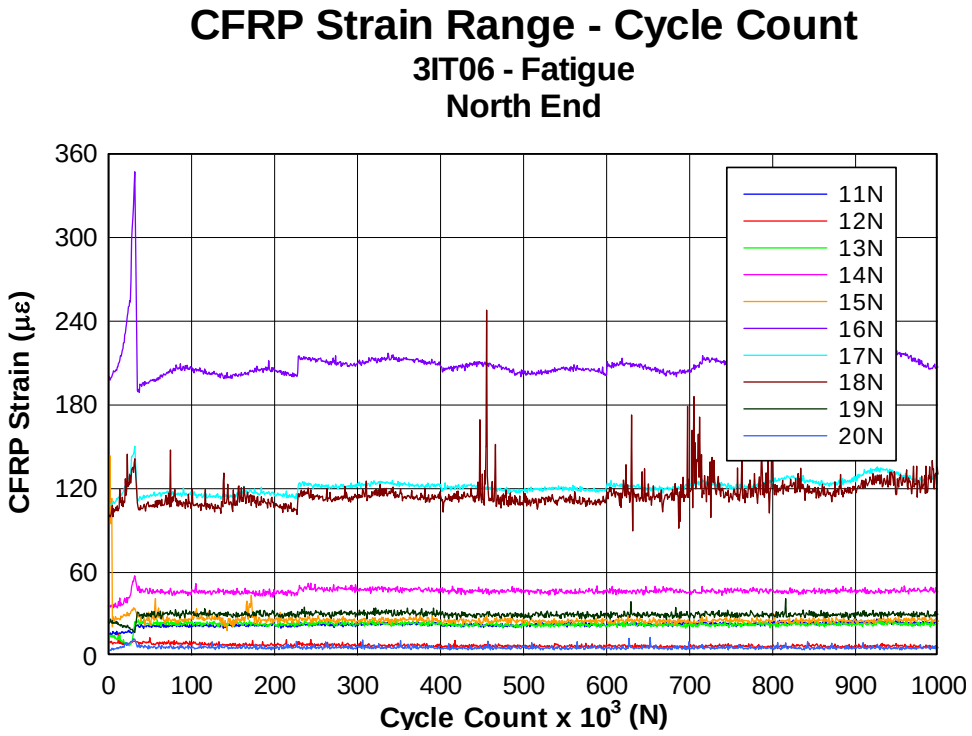
CFRP Strain Range - Cycle Count
3IT06 - Fatigue
North End
CFRP Strain (με)
Cycle Count x 10^3 (N)
11N
12N
13N
14N
15N
16N
17N
18N
19N
20N
0
60
120
180
240
300
360
0
100
200
300
400
500
600
700
800
900
1000

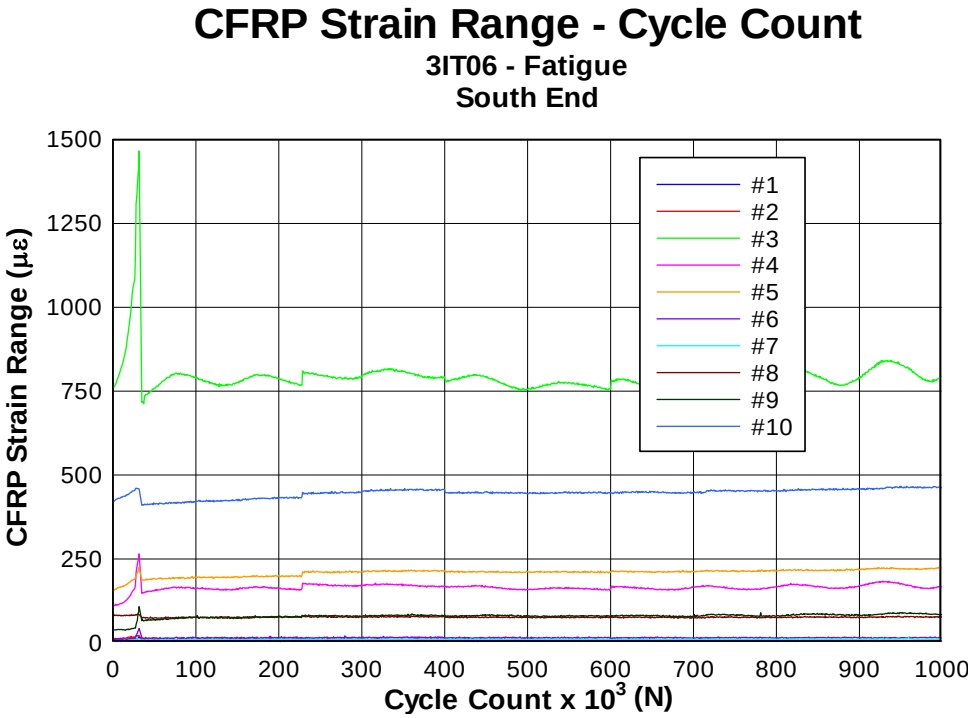
CFRP Strain Range - Cycle Count
3IT06 - Fatigue
South End
CFRP Strain Range (με)
1500
1250
1000
750
500
250
0
0
100
200
300
400
500
600
700
800
900
1000
Cycle Count x 10^3 (N)
#1
#2
#3
#4
#5
#6
#7
#8
#9
#10

CAST 4 – SPECIMEN 4IT07

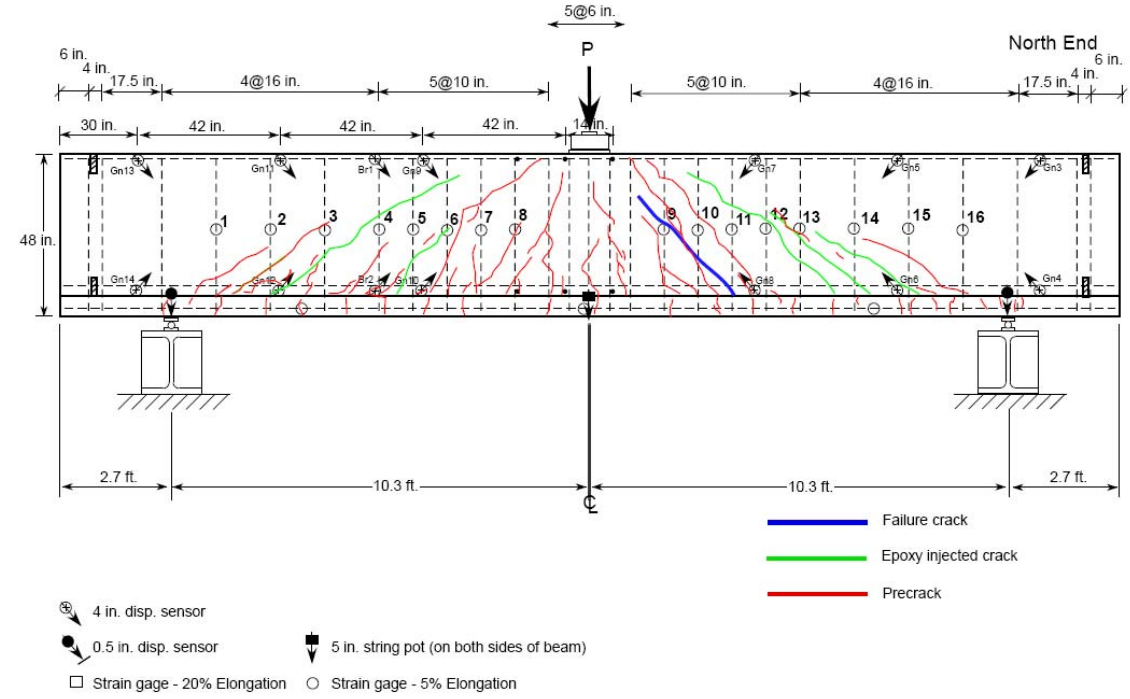

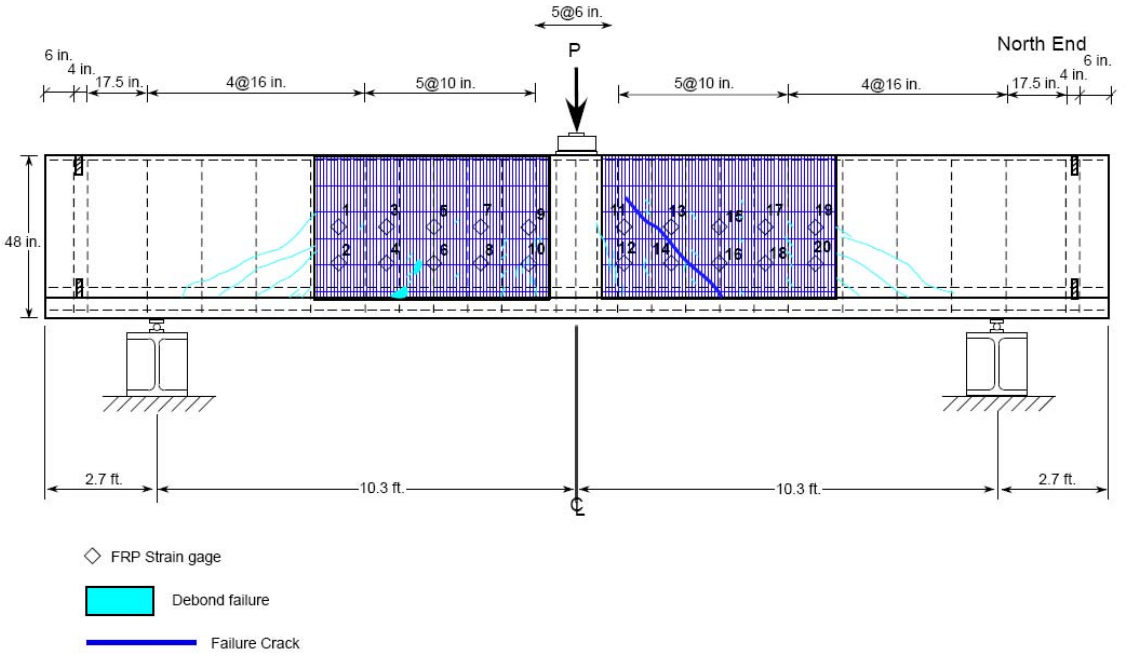

Cast 4 - Specimen 7
Negative Bending (IT-Beam)
East Face of Specimen

SPECIMEN 4IT07 – PRECRACK LOAD PLOTS

Force - Midspan Displacement

4IT07 - Precrack

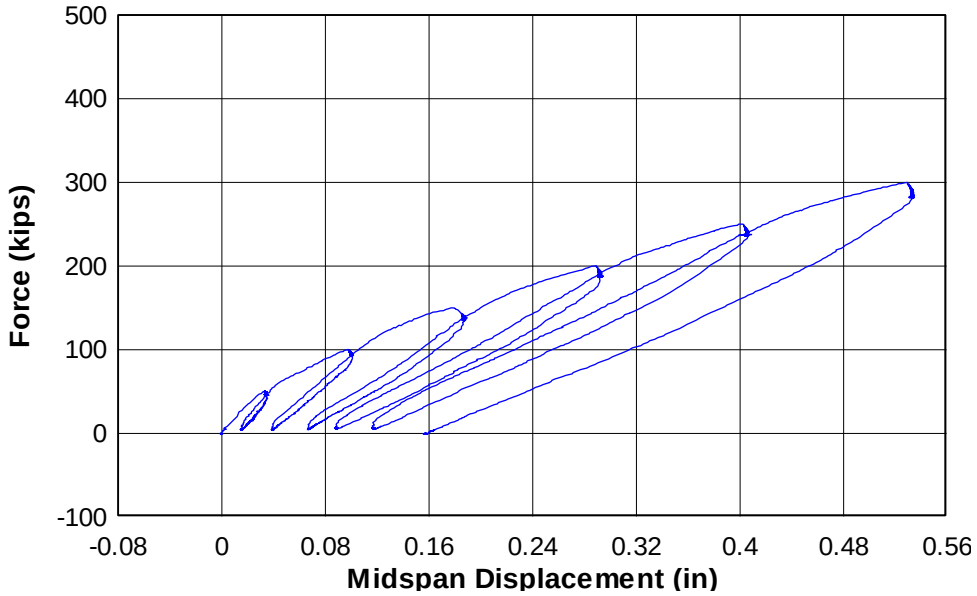

Force - Flexural Reinforcement Strain

4IT07 - Precrack
Detail Locations

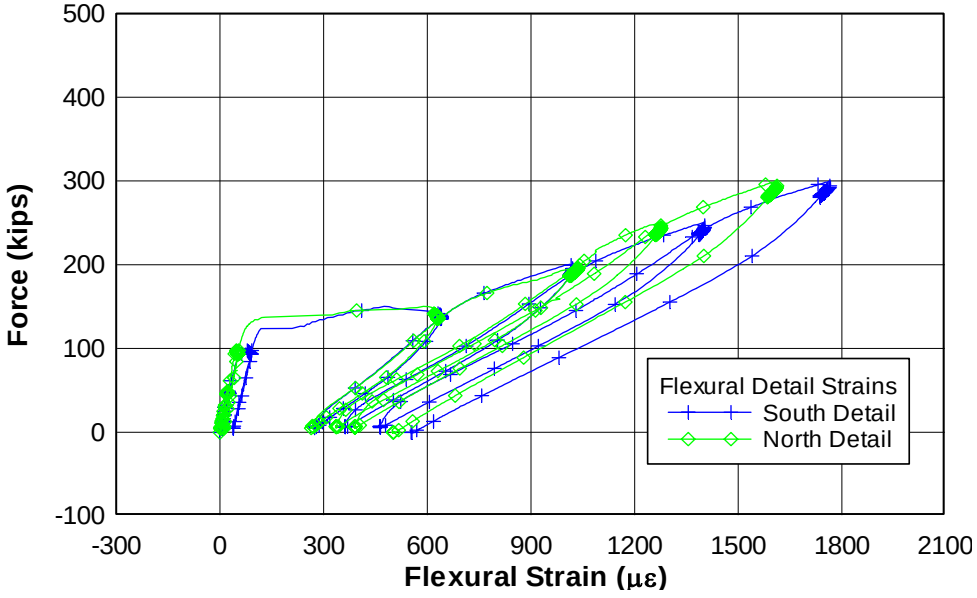

Force - Diagonal Displacement
4IT07 - Precrack
North End

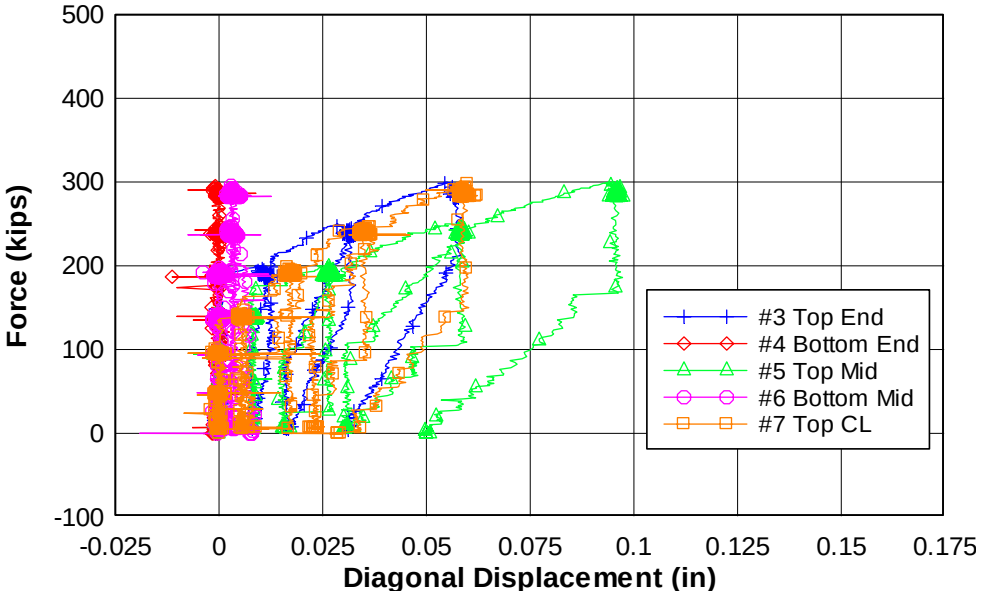

Force - Diagonal Displacement
4IT07 - Precrack
South End

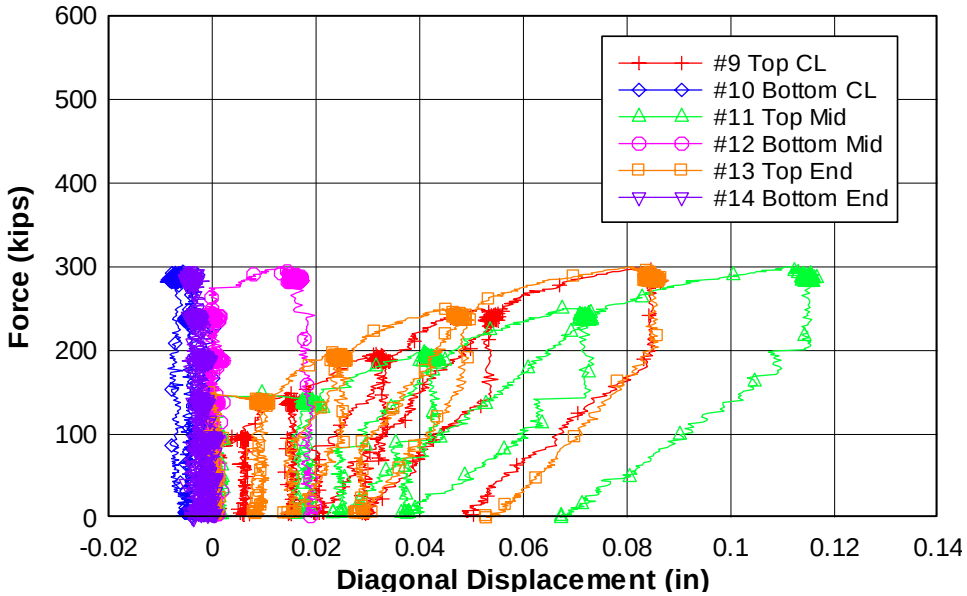

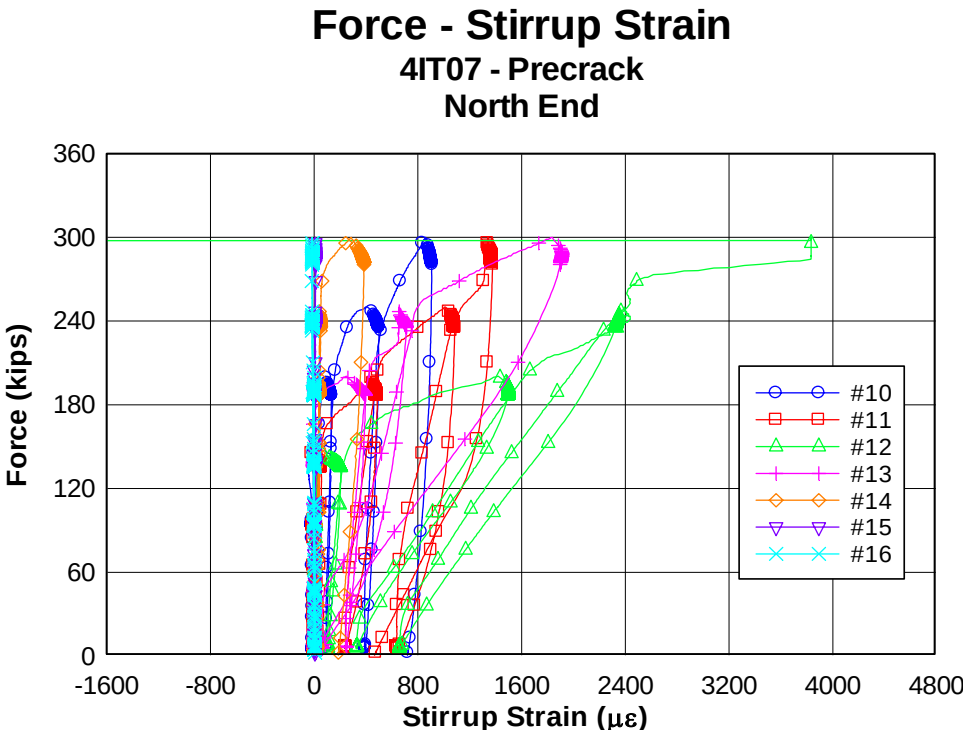
Force - Stirrup Strain
4IT07 - Precrack
North End
Force (kips)
Stirrup Strain (με)
360
300
240
180
120
60
0
-1600
-800
0
800
1600
2400
3200
4000
4800
#10
#11
#12
#13
#14
#15
#16

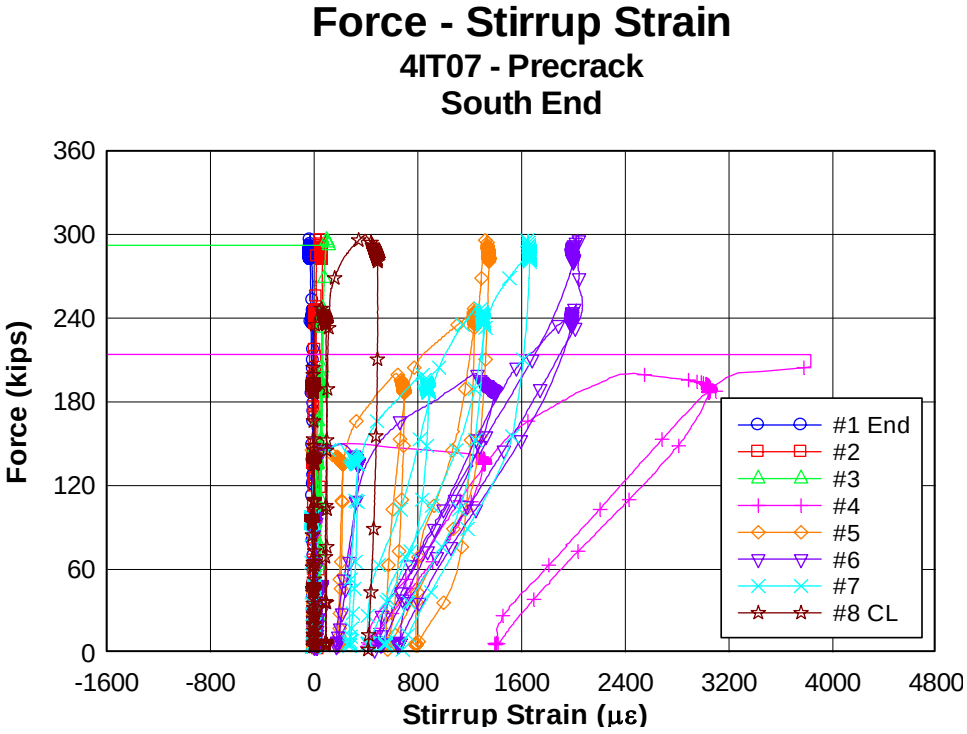
Force - Stirrup Strain
4IT07 - Precrack
South End
Force (kips)
Stirrup Strain (με)
360
300
240
180
120
60
0
-1600
-800
0
800
1600
2400
3200
4000
4800
#1 End
#2
#3
#4
#5
#6
#7
#8 CL

SPECIMEN 4IT07 – FAILURE LOAD PLOTS

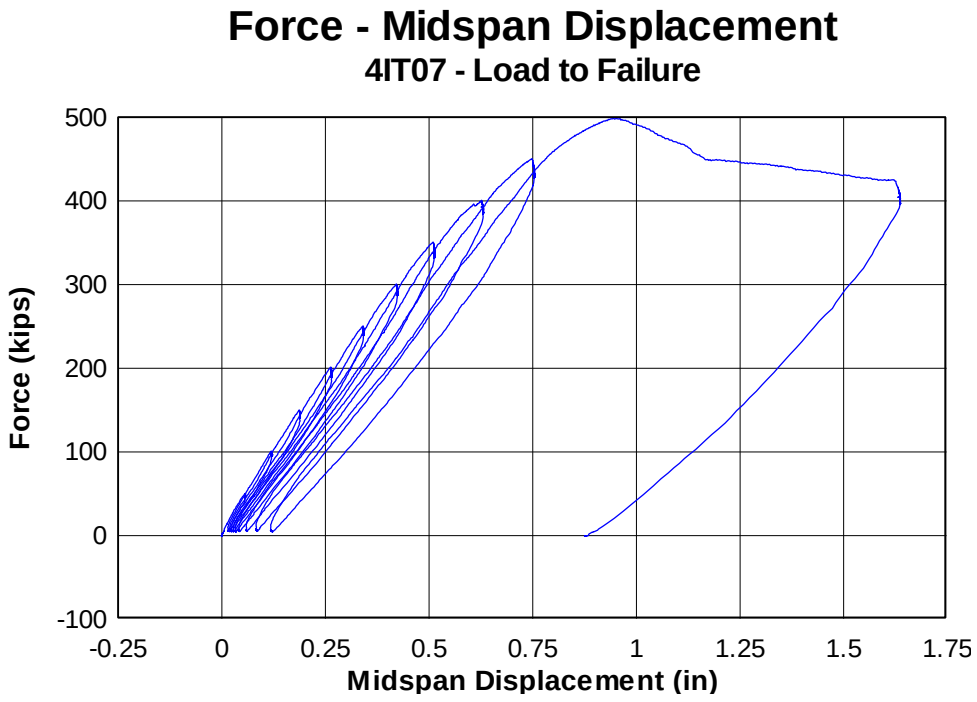
Force - Midspan Displacement
4IT07 - Load to Failure
Force (kips)
500
400
300
200
100
0
-100
-0.25
0
0.25
0.5
0.75
1
1.25
1.5
1.75
Midspan Displacement (in)

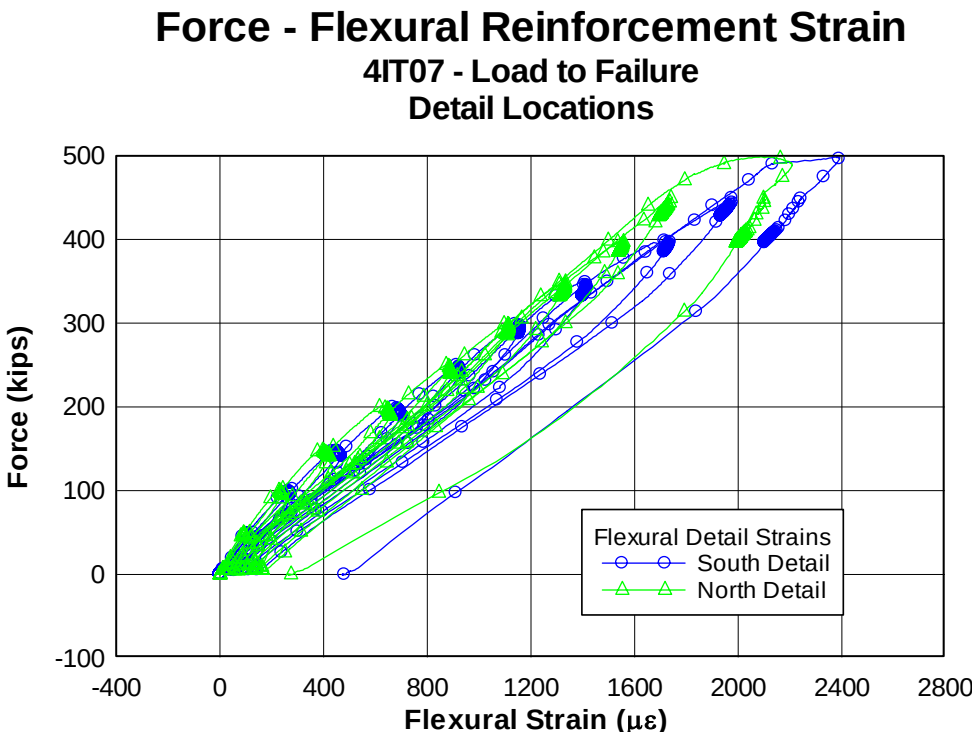
Force - Flexural Reinforcement Strain
4IT07 - Load to Failure
Detail Locations
Force (kips)
500
400
300
200
100
0
-100
-400
0
400
800
1200
1600
2000
2400
2800
Flexural Strain (με)
Flexural Detail Strains
South Detail
North Detail

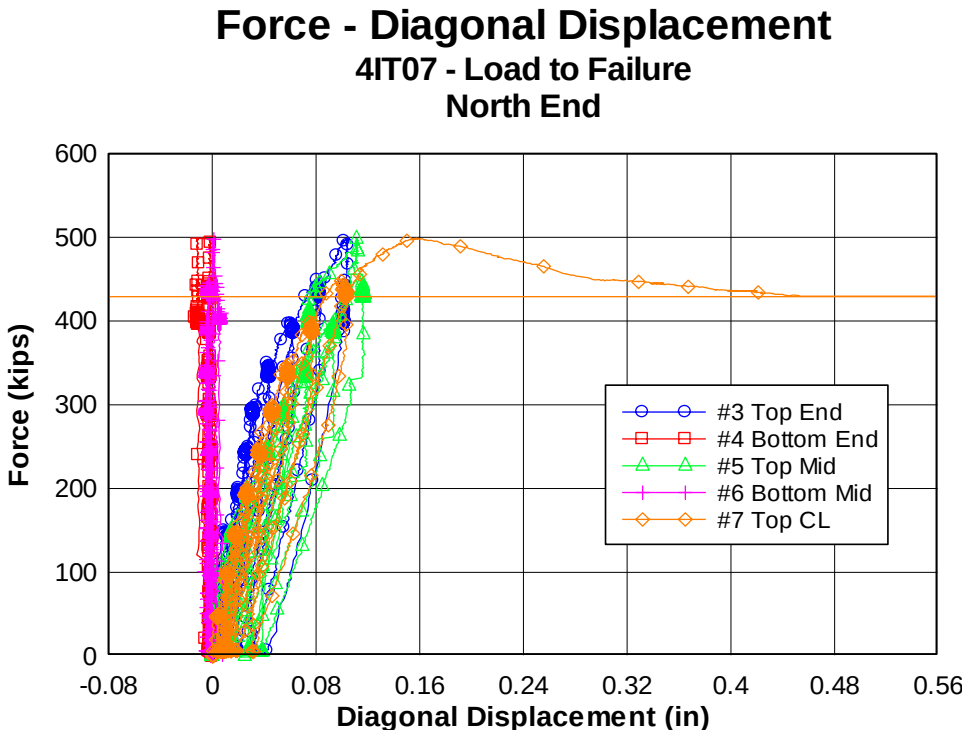
Force - Diagonal Displacement
4IT07 - Load to Failure
North End
Force (kips)
600
500
400
300
200
100
0
-0.08
0
0.08
0.16
0.24
0.32
0.4
0.48
0.56
Diagonal Displacement (in)
#3 Top End
#4 Bottom End
#5 Top Mid
#6 Bottom Mid
#7 Top CL

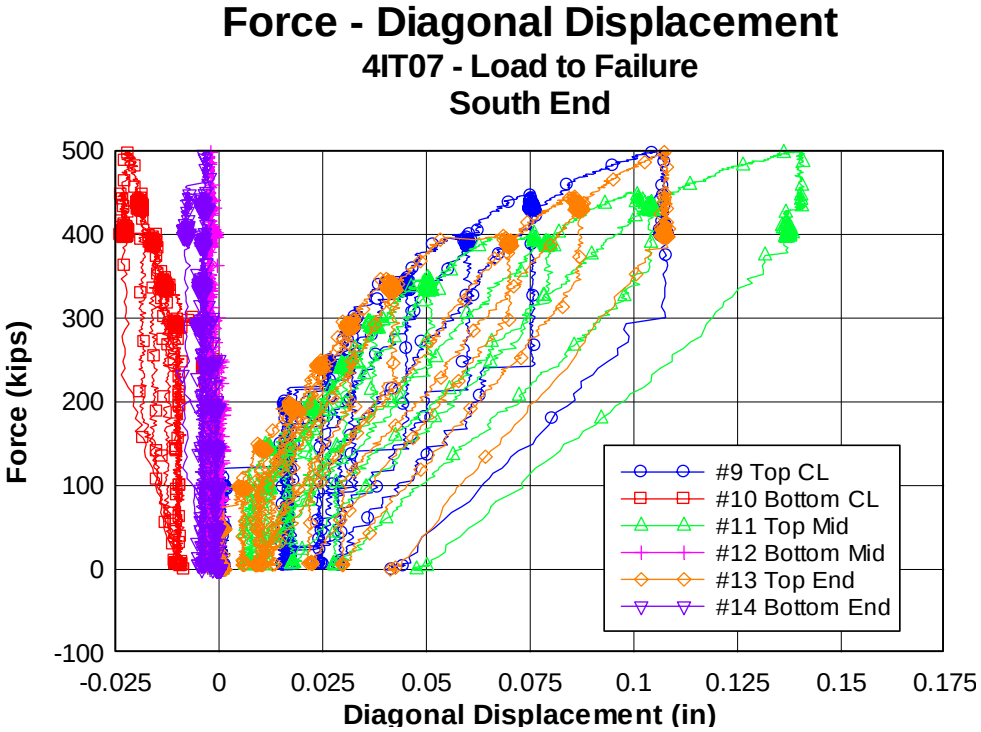
Force - Diagonal Displacement
4IT07 - Load to Failure
South End
Force (kips)
500
400
300
200
100
0
-100
-0.025
0
0.025
0.05
0.075
0.1
0.125
0.15
0.175
Diagonal Displacement (in)
#9 Top CL
#10 Bottom CL
#11 Top Mid
#12 Bottom Mid
#13 Top End
#14 Bottom End

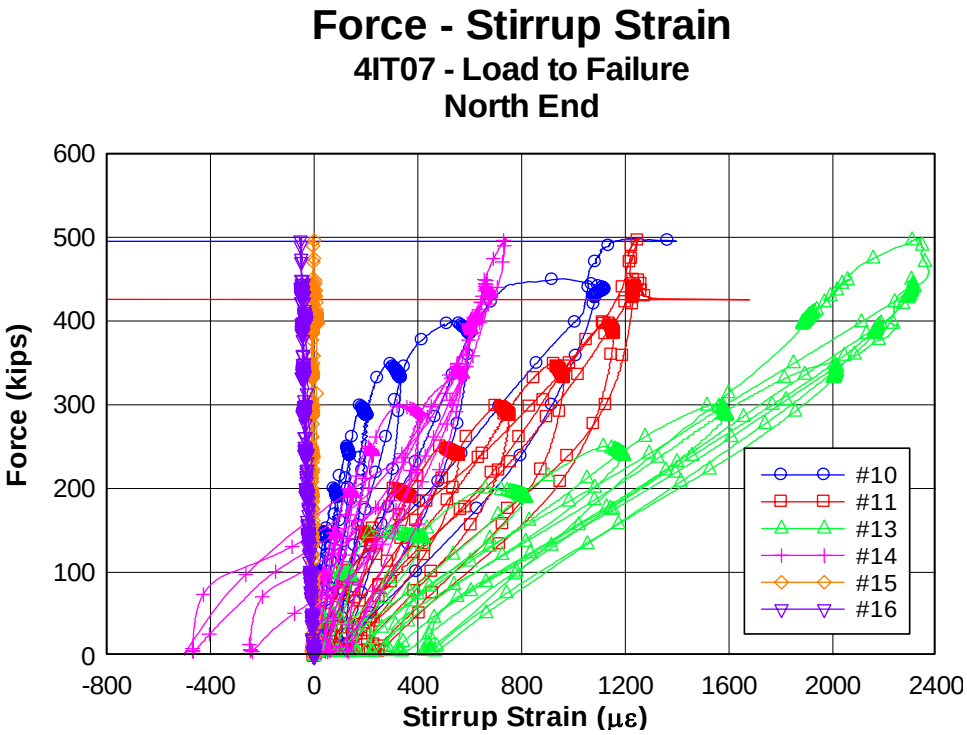
Force - Stirrup Strain
4IT07 - Load to Failure
North End
Force (kips)
Stirrup Strain (με)
600
500
400
300
200
100
0
-800
-400
0
400
800
1200
1600
2000
2400
#10
#11
#13
#14
#15
#16

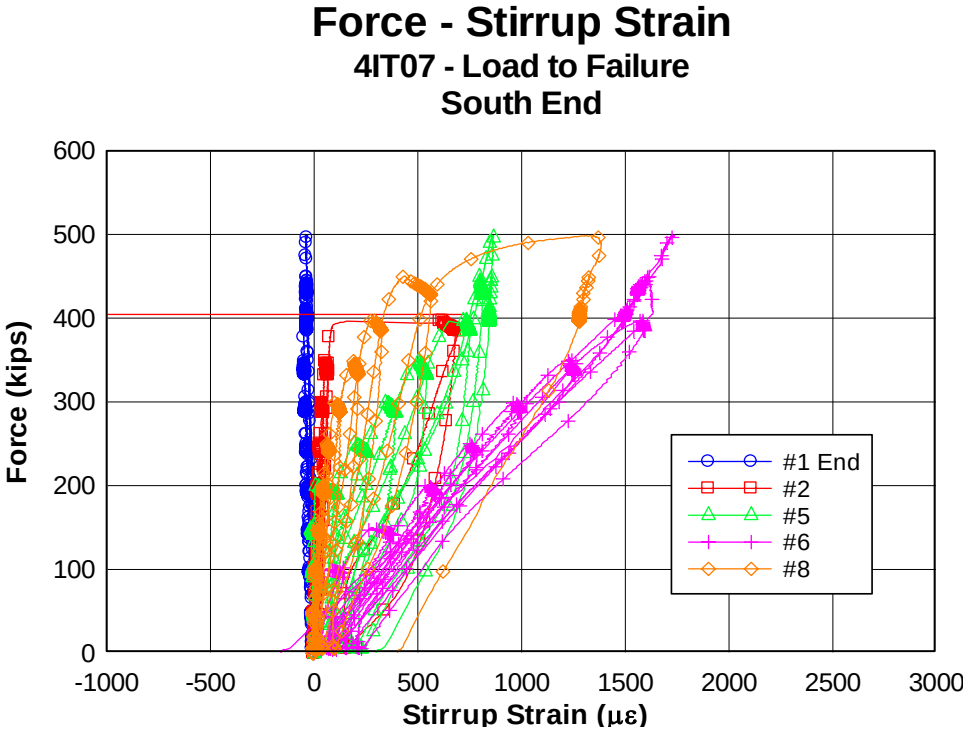
Force - Stirrup Strain
4IT07 - Load to Failure
South End
Force (kips)
Stirrup Strain (με)
600
500
400
300
200
100
0
-1000
-500
0
500
1000
1500
2000
2500
3000
#1 End
#2
#5
#6
#8

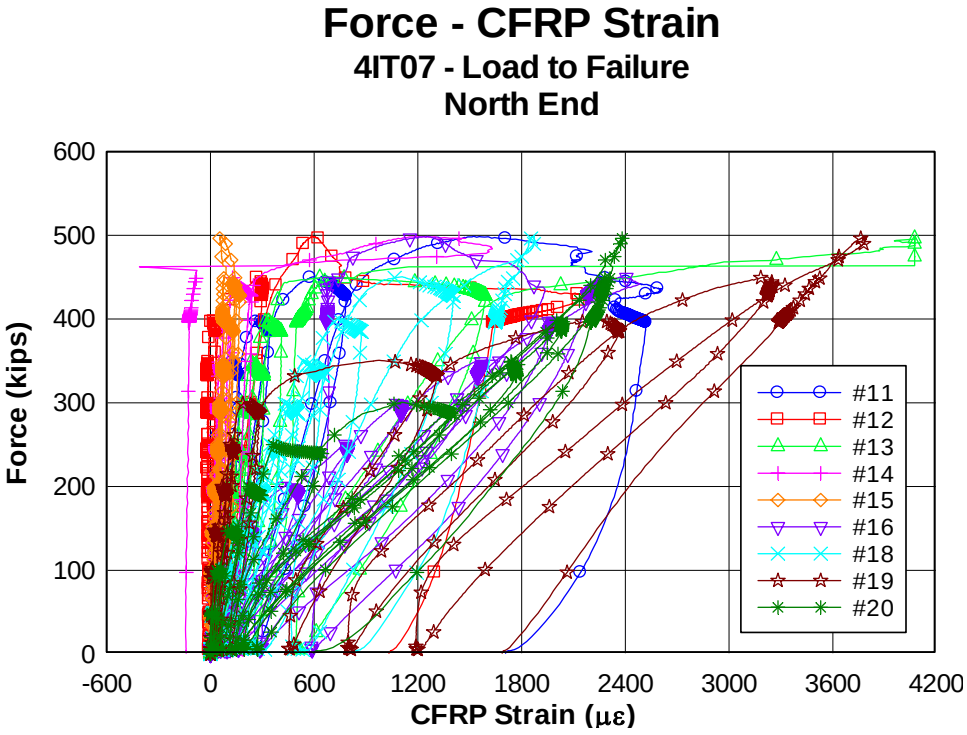
Force - CFRP Strain
4IT07 - Load to Failure
North End
Force (kips)
CFRP Strain (με)
600
500
400
300
200
100
0
-600
0
600
1200
1800
2400
3000
3600
4200
#11
#12
#13
#14
#15
#16
#18
#19
#20

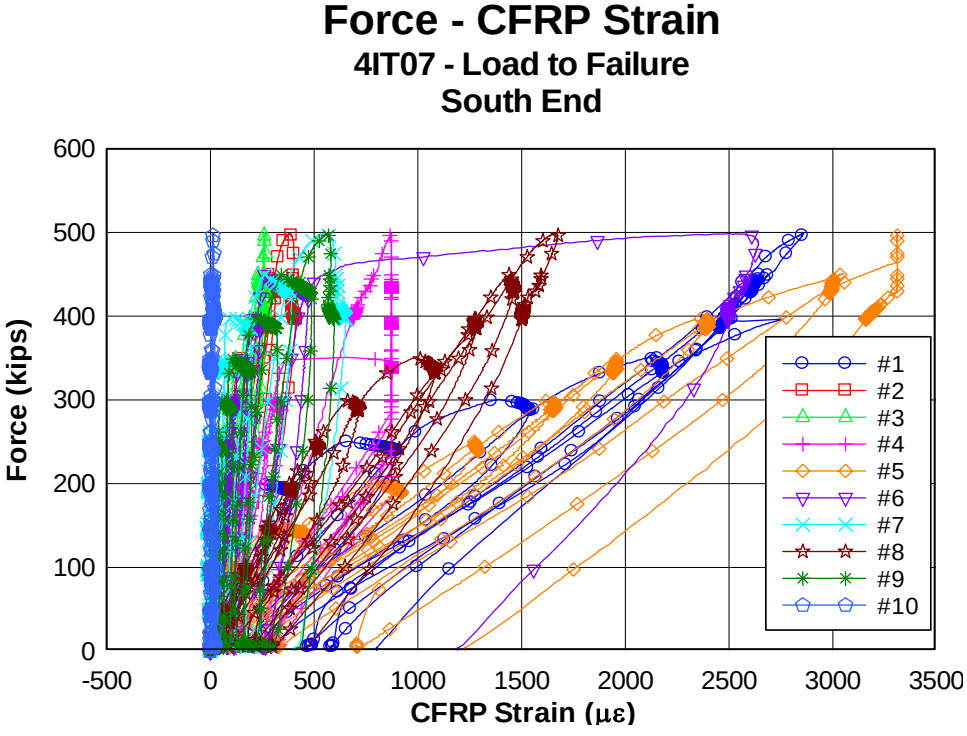
Force - CFRP Strain
4IT07 - Load to Failure
South End
Force (kips)
CFRP Strain (με)
600
500
400
300
200
100
0
-500
0
500
1000
1500
2000
2500
3000
3500
#1
#2
#3
#4
#5
#6
#7
#8
#9
#10

CAST 4 – SPECIMEN 4IT08

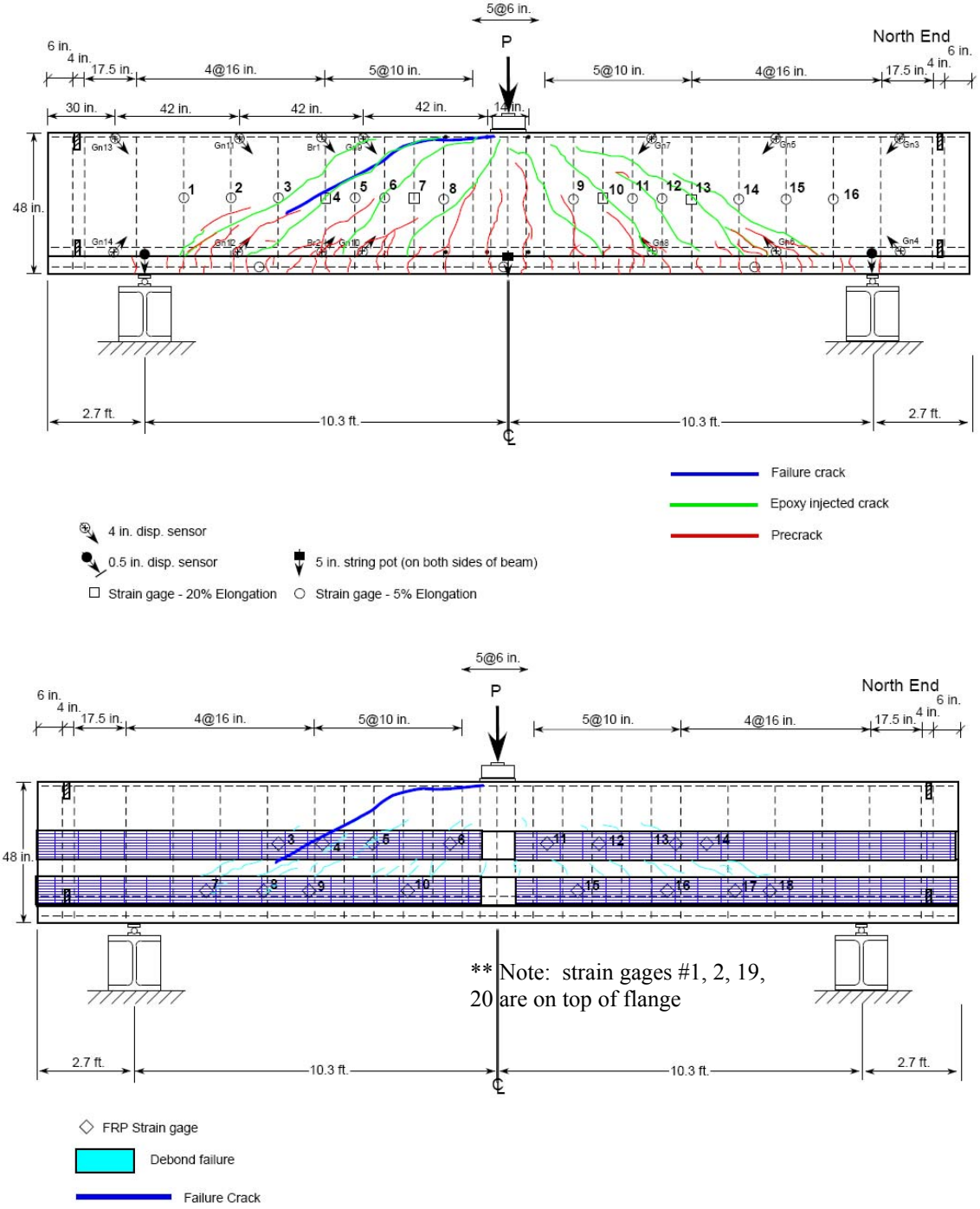

Cast 4 - Specimen 8
Negative Bending (IT-Beam)
East Face of Specimen

SPECIMEN 4IT08 – PRECRACK LOAD PLOTS

Force - Midspan Displacement

4IT08 - Precrack

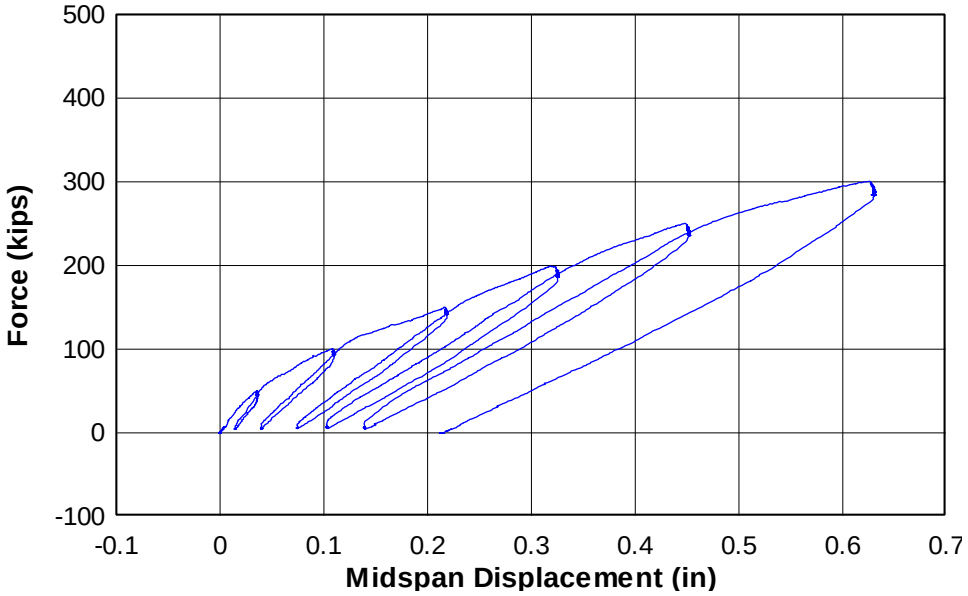

Force - Flexural Reinforcement Strain

4IT08 - Precrack
Detail Locations

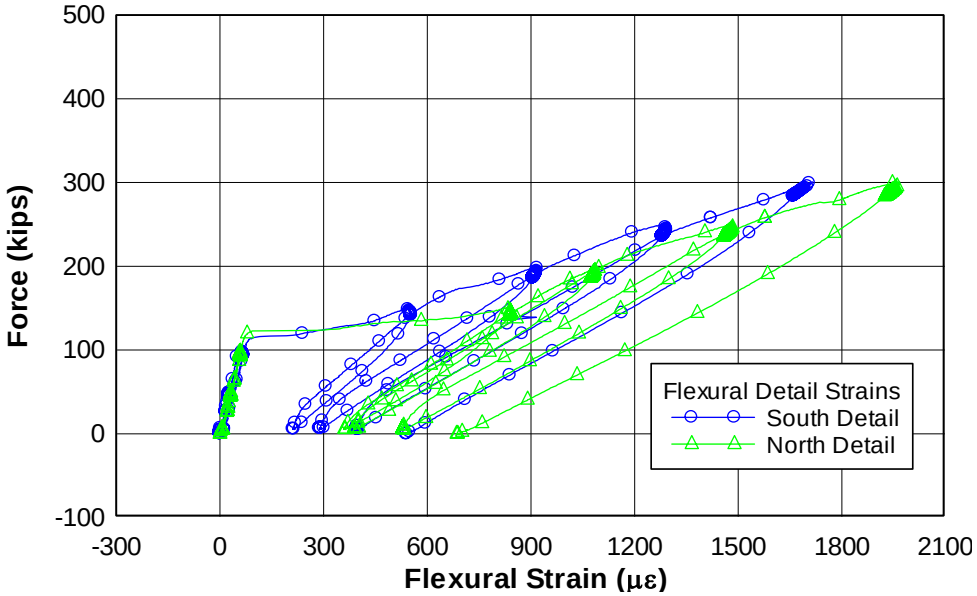

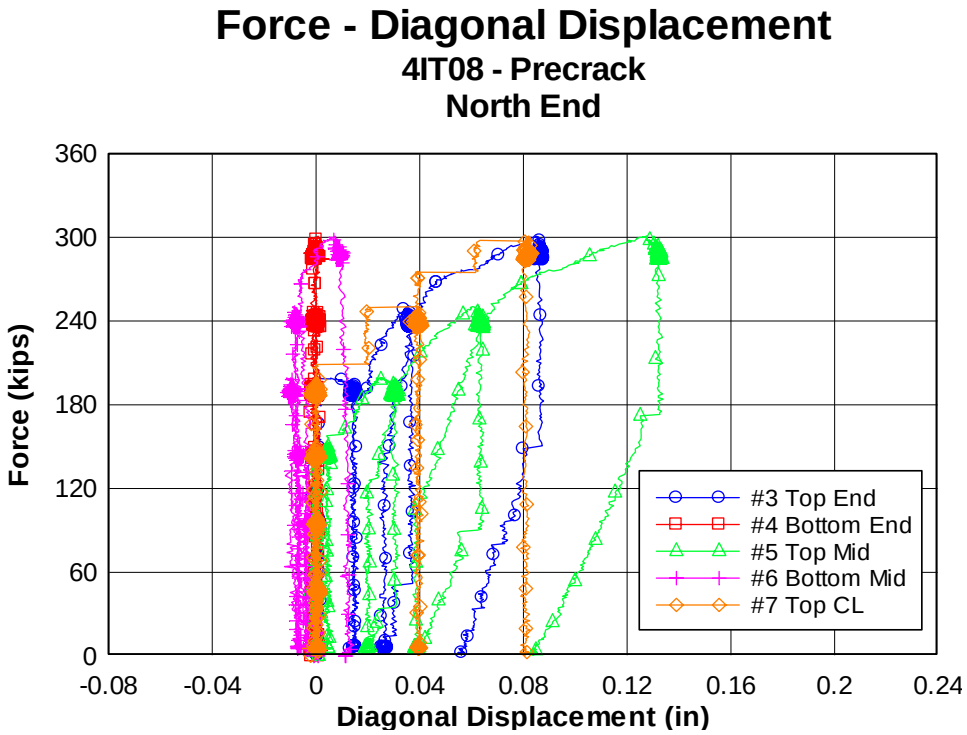
Force - Diagonal Displacement
4IT08 - Precrack
North End
Force (kips)
360
300
240
180
120
60
0
-0.08
-0.04
0
0.04
0.08
0.12
0.16
0.2
0.24
Diagonal Displacement (in)
#3 Top End
#4 Bottom End
#5 Top Mid
#6 Bottom Mid
#7 Top CL

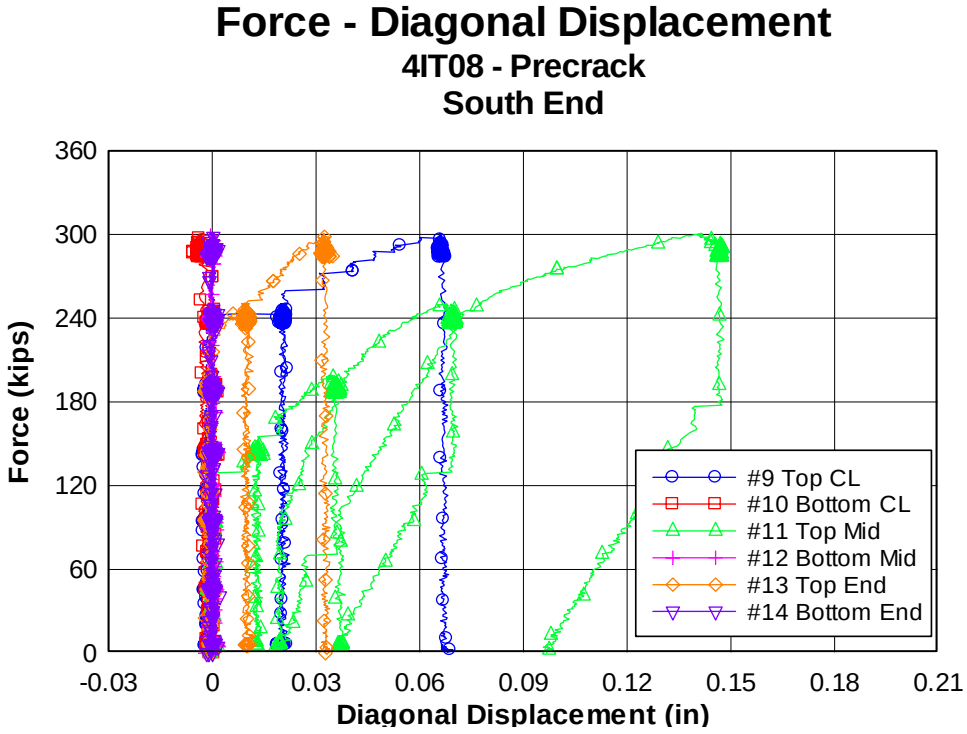
Force - Diagonal Displacement
4IT08 - Precrack
South End
Force (kips)
360
300
240
180
120
60
0
-0.03
0
0.03
0.06
0.09
0.12
0.15
0.18
0.21
Diagonal Displacement (in)
#9 Top CL
#10 Bottom CL
#11 Top Mid
#12 Bottom Mid
#13 Top End
#14 Bottom End

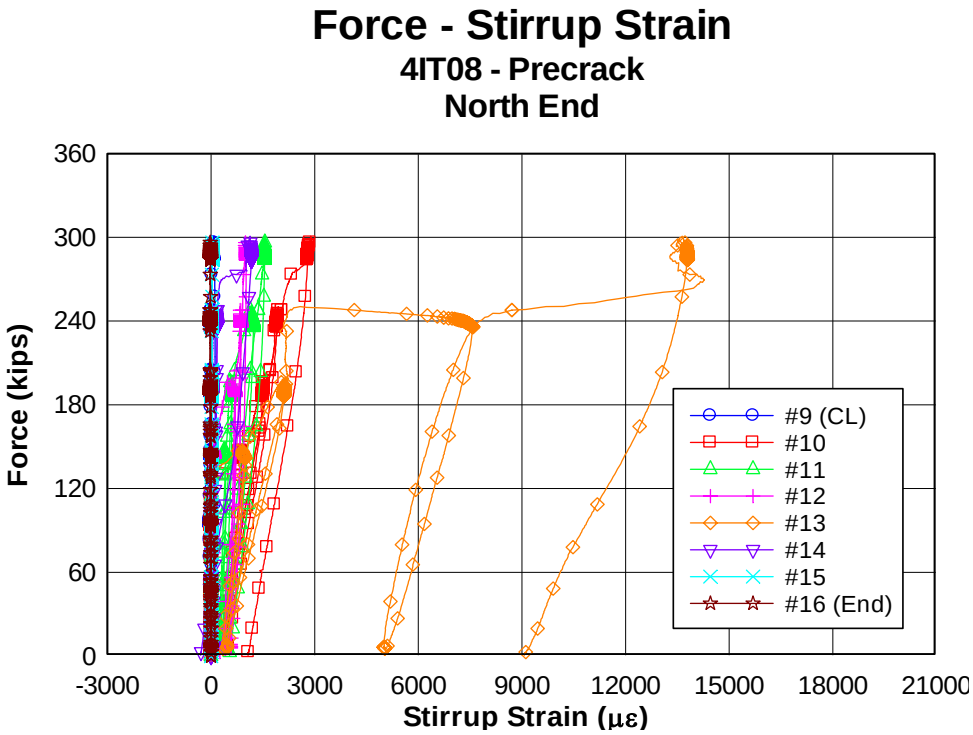
Force - Stirrup Strain
4IT08 - Precrack
North End
Force (kips)
Stirrup Strain (με)
360
300
240
180
120
60
0
-3000
0
3000
6000
9000
12000
15000
18000
21000
#9 (CL)
#10
#11
#12
#13
#14
#15
#16 (End)

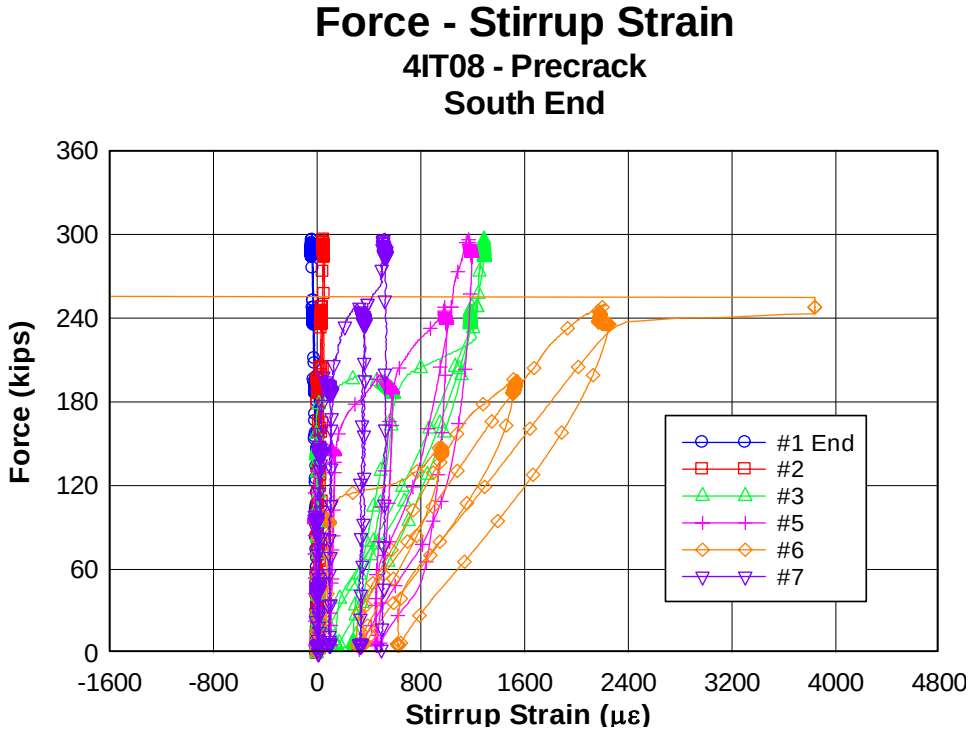
Force - Stirrup Strain
4IT08 - Precrack
South End
Force (kips)
Stirrup Strain (με)
360
300
240
180
120
60
0
-1600
-800
0
800
1600
2400
3200
4000
4800
#1 End
#2
#3
#5
#6
#7

SPECIMEN 4IT08 – FAILURE LOAD PLOTS

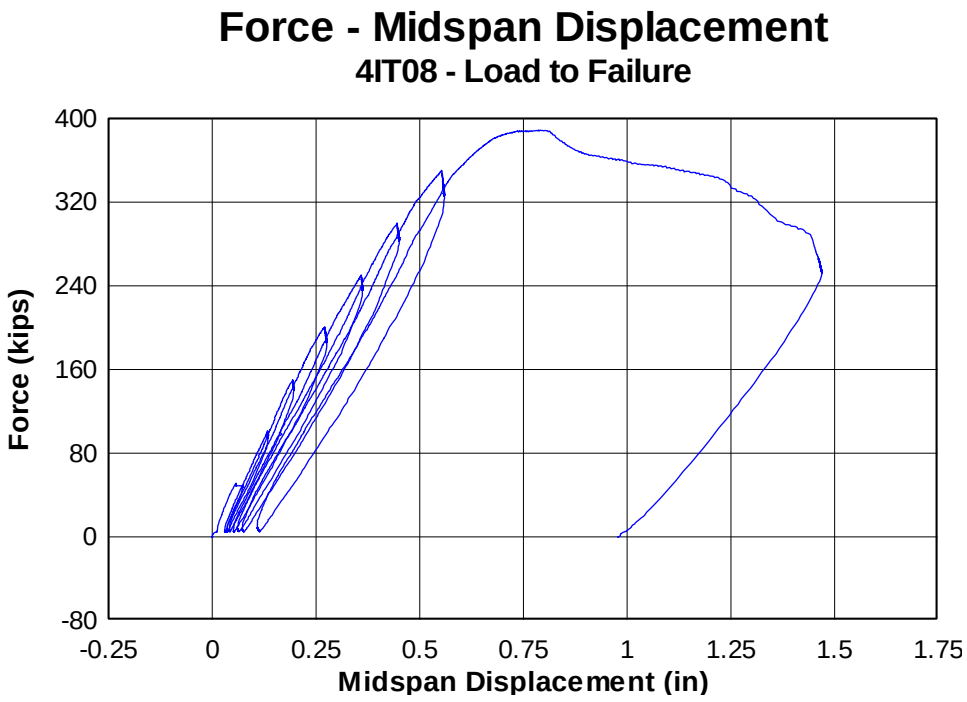
Force - Midspan Displacement
4IT08 - Load to Failure
Force (kips)
400
320
240
160
80
0
-80
-0.25
0
0.25
0.5
0.75
1
1.25
1.5
1.75
Midspan Displacement (in)

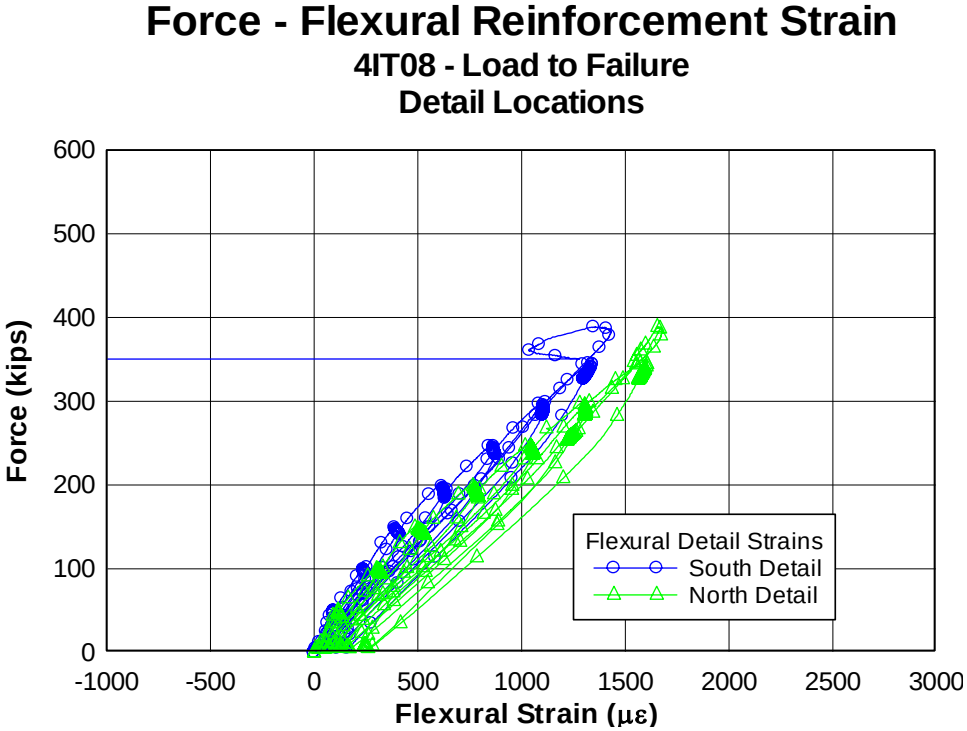
Force - Flexural Reinforcement Strain
4IT08 - Load to Failure
Detail Locations
Force (kips)
600
500
400
300
200
100
0
-1000
-500
0
500
1000
1500
2000
2500
3000
Flexural Strain (με)
Flexural Detail Strains
South Detail
North Detail

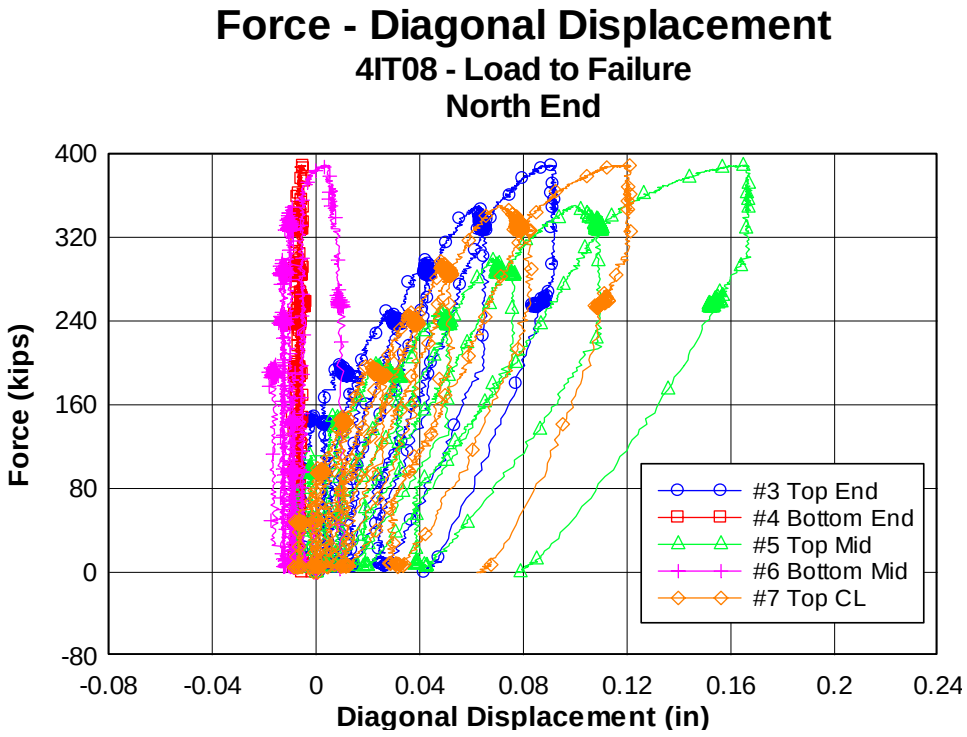
Force - Diagonal Displacement
4IT08 - Load to Failure
North End
Force (kips)
400
320
240
160
80
0
-80
-0.08
-0.04
0
0.04
0.08
0.12
0.16
0.2
0.24
Diagonal Displacement (in)
#3 Top End
#4 Bottom End
#5 Top Mid
#6 Bottom Mid
#7 Top CL

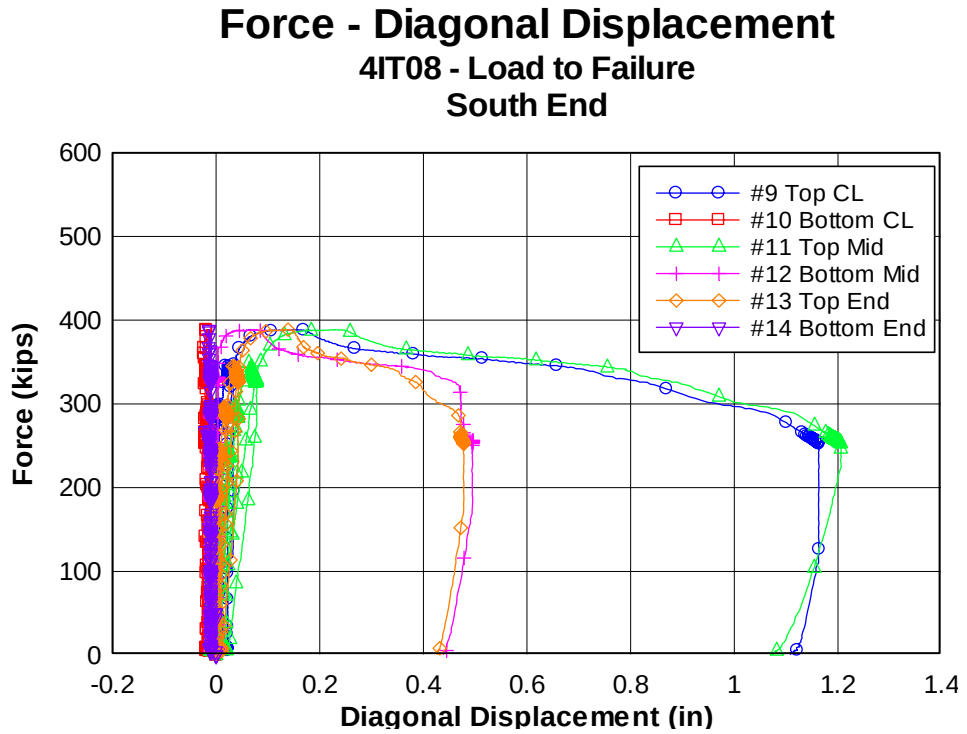
Force - Diagonal Displacement
4IT08 - Load to Failure
South End
Force (kips)
600
500
400
300
200
100
0
-0.2
0
0.2
0.4
0.6
0.8
1
1.2
1.4
Diagonal Displacement (in)
#9 Top CL
#10 Bottom CL
#11 Top Mid
#12 Bottom Mid
#13 Top End
#14 Bottom End

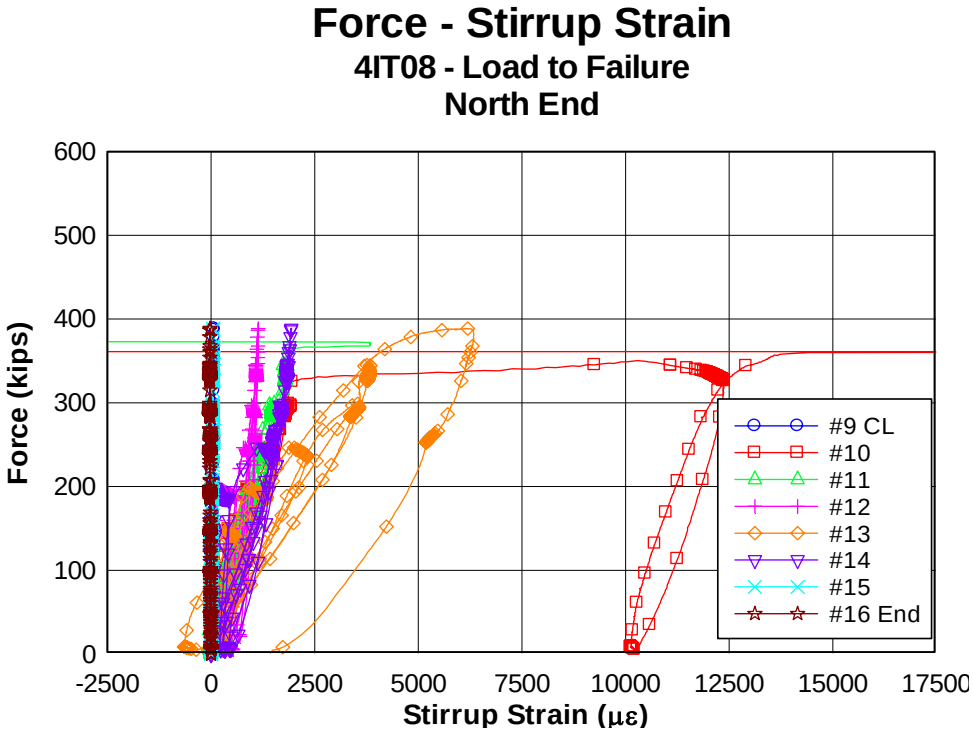
Force - Stirrup Strain
4IT08 - Load to Failure
North End
Force (kips)
Stirrup Strain (με)
600
500
400
300
200
100
0
-2500
0
2500
5000
7500
10000
12500
15000
17500
#9 CL
#10
#11
#12
#13
#14
#15
#16 End

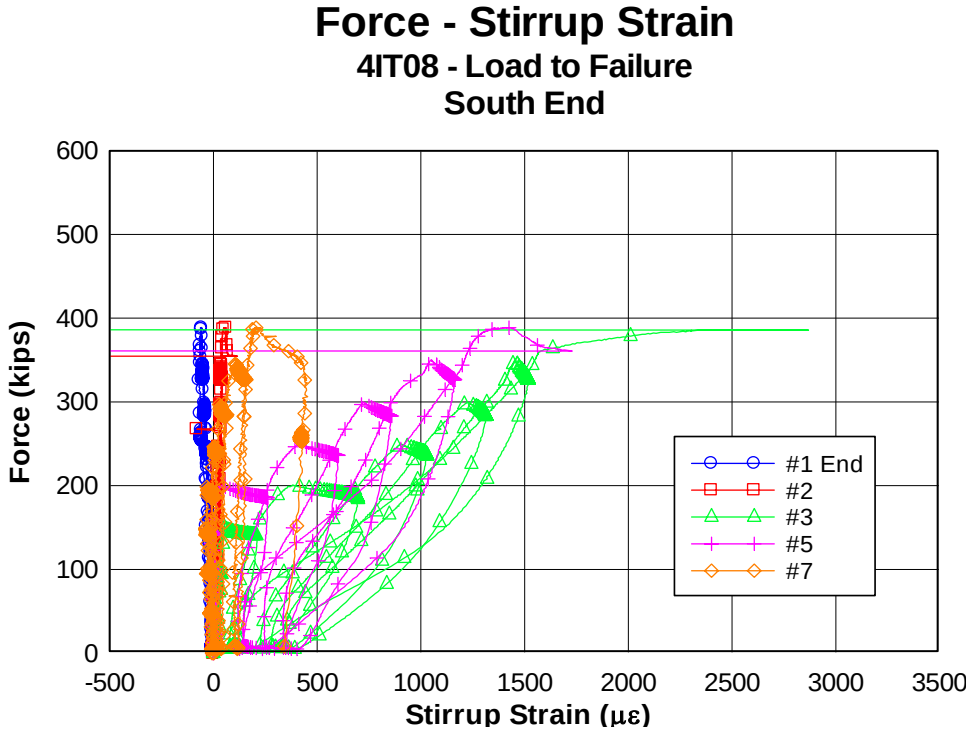
Force - Stirrup Strain
4IT08 - Load to Failure
South End
Force (kips)
Stirrup Strain (με)
600
500
400
300
200
100
0
-500
0
500
1000
1500
2000
2500
3000
3500
#1 End
#2
#3
#5
#7

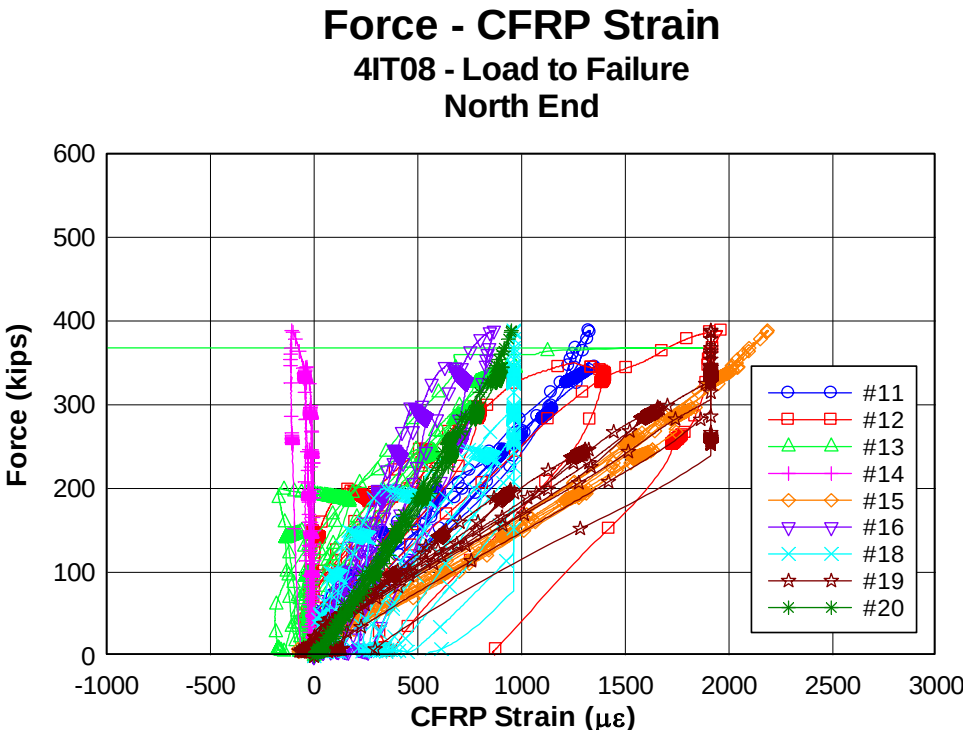
Force - CFRP Strain
4IT08 - Load to Failure
North End
Force (kips)
CFRP Strain (με)
600
500
400
300
200
100
0
-1000
-500
0
500
1000
1500
2000
2500
3000
#11
#12
#13
#14
#15
#16
#18
#19
#20

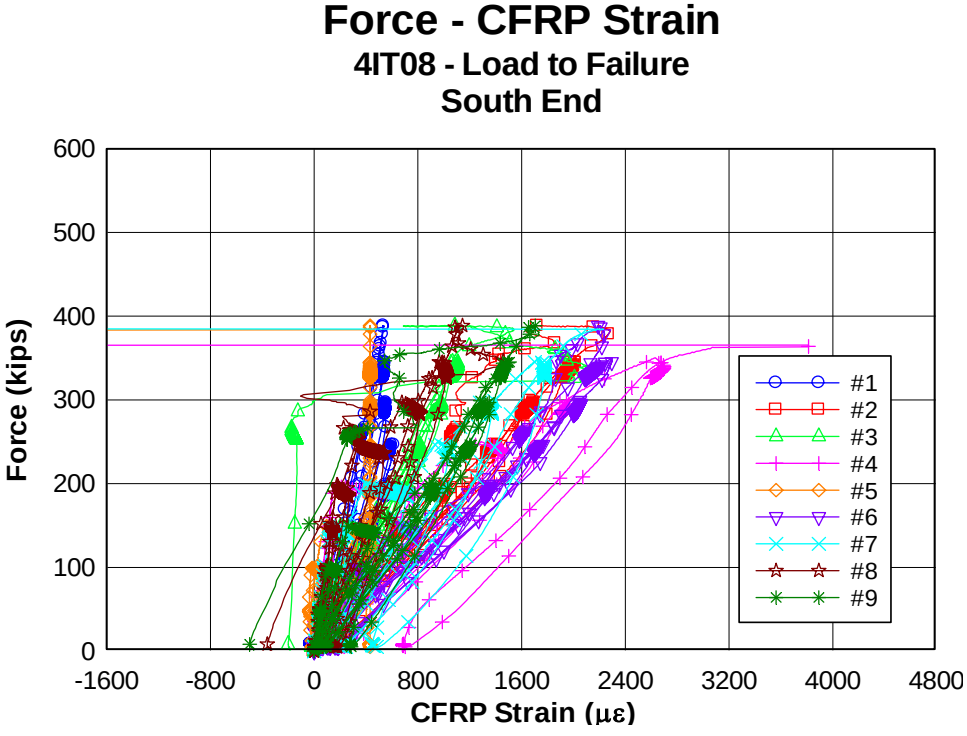
Force - CFRP Strain
4IT08 - Load to Failure
South End
Force (kips)
CFRP Strain (με)
600
500
400
300
200
100
0
-1600
-800
0
800
1600
2400
3200
4000
4800
#1
#2
#3
#4
#5
#6
#7
#8
#9

APPENDIX F: CAPACITY CALCULATIONS PREDICTED BY NATIONAL AND INTERNATIONAL DESIGN METHODS

Capacity Calculations Predicted by National and International Design Methods

Design guides for concrete structures reinforced with FRP are available worldwide. Four codified approaches were applied to each of the test specimens to calculate the strength of the members with the FRP. The four codes considered are: The American Concrete Institute's ACI-440.2R-02 (2004) with the ACI-318-05 (2005); The Canadian Standards Association's CSA S806-02 (2002); the International Federation of Structural Concrete's FIB Bulletin 14 (2001) with the European standard, Eurocode 2, (British Standard, BS EN 2004); and the Japan Society of Civil Engineer's (JSCE) Concrete Engineering Series #41, (2001). One additional approach developed by Monti & Liotta (Italy, 2005) was also applied. A summary follows that compares the predicted capacities with the experimentally measured capacities for the FRP repaired specimens. All partial safety factors were set to 1.0 to provide uniformity of comparisons.

All of the methods calculate capacity as the superposition of the individual resistance components: concrete, steel, and FRP, as:

$$V_n = V_c + V_s + V_f \qquad \text{[1.AppF]}$$

where V_n is the nominal shear resistance, V_c is the concrete contribution to the shear resistance, V_s is the transverse steel contribution to the shear resistance, and V_f is the FRP contribution to the shear resistance.

ACI-440

The American Concrete Institute (ACI) established guidelines for the design of reinforced concrete structures with FRP components in ACI-440 (2004) that are based on limit-states design principles. That document, along with ACI-318 (2005), is used to determine the shear capacity of an RC beam with FRP. All ACI equations presented below use US customary units. The simplified equation for the concrete contribution to shear is computed as:

$$V_c\,(lb) = 2\sqrt{f'_c}\,b_w d \qquad \text{[2.AppF]}$$

where f'_c (psi) is the compressive strength of the concrete (f'_c shall not exceed 10,000 psi), b_w (in.) is the web width of the beam, and d (in.) is the effective depth. It is also permissible to use the more detailed equation for V_c that incorporates the shear-to-moment ratio as well as the longitudinal reinforcing ratio.

The steel contribution to the shear capacity for stirrups perpendicular to the member axis is calculated as:

$$V_s\,(lb) = \frac{A_v f_{v,y} d}{s} \le 8\sqrt{f'_c}\,b_w d \qquad \text{[3.AppF]}$$

where A_v (in.^{2}) is the area of the transverse steel, $f_{v,y}$ (psi) is the yield strength of the transverse steel, d (in.) is the effective depth, and s (in.) is the spacing of the transverse steel.

The FRP contribution to the shear capacity is:

$$V_f\left(lb\right) = \frac{A_{fv} f_{fe} (\sin\alpha + \cos\alpha) d_f}{s_f} \qquad \text{[4.AppF]}$$

where α is the angle of inclination of the FRP stirrups, d_f (in.) is the depth of FRP shear reinforcement as defined in Fig. App.F1, s_f (in.) is the spacing of the FRP strips, and A_{fv} (in.^{2}) is the area of the FRP shear reinforcement and is calculated as:

$$A_{fv} = 2nt_f w_f \qquad \text{[4.1.AppF]}$$

where n is the number of FRP plies, t_f (in.) is the nominal thickness of one ply of the FRP reinforcement, and w_f (in.) is the width of the FRP reinforcing plies;

and f_{fe} (psi) is the effective stress in the FRP (i.e. the stress magnitude at failure) and is calculated as:

$$f_{fe} = \varepsilon_{fe} E_f \qquad \text{[4.2.AppF]}$$

where ε_f (in./in.) is the strain level in the FRP, and is calculated, for bonded u-wraps or face plies as:

$$\varepsilon_{fe} = \kappa_v \varepsilon_{fu} \le 0.004 \qquad \text{[4.2.1.AppF]}$$

where κ_v is the bond dependent coefficient for shear calculated as:

$$\kappa_v = \frac{k_1 k_2 L_e}{468\varepsilon_{fu}} \le 0.75 \qquad \text{[4.2.1.1.AppF]}$$

where k_1 is the modification factor applied to κ_v to account for the concrete strength and is calculated as:

$$k_1 = \left(\frac{f_c^{'}}{4000}\right)^{\frac{2}{3}} \qquad \text{[4.2.1.1a.AppF]}$$

where f'_c (psi) is the specified compressive strength of concrete;

and where k_2 is the modification factor applied to κ_v to account for the wrapping scheme and is calculated as:

$$k_2 = \frac{d_f - L_e}{d_f} \qquad \text{[4.2.1.1b.AppF]}$$

where L_e (in.) is the active bond length of FRP laminate and is calculated as:

$$L_e = \frac{2500}{\left(nt_f E_f\right)^{0.58}} \qquad \text{[4.2.1.1c.AppF]}$$

where E_f (psi) is the tensile modulus of elasticity of FRP.

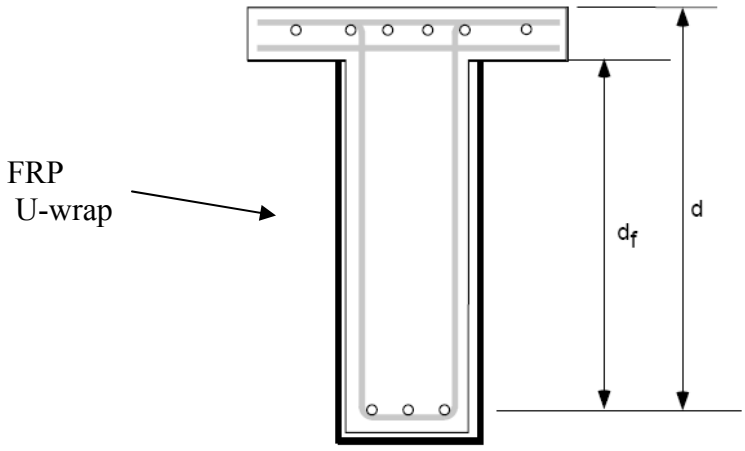

Figure App.F1. Graphical definition of d_f from ACI-440.

Debonding of the FRP is a dominant failure mode for FRP reinforced beams and all of the design methods consider, in some way, that the FRP material strength will not be fully utilized due to this mode of failure. The equation for the effective FRP stress in ACI-440 incorporates factors that take into account the stiffness of the FRP, the concrete strength, and the wrapping scheme, to limit the capacity due to the debonding failure mode. There is also a separate bond strength reduction factor, ψ, in addition to the typical member resistance factor, φ, applied to all components. This bond strength reduction factor is a function of the FRP wrapping scheme and is 0.95 for members that are completely wrapped (contact-critical shear reinforcing), and 0.85 for three-sided u-wraps or bonded face plies (bond-critical shear reinforcing).

Limits are imposed on the total amount of reinforcement in ACI-440. A total reinforcement limit (steel + FRP) is specified that is based on the limit for steel reinforcing alone found in ACI-318. This limit prevents over-reinforcing to avoid concrete crushing failure modes and is based on the concrete strength. The limit is given as:

$$V_s + V_f \le 0.66\sqrt{f'_c}\, b_w d \qquad \text{[5.AppF]}$$

There are also limits imposed due to other design considerations, such as FRP strip spacing must meet the same limits as those set forth in ACI-318 for internal steel reinforcement for shear.

Durability is another potential limiting factor for FRP strengthened beams. There is limited experience with long-term use of FRP's that has made long-term durability uncertain. Environmental reduction factors for various FRP applications and exposure conditions are given in ACI-440 and account for the degradation of bond as well as long-term durability uncertainty. Fatigue is addressed by ACI only in the flexural strengthening section where limits are imposed on the ultimate tensile strength of the FRP. Furthermore, the strength and serviceability requirements from ACI-318 must still be satisfied to ensure an adequate design.

Areas of uncertainty arose in applying the ACI-440 design method for shear in continuous bridges (members containing high shear with both positive and negative moment regions). The depth of FRP reinforcing, d_f, is shown in ACI-440 only for FRP applied to a T-beam subjected to a positive bending moment where the FRP edges terminate in, or near, the compression zone. However, in the present study, six inverted T-beams were tested for a negative bending moment. The terminating edge of the CFRP strips was located in the flexural-tension zone. The value that should be used for the depth of reinforcing in this case is not apparent. The termination of the FRP in the tension zone would be weaker than the T-beam where the termination occurs in the compression zone and is more likely to be subjected to peeling or debonding. As a result, a conservative estimate for d_f or a more conservative bond stress may be more appropriate.

For the FRP strip width and spacing used in the present study (12 in. width with 2 in. gap), and for the ACI assumption of a 45° crack angle at failure, a full crack is crossed by three FRP strips (Fig. App.F2). Therefore, to adequately characterize the condition at failure, the authors recommend a strip spacing that is based on the FRP strip width, the crack angle, and the web height that will ensure ***at least*** one strip crosses the diagonal crack with an anchorage length of at least one-half the height of the web. The spacing between strips to ensure this condition is:

$$g = \frac{1}{2}\left(\frac{h_w}{\tan\theta} - 3w_f \right) \qquad \text{[6.AppF]}$$

where g (in.) is the gap spacing between FRP strips, h_w (in.) is the height of the web, θ is the crack angle, and w_f (in.) is the FRP strip width. The smaller the crack angle, the wider the gap permitted between strips.

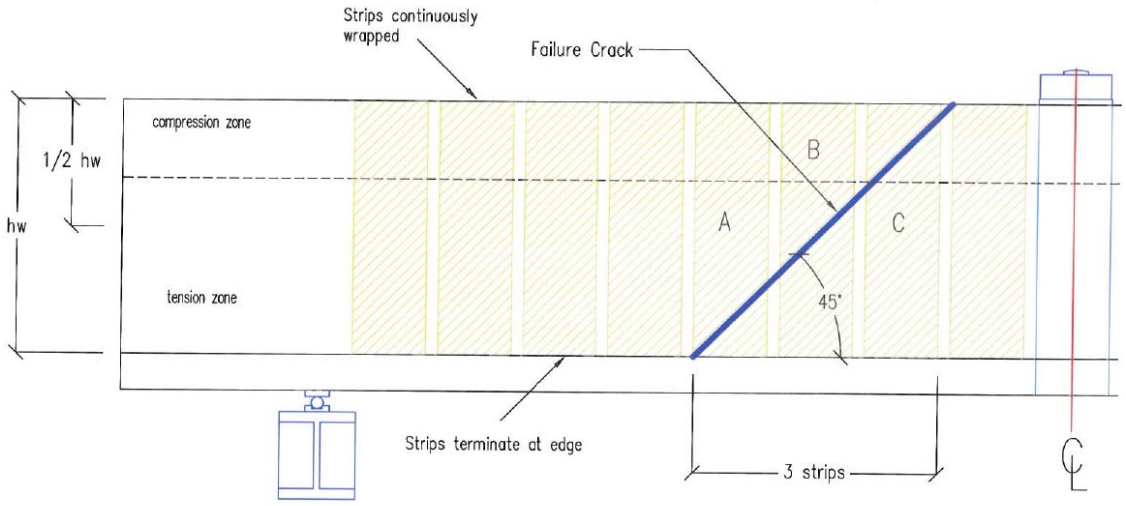

Figure App.F2. FRP Strip Coverage.

In the above figure, strip **A** crosses the crack in the tension zone where the terminating edge of the FRP will likely have debonded from the inadequate bond past the crack. Therefore, minimal strength will be gained from this strip. Strip **C** crosses the crack primarily in the compression zone where, again, minimal strength will be gained from the addition of the FRP as the shear will be primarily carried through the concrete compressive zone in this section. Therefore, strip **B**, is the sole strip that the authors believe can be relied upon to strengthen the beam in shear for strips terminating in the flexural tension zone.

CSA S806-02

The Canadian Standards Association (CSA) created a manual to aid in the design of FRP reinforced structures (2002) with chapter 11 devoted to the strengthening of concrete and masonry components with surface bonded FRP. The approach is very similar to ACI-440 although all units are presented in SI units for the Canadian approach and all subsequent design methods. Again, all resistance factors for the individual components were set to 1.0. The concrete contribution to shear strength is calculated as:

$$V_c(N) = 0.2\lambda\sqrt{f_c'}\,b_w d \qquad \text{[7.AppF]}$$

where λ is a factor to account for concrete density (set to 1.0 for normal density concrete), f'_c (MPa) is the specified compressive strength of concrete, b_w (mm) is the web width of the beam, and d (mm) is the distance from the extreme compression fiber to the centroid of the tension reinforcement.

The steel contribution to shear is calculated as:

$$V_s(N) = \frac{A_v f_y d}{s} \qquad \text{[8.AppF]}$$

where A_v (mm^2) is the area of the shear reinforcement perpendicular to the axis of a member within a distance s_f (mm), the spacing of the FRP strips, f_y (MPa) is the yield strength of the transverse steel, d (mm) is the distance from the extreme compression fiber to the centroid of the tension reinforcement, s (mm) is the stirrup spacing in the beam.

It should be noted here that the definition for the A_v term appears to produce overly large steel contributions that increase as the FRP spacing increased. This was a result of the area calculation being based on the spacing of the FRP stirrups as opposed to the steel stirrups, as is common. In the limiting case, as the spacing of FRP strips increases to infinity, so does the steel contribution to the shear capacity. This does not seem to be the intent of the code and the value was taken to be the area of the shear reinforcement perpendicular to the axis of a member within a distance, s, instead to bring it in line with the other code equations.

The FRP contribution to shear is calculated as:

$$V_f\left(N\right) = \frac{A_f E_f \varepsilon_f d_f}{s_f} \qquad \text{[9.AppF]}$$

where A_f (mm^2) is the cross-sectional area of the FRP shear reinforcement, E_f (mm^2) is the modulus of elasticity of the FRP composite, ε_f (mm/mm) is the tensile strain at the level of FRP composites under factored loads (taken as 4000με for U-wrapped FRP if more precise information is lacking), d_f (mm) is the distance from the extreme compression fiber to centroid of tension FRP reinforcement, and s_f (mm) is the spacing of the FRP strips.

Application of the above FRP contribution to shear required some interpretation of the equation. The tensile strain used as input for the FRP contribution is not information that would be readily available to the analyst. A value is proposed in the standard that is reportedly conservative and depends on the type of FRP scheme used. However, the recommended value gives design values that were not conservative for girders in the present study that were reinforced with the thicker CFRP wrap. Also the definition of the d_f term is unclear. It was assumed to be the distance to the centroid of the "flexural" tension FRP reinforcement. There is no FRP flexural reinforcement for the specimens but a zero for this term would indicate no contribution of the FRP to the shear capacity which is not an accurate representation. Therefore, in the calculations, the d_f term was taken to be the distance between the flexural tension and compression force resultants (the d_v term common to MCFT).

There are fewer limiting factors in the Canadian code compared to that in the ACI-440. There is no limit due to the wrapping scheme but a note is added that if anything is used other than a full-wrap, adequate anchorage must be provided. A limit is imposed on the overall nominal shear strength increase and is a function of the concrete contribution and the concrete strength. There are further limits imposed on the strain of the concrete (0.0035) and FRP (0.007) for flexural strengthening but these are not imposed in the shear strengthening section. Further, there are design considerations for failure modes as well as initial, pre-strengthening application, strains and stresses that are not explicitly applied to the shear mode. It is unclear if this was the

intention of the authors. Finally, there is an upper limit on the total shear capacity (V_r) of the components defined as:

$$V_r\left(N\right)_{\max} = V_c + 0.6\lambda\sqrt{f'_c}b_w d \qquad \text{[10.AppF]}$$

FIB 14 and Eurocode 2

FIB 14 is intended to be a state-of-the-art review on progress made in designing concrete structures with FRP. An entire chapter is devoted to shear strengthening. The document was used in conjunction with Eurocode 2, British Standard, (BS EN 2004) to develop the strength capacities of the test specimens. The concrete contribution to the shear strength as defined in BS EN is calculated as:

$$V_{Rd,c}(N) = [C_{Rd,c}k\left(100\rho_l f_{ck}\right)^{1/3} + k_1\sigma_{cp}]b_w d \qquad \text{[11.AppF]}$$

where $C_{Rd,c}$, and k_1 are limiting factors that vary by country (recommended values are 0.18 and 0.15, respectively), f_{ck} (MPa) is the characteristic concrete cylinder strength, b_w (mm) is the smallest width of the cross-section in the flexural tensile area, d (mm) is the depth from the compression fiber to the steel tensile reinforcement, σ_{cp} (MPa) is the axial stress in the section due to loading or prestressing (positive for compression, but zero for the current case) and k and ρ_l are calculated as:

$$k = 1 + \sqrt{\frac{200}{d}} \le 2.0 \qquad \text{[11.1..AppF]}$$

$$\rho_l = \frac{A_{sl}}{b_w d} \le 0.02 \qquad \text{[11.2.AppF]}$$

where A_{sl} (mm^2) is the area of the tensile reinforcement, which extends $\geq$ (l_{bd}+d) beyond the section considered (where l_{bd} is the design anchorage length, assumed to be *10* bar diameters).

The steel contribution to the shear strength as defined in Eurocode 2 was calculated as:

$$V_{Rd,s}(N) = \frac{A_{sw}}{s} f_{yd} z \cot\theta \qquad \text{[12.AppF]}$$

where A_{sw} (mm^2) is the cross-sectional area of the shear reinforcement, s (mm) is the spacing of the stirrups, z (mm) is the lever arm of internal forces (assumed to be *0.9d* per Eurocode 2), f_{yd} (MPa) is the design yield strength of the shear reinforcement, and θ is the angle of diagonal crack with respect to the member axis (assumed 45° with a limit:$1 \le \cot\theta \le 2.5$).

The maximum limiting value for $V_{rd,s}$ is defined as:

$$V_{rd,s\max} = \alpha_{cw} b_w v_1 f_{cd}\left(\cot\theta + \tan\theta\right) \qquad \text{[13.AppF]}$$

where α_{cw} is a coefficient accounting for stress in the compression cord (=1.0 for nonprestressed members), f_{cd} is the design compressive strength of concrete (= $f_{ck}(\alpha_{cc}/\gamma_C)$, α_{cc} a coefficient accounting for long term effects on strength and unfavorable effects from the manner in which the load is applied, and γ_C, a safety factor, (both taken as 1.0 for the current study), and v_1 is a strength reduction factor for concrete cracked in shear recommended to be taken as:

$$v_1 = 0.6\left[1 - \frac{f_{ck}}{250}\right] \qquad \text{[13.1.AppF]}$$

The FRP contribution to shear strength, defined in FIB 14, is calculated as:

$$V_{fd}(N) = 0.9\varepsilon_{fd,e}E_{fu}\rho_f b_w d\left(\cot\theta + \cot\alpha\right)\sin\alpha \qquad \text{[14.AppF]}$$

where $\varepsilon_{fd,e}$ (mm/mm) is the design value of effective FRP strain calculated as:

$$\varepsilon_{fd,e} = \frac{\varepsilon_{fk,e}}{\gamma_f} \qquad \text{[14.2.AppF]}$$

where γ_f is a safety factor, (set to 1.0 for purposes of comparison), and thus $\varepsilon_{fd,e}$ equals $\varepsilon_{fk,e}$ and it may be estimated as $0.8\varepsilon_{f,e}$ where $\varepsilon_{f,e}$ is the effective FRP strain and is calculated as:

$$\varepsilon_{f,e} = \min\left[0.65\left(\frac{f_{cm}^{2/3}}{E_{fu}\rho_f}\right)^{0.56} \times 10^{-3}, 0.17\left(\frac{f_{cm}^{2/3}}{E_{fu}\rho_f}\right)^{0.30}\varepsilon_{fu}\right] \qquad \text{[14.2.1.AppF]}$$

where f_{cm} (MPa) is the mean value of the concrete compressive strength and is estimated to be, f_{ck} + 8(MPa) and ε_{fu} is the ultimate FRP strain (taken as the value reported from the manufacturer);

and where E_{fu} (MPa) is the elastic modulus of FRP in the principal fiber orientation, b_w (mm) is the minimum width of the cross section over the effective depth, d (mm) is the effective depth of cross section, θ is the angle of diagonal crack with respect to the member axis (assumed = 45°), and α is the angle between principal fiber orientation and longitudinal axis of member (90° for the current study), ρ_f is the FRP reinforcement ratio calculated as:

$$\rho_f = \frac{2t_f}{b_w}\left(\frac{b_f}{s_f}\right) \qquad \text{[14.1.AppF]}$$

where t_f(mm), b_f(mm), s_f(mm) is the thickness, width, and spacing of the FRP shear reinforcement respectively.

The effective strain equations were derived from a detailed analysis of the experimental results reported in literature on shear strengthening of RC members with FRP (up through 1999). It is also reported that a strain limit of 0.006 is recommended by some researchers but is necessary only if the activation of the aggregate interlock mechanism within the concrete is necessary.

The only other limit is for the spacing of the FRP strips to ensure that no diagonal crack exists without crossing an FRP strip. This limit for T-beams is: $d\text{-}h_f\text{-}b_f/2$, with h_f equal to the slab thickness.

JSCE #41

Japan's Society of Civil Engineers have compiled document #41 (2001) which provides standards on upgrading concrete structures with continuous fiber sheets (CFS). The concrete contribution to the shear strength was calculated as:

$$V_{cd}(N) = \beta_d \beta_p \beta_n f_{vcd} b_w d \qquad \text{[15.AppF]}$$

where b_w (mm) is the smallest width of the cross-section in the flexural tensile area, d (mm) is the effective depth, f_{vcd} (MPa) is the concrete strength calculated as:

$$f_{vcd} = 0.20\sqrt[3]{f'_{cd}} \le 0.72(MPa) \qquad \text{[15.1AppF]}$$

where f'_{cd} (MPa) is the design compressive strength of concrete;

and where β_d, β_p, β_n, are calculated as follows:

$$\beta_d = \sqrt[4]{1/d}\ ; with\ d(m) \qquad \text{[15.2.AppF]}$$

$$\beta_p = \sqrt[3]{100\, p_w} \qquad \text{[15.3.AppF]}$$

where p_w is the longitudinal reinforcing ratio;

$$*\beta_n = 0.75 + \frac{1.4}{a/d} \qquad \text{[15.4.AppF]}$$

where a (mm) is the shear span (taken as the distance between the closest distance between the loading point and the support). *****NOTE: This is not the JSCE code equation for β_n but rather an equation used in lieu of the code equation in a study by Miyauchi et al. (1997). This substitution was made because the JSCE code β_n equation is a function of the design forces not available for comparisons of capacity.

The steel contribution to the shear strength is calculated as:

$$V_{sd}(N) = \left[A_w f_{wyd} \left(\sin\alpha_s + \cos\alpha_s \right) / s_s \right] z \qquad \text{[16.AppF]}$$

where s_s (mm) is the spacing of the steel shear reinforcement, A_w (mm^2) is the total cross-sectional area of shear reinforcement within s_s, f_{wyd} (MPa) is the design tension yield strength of shear reinforcement (400 MPa max.), α_s is the angle formed by shear reinforcement about the member axis, and z is the lever arm length (typically set to d/1.15 (~0.86d) per the JSCE code).

The FRP contribution to shear strength was calculated as:

$$V_{fd}(N) = K \left[A_f f_{fud} \left(\sin\alpha_f + \cos\alpha_f \right) / s_f \right] z \qquad \text{[17.AppF]}$$

where A_f (mm^2) is the total cross-sectional area of continuous fiber sheets (CFS) in space s_f, f_{fud} (MPa) is the design tensile strength of the CFS, α_f is the angle formed by the CFS about the member axis, s_f(mm) is the spacing of the CFS, and K is the shear reinforcing efficiency factor for the CFS which is calculated as:

$$K = 1.68 - 0.67R, \left(0.4 \le K \le 0.8\right) \qquad \text{[17.1AppF]}$$

where R is calculated as:

$$R = \left(\rho_f E_f\right)^{1/4} \left(\frac{f_{fud}}{E_f} \right)^{2/3} \left(\frac{1}{f_{cd}'} \right)^{1/3}, \left(0.5 \le R \le 2.0\right) \qquad \text{[17.1.2.AppF]}$$

where E_f(GPa) is the modulus of elasticity of the CFS and ρ_f is calculated as:

$$\rho_f = \frac{A_f}{b_w s_f} \qquad \text{[17.1.2.1AppF]}$$

The value for the design tensile strength is not explicitly defined in the JSCE #41 code. It was taken here as: $f_{fu} = E_f \varepsilon_f$ for purposes of this comparison. Since the strain in the FRP at ultimate has been found to not be reached due to debond failures at much lower strains, a constant value of 0.007 for the FRP strain was selected from recommendations by the Japan Building Disaster Prevention Association (JBDPA) based on investigations of FRP strains at failure in shear (Tumialan *et al.* 2001).

There appears to be a conflict with the limiting factors R and K in the design code. Based on the limits for K, the input values of R are between 1.31 and 1.91 only which does not match those given in the code of 0.5-2.0. There may be an error here which would permit further limitations on the FRP strength but it is unable to be determined without further information.

The JSCE #41 method presented relies on the assumption of a 35° shear crack angle, rigid body rotation after shear cracking, the bond constitutive law between the concrete (rigid body) and the CFS (elastic body) is valid, and the strain in the concrete compression zones is a function of the angle of rotation of the assumed rigid body.

Monti & Liotta (Italy)

A recent approach for characterizing the design capacity of FRP reinforced concrete beams in shear was developed by Monti & Liotta (2005). Analytical expressions were developed for the shear capacity by accounting for the constitutive properties of the FRP bonded to the concrete, compatibility imposed by the shear crack, and the boundary conditions for the specific wrap configuration.

The concrete and steel contributions to the overall nominal strength are based on the design approach proposed by Eurocode 2. The concrete contribution is defined by Monti & Liotta and calculated as:

$$V_{Rd,ct}(N) = 0.18 * b_w d * \min\left(1 + \frac{200mm}{d}, 2\right) * \sqrt[3]{100 * \min(0.02, \rho_{sl}) f_{ck}} \qquad [18.AppF]$$

where b_w (mm) is the beam web width, d (mm) is the effective beam depth, ρ_{sl} is the longitudinal geometric ratio, f_{ck} (MPa) is the concrete characteristic cylindrical strength.

The steel contribution to shear was calculated as:

$$V_{Rd,s}(N) = 0.9d * f_{yd} \frac{n_{st} A_{st}}{s_{st}} (\cot\theta + \cot\beta_{st}) \sin\beta_{st} \qquad [19.AppF]$$

where d (mm) is the effective beam depth, f_{yd} (MPa) is the design steel yield strength, n_{st} is the transverse reinforcement arm number, A_{st} (mm^2) is the area of one arm of the transverse reinforcement, s_{st} (mm) is the spacing of the transverse reinforcement, θ is the assumed crack angle with respect to the beam axis (assumed = 45°) and β_{st} is the angle of the stirrups.

The FRP contribution to shear is calculated as: $V_{Rd,f}(N) = 0.9d * f_{fed} 2t_f (\cot\theta + \cot\beta) \frac{w_f}{p_f}$

[20.AppF]

where d (mm) is the effective beam depth, where t_f (mm) is the FRP sheet thickness, θ is the crack angle to the beam axis, β is the angle of strip/sheet to the beam axis, w_f is the FRP strip width measured orthogonally to β, p_f is the FRP strip spacing measured orthogonally to β, and f_{fed} (MPa) is the effective bonding strength of the FRP and is calculated for U-wrapping schemes as:

$$f_{fed} = f_{fdd}\left[1 - \frac{1}{3}\frac{l_e \sin\beta}{\left[\min\{0.9d, h_w\}\right]}\right] \qquad [20.1.AppF]$$

where h_w (mm) is the height of the web and f_{fdd} (MPa) is the debonding strength calculated as:

$$f_{fdd} = 0.80\sqrt{\frac{2E_f \Gamma_{Fk}}{t_f}} \qquad \text{[20.1.1.AppF]}$$

where E_f (MPa) is the FRP sheet elastic modulus and Γ_{Fk} is the specific rupture energy calculated as:

$$\Gamma_{Fk} = 0.03 k_b \sqrt{f_{ck} f_{ctm}} \qquad \text{[20.1.1.AppF]}$$

where f_{ck} (MPa) is the concrete characteristic cylindrical strength, k_b (MPa) is the covering scale coefficient calculated as:

$$k_b = \sqrt{\frac{2 - {w_f}/{p_f}}{1 + {w_f}/{400}}} \geq 1 \qquad \text{[20.1.1.1.AppF]}$$

and f_{ctm} (MPa) is the concrete mean tensile strength calculated as:

$$f_{ctm} = 0.27 R_{ck}^{2/3} \qquad \text{[20.1.1.2.AppF]}$$

where R_{ck} (MPa) is the concrete characteristic cubic strength taken as the concrete characteristic cylindrical strength, f_{ck} /0.8 (as estimated value from a table of converted concrete strengths reported by BSI);

and where l_e (mm) is the effective bond length (optimum anchorage length) and is calculated as:

$$l_e = \sqrt{\frac{E_f t_f}{2 f_{ctm}}} \qquad \text{[20.1.2.AppF]}$$

The effective design strength takes into account the limit on the strength gained due to debonding failure. It is a function of wrapping scheme, effective bond length, FRP stiffness, and concrete strength. There is also an overall limit to the shear resistance based on the strength of the concrete strut. This method is the only one to not include the strength as a function of FRP strain.

$$V_{Rd,\max}(N) = 0.9 d\, b_w v\, f_{cd} \left(\cot\theta + \cot\beta_{st}\right) / \left(1 + \cot^2\theta\right) \qquad \text{[21.AppF]}$$

Results and Sample Calculations

Quantitative Comparisons between Code Approaches

Results from the application of all five codified methods to the test specimens are compared and presented in this appendix. In addition, hand calculations for Specimen 1IT01 are provided to illustrate the calculations required of the various methods. Specimen 4IT08, which was strengthened with longitudinal FRP, was not included in these comparisons as the horizontal fiber orientation was found not to contribute to the shear strength of the beam.

The predicted shear capacities were calculated for each of the design methods using their respective procedures, as detailed previously. Response 2000 (R2K) was used to calculate the unrepaired member capacity, V_{R2K}. This program was found to predict the shear-moment capacity of full-size RC girders without FRP, of the size and type used in this research study to within 2% (Higgins *et al*. 2004). Thus, R2K predicted capacity is anticipated to very closely estimate the shear-moment capacity of the unrepaired specimens. The R2K predicted capacity for specimen 4IT08 was predicted within 2% of the experimentally measured shear further validating the approach used to estimate the unrepaired capacity of the members. The V_{R2K} predicted capacity was taken to represent the combined experimental concrete (V_c) and steel contribution (V_s) to shear strength as:

$$V_{R2K} = V_c + V_s \qquad \text{[22.AppF]}$$

In general the experimental steel stirrup contribution to shear can be reasonably estimated by determining the number of stirrups that cross the failure diagonal crack and multiplying by the yield stress and area of the stirrup legs as:

$$V_s = A_v f_y n \qquad \text{[22.AppF]}$$

To estimate the experimental concrete contribution to shear, V_c, the experimental steel contribution was subtracted from the R2K predicted shear capacity as:

$$V_c = V_{R2K} - V_s \qquad \text{[23.AppF]}$$

Finally, the experimental FRP contribution to capacity, V_{frp}, was determined as the measured maximum applied shear from the actuator, plus the dead load shear, V_{dead}, from the specimen self-weight at the failure crack, minus the concrete and steel value predicted by R2K as:

$$V_{frp} = V_{app} + V_{dead} - V_{R2K} \qquad \text{[24.AppF]}$$

Figures AppF3-AppF5 summarize the steel, concrete, and FRP contributions, respectively, showing the experimentally measured values for the test specimens and the different code predicted values.

The five code approaches provided similar steel stirrup contributions. Canada, the United States, and Japan have assumed crack angles built into the formulations (45° for CSA-S806 and ACI-440 and 35° for JSCE #41) while Eurocode 2 and the Monti & Liotta equations for the steel contribution allows for input of the diagonal crack angle. Figure App.F3 shows the steel stirrup contributions of the experimental values compared well with the predicted and were similar to each other, as expected, since the formulae were similar with the only difference being the input diagonal crack angle (the measured versus the code assumed crack angle).

The concrete contribution varied a bit more widely between the different code approaches. All take into account the geometry of the section and the concrete strength but Canada and the United States use the square root of the compressive strength while the others use the cube root. The Japanese and European approaches take into account the longitudinal steel reinforcement ratio and the Japanese also include a moment-shear ratio at the section of interest. Figure AppF4

shows that the concrete contribution was conservative for all the methods and the relatively tight scatter of the data reflects the uniformity in the code equations with most of the variation due to the dependence on the square versus the cube root of the concrete strength.

Finally, the FRP contribution varied the most between the different design equations as seen in Fig. AppF5. When simplified, the various code equations differ in two basic ways; the stress in the FRP, and the flexural lever arm. CSA-S806 uses the simplest stress calculation taken as the FRP modulus of elasticity times the strain with a given FRP strain of 0.004. The Monti & Liotta approach calculates the FRP stress including effective bond length, FRP rupture energy, concrete strength, and a covering coefficient. The effective FRP strain has a large impact on the overall FRP strength. For example, if the effective strain limit employed in CSA-S806 (0.004), is replaced with the limit suggested by the JSCE #41 (0.007), then the shear strength contribution of the FRP increases 15% for the typical inverted-T specimens considered. Thus, the method used for calculating an effective FRP strain and the value for the limiting FRP strain are of critical importance for an effective and reliable design approach. Further, FRP debonding failure modes must also be reflected in the methodology.

The code predicted FRP contributions were not well correlated with the experimental results (with the exception being the Monti & Liotta approach (ITA), which was more complex to implement). Further results varied significantly among the different methods with a nearly 90% difference between the predicted values for the IT group. This analysis excludes specimen 4IT07 which is shown in Figure App.F6 to vary much more between the different approaches. This specimen had thicker FRP material (equivalent of 2 layers) and the different code approaches treated this additional material to this differently. If no limit was placed on the FRP strain, the strength predicted from the additional layer doubled (JSCE #41). Clearly from the experimental results, the capacity of the specimen with the thicker material was essentially equal to that of the thinner FRP material specimens. The lack of additional capacity is likely due to the premature debonding of the FRP material before the capacity of the additional material thickness is realized. This was the typical failure mode for the IT specimens due to the termination of the FRP strips in the flexural-tension region at the deck soffitt (the T-beam also failed due to the bonding, but at higher loads). The uniformity of the FRP failure capacity for the IT specimens suggests that the termination of the FRP strips in the flexural-tension zone are more prone to peeling and debonding at lower stress levels than that of the T-beams which terminate near the flexural-compression zone. This further highlights that FRP debonding in many practical bridge girder strengthening cases will likely control capacity (where full wraps are not possible due to the deck) and that additional limits are necessary to reasonably predict capacity when bond failures control the behavior.

The predicted total shear capacity of the specimens, with all with the safety factors set to unity for purposes of this analysis, appeared to be generally conservative as seen in Fig. AppF7. Differences between predicted and measured ranged from a low of 20% unconservative to a high of 61% conservative but most fell in a more modest range. The overall degree of conservatism for the different code approaches however, is not an indication of the accuracy for the prediction of the FRP shear strength contribution. As seen in Figures App.F4 and App.F5, the overly conservative concrete strength contribution masks the inaccuracies and unconservative design values in the FRP contributions. This suggests that there are compensating errors that, in the end,

provide total shear capacities that are reasonable, but that the FRP contribution taken alone may be unconservative, particularly for cases where the strips terminate in the flexural-tension zone.

When percent differences between experimental and predicted shear capacities were compared between T and IT-beam specimens, it is clear that the T-beam provide a higher degree of conservatism. Considering just the ACI-440 approach, the difference between the average predicted and experimental shear capacity for the IT specimens was 11% while for the two T-beam specimens was 30%. To bring a more consistent degree of conservatism to the IT specimens (similar to the T-beams), the FRP stress should be further limited to a value less than that currently permissible in ACI-440. A value for the FRP stress of half the current ACI-440 permitted value provided a level of design conservatism for the IT specimens of 27%, which was more consistent with that of the T-beam. Most of the previous research has been done on smaller scale specimens with anchorages or terminations in or near the flexural-compression zone. Thus, the results reported here indicate that additional limits may be needed to prevent premature debonding failures when FRP strips are terminated in the flexural-tension zone. Results are based on comparisons with just two T-beams (only one failing in shear) and further verification of these findings should be investigated.

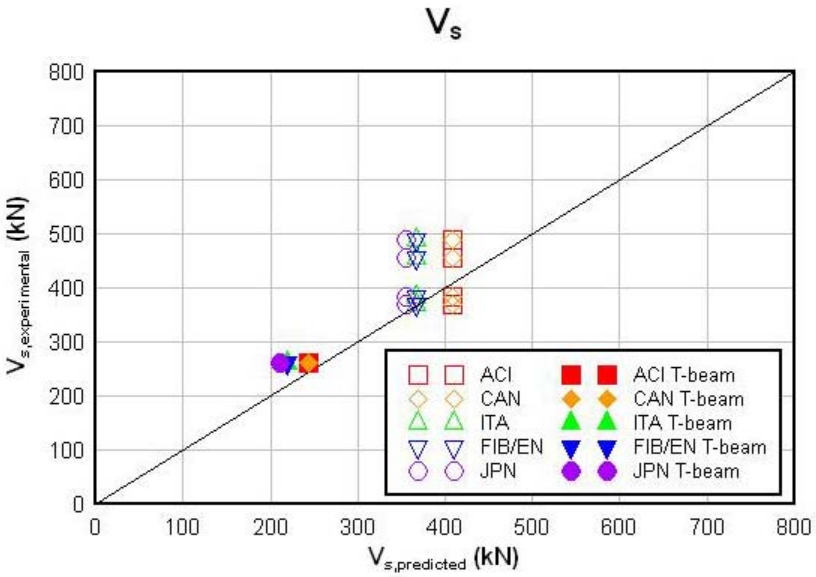

Figure App.F3. Comparison of experimental versus code predicted steel shear strength contribution.

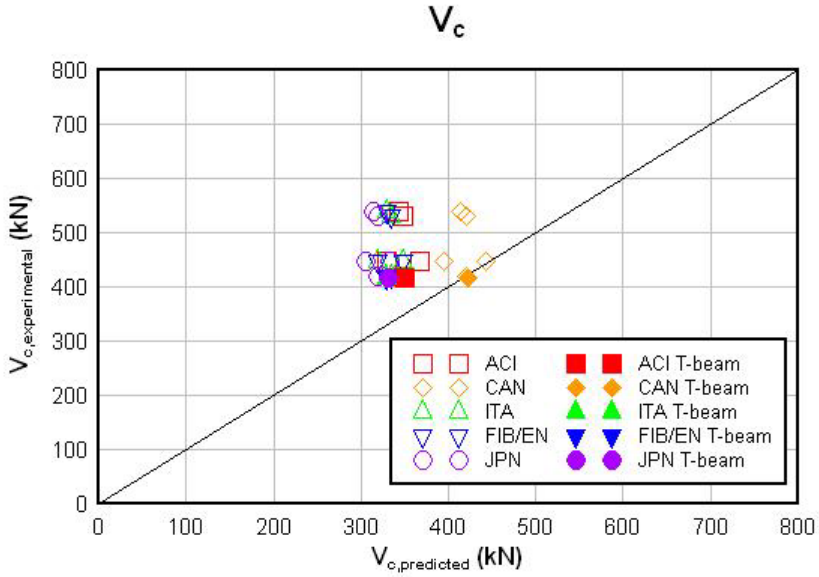

Figure App.F4. Comparison of experimental versus code predicted concrete shear strength contribution.

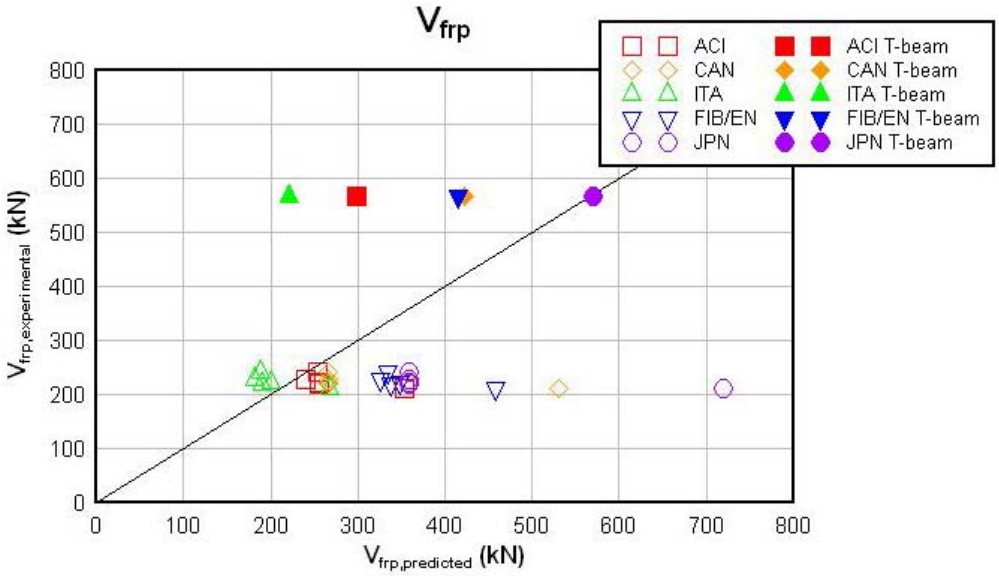

Figure App.F5. Comparison of experimental versus code predicted FRP shear strength contribution.

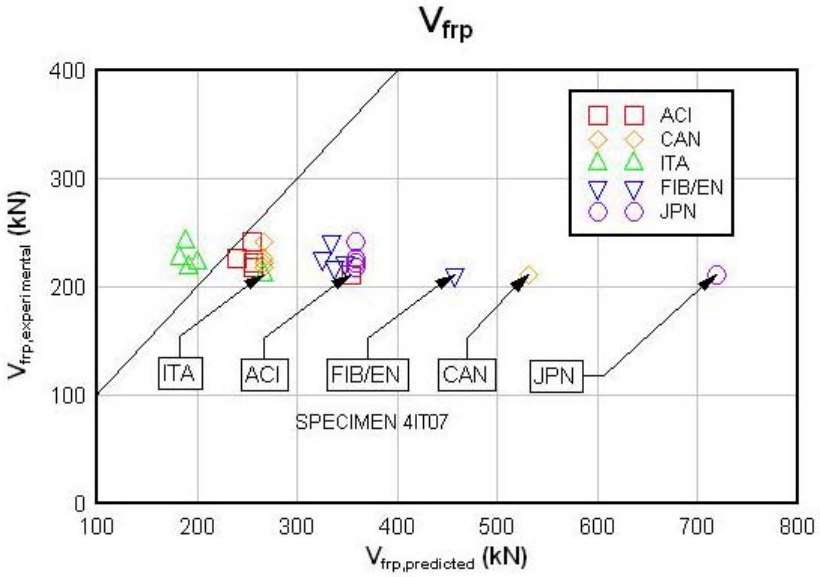

Figure App.F6. Detailed view of V_{frp} for all IT specimens.

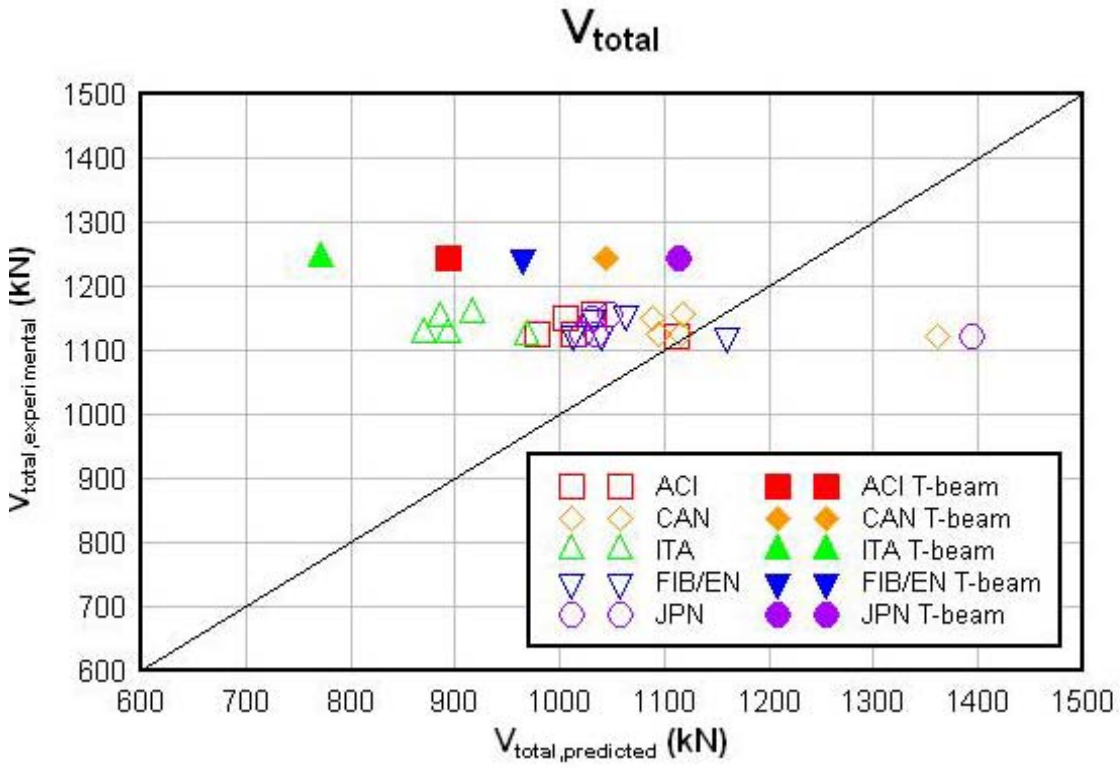

Figure App.F7. Comparison of experimental versus code predicted total shear capacity.

ACI Design Capacity Calculations

Test specimen 1IT01 - ACI Method

input		
*E_f	227	Gpa
*ε_{fu}	0.017	
*t_f	0.165	mm
f'_c	29.3	MPa
w_f	305	mm
d	1150	mm
d_f	998	mm
s_f	356	mm
b_w	356	mm
n	1	
s_s	254	mm
f_y	350	MPa
A_{sv}	258	mm^2
α	90	deg
V_{test}	1145	kN
V_{dead}	11.4	kN

*Manufacturer's reported FRP system properties

calculations		
f'_{fe}	908	Mpa
A_{fv}	101	mm^2
ε_{fe}	0.004	
L_e	52	mm
k_1	1.056	
k_2	0.95	
κ_v	0.257	

V		
V_{FRP}	256	kN
V_{steel}	409	kN
$V_{concrete}$	368	kN
V_{total}	1033	kN
difference	12%	

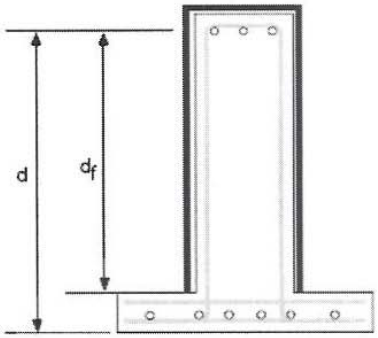

E_f = tensile modulus of elasticity

ε_{fu} = design rupture strain

t_f = nominal thickness of one ply of FRP

f'_c = specified compressive strength of concrete

w_f = FRP strip width

d = distance from extreme compression fiber to the neutral axis

d_f = depth of FRP shear reinforcement (see figure)

s_f = FRP strip spacing

b_w = web width

n = number of FRP plies

s_s = steel stirrup spacing

f_y = specified yield strength of steel

A_{sv} = area of steel shear reinforcement

α = angle of FRP stirrups

V_{test} = applied failure load

f'_{fe} = effective stress in FRP, stress level at section failure

A_{fv} = area of FRP shear reinforcement ($2*n*t_f*w_f$)

ε_{fe} = effective strain in FRP, strain level at section failure

L_e = active bond length of FRP

k_1 = concrete strength modification factor

k_2 = wrapping scheme modification factor

κ_v = bond dependent coefficient for shear

Test specimen 1IT02 - ACI Method

input		
$*E_f$	227	Gpa
$*\varepsilon_{fu}$	0.017	
$*t_f$	0.165	mm
f'_c	26.34	MPa
w_f	305	mm
d	1150	mm
d_f	998	mm
s_f	356	mm
b_w	356	mm
n	1	
s_s	254	mm
f_y	350	MPa
A_{sv}	258	mm^2
α	90	deg
V_{test}	1112	kN
V_{dead}	12.7	kN

calculations		
f'_{fe}	908	Mpa
A_{fv}	101	mm^2
ε_{fe}	0.004	
L_e	52	mm
k_1	0.984	
k_2	0.95	
κ_v	0.239	

V		
V_{FRP}	256	kN
V_{steel}	409	kN
$V_{concrete}$	349	kN
V_{total}	1014	kN
difference	11%	

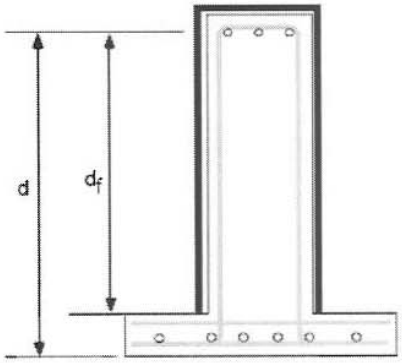

*Manufacturer's reported FRP system properties

E_f = tensile modulus of elasticity

ε_{fu} = design rupture strain

t_f = nominal thickness of one ply of FRP

f'_c = specified compressive strength of concrete

w_f = FRP strip width

d = distance from extreme compression fiber to the neutral axis

d_f = depth of FRP shear reinforcement (see figure)

s_f = FRP strip spacing

b_w = web width

n = number of FRP plies

s_s = steel stirrup spacing

f_y = specified yield strength of steel

A_{sv} = area of steel shear reinforcement

α = angle of FRP stirrups

V_{test} = applied failure load

f'_{fe} = effective stress in FRP, stress level at section failure

A_{fv} = area of FRP shear reinforcement ($2*n*t_f*w_f$)

ε_{fe} = effective strain in FRP, strain level at section failure

L_e = active bond length of FRP

k_1 = concrete strength modification factor

k_2 = wrapping scheme modification factor

κ_v = bond dependent coefficient for shear

Test specimen 2T03 - ACI Method

input		
$*E_f$	227	Gpa
$*\varepsilon_{fu}$	0.017	
$*t_f$	0.33	mm
f'_c	25.4	MPa
w_f	254	mm
d	1096	mm
d_f	943.5	mm
s_f	356	mm
b_w	356	mm
n	1	
s_s	508	mm
f_y	350	MPa
A_{sv}	258	mm^2
α	90	deg
V_{test}	956	kN
V_{dead}	0	kN

*Manufacturer's reported FRP system properties

calculations		
f'_{fe}	612	Mpa
A_{fv}	168	mm^2
ε_{fe}	0.0027	
L_e	35	mm
k_1	0.960	
k_2	0.96	
κ_v	0.159	

V		
V_{FRP}	272	kN
V_{steel}	195	kN
$V_{concrete}$	327	kN
V_{total}	793	kN
difference	21%	

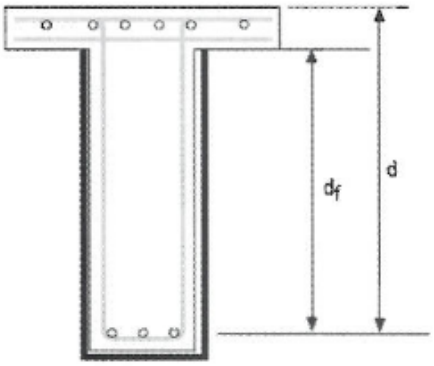

E_f = tensile modulus of elasticity

ε_{fu} = design rupture strain

t_f = nominal thickness of one ply of FRP

f'_c = specified compressive strength of concrete

w_f = FRP strip width

d = distance from extreme compression fiber to the neutral axis

d_f = depth of FRP shear reinforcement (see figure)

s_f = FRP strip spacing

b_w = web width

n = number of FRP plies

s_s = steel stirrup spacing

f_y = specified yield strength of steel

A_{sv} = area of steel shear reinforcement

α = angle of FRP stirrups

V_{test} = applied failure load

f'_{fe} = effective stress in FRP, stress level at section failure

A_{fv} = area of FRP shear reinforcement ($2*n*t_f*w_f$)

ε_{fe} = effective strain in FRP, strain level at section failure

L_e = active bond length of FRP

k_1 = concrete strength modification factor

k_2 = wrapping scheme modification factor

κ_v = bond dependent coefficient for shear

Test specimen 2T04 - ACI Method

input		
$*E_f$	227	Gpa
$*\varepsilon_{fu}$	0.017	
$*t_f$	0.33	mm
f'_c	29.37	MPa
w_f	254	mm
d	1096	mm
d_f	943.5	mm
s_f	356	mm
b_w	356	mm
n	1	
s_s	406.4	mm
f_y	350	MPa
A_{sv}	258	mm^2
α	90	deg
V_{test}	1225	kN
V_{dead}	18.3	kN

*Manufacturer's reported FRP system properties

calculations		
f'_{fe}	674	Mpa
A_{fv}	168	mm^2
ε_{fe}	0.0030	
L_e	35	mm
k_1	1.058	
k_2	0.96	
κ_v	0.175	

V		
V_{FRP}	299	kN
V_{steel}	244	kN
$V_{concrete}$	351	kN
V_{total}	894	kN
difference	39%	

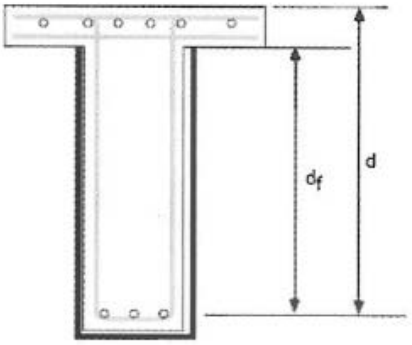

E_f = tensile modulus of elasticity
ε_{fu} = design rupture strain
t_f = nominal thickness of one ply of FRP
f'_c = specified compressive strength of concrete
w_f = FRP strip width
d = distance from extreme compression fiber to the neutral axis
d_f = depth of FRP shear reinforcement (see figure)
s_f = FRP strip spacing
b_w = web width
n = number of FRP plies
s_s = steel stirrup spacing
f_y = specified yield strength of steel
A_{sv} = area of steel shear reinforcement
α = angle of FRP stirrups
V_{test} = applied failure load
f'_{fe} = effective stress in FRP, stress level at section failure
A_{fv} = area of FRP shear reinforcement ($2*n*t_f*w_f$)
ε_{fe} = effective strain in FRP, strain level at section failure
L_e = active bond length of FRP
k_1 = concrete strength modification factor
k_2 = wrapping scheme modification factor
κ_v = bond dependent coefficient for shear

Test specimen 3IT05 - ACI Method

input		
*E_f	227	Gpa
*ε_{fu}	0.017	
*t_f	0.165	mm
f'_c	25.39	MPa
w_f	305	mm
d	1150	mm
d_f	998	mm
s_f	356	mm
b_w	356	mm
n	1	
s_s	254	mm
f_y	350	MPa
A_{sv}	258	mm^2
α	90	deg
V_{test}	1134	kN
V_{dead}	13	kN

calculations		
f'_{fe}	900	Mpa
A_{fv}	101	mm^2
ε_{fe}	0.004	
L_e	52	mm
k_1	0.960	
k_2	0.95	
κ_v	0.233	

V		
V_{FRP}	254	kN
V_{steel}	409	kN
$V_{concrete}$	343	kN
V_{total}	1005	kN
difference	14%	

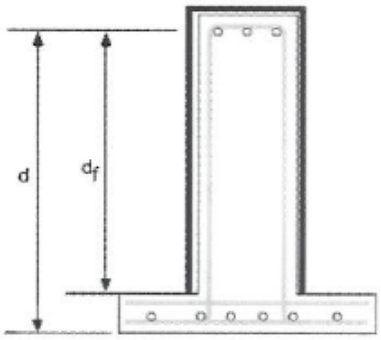

*Manufacturer's reported FRP system properties

E_f = tensile modulus of elasticity
ε_{fu} = design rupture strain
t_f = nominal thickness of one ply of FRP
f'_c = specified compressive strength of concrete
w_f = FRP strip width
d = distance from extreme compression fiber to the neutral axis
d_f = depth of FRP shear reinforcement (see figure)
s_f = FRP strip spacing
b_w = web width
n = number of FRP plies
s_s = steel stirrup spacing
f_y = specified yield strength of steel
A_{sv} = area of steel shear reinforcement
α = angle of FRP stirrups
V_{test} = applied failure load
f'_{fe} = effective stress in FRP, stress level at section failure
A_{fv} = area of FRP shear reinforcement ($2*n*t_f*w_f$)
ε_{fe} = effective strain in FRP, strain level at section failure
L_e = active bond length of FRP
k_1 = concrete strength modification factor
k_2 = wrapping scheme modification factor
κ_v = bond dependent coefficient for shear

Test specimen 3IT06 - ACI Method

input		
$*E_f$	227	Gpa
$*\varepsilon_{fu}$	0.017	
$*t_f$	0.165	mm
f'_c	23.33	MPa
w_f	305	mm
d	1150	mm
d_f	998	mm
s_f	356	mm
b_w	356	mm
n	1	
s_s	254	mm
f_y	350	MPa
A_{sv}	258	mm^2
α	90	deg
V_{test}	1116	kN
V_{dead}	9.3	kN

calculations		
f'_{fe}	851	Mpa
A_{fv}	101	mm^2
ε_{fe}	0.004	
L_e	52	mm
k_1	0.907	
k_2	0.95	
κ_v	0.220	

V		
V_{FRP}	240	kN
V_{steel}	409	kN
$V_{concrete}$	329	kN
V_{total}	977	kN
difference	15%	

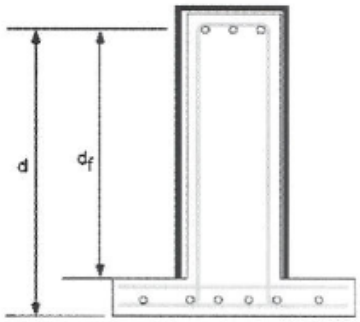

*Manufacturer's reported FRP system properties

E_f = tensile modulus of elasticity

ε_{fu} = design rupture strain

t_f = nominal thickness of one ply of FRP

f'_c = specified compressive strength of concrete

w_f = FRP strip width

d = distance from extreme compression fiber to the neutral axis

d_f = depth of FRP shear reinforcement (see figure)

s_f = FRP strip spacing

b_w = web width

n = number of FRP plies

s_s = steel stirrup spacing

f_y = specified yield strength of steel

A_{sv} = area of steel shear reinforcement

α = angle of FRP stirrups

V_{test} = applied failure load

f'_{fe} = effective stress in FRP, stress level at section failure

A_{fv} = area of FRP shear reinforcement ($2*n*t_f*w_f$)

ε_{fe} = effective strain in FRP, strain level at section failure

L_e = active bond length of FRP

k_1 = concrete strength modification factor

k_2 = wrapping scheme modification factor

κ_v = bond dependent coefficient for shear

Test specimen 4IT07 - ACI Method

input		
$*E_f$	227	Gpa
$*\varepsilon_{fu}$	0.017	
$*t_f$	0.33	mm
f'_c	26.27	MPa
w_f	305	mm
d	1150	mm
d_f	998	mm
s_f	356	mm
b_w	356	mm
n	1	
s_s	254	mm
f_y	350	MPa
A_{sv}	258	mm^2
α	90	deg
V_{test}	1110	kN
V_{dead}	9.2	kN

*Manufacturer's reported FRP system properties

calculations		
f'_{fe}	627	Mpa
A_{fv}	201	mm^2
ε_{fe}	0.003	
L_e	35	mm
k_1	0.982	
k_2	0.97	
κ_v	0.162	

V		
V_{FRP}	354	kN
V_{steel}	409	kN
$V_{concrete}$	349	kN
V_{total}	1111	kN
difference	1%	

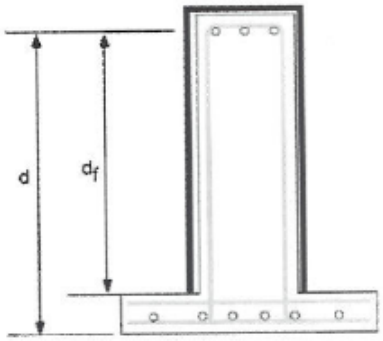

E_f = tensile modulus of elasticity

ε_{fu} = design rupture strain

t_f = nominal thickness of one ply of FRP

f'_c = specified compressive strength of concrete

w_f = FRP strip width

d = distance from extreme compression fiber to the neutral axis

d_f = depth of FRP shear reinforcement (see figure)

s_f = FRP strip spacing

b_w = web width

n = number of FRP plies

s_s = steel stirrup spacing

f_y = specified yield strength of steel

A_{sv} = area of steel shear reinforcement

α = angle of FRP stirrups

V_{test} = applied failure load

f'_{fe} = effective stress in FRP, stress level at section failure

A_{fv} = area of FRP shear reinforcement ($2*n*t_f*w_f$)

ε_{fe} = effective strain in FRP, strain level at section failure

L_e = active bond length of FRP

k_1 = concrete strength modification factor

k_2 = wrapping scheme modification factor

κ_v = bond dependent coefficient for shear

$V_r = V_s + V_c + V_f$

$V_s = \frac{A_v f_y d}{s} = \frac{258mm^2(350N/mm^2)(1150mm)}{254mm} = 409kN$

$A_v = 2\ \#13\ BARS\ (\#4) = 129mm^2(2) = 258mm^2$
$f_y = 350\ MPa = 350\ N/mm^2$
$d = 1219mm - 69mm = 1150mm$
$s = 254\ mm$

$V_c = 2\sqrt{f'_c}\, b_w d$; $\sqrt{f'_c}$ = psi

$f'_c = 29.3\ MPa = 4250\ psi$
$b_w = 356mm = 14"$
$d = 1150mm = 45.3"$

$V_c = 2\sqrt{4250psi}\,(14")(45.3") = 82,690\,lb = 368kN$

$V_f = \frac{A_{fv} f_{fe} (\sin\alpha + \cos\alpha) d_f}{s_f}$ (10-3)

$A_{fv} = 2nt_f w_f = 2(1)(.165mm)(305mm) = 100.7mm^2$
$f_{fe} = \varepsilon_{fe} E_f$

$\varepsilon_{fe} = K_v \varepsilon_{fu} \le 0.004 \le 0.75\varepsilon_{fu}$ (10-6(a))
$K_v = \frac{k_1 k_2 L_e}{11,900\,\varepsilon_{fu}}$ (U-WRAPS OR SIDE BOND)

$k_1 = \left(\frac{f'_c}{27}\right)^{2/3} = \left(\frac{29.3}{27}\right)^{2/3} = 1.056$ (10-9)
$f'_c = 29.3MPa$

$k_2 = \frac{d_f - L_e}{d_f}$ (U-WRAPS) (10-10)

$d_f = d - t_s = 1150mm - 152mm = 998$
$L_e = \frac{23,300}{(nt_f E_f)^{0.58}}$ (10-8)
$E_f = 227 \times 10^3\ MPa$
$L_e = \frac{23,300}{[(1)(.165mm)(227\times10^3 MPa)]^{0.58}} = 51.8mm$

$k_2 = \frac{998mm - 51.8mm}{998mm} = .948$

$\varepsilon_{fu} = .017$

$$k_v = \frac{(1.06)(0.948)(51.8mm)}{11,900(.017)} = .257$$

$$\varepsilon_{fe} = k_v \varepsilon_{fu} = .257(.017) = .0043$$

$.0043 \not< .004 \; (.75\varepsilon_{fu}) \therefore \varepsilon_{fe} = .004$

$f_{fe} = .004(227\times10^3 MPa) = 908 MPa = 908 N/mm^2$

$\alpha = 90°$

$s_f = 356mm$

$$V_f = \frac{100.7mm^2(908 N/mm^2)(\sin 90° + \cos 90°)998mm}{356mm} = \underline{256kN}$$

$V_T = 409kN + 368kN + 256kN = \boxed{1033kN}$

$V_{T\,ACTUAL} = V_{TEST} + V_{DEAD} = 1145kN + 11.4kN = 1156kN$ (DIFFERENCE = 12%)

CHECK: $V_s + V_f \leq 0.66\sqrt{f'_c}\, b_w d$ (10-11)

$409kN + 256kN \leq 0.66\sqrt{28MPa}(356mm)(1150mm)$

$665kN \leq 1430kN$ O.K.

Canada Design Capacity Calculations

Test specimen 1IT01 - Canadian Standards Assoc. Method

input		
*E_f	227	Gpa
**ε_f	0.004	
*t_f	0.165	mm
f'_c	29.3	MPa
w_f	305	mm
d	1150	mm
d_f	1035	mm
s_f	356	mm
b_w	356	mm
n	1	
s	254	mm
f_y	350	MPa
A_v	258	mm^2
V_{test}	1145	kN
V_{dead}	11.4	kN

*Manufacturer's reported FRP system properties
**assumed value per code

calculations		
A_f	101	mm^2

V		
V_{FRP}	266	kN
V_{steel}	409	kN
$V_{concrete}$	443	kN
V_{total}	1118	kN
difference	3%	

E_f = Modulus of elasticity of FRP composite
ε_f = tensile strain at the level of FRP composites under factored loads
t_f = nominal thickness of one ply of FRP
f'_c = specified compressive strength of concrete
w_f = FRP strip width
d = distance from extreme compression fibre to centroid of tension reinforcement
d_f = assumed to be 0.9*d (not per the CAN code)
s_f = spacing of FRP shear reinforcement of a beam or unit width for continuous FRP sheet
b_w = width of the web of a beam
n = number of FRP plies
s = spacing of stirrup of a beam
f_y = specified yield strength of steel reinforcement
A_v = area of shear reinforcement perpendicular to the axis of a member within a distance, s (not s_f as per the CAN code)
V_{test} = applied failure load
A_f = cross-sectional area of FRP composite reinforcement of unit wide for continuous FRP sheet

Test specimen 1IT02 - Canadian Standards Assoc. Method

input		
*E_f	227	Gpa
**ε_f	0.004	
*t_f	0.165	mm
f'_c	26.34	MPa
w_f	305	mm
d	1150	mm
d_f	1035	mm
s_f	356	mm
b_w	356	mm
n	1	
s	254	mm
f_y	350	MPa
A_v	258	mm^2
V_{test}	1112	kN
V_{dead}	12.7	kN

calculations		
A_f	101	mm^2

V		
V_{FRP}	266	kN
V_{steel}	409	kN
$V_{concrete}$	420	kN
V_{total}	1095	kN
difference	3%	

*Manufacturer's reported FRP system properties
**assumed value per code

E_f = Modulus of elasticity of FRP composite
ε_f = tensile strain at the level of FRP composites under factored loads
t_f = nominal thickness of one ply of FRP
f'_c = specified compressive strength of concrete
w_f = FRP strip width
d = distance from extreme compression fibre to centroid of tension reinforcement
d_f = assumed to be 0.9*d (not per the CAN code)
s_f = spacing of FRP shear reinforcement of a beam or unit width for continuous FRP sheet
b_w = width of the web of a beam
n = number of FRP plies
s = spacing of stirrup of a beam
f_y = specified yield strength of steel reinforcement
A_v = area of shear reinforcement perpendicular to the axis of a member within a distance, s (not s_f as per the CAN code)
V_{test} = applied failure load
A_f = cross-sectional area of FRP composite reinforcement of unit wide for continuous FRP sheet

Test specimen 2T03 - Canadian Standards Assoc. Method

input		
*E_f	227	Gpa
**ε_f	0.004	
*t_f	0.33	mm
f'_c	25.4	MPa
w_f	254	mm
d	1096	mm
d_f	986.4	mm
s_f	356	mm
b_w	356	mm
n	1	
s	508	mm
f_y	350	MPa
A_v	258	mm^2
V_{test}	1225	kN
V_{dead}	0	kN

*Manufacturer's reported FRP system properties
**assumed value per code

calculations		
A_f	168	mm^2

V		
V_{FRP}	422	kN
V_{steel}	195	kN
$V_{concrete}$	393	kN
V_{total}	1010	kN
difference	21%	

E_f = Modulus of elasticity of FRP composite
ε_f = tensile strain at the level of FRP composites under factored loads
t_f = nominal thickness of one ply of FRP
f'_c = specified compressive strength of concrete
w_f = FRP strip width
d = distance from extreme compression fibre to centroid of tension reinforcement
d_f = assumed to be 0.9*d (not per the CAN code)
s_f = spacing of FRP shear reinforcement of a beam or unit width for continuous FRP sheet
b_w = width of the web of a beam
n = number of FRP plies
s = spacing of stirrup of a beam
f_y = specified yield strength of steel reinforcement
A_v = area of shear reinforcement perpendicular to the axis of a member within a distance, s (not s_f as per the CAN code)
V_{test} = applied failure load
A_f = cross-sectional area of FRP composite reinforcement of unit wide for continuous FRP sheet

Test specimen 2T04 - Canadian Standards Assoc. Method

input		
*E_f	227	Gpa
**ε_f	0.004	
*t_f	0.33	mm
f'_c	29.37	MPa
w_f	254	mm
d	1096	mm
d_f	986.4	mm
s_f	356	mm
b_w	356	mm
n	1	
s	406.4	mm
f_y	350	MPa
A_v	258	mm^2
V_{test}	1225	kN
V_{dead}	18.3	kN

*Manufacturer's reported FRP system properties

**assumed value per code

calculations		
A_f	168	mm^2

V		
V_{FRP}	422	kN
V_{steel}	244	kN
$V_{concrete}$	423	kN
V_{total}	1088	kN
difference	14%	

E_f = Modulus of elasticity of FRP composite

ε_f = tensile strain at the level of FRP composites under factored loads

t_f = nominal thickness of one ply of FRP

f'_c = specified compressive strength of concrete

w_f = FRP strip width

d = distance from extreme compression fibre to centroid of tension reinforcement

d_f = assumed to be 0.9*d (not per the CAN code)

s_f = spacing of FRP shear reinforcement of a beam or unit width for continuous FRP sheet

b_w = width of the web of a beam

n = number of FRP plies

s = spacing of stirrup of a beam

f_y = specified yield strength of steel reinforcement

A_v = area of shear reinforcement perpendicular to the axis of a member within a distance, s (not s_f as per the CAN code)

V_{test} = applied failure load

A_f = cross-sectional area of FRP composite reinforcement of unit wide for continuous FRP sheet

Test specimen 3IT05 - Canadian Standards Assoc. Method

input		
*E_f	227	Gpa
**ε_f	0.004	
*t_f	0.165	mm
f'_c	25.39	MPa
w_f	305	mm
d	1150	mm
d_f	1035	mm
s_f	356	mm
b_w	356	mm
n	1	
s	254	mm
f_y	350	MPa
A_v	258	mm^2
V_{test}	1134	kN
V_{dead}	13	kN

calculations		
A_f	101	mm^2

V		
V_{FRP}	266	kN
V_{steel}	409	kN
$V_{concrete}$	413	kN
V_{total}	1087	kN
difference	6%	

*Manufacturer's reported FRP system properties
**assumed value per code

E_f = Modulus of elasticity of FRP composite
ε_f = tensile strain at the level of FRP composites under factored loads
t_f = nominal thickness of one ply of FRP
f'_c = specified compressive strength of concrete
w_f = FRP strip width
d = distance from extreme compression fibre to centroid of tension reinforcement
d_f = assumed to be 0.9*d (not per the CAN code)
s_f = spacing of FRP shear reinforcement of a beam or unit width for continuous FRP sheet
b_w = width of the web of a beam
n = number of FRP plies
s = spacing of stirrup of a beam
f_y = specified yield strength of steel reinforcement
A_v = area of shear reinforcement perpendicular to the axis of a member within a distance, s (not s_f as per the CAN code)
V_{test} = applied failure load
A_f = cross-sectional area of FRP composite reinforcement of unit wide for continuous FRP sheet

Test specimen 3IT06 - Canadian Standards Assoc. Method

input		
*E_f	227	Gpa
**ε_f	0.004	
*t_f	0.165	mm
f'_c	23.33	MPa
w_f	305	mm
d	1150	mm
d_f	1035	mm
s_f	356	mm
b_w	356	mm
n	1	
s	254	mm
f_y	350	MPa
A_v	258	mm^2
V_{test}	1116	kN
V_{dead}	9.3	kN

*Manufacturer's reported FRP system properties
**assumed value per code

calculations		
A_f	101	mm^2

V		
V_{FRP}	266	kN
V_{steel}	409	kN
$V_{concrete}$	395	kN
V_{total}	1070	kN
difference	5%	

E_f = Modulus of elasticity of FRP composite
ε_f = tensile strain at the level of FRP composites under factored loads
t_f = nominal thickness of one ply of FRP
f'_c = specified compressive strength of concrete
w_f = FRP strip width
d = distance from extreme compression fibre to centroid of tension reinforcement
d_f = assumed to be 0.9*d (not per the CAN code)
s_f = spacing of FRP shear reinforcement of a beam or unit width for continuous FRP sheet
b_w = width of the web of a beam
n = number of FRP plies
s = spacing of stirrup of a beam
f_y = specified yield strength of steel reinforcement
A_v = area of shear reinforcement perpendicular to the axis of a member within a distance, s (not s_f as per the CAN code)
V_{test} = applied failure load
A_f = cross-sectional area of FRP composite reinforcement of unit wide for continuous FRP sheet

Test specimen 4IT07 - Canadian Standards Assoc. Method

input		
*E_f	227	Gpa
**ε_f	0.004	
*t_f	0.33	mm
f'_c	26.27	MPa
w_f	305	mm
d	1150	mm
d_f	1035	mm
s_f	356	mm
b_w	356	mm
n	1	
s	254	mm
f_y	350	MPa
A_v	258	mm^2
V_{test}	1110	kN
V_{dead}	9.2	kN

*Manufacturer's reported FRP system properties
**assumed value per code

calculations		
A_f	201	mm^2

V		
V_{FRP}	531	kN
V_{steel}	409	kN
$V_{concrete}$	420	kN
V_{total}	1360	kN
difference	-18%	

E_f = Modulus of elasticity of FRP composite
ε_f = tensile strain at the level of FRP composites under factored loads
t_f = nominal thickness of one ply of FRP
f'_c = specified compressive strength of concrete
w_f = FRP strip width
d = distance from extreme compression fibre to centroid of tension reinforcement
d_f = assumed to be 0.9*d (not per the CAN code)
s_f = spacing of FRP shear reinforcement of a beam or unit width for continuous FRP sheet
b_w = width of the web of a beam
n = number of FRP plies
s = spacing of stirrup of a beam
f_y = specified yield strength of steel reinforcement
A_v = area of shear reinforcement perpendicular to the axis of a member within a distance, s (not s_f as per the CAN code)
V_{test} = applied failure load
A_f = cross-sectional area of FRP composite reinforcement of unit wide for continuous FRP sheet

CANADIAN STAND. S806-02	SPECIMEN IIT07	SHEAR CAPACITY CALCS	1/1

$V_r = V_c + V_s + V_f$

$V_c = 0.2 \lambda \phi_c \sqrt{f'_c}\, A_e$

$\lambda = \phi_c$ = REDUCTION FACTORS = 1

$= 0.2\sqrt{f'_c}\, b_w d$ (11-3)

$f'_c = 29.3 MPa$

$b_w = 356mm$

$d = 1219mm - 69mm = 1150mm$

$V_c = 2\sqrt{29.3 MPa}\,(356mm)(1150mm) = \underline{443 kN}$

$V_s = \phi_s \dfrac{A_v f_y d}{s}$ (SAME AS ACI) (11-4)

$\phi_s = 1$

$A_v = 258mm^2$ (NOTE: NOT USING CODE, A_v WITHIN DISTANCE S_f)

$f_y = 350 MPa$

$s = 254 mm$

2 #15(A) BARS = $258mm^2 = A_{3V}$

$V_s = \dfrac{1\,(258mm^2)(350MPa)(1150mm)}{254mm} = \underline{409 kN}$

$V_f = \dfrac{\phi_f A_f E_f \epsilon_f d_f}{S_f}$ (11-5)

$\phi_f = 1$

$A_f = 2(.165mm)(305mm) = 101mm^2$

$E_f = 227 \times 10^3 MPa$

$\epsilon_f = .004$ (CONSERVATIVE ASSUMPTION PER CODE)

$d_f = 0.9d = 1035mm$

$S_f = 356mm$

$V_f = \dfrac{101mm^2 (227 \times 10^3 MPa)(.004)(1035mm)}{356mm} = \underline{266 kN}$

$V_r = 443kN + 409kN + 266kN = \boxed{1118kN}$

$V_{r\,ACTUAL} = 1145 kN$ (DIFFERENCE = 3%)

FIB Design Capacity Calculations

Test specimen 1IT01 - fib

input		
E_f	227	Gpa
ε_{fu}	0.017	
t_f	0.165	mm
f_{ck}	29.3	MPa
b_f	305	mm
s_f	356	mm
d	1150	mm
b_w	356	mm
A_{sw}	258	mm^2
s_{sw}	254	mm
f_{ywd}	350	MPa
$A_{sl(total)}$	5161	mm^2
θ_{actual}	37	deg
$\theta_{theoretical}$	45	deg
α	90	deg
V_{test}	1145	kN
V_{dead}	11.4	kN

calculations		
$C_{Rd,c}$	0.18	
k	1.42	
z	1035	
ρ_l	0.013	
$\varepsilon_{fd,e}$	0.005	
$\varepsilon_{fk,e}$	0.005	
f_{cm}	37.3	MPa
ρ_f	0.00079	
$\varepsilon_{f,e}$	0.00655	

$V_{actual\theta}$	
V_{fd}	462
V_{wd}	488
V_{cd}	348
V_{Rd}	1298
difference	-11%

$V_{theoretical\theta}$	
V_{fd}	348
V_{wd}	368
V_{cd}	348
V_{Rd}	1064
difference	9%

E_f = FRP sheet elastic modulus

ε_{fu} = ultimate FRP strain

t_f = sheet thickness

f_{ck} = concrete characteristic cylindrical strength, 28 day

b_f = width of FRP

s_f = spacing of FRP strips

d = beam effective depth

b_w = smallest width of x-section in tensile area

A_{sw} = area of transverse reinforcement

s_{sw} = spacing of transverse reinforcement

f_{ywd} = design steel yield strength

$A_{sl(total)}$ = area of tensile steel reinforcement

θ_{actual} = actual crack angle as measured in test

$\theta_{theoretical}$ = assumed crack angle as measured from the beam axis

α = angle between principal fibre orientation and longitudinal axis of member

V_{test} = applied failure load

V_{dead} = estimated shear from concrete dead load below the failure crack

$C_{Rd,c}$ = limitng coefficient

k = limitng coefficient

z = lever arm (d_v in MCFT)

ρ_l = steel longitudinal geometric ratio

$\varepsilon_{fd,e}$ = design value of effective FRP strain

$\varepsilon_{fk,e}$ = characteristic value of effective FRP strain

f_{cm} = mean value concrete compressive strength

ρ_f = FRP reinforcement ratio

$\varepsilon_{f,e}$ = effective FRP strain

Test specimen 1IT02 - fib

input		
E_f	227	Gpa
ε_{fu}	0.017	
t_f	0.165	mm
f_{ck}	26.34	MPa
b_f	305	mm
s_f	356	mm
d	1150	mm
b_w	356	mm
A_{sw}	258	mm^2
s_{sw}	254	mm
f_{ywd}	350	MPa
$A_{sl(total)}$	5103	mm^2
θ_{actual}	37	deg
$\theta_{theoretical}$	45	deg
α	90	deg
V_{test}	1112	kN
V_{dead}	12.7	kN

calculations		
$C_{Rd,c}$	0.18	
k	1.42	
z	1035	
ρ_l	0.012	
$\varepsilon_{fd,e}$	0.005	
$\varepsilon_{fk,e}$	0.005	
f_{cm}	34.34	MPa
ρ_f	0.00079	
$\varepsilon_{f,e}$	0.00635	

$V_{actual\theta}$	
V_{fd}	448
V_{wd}	488
V_{cd}	334
V_{Rd}	1271
difference	-11%

$V_{theoretical\theta}$	
V_{fd}	338
V_{wd}	368
V_{cd}	334
V_{Rd}	1040
difference	8%

E_f = FRP sheet elastic modulus
ε_{fu} = ultimate FRP strain
t_f = sheet thickness
f_{ck} = concrete characteristic cylindrical strength,28 day
b_f = width of FRP
s_f = spacing of FRP strips
d = beam effective depth
b_w = smallest width of x-section in tensile area
A_{sw} = area of transverse reinforcement
s_{sw} = spacing of transverse reinforcement
f_{ywd} = design steel yield strength
$A_{sl(total)}$ = area of tensile steel reinforcement
θ_{actual} = actual crack angle as measured in test
$\theta_{theoretical}$ = assumed crack angle as measured from the beam axis
α = angle between principal fibre orientation and longitudinal axis of member
V_{test} = applied failure load
V_{dead} = estimated shear from concrete dead load below the failure crack

$C_{Rd,c}$ = limitng coefficient
k = limitng coefficient
z = lever arm (d_v in MCFT)
ρ_l = steel longitudinal geometric ratio
$\varepsilon_{fd,e}$ = design value of effective FRP strain
$\varepsilon_{fk,e}$ = characteristic value of effective FRP strain
f_{cm} = mean value concrete compressive strength
ρ_f = FRP reinforcement ratio
$\varepsilon_{f,e}$ = effective FRP strain

Test specimen 2T03 - fib

input		
E_f	227	Gpa
ε_{fu}	0.017	
t_f	0.33	mm
f_{ck}	25.4	MPa
b_f	254	mm
s_f	356	mm
d	1096	mm
b_w	356	mm
A_{sw}	258	mm^2
s_{sw}	508	mm
f_{ywd}	350	MPa
$A_{sl(total)}$	5593	mm^2
θ_{actual}	90	deg
$\theta_{theoretical}$	45	deg
α	90	deg
V_{test}	956	kN
V_{dead}	0	kN

calculations		
$C_{Rd,c}$	0.18	
k	1.43	
z	986	
ρ_l	0.014	
$\varepsilon_{fd,e}$	0.004	
$\varepsilon_{fk,e}$	0.004	
f_{cm}	33.4	MPa
ρ_f	0.00132	
$\varepsilon_{f,e}$	0.00472	

$V_{actual\theta}$	
V_{fd}	0
V_{wd}	0
V_{cd}	332
V_{Rd}	332
difference	188%

$V_{theoretical\theta}$	
V_{fd}	399
V_{wd}	175
V_{cd}	332
V_{Rd}	906
difference	5.5%

E_f = FRP sheet elastic modulus
ε_{fu} = ultimate FRP strain
t_f = sheet thickness
f_{ck} = concrete characteristic cylindrical strength, 28 day
b_f = width of FRP
s_f = spacing of FRP strips
d = beam effective depth
b_w = smallest width of x-section in tensile area
A_{sw} = area of transverse reinforcement
s_{sw} = spacing of transverse reinforcement
f_{ywd} = design steel yield strength
$A_{sl(total)}$ = area of tensile steel reinforcement
θ_{actual} = actual crack angle as measured in test
$\theta_{theoretical}$ = assumed crack angle as measured from the beam axis
α = angle between principal fibre orientation and longitudinal axis of member
V_{test} = applied failure load
V_{dead} = estimated shear from concrete dead load below the failure crack

$C_{Rd,c}$ = limitng coefficient
k = limitng coefficient
z = lever arm (d_v in MCFT)
ρ_l = steel longitudinal geometric ratio
$\varepsilon_{fd,e}$ = design value of effective FRP strain
$\varepsilon_{fk,e}$ = characteristic value of effective FRP strain
f_{cm} = mean value concrete compressive strength
ρ_f = FRP reinforcement ratio
$\varepsilon_{f,e}$ = effective FRP strain

Test specimen 2T04 - fib

input		
E_f	227	Gpa
ε_{fu}	0.017	
t_f	0.33	mm
f_{ck}	29.37	MPa
b_f	254	mm
s_f	356	mm
d	1096	mm
b_w	356	mm
A_{sw}	258	mm^2
s_{sw}	406.4	mm
f_{ywd}	350	MPa
$A_{sl(total)}$	4722	mm^2
θ_{actual}	40	deg
$\theta_{theoretical}$	45	deg
α	90	deg
V_{test}	1225	kN
V_{dead}	18.3	kN

calculations		
$C_{Rd,c}$	0.18	
k	1.43	
z	986	
ρ_l	0.012	
$\varepsilon_{fd,e}$	0.004	
$\varepsilon_{fk,e}$	0.004	
f_{cm}	37.37	MPa
ρ_f	0.00132	
$\varepsilon_{f,e}$	0.00493	

$V_{actual\theta}$	
V_{fd}	495
V_{wd}	261
V_{cd}	330
V_{Rd}	1086
difference	14%

$V_{theoretical\theta}$	
V_{fd}	416
V_{wd}	219
V_{cd}	330
V_{Rd}	964
difference	28.9%

E_f = FRP sheet elastic modulus

ε_{fu} = ultimate FRP strain

t_f = sheet thickness

f_{ck} = concrete characteristic cylindrical strength, 28 day

b_f = width of FRP

s_f = spacing of FRP strips

d = beam effective depth

b_w = smallest width of x-section in tensile area

A_{sw} = area of transverse reinforcement

s_{sw} = spacing of transverse reinforcement

f_{ywd} = design steel yield strength

$A_{sl(total)}$ = area of tensile steel reinforcement

θ_{actual} = actual crack angle as measured in test

$\theta_{theoretical}$ = assumed crack angle as measured from the beam axis

α = angle between principal fibre orientation and longitudinal axis of member

V_{test} = applied failure load

V_{dead} = estimated shear from concrete dead load below the failure crack

$C_{Rd,c}$ = limitng coefficient

k = limitng coefficient

z = lever arm (d_v in MCFT)

ρ_l = steel longitudinal geometric ratio

$\varepsilon_{fd,e}$ = design value of effective FRP strain

$\varepsilon_{fk,e}$ = characteristic value of effective FRP strain

f_{cm} = mean value concrete compressive strength

ρ_f = FRP reinforcement ratio

$\varepsilon_{f,e}$ = effective FRP strain

Test specimen 3IT05 - fib

input		
E_f	227	Gpa
ε_{fu}	0.017	
t_f	0.165	mm
f_{ck}	25.39	MPa
b_f	305	mm
s_f	356	mm
d	1150	mm
b_w	356	mm
A_{sw}	258	mm^2
s_{sw}	254	mm
f_{ywd}	350	MPa
$A_{sl(total)}$	5084	mm^2
θ_{actual}	45	deg
$\theta_{theoretical}$	45	deg
α	90	deg
V_{test}	1134	kN
V_{dead}	13	kN

calculations		
$C_{Rd,c}$	0.18	
k	1.42	
z	1035	
ρ_l	0.012	
$\varepsilon_{fd,e}$	0.005	
$\varepsilon_{fk,e}$	0.00503	
f_{cm}	33.39	MPa
ρ_f	0.00079	
$\varepsilon_{f,e}$	0.00629	

$V_{actual@}$	
V_{fd}	334
V_{wd}	368
V_{cd}	330
V_{Rd}	1032
difference	11%

$V_{theoretical@}$	
V_{fd}	334
V_{wd}	368
V_{cd}	330
V_{Rd}	1032
difference	11%

E_f = FRP sheet elastic modulus

ε_{fu} = ultimate FRP strain

t_f = sheet thickness

f_{ck} = concrete characteristic cylindrical strength, 28 day

b_f = width of FRP

s_f = spacing of FRP strips

d = beam effective depth

b_w = smallest width of x-section in tensile area

A_{sw} = area of transverse reinforcement

s_{sw} = spacing of transverse reinforcement

f_{ywd} = design steel yield strength

$A_{sl(total)}$ = area of tensile steel reinforcement

θ_{actual} = actual crack angle as measured in test

$\theta_{theoretical}$ = assumed crack angle as measured from the beam axis

α = angle between principal fibre orientation and longitudinal axis of member

V_{test} = applied failure load

V_{dead} = estimated shear from concrete dead load below the failure crack

$C_{Rd,c}$ = limitng coefficient

k = limitng coefficient

z = lever arm (d_v in MCFT)

ρ_l = steel longitudinal geometric ratio

$\varepsilon_{fd,e}$ = design value of effective FRP strain

$\varepsilon_{fk,e}$ = characteristic value of effective FRP strain

f_{cm} = mean value concrete compressive strength

ρ_f = FRP reinforcement ratio

$\varepsilon_{f,e}$ = effective FRP strain

Test specimen 3IT06 - fib

input		
E_f	227	Gpa
ε_{fu}	0.017	
t_f	0.165	mm
f_{ck}	23.33	MPa
b_f	305	mm
s_f	356	mm
d	1150	mm
b_w	356	mm
A_{sw}	258	mm^2
s_{sw}	254	mm
f_{ywd}	350	MPa
$A_{sl(total)}$	5039	mm^2
θ_{actual}	39	deg
$\theta_{theoretical}$	45	deg
α	90	deg
V_{test}	1116	kN
V_{dead}	9.3	kN

calculations		
$C_{Rd,c}$	0.18	
k	1.42	
z	1035	
ρ_l	0.012	
$\varepsilon_{fd,e}$	0.005	
$\varepsilon_{fk,e}$	0.005	
f_{cm}	31.33	MPa
ρ_f	0.00079	
$\varepsilon_{f,e}$	0.00614	

$V_{actual\theta}$	
V_{fd}	403
V_{wd}	454
V_{cd}	320
V_{Rd}	1177
difference	-4%

$V_{theoretical\theta}$	
V_{fd}	326
V_{wd}	368
V_{cd}	320
V_{Rd}	1014
difference	11%

E_f = FRP sheet elastic modulus
ε_{fu} = ultimate FRP strain
t_f = sheet thickness
f_{ck} = concrete characteristic cylindrical strength, 28 day
b_f = width of FRP
s_f = spacing of FRP strips
d = beam effective depth
b_w = smallest width of x-section in tensile area
A_{sw} = area of transverse reinforcement
s_{sw} = spacing of transverse reinforcement
f_{ywd} = design steel yield strength
$A_{sl(total)}$ = area of tensile steel reinforcement
θ_{actual} = actual crack angle as measured in test
$\theta_{theoretical}$ = assumed crack angle as measured from the beam axis
α = angle between principal fibre orientation and longitudinal axis of member
V_{test} = applied failure load
V_{dead} = estimated shear from concrete dead load below the failure crack

$C_{Rd,c}$ = limitng coefficient
k = limitng coefficient
z = lever arm (d_v in MCFT)
ρ_l = steel longitudinal geometric ratio
$\varepsilon_{fd,e}$ = design value of effective FRP strain
$\varepsilon_{fk,e}$ = characteristic value of effective FRP strain
f_{cm} = mean value concrete compressive strength
ρ_f = FRP reinforcement ratio
$\varepsilon_{f,e}$ = effective FRP strain

Test specimen 4IT07 - fib

input		
E_f	227	Gpa
ε_{fu}	0.017	
t_f	0.33	mm
f_{ck}	26.27	MPa
b_f	305	mm
s_f	356	mm
d	1150	mm
b_w	356	mm
A_{sw}	258	mm^2
s_{sw}	254	mm
f_{ywd}	350	MPa
$A_{sl(total)}$	5103	mm^2
θ_{actual}	44	deg
$\theta_{theoretical}$	45	deg
α	90	deg
V_{test}	1110	kN
V_{dead}	9.2	kN

calculations		
$C_{Rd,c}$	0.18	
k	1.42	
z	1035	
ρ_l	0.012	
$\varepsilon_{fd,e}$	0.003	
$\varepsilon_{fk,e}$	0.003	
f_{cm}	34.27	MPa
ρ_f	0.00159	
$\varepsilon_{f,e}$	0.00431	

$V_{actual\theta}$	
V_{fd}	474
V_{wd}	381
V_{cd}	334
V_{Rd}	1189
difference	-6%

$V_{theoretical\theta}$	
V_{fd}	458
V_{wd}	368
V_{cd}	334
V_{Rd}	1160
difference	-3%

E_f = FRP sheet elastic modulus
ε_{fu} = ultimate FRP strain
t_f = sheet thickness
f_{ck} = concrete characteristic cylindrical strength, 28 day
b_f = width of FRP
s_f = spacing of FRP strips
d = beam effective depth
b_w = smallest width of x-section in tensile area
A_{sw} = area of transverse reinforcement
s_{sw} = spacing of transverse reinforcement
f_{ywd} = design steel yield strength
$A_{sl(total)}$ = area of tensile steel reinforcement
θ_{actual} = actual crack angle as measured in test
$\theta_{theoretical}$ = assumed crack angle as measured from the beam axis
α = angle between principal fibre orientation and longitudinal axis of member
V_{test} = applied failure load
V_{dead} = estimated shear from concrete dead load below the failure crack

$C_{Rd,c}$ = limitng coefficient
k = limitng coefficient
z = lever arm (d_v in MCFT)
ρ_l = steel longitudinal geometric ratio
$\varepsilon_{fd,e}$ = design value of effective FRP strain
$\varepsilon_{fk,e}$ = characteristic value of effective FRP strain
f_{cm} = mean value concrete compressive strength
ρ_f = FRP reinforcement ratio
$\varepsilon_{f,e}$ = effective FRP strain

$V_{Rd} = \min(V_{cd} + V_{wd} + V_{fd},\ V_{Rd,c})$

$V_{cd} = [C_{Rd,c}\, k\, (100\rho_1 f_{ck})^{1/3} + k_1 \sigma_{cp}]\, b_w d$ EC (6.2.a)

$C_{Rd,c} = \frac{0.18}{\gamma_c}$; Assume $\gamma_c = 1.0$

$k = 1 + \sqrt{\frac{200}{d}} \le 2.0 = 1 + \sqrt{\frac{200}{1150}} = 1.42$

d = DISTANCE FROM COMP. FIBER TO CENTROID OF LONGITUDINAL REINFORCEMENT (mm) = 1150mm

$\rho_1 = \frac{A_{s1}}{b_w d} \le 0.02 = \frac{5161\,mm^2}{356(1150)} = .013$

$A_{s1} = 5161\ mm^2$
$b_w = 356mm$
$d = 1150$

$f_{ck} = 29.3\ MPa$

$k_1 = 0.15$

$\sigma_{cp} = \emptyset$

$V_{cd} = [0.18(1.42)(100(0.013)(29.3))^{1/3}](356)(1150) = \underline{348\,kN}$ EC (6.8)

CHECKS

CHECK MIN $V_{cd} = (v_{min} + k_1 \sigma_{cp}) b_w d$

$v_{min} = 0.035(k)^{3/2}(f_{ck})^{1/2} = .035(1.42)^{3/2}(29.3)^{1/2} = .32$

$V_{cd,min} = (.32)(356)(1150) = 131\,kN$ (O.K.)

$V_{wd} = (V_s) = \frac{A_{sw}}{s} z (f_{ywd}) \cot\theta$

$A_{sw} = 258.1\,mm^2$

$s = 254\,mm$

$z = [d_v (mcot)] = .9d = 1035mm$

$f_{ywd} = 350\,MPa$

$\theta = 45°$

$V_{wd} = \frac{258}{254}(1035)(350)(\cot 45) = \underline{368\,kN}$

CHECK

$$A_{sw,MAX} \leq \frac{b_w s \frac{1}{2} \alpha_{cw} \nu_1 f_{cd}}{f_{ywd}}$$

$\alpha_{cw} = 1$

$\nu_1 = \nu = 0.6\left[1 - \frac{f_{ck}}{250}\right] = 0.6\left[1 - \frac{29.3}{250}\right] = .53$

f_{cd} = DESIGN COMPRESSIVE STRENGTH

$= \frac{\alpha_{cc} f_{ck}}{\gamma_c} = \frac{29.3}{1.5} = 19.5\ MPa$

$\alpha_{cc} = 1$

$\gamma_c = 1.5$

$A_{sw,MAX} = \frac{356(254)\frac{1}{2}(1)(.53)(19.5^{MPa})}{350^{MPa}} = 1335 mm^2 > 258$ O.K.

CHECK

$V_{Rd,MAX} > V_{Rd,s}$

$V_{Rd,MAX} = \alpha_{cw} b_w z \nu_1 f_{cd} (\cot\theta + \cot\alpha)/(1+\cot^2\theta)$

$= (1)(356)(1035)(.53)(19.5)(\cot 45° + \cot 90°)/(1+\cot^2 45°)$

$V_{Rd,MAX} = 3808 kN > V_{Rd,s}$ O.K.

$V_{fd} = 0.9 \epsilon_{fd,e} E_{fu} \rho_f b_w d (\cot\theta + \cot\alpha) \sin\alpha$ fib (5-2)

$\epsilon_{fd,e} = \epsilon_{fk,e}/\gamma_f$

$\epsilon_{fk,e} = k \epsilon_{f,e}$

$k = 0.8$

$\epsilon_{f,e} = MIN\left[0.65\left(\frac{f_{cm}^{2/3}}{E_{fu}\rho_f}\right)^{0.56} \times 10^{-3}, 0.17\left(\frac{f_{cm}^{2/3}}{E_{fu}\rho_f}\right)^{0.30} \epsilon_{fu}\right]$

$f_{cm} = f_{ck} + 8(MPa) = 29.3 + 8 = 37.3 MPa$

$E_{fu} = 227 GPa$

$\rho_f = \frac{2 t_f}{b_w}\left(\frac{b_f}{s_f}\right) = \frac{2(.165)}{356}\left(\frac{305}{356}\right) = .0008$

$t_f = 0.165 mm$

$b_f = 305 mm$

$s_f = 356 mm$

FIB/EUROCODE 2 | SPECIMEN 1IT01 | SHEAR CAPACITY | 3/3

$$\epsilon_{f,e} = 0.65\left(\frac{37.3^{2/3}}{227(.0008)}\right)^{0.56} \times 10^{-3} = .007 \quad \text{CONTROLS}$$

OR

$$0.17\left(\frac{37.3^{2/3}}{227(.0008)}\right)^{0.30} .017 = .01$$

$$\epsilon_{fk,e} = 0.8(.007) = .005$$

$$\epsilon_{fd,e} = \epsilon_{fk,e}/\gamma_f \; ; \; \gamma_f = 1.0, \; \therefore = .005$$

$$V_{fd} = 0.9(.005)(227\times10^3)(.0008)(356)(1150)(\cot 45^\circ + \cot 90^\circ)\sin 90^\circ = 348\,kN$$

$$V_{cd} + V_{wd} + V_{fd} = 318\,kN + 368\,kN + 348\,kN = 1034\,kN$$

Japan Design Capacity Calculations

Test specimen 1IT01 - Japan Method

input		
*E_f	227	Gpa
*t_f	0.165	mm
$\varepsilon_{f(limit)}$	0.007	
f'_{cd}	29.3	MPa
b_f	305	mm
d	1150	mm
s_f	356	mm
α_f	90	deg
b_w	356	mm
a	3139	mm
s_s	254	mm
f_{wyd}	350	MPa
A_w	258	mm^2
α_s	90	deg
A_s	5161	mm^2
V_{test}	1145	kN
V_{dead}	11.4	kN

*Manufacturer's reported FRP system properties

calculations		
β_d	0.966	
β_p	1.08	
**β_n	1.263	
f_{vcd}	0.617	MPa
f_{fud}	1589	MPa
z	1000	mm
p_w	0.013	
ρ_f	0.0008	
R	0.773	
K	0.80	

**Design factor estimated usign equation from literature (Miyauchi et al. 1997)

V		
V_{FRP}	359	kN
V_{steel}	356	kN
V_{cd}	333	kN
V_{total}	1047	kN
difference	10%	

E_f = tensile modulus of elasticity

t_f = nominal thickness of one ply of FRP

$\varepsilon_{f(limit)}$ = upper limit design strain (taken from literature, Tumlian et al. 2001)

f'_{cd} = design compressive strength of concrete

b_f = FRP strip width

d = effective depth

s_f = spacing of continuous fiber sheet

α_f = angle formed by continuous fiber sheet about the member axis

b_w = web width

a = shear span

s_s = steel stirrup spacing

f_{wyd} = design tension yield strength of shear reinforcement (400 MPa max)

A_w = total cross-sectional area of shear reinforcement in space s_s

α_s = angle formed by shear reinforcement about the member axis

A_s = cross-sectional area of reinforcing bars in tension side

V_{test} = applied failure load

V_{dead} = estimated shear from concrete dead load below the failure crack

β's limit factors

f_{vcd} = 0.20*(f'cd)^(1/3)

f_{fud} = design tension strength of continuous fiber sheet

z = lever arm length

ρ_f, ρ_w = reinforcement ratios

R, K = limiting factors

Test specimen 1IT02 - Japan Method

input		
*E_f	227	Gpa
*t_f	0.165	mm
$\varepsilon_{f(limit)}$	0.007	
f'_{cd}	26.34	MPa
b_f	305	mm
d	1150	mm
s_f	356	mm
b_w	356	mm
a	3139	mm
s_s	254	mm
f_{wyd}	350	MPa
A_{sv}	258	mm^2
α_f	90	deg
$A_{sl(total)}$	5103	mm^2
V_{test}	1112	kN
V_{dead}	12.7	kN

*Manufacturer's reported FRP system properties

calculations		
β_d	0.966	
β_p	1.08	
**β_n	1.263	
f_{vcd}	0.595	MPa
f_{fud}	1589	MPa
z	1000	mm
ρ_w	0.012	
ρ_f	0.0008	
R	0.801	
K	0.80	

**Design factor estimated usign equation from literature (Miyauchi et al. 1997)

V		
V_{FRP}	359	kN
V_{steel}	356	kN
V_{cd}	320	kN
V_{total}	1035	kN
difference	9%	

E_f = tensile modulus of elasticity

t_f = nominal thickness of one ply of FRP

$\varepsilon_{f(limit)}$ = upper limit design strain (taken from literature, Tumlian et al. 2001)

f'_{cd} = design compressive strength of concrete

b_f = FRP strip width

d = effective depth

s_f = spacing of continuous fiber sheet

α_f = angle formed by continuous fiber sheet about the member axis

b_w = web width

a = shear span

s_s = steel stirrup spacing

f_{wyd} = design tension yield strength of shear reinforcement (400 Mpa max)

A_w = total cross-sectional area of shear reinforcement in space s_s

α_s = angle formed by shear reinforcement about the member axis

A_s = cross-sectional area of reinforcing bars in tension side

V_{test} = applied failure load

V_{dead} = estimated shear from concrete dead load below the failure crack

β's limit factors

f_{vcd} = 0.20*(f'cd)^(1/3)

f_{fud} = design tension strength of continuous fiber sheet

z = lever arm length

ρ_f, ρ_w = reinforcement ratios

R, K = limiting factors

Test specimen 2T03 - Japan Method

input		
*E_f	227	Gpa
*t_f	0.33	mm
$\varepsilon_{f(limit)}$	0.007	
f'_{cd}	25.4	MPa
b_f	254	mm
d	1096	mm
s_f	356	mm
α_f	90	deg
b_w	356	mm
a	2667	mm
s_s	508	mm
f_{wyd}	350	MPa
A_w	258	mm^2
α_s	90	deg
A_s	5593	mm^2
V_{test}	956	kN
V_{dead}	0	kN

*Manufacturer's reported FRP system properties

calculations		
β_d	0.977	
β_p	1.13	
**β_n	1.325	
f_{vcd}	0.588	MPa
f_{fud}	1589	MPa
z	953	mm
p_w	0.014	
ρ_f	0.0013	
R	0.922	
K	0.80	

**Design factor estimated usign equation from literature (Miyauchi et al. 1997)

V		
V_{FRP}	570	kN
V_{steel}	169	kN
V_{cd}	335	kN
V_{total}	1075	kN
difference	-11%	

E_f = tensile modulus of elasticity

t_f = nominal thickness of one ply of FRP

$\varepsilon_{f(limit)}$ = upper limit design strain (taken from literature, Tumlian et al. 2001)

f'_{cd} = design compressive strength of concrete

b_f = FRP strip width

d = effective depth

s_f = spacing of continuous fiber sheet

α_f = angle formed by continuous fiber sheet about the member axis

b_w = web width

a = shear span

s_s = steel stirrup spacing

f_{wyd} = design tension yield strength of shear reinforcement (400 MPa max)

A_w = total cross-sectional area of shear reinforcement in space s_s

α_s = angle formed by shear reinforcement about the member axis

A_s = cross-sectional area of reinforcing bars in tension side

V_{test} = applied failure load

V_{dead} = estimated shear from concrete dead load below the failure crack

β's limit factors

f_{vcd} = 0.20*(f'cd)^(1/3)

f_{fud} = design tension strength of continuous fiber sheet

z = lever arm length

ρ_f, p_w = reinforcement ratios

R, K = limiting factors

Test specimen 2T04 - Japan Method

input		
*E_f	227	Gpa
*t_f	0.33	mm
$\varepsilon_{f(limit)}$	0.007	
f'_{cd}	29.37	MPa
b_f	254	mm
d	1096	mm
s_f	356	mm
α_f	90	deg
b_w	356	mm
a	2667	mm
s_s	406.4	mm
f_{wyd}	350	MPa
A_w	258	mm^2
α_s	90	deg
A_s	4722	mm^2
V_{test}	1225	kN
V_{dead}	18.3	kN

*Manufacturer's reported FRP system properties

calculations		
β_d	0.977	
β_p	1.07	
$**\beta_n$	1.325	
f_{vcd}	0.617	MPa
f_{fud}	1589	MPa
z	953	mm
ρ_w	0.012	
ρ_f	0.0013	
R	0.878	
K	0.80	

**Design factor estimated usign equation from literature (Miyauchi et al. 1997)

V		
V_{FRP}	570	kN
V_{steel}	212	kN
V_{cd}	332	kN
V_{total}	1115	kN
difference	11.5%	

E_f = tensile modulus of elasticity

t_f = nominal thickness of one ply of FRP

$\varepsilon_{f(limit)}$ = upper limit design strain (taken from literature, Tumlian et al. 2001)

f'_{cd} = design compressive strength of concrete

b_f = FRP strip width

d = effective depth

s_f = spacing of continuous fiber sheet

α_f = angle formed by continuous fiber sheet about the member axis

b_w = web width

a = shear span

s_s = steel stirrup spacing

f_{wyd} = design tension yield strength of shear reinforcement (400 MPa max)

A_w = total cross-sectional area of shear reinforcement in space s_s

α_s = angle formed by shear reinforcement about the member axis

A_s = cross-sectional area of reinforcing bars in tension side

V_{test} = applied failure load

V_{dead} = estimated shear from concrete dead load below the failure crack

β's limit factors

$f_{vcd} = 0.20*(f'_{cd})^{(1/3)}$

f_{fud} = design tension strength of continuous fiber sheet

z = lever arm length

ρ_f, ρ_w = reinforcement ratios

R, K = limiting factors

Test specimen 3IT05 - Japan Method

input		
*E_f	227	Gpa
*t_f	0.165	mm
$\varepsilon_{f(limit)}$	0.007	
f'_{cd}	25.39	MPa
b_f	305	mm
d	1150	mm
s_f	356	mm
b_w	356	mm
a	3139	mm
s_s	254	mm
f_{wyd}	350	MPa
A_{sv}	258	mm^2
α_f	90	deg
$A_{sl(total)}$	5084	mm^2
V_{test}	1134	kN
V_{dead}	13	kN

*Manufacturer's reported FRP system properties

calculations		
β_d	0.966	
β_p	1.07	
**β_n	1.263	
f_{vcd}	0.588	MPa
f_{fud}	1589	MPa
z	1000	mm
p_w	0.012	
ρ_f	0.0008	
R	0.811	
K	0.80	

**Design factor estimated usign equation from literature (Miyauchi et al. 1997)

V		
V_{FRP}	359	kN
V_{steel}	356	kN
V_{cd}	315	kN
V_{total}	1030	kN
difference	11%	

E_f = tensile modulus of elasticity

t_f = nominal thickness of one ply of FRP

$\varepsilon_{f(limit)}$ = upper limit design strain (taken from literature, Tumlian et al. 2001)

f'_{cd} = design compressive strength of concrete

b_f = FRP strip width

d = effective depth

s_f = spacing of continuous fiber sheet

α_f = angle formed by continuous fiber sheet about the member axis

b_w = web width

a = shear span

s_s = steel stirrup spacing

f_{wyd} = design tension yield strength of shear reinforcement (400 MPa max)

A_v = total cross-sectional area of shear reinforcement in space s_s

α_s = angle formed by shear reinforcement about the member axis

A_s = cross-sectional area of reinforcing bars in tension side

V_{test} = applied failure load

V_{dead} = estimated shear from concrete dead load below the failure crack

β's limit factors

f_{vcd} = 0.20*(f'cd)^(1/3)

f_{fud} = design tension strength of continuous fiber sheet

z = lever arm length

ρ_f, p_w = reinforcement ratios

R, K = limiting factors

Test specimen 3IT06 - Japan Method

input		
*E_f	227	Gpa
*t_f	0.165	mm
$\varepsilon_{f(limit)}$	0.007	
f'_{cd}	23.33	MPa
b_f	305	mm
d	1150	mm
s_f	356	mm
b_w	356	mm
a	3139	mm
s_s	254	mm
f_{wyd}	350	MPa
A_{sv}	258	mm^2
α_f	90	deg
$A_{sl(total)}$	5039	mm^2
V_{test}	1116	kN
V_{dead}	9.3	kN

*Manufacturer's reported FRP system properties

calculations		
β_d	0.966	
β_p	1.07	
**β_n	1.263	
f_{vcd}	0.571	MPa
f_{fud}	1589	MPa
z	1000	mm
p_w	0.012	
ρ_f	0.0008	
R	0.834	
K	0.80	

**Design factor estimated usign equation from literature (Miyauchi et al. 1997)

V		
V_{FRP}	359	kN
V_{steel}	356	kN
V_{cd}	306	kN
V_{total}	1021	kN
difference	10%	

E_f = tensile modulus of elasticity

t_f = nominal thickness of one ply of FRP

$\varepsilon_{f(limit)}$ = upper limit design strain (taken from literature, Tumlian et al. 2001)

f'_{cd} = design compressive strength of concrete

b_f = FRP strip width

d = effective depth

s_f = spacing of continuous fiber sheet

α_f = angle formed by continuous fiber sheet about the member axis

b_w = web width

a = shear span

s_s = steel stirrup spacing

f_{wyd} = design tension yield strength of shear reinforcement (400 MPa max)

A_w = total cross-sectional area of shear reinforcement in space s_s

α_s = angle formed by shear reinforcement about the member axis

A_s = cross-sectional area of reinforcing bars in tension side

V_{test} = applied failure load

V_{dead} = estimated shear from concrete dead load below the failure crack

β's limit factors

f_{vcd} = 0.20*(f'cd)^(1/3)

f_{fud} = design tension strength of continuous fiber sheet

z = lever arm length

ρ_f, p_w = reinforcement ratios

R, K = limiting factors

Test specimen 4IT07 - Japan Method

input		
*E_f	227	Gpa
*t_f	0.33	mm
$\varepsilon_{f(limit)}$	0.007	
f'_{cd}	26.27	MPa
b_f	305	mm
d	1150	mm
s_f	356	mm
b_w	356	mm
a	3139	mm
s_s	254	mm
f_{wyd}	350	MPa
A_{sv}	258	mm^2
α_f	90	deg
$A_{sl(total)}$	5103	mm^2
V_{test}	1110	kN
V_{dead}	9.2	kN

*Manufacturer's reported FRP system properties

calculations		
β_d	0.966	
β_p	1.08	
**β_n	1.263	
f_{vcd}	0.595	MPa
f_{fud}	1589	MPa
z	1000	mm
ρ_w	0.012	
ρ_f	0.0016	
R	0.954	
K	0.80	

**Design factor estimated usign equation from literature (Miyauchi et al. 1997)

V		
V_{FRP}	719	kN
V_{steel}	356	kN
V_{cd}	319	kN
V_{total}	1394	kN
difference	-20%	

E_f = tensile modulus of elasticity

t_f = nominal thickness of one ply of FRP

$\varepsilon_{f(limit)}$ = upper limit design strain (taken from literature, Tumlian et al. 2001)

f'_{cd} = design compressive strength of concrete

b_f = FRP strip width

d = effective depth

s_f = spacing of continuous fiber sheet

α_f = angle formed by continuous fiber sheet about the member axis

b_w = web width

a = shear span

s_s = steel stirrup spacing

f_{wyd} = design tension yield strength of shear reinforcement (400 MPa max)

A_w = total cross-sectional area of shear reinforcement in space s_s

α_s = angle formed by shear reinforcement about the member axis

A_s = cross-sectional area of reinforcing bars in tension side

V_{test} = applied failure load

V_{dead} = estimated shear from concrete dead load below the failure crack

β's = limit factors

f_{vcd} = 0.20*(f'cd)^(1/3)

f_{fud} = design tension strength of continuous fiber sheet

z = lever arm length

ρ_f, ρ_w = reinforcement ratios

R, K = limiting factors

$V_{yd} = V_{cd} + V_{sd} + V_{fd}$

$V_{cd} = \beta_d \beta_p \beta_n f_{vcd} b_w d / \gamma_b$

$f_{vcd} = 0.20 \sqrt[3]{f'_{cd}}$ (0.72 max)

$f'_{cd} = 28.1$ MPa (N/mm²)

$= 0.20 \sqrt[3]{29.3} = .62$ MPa

$\beta_d = \sqrt[4]{1/d}$ (1.5 max)

$d = 1150$ mm

$= \sqrt[4]{1/1.15} = .97$

$\beta_p = \sqrt[3]{100 p_w}$ (1.5 max)

$p_w = \frac{A_s}{b_w d} = \frac{5161\ mm^2}{356mm(1150mm)} = .013$

$= \sqrt[3]{100(.013)} = 1.08$

(Niwa et al 1987) $\beta_n = 0.75 + 1.4/(1/d) = 0.75 + 1.4/(\frac{3139mm}{1000mm}) = 1.26$

$a = 3139$ mm

$V_{cd} = .97(1.08)(1.26)(0.62\ MPa)(356)(1150mm) = 333kN$

$V_{sd} = [A_w \cdot f_{wyd} (\sin\alpha_s + \cos\alpha_s)/s_s] z / \gamma_b$

$A_w = 258 mm^2$

$f_{wyd} = 350$ MPa

$\alpha_s = 90°$

$s_s = 254$ mm

$z = \frac{d}{1.15} = \frac{1150}{1.15} = 1000$ mm

$V_{sd} = \frac{258(350)(1)}{254} 1000mm$ 356 kN

ISCE #41	SPECIMEN 11T01	SHEAR CAPACITY	2/2

$$V_{fd} = K \cdot [A_f \cdot f_{fud} (\sin\alpha_f + \cos\alpha_f)/s_f] \cdot z/\gamma_b$$

$$K = 1.68 - 0.67R \quad (0.4 \le K \le 0.8)$$

$$R = [\rho_f \cdot E_f]^{1/4} \cdot \left[\frac{f_{fud}}{E_f}\right]^{2/3} \left(\frac{1}{f_{cd}}\right)^{1/3} \quad (0.5 \le R \le 2.0)$$

$$\rho_f = \frac{A_f}{b_w \cdot s_f} = \frac{0.165mm \cdot (305mm)(2)}{356mm\,(356mm)} = .0008$$

$E_f = 227\ GPa$

$f_{fud} = E_f(\varepsilon_f) = 227 \times 10^3 (.007) = 1589\ MPa$

$\alpha_f = 90°$

$s_f = 356mm$

$$R = (.0008 \cdot 227)^{1/4} \left(\frac{1589}{227}\right)^{2/3} \left(\frac{1}{27.3}\right)^{1/3} =$$

$$R = .652\,(3.66)(.329) = 0.773$$

$$K = 1.68 - 0.67(.786) = 1.15 \quad (\therefore K = 0.8)$$

$\gamma_b = 1.25$ (per code)

$$V_{fd} = \frac{0.8[(0.165(305)(2)mm^2)(1589\,MPa)(1)/356mm] \cdot 1000mm}{(1000)} = 359\,kN$$

$$V_{fyd} = 333 + 356 + 359 = \boxed{1047\,kN}$$

DIFFERENCE = 10%

Monti & Liotta (Italy) Design Capacity Calculations

Test specimen 1IT01 - Monti & Liotta

input		
E_f	227	Gpa
t_f	0.165	mm
f_{ck}	29.3	MPa
w_f	305	mm
p_f	356	mm
d	1150	mm
h_w	1067	mm
b_w	356	mm
n_{st}	2	
A_{st}	129	mm^2
s_{st}	254	mm
f_{yd}	350	MPa
$A_{sl(total)}$	5161	mm^2
θ_{actual}	37	deg
$\theta_{theoretical}$	45	deg
β	90	deg
V_{test}	1145	kN
V_{dead}	11.4	kN

calculations	
R_{ck}	36.625
f_{ctm}	2.98
l_e	79
k_b	1
Γ_{Fk}	0.28
f_{fdd}	702
f_{fed}	685
ρ_{sl}	0.013

$V_{actual\theta}$	
$V_{Rd,FRP}$	266
$V_{Rd,steel}$	488
$V_{Rd,concrete}$	348
$V_{Rd,total}$	1102
difference	5%

$V_{theoretical\theta}$	
$V_{Rd,FRP}$	200
$V_{Rd,steel}$	368
$V_{Rd,concrete}$	348
$V_{Rd,total}$	916
difference	26%

E_f = FRP sheet elastic modulus
t_f = sheet thickness
f_{ck} = concrete characteristic cylindrical strength
w_f = FRP strip width measured orthogonally to β
p_f = FRP strip spacing measured orthogonally to β
d = beam effective depth
h_w = beam web depth
b_w = web section width
n_{st} = transverse reinforcement arm number
A_{st} = area (one arm) of transverse reinforcement
s_{st} = spacing of transverse reinforcement
f_{yd} = design steel yield strength
$A_{sl(total)}$ = area of longitudinal steel reinforcement
θ_{actual} = actual crack angle as measured in test
$\theta_{theoretical}$ = assumed crack angle as measured from the beam axis
β = angle of strip or sheet to the beam axis
V_{test} = applied failure load

R_{ck} = concrete characteristic cubic strength
f_{ctm} = concrete mean tensile strength
l_e = effective bond length
k_b = convering/scale coefficient
Γ_{Fk} = specific rupture energy of the bond
f_{fdd} = debonding strength
f_{fed} = effective debonding strength
ρ_{sl} = steel longitudinal geometric ratio

Test specimen 1IT02 - Monti & Liotta

input		
E_f	227	Gpa
t_f	0.165	mm
f_{ck}	26.34	MPa
w_f	305	mm
p_f	356	mm
d	1150	mm
h_w	1067	mm
b_w	356	mm
n_{st}	2	
A_{st}	129	mm^2
s_{st}	254	mm
f_{yd}	350	MPa
$A_{sl(total)}$	5103	mm^2
θ_{actual}	37	deg
$\theta_{theoretical}$	45	deg
β	90	deg
V_{test}	1112	kN
V_{dead}	12.7	kN

calculations	
R_{ck}	32.925
f'_{ctm}	2.77
l_e	82
k_b	1
Γ_{Fk}	0.26
f_{fdd}	672
f_{fed}	654
ρ_{sl}	0.012

$V_{actual\theta}$	
$V_{Rd,FRP}$	254
$V_{Rd,steel}$	488
$V_{Rd,concrete}$	334
$V_{Rd,total}$	1077
difference	4%

$V_{theoretical\theta}$	
$V_{Rd,FRP}$	191
$V_{Rd,steel}$	368
$V_{Rd,concrete}$	334
$V_{Rd,total}$	894
difference	26%

E_f = FRP sheet elastic modulus
t_f = sheet thickness
f_{ck} = concrete characteristic cylindrical strength
w_f = FRP strip width measured orthogonally to β
p_f = FRP strip spacing measured orthogonally to β
d = beam effective depth
h_w = beam web depth
b_w = web section width
n_{st} = transverse reinforcement arm number
A_{st} = area (one arm) of transverse reinforcement
s_{st} = spacing of transverse reinforcement
f_{yd} = design steel yield strength
$A_{sl(total)}$ = area of longitudinal steel reinforcement
θ_{actual} = actual crack angle as measured in test
$\theta_{theoretical}$ = assumed crack angle as measured from the beam axis
β = angle of strip or sheet to the beam axis
V_{test} = applied failure load

R_{ck} = concrete characteristic cubic strength
f'_{ctm} = concrete mean tensile strength
l_e = effective bond length
k_b = convering/scale coefficient
Γ_{Fk} = specific rupture energy of the bond
f_{fdd} = debonding strength
f_{fed} = effective debonding strength
ρ_{sl} = steel longitudinal geometric ratio

Test specimen 2IT03 - Monti & Liotta

input		
E_f	227	Gpa
t_f	0.33	mm
f_{ck}	25.4	MPa
w_f	254	mm
p_f	356	mm
d	1096	mm
h_w	1067	mm
b_w	356	mm
n_{st}	2	
A_{st}	129	mm^2
s_{st}	508	mm
f_{yd}	350	MPa
$A_{sl(total)}$	5593	mm^2
θ_{actual}	90	deg
$\theta_{theoretical}$	45	deg
β	90	deg
V_{test}	956	kN
V_{dead}	0	kN

calculations	
R_{ck}	31.75
f'_{ctm}	2.71
l_e	118
k_b	1
Γ_{Fk}	0.25
f_{fdd}	468
f_{fed}	449
ρ_{sl}	0.014

$V_{actual\theta}$	
$V_{Rd,FRP}$	0
$V_{Rd,steel}$	0
$V_{Rd,concrete}$	332
$V_{Rd,total}$	332
difference	188%

$V_{theoretical\theta}$	
$V_{Rd,FRP}$	209
$V_{Rd,steel}$	175
$V_{Rd,concrete}$	332
$V_{Rd,total}$	716
difference	33%

E_f = FRP sheet elastic modulus
t_f = sheet thickness
f_{ck} = concrete characteristic cylindrical strength
w_f = FRP strip width measured orthogonally to β
p_f = FRP strip spacing measured orthogonally to β
d = beam effective depth
h_w = beam web depth
b_w = web section width
n_{st} = transverse reinforcement arm number
A_{st} = area (one arm) of transverse reinforcement
s_{st} = spacing of transverse reinforcement
f_{yd} = design steel yield strength
$A_{sl(total)}$ = area of longitudinal steel reinforcement
θ_{actual} = actual crack angle as measured in test
$\theta_{theoretical}$ = assumed crack angle as measured from the beam axis
β = angle of strip or sheet to the beam axis
V_{test} = applied failure load

R_{ck} = concrete characteristic cubic strength
f'_{ctm} = concrete mean tensile strength
l_e = effective bond length
k_b = convering/scale coefficient
Γ_{Fk} = specific rupture energy of the bond
f_{fdd} = debonding strength
f_{fed} = effective debonding strength
ρ_{sl} = steel longitudinal geometric ratio

Test specimen 2IT04 - Monti & Liotta

input		
E_f	227	Gpa
t_f	0.33	mm
f_{ck}	29.37	MPa
w_f	254	mm
p_f	356	mm
d	1096	mm
h_w	1067	mm
b_w	356	mm
n_{st}	2	
A_{st}	129	mm^2
s_{st}	406.4	mm
f_{yd}	350	MPa
$A_{sl(total)}$	4722	mm^2
θ_{actual}	40	deg
$\theta_{theoretical}$	45	deg
β	90	deg
V_{test}	1225	kN
V_{dead}	18.3	kN

calculations	
R_{ck}	36.7125
f'_{ctm}	2.98
l_e	112
k_b	1
Γ_{Fk}	0.28
f_{fdd}	497
f_{fed}	478
ρ_{sl}	0.012

$V_{actual\theta}$	
$V_{Rd,FRP}$	265
$V_{Rd,steel}$	261
$V_{Rd,concrete}$	330
$V_{Rd,total}$	856
difference	45%

$V_{theoretical\theta}$	
$V_{Rd,FRP}$	222
$V_{Rd,steel}$	219
$V_{Rd,concrete}$	330
$V_{Rd,total}$	771
difference	61%

E_f = FRP sheet elastic modulus
t_f = sheet thickness
f_{ck} = concrete characteristic cylindrical strength
w_f = FRP strip width measured orthogonally to β
p_f = FRP strip spacing measured orthogonally to β
d = beam effective depth
h_w = beam web depth
b_w = web section width
n_{st} = transverse reinforcement arm number
A_{st} = area (one arm) of transverse reinforcement
s_{st} = spacing of transverse reinforcement
f_{yd} = design steel yield strength
$A_{sl(total)}$ = area of longitudinal steel reinforcement
θ_{actual} = actual crack angle as measured in test
$\theta_{theoretical}$ = assumed crack angle as measured from the beam axis
β = angle of strip or sheet to the beam axis
V_{test} = applied failure load

R_{ck} = concrete characteristic cubic strength
f'_{ctm} = concrete mean tensile strength
l_e = effective bond length
k_b = convering/scale coefficient
Γ_{Fk} = specific rupture energy of the bond
f_{fdd} = debonding strength
f_{fed} = effective debonding strength
ρ_{sl} = steel longitudinal geometric ratio

Test specimen 3IT05 - Monti & Liotta

input		
E_f	227	Gpa
t_f	0.165	mm
f_{ck}	25.39	MPa
w_f	305	mm
p_f	356	mm
d	1150	mm
h_w	1067	mm
b_w	356	mm
n_{st}	2	
A_{st}	129	mm^2
s_{st}	254	mm
f_{yd}	350	MPa
$A_{sl(total)}$	5084	mm^2
θ_{actual}	45	deg
$\theta_{theoretical}$	45	deg
β	90	deg
V_{test}	1134	kN
V_{dead}	13	kN

calculations	
R_{ck}	31.7375
f'_{ctm}	2.71
l_e	83
k_b	1
Γ_{Fk}	0.25
f_{fdd}	662
f_{fed}	644
ρ_{sl}	0.012

$V_{actual\theta}$	
$V_{Rd,FRP}$	188
$V_{Rd,steel}$	368
$V_{Rd,concrete}$	330
$V_{Rd,total}$	886
difference	29%

$V_{theoretical\theta}$	
$V_{Rd,FRP}$	188
$V_{Rd,steel}$	368
$V_{Rd,concrete}$	330
$V_{Rd,total}$	886
difference	29%

E_f = FRP sheet elastic modulus
t_f = sheet thickness
f_{ck} = concrete characteristic cylindrical strength
w_f = FRP strip width measured orthogonally to β
p_f = FRP strip spacing measured orthogonally to β
d = beam effective depth
h_w = beam web depth
b_w = web section width
n_{st} = transverse reinforcement arm number
A_{st} = area (one arm) of transverse reinforcement
s_{st} = spacing of transverse reinforcement
f_{yd} = design steel yield strength
$A_{sl(total)}$ = area of longitudinal steel reinforcement
θ_{actual} = actual crack angle as measured in test
$\theta_{theoretical}$ = assumed crack angle as measured from the beam axis
β = angle of strip or sheet to the beam axis
V_{test} = applied failure load

R_{ck} = concrete characteristic cubic strength
f'_{ctm} = concrete mean tensile strength
l_e = effective bond length
k_b = convering/scale coefficient
Γ_{Fk} = specific rupture energy of the bond
f_{fdd} = debonding strength
f_{fed} = effective debonding strength
ρ_{sl} = steel longitudinal geometric ratio

Test specimen 3IT06- Monti & Liotta

input		
E_f	227	Gpa
t_f	0.165	mm
f_{ck}	23.33	MPa
w_f	305	mm
p_f	356	mm
d	1150	mm
h_w	1067	mm
b_w	356	mm
n_{st}	2	
A_{st}	129	mm^2
s_{st}	254	mm
f_{yd}	350	MPa
$A_{sl(total)}$	5039	mm^2
θ_{actual}	39	deg
$\theta_{theoretical}$	45	deg
β	90	deg
V_{test}	1116	kN
V_{dead}	9.3	kN

calculations	
R_{ck}	29.1625
f'_{ctm}	2.56
l_e	86
k_b	1
Γ_{Fk}	0.23
f_{fdd}	639
f_{fed}	621
ρ_{sl}	0.012

$V_{actual\theta}$	
$V_{Rd,FRP}$	224
$V_{Rd,steel}$	454
$V_{Rd,concrete}$	320
$V_{Rd,total}$	999
difference	13%

$V_{theoretical\theta}$	
$V_{Rd,FRP}$	182
$V_{Rd,steel}$	368
$V_{Rd,concrete}$	320
$V_{Rd,total}$	870
difference	29%

E_f = FRP sheet elastic modulus
t_f = sheet thickness
f_{ck} = concrete characteristic cylindrical strength
w_f = FRP strip width measured orthogonally to β
p_f = FRP strip spacing measured orthogonally to β
d = beam effective depth
h_w = beam web depth
b_w = web section width
n_{st} = transverse reinforcement arm number
A_{st} = area (one arm) of transverse reinforcement
s_{st} = spacing of transverse reinforcement
f_{yd} = design steel yield strength
$A_{sl(total)}$ = area of longitudinal steel reinforcement
θ_{actual} = actual crack angle as measured in test
$\theta_{theoretical}$ = assumed crack angle as measured from the beam axis
β = angle of strip or sheet to the beam axis
V_{test} = applied failure load

R_{ck} = concrete characteristic cubic strength
f'_{ctm} = concrete mean tensile strength
l_e = effective bond length
k_b = convering/scale coefficient
Γ_{Fk} = specific rupture energy of the bond
f_{fdd} = debonding strength
f_{fed} = effective debonding strength
ρ_{sl} = steel longitudinal geometric ratio

Test specimen 4IT07 - Monti & Liotta

input		
E_f	227	Gpa
t_f	0.33	mm
f_{ck}	26.27	MPa
w_f	305	mm
p_f	356	mm
d	1150	mm
h_w	1067	mm
b_w	356	mm
n_{st}	2	
A_{st}	129	mm^2
s_{st}	254	mm
f_{yd}	350	MPa
$A_{sl(total)}$	5103	mm^2
θ_{actual}	44	deg
$\theta_{theoretical}$	45	deg
β	90	deg
V_{test}	1110	kN
V_{dead}	9.2	kN

calculations	
R_{ck}	32.8375
f_{ctm}	2.77
l_e	116
k_b	1
Γ_{Fk}	0.26
f_{fdd}	475
f_{fed}	457
ρ_{sl}	0.012

$V_{actual\theta}$	
$V_{Rd,FRP}$	277
$V_{Rd,steel}$	381
$V_{Rd,concrete}$	334
$V_{Rd,total}$	992
difference	13%

$V_{theoretical\theta}$	
$V_{Rd,FRP}$	267
$V_{Rd,steel}$	368
$V_{Rd,concrete}$	334
$V_{Rd,total}$	969
difference	15%

E_f = FRP sheet elastic modulus
t_f = sheet thickness
f_{ck} = concrete characteristic cylindrical strength
w_f = FRP strip width measured orthogonally to β
p_f = FRP strip spacing measured orthogonally to β
d = beam effective depth
h_w = beam web depth
b_w = web section width
n_{st} = transverse reinforcement arm number
A_{st} = area (one arm) of transverse reinforcement
s_{st} = spacing of transverse reinforcement
f_{yd} = design steel yield strength
$A_{sl(total)}$ = area of longitudinal steel reinforcement
θ_{actual} = actual crack angle as measured in test
$\theta_{theoretical}$ = assumed crack angle as measured from the beam axis
β = angle of strip or sheet to the beam axis
V_{test} = applied failure load

R_{ck} = concrete characteristic cubic strength
f_{ctm} = concrete mean tensile strength
l_e = effective bond length
k_b = convering/scale coefficient
Γ_{Fk} = specific rupture energy of the bond
f_{fdd} = debonding strength
f_{fed} = effective debonding strength
ρ_{sl} = steel longitudinal geometric ratio

FRPRCS-7 pp. 543-562	SPECIMEN IIT01	SHEAR CAPACITY CALCS	1/2

$$V_{Rd} = V_{Rd,cc} + V_{Rd,s} + V_{Rd,f}$$

$$V_{Rd,cc} = \frac{0.18}{\gamma_c} b_w d \cdot \min\left\{1 + \sqrt{\frac{200mm}{d}}, 2\right\} \cdot \sqrt[3]{100 \cdot \min\{0.02, \rho_{sl}\} \cdot f_{ck}} \quad (21)$$

$\gamma_c = 1.0$
$b_w = 356mm$
$d = 1219mm - 69mm = 1150mm$
$1 + \sqrt{\frac{200mm}{d}} = 1 + \sqrt{\frac{200}{1150}} = 1.42 < 2$
$\rho_{sl} = \frac{A_s}{b_w d} = \frac{516 mm^2}{356mm(1150mm)} = .013 \leq .02$
$A_s = 516 mm^2$ (@ d AWAY FROM LOAD)
$f_{ck} = 29.3 MPa$ (CYLINDRICAL).

$$V_{Rd,cc} = \frac{0.18}{1}(356mm)(1150mm)(1.42)\sqrt[3]{100(.013)(29.3MPa)} = 348 kN$$

$$V_{Rd,s} = 0.9d \cdot f_{yd} \cdot \frac{n_{st} A_{sr}}{s_{sr}} (\cot\theta + \cot\beta_{sr}) \sin\beta_{sr} \quad (22)$$

$f_{yd} = 350 MPa = 350 N/mm^2$
$n_{st} = 2$
$A_{sr} = 129 mm^2$ (1 # 13 BAR)
$s_{sr} = 254mm$
$\theta = 45°$ (THEORETICAL CRACK ANGLE)
$\beta_{sr} = 90°$

$$V_{Rd,s} = 0.9(1150mm)(350 MPa)\left(\frac{2(129mm^2)}{254}\right)(\cot 45° + \cot 90°)\sin 90°$$

$V_{Rd,s} = 368 kN$

$$V_{Rd,f} = \frac{1}{\gamma_{Rd}} 0.9d \cdot f_{fed} \cdot 2t_f (\cot\theta + \cot\beta) \cdot \frac{w_f}{p_f} \quad (16)$$

$\gamma_{Rd} = 1$

$$f_{fed} = f_{fdd} \cdot \left[1 - \frac{1}{3}\frac{l_e \sin\beta}{\min\{0.9d, h_w\}}\right] \quad \text{(U-WRAP)} \quad (13)$$

$$f_{fdd} = \frac{0.80}{\gamma_{f,d}} \sqrt{\frac{2 E_f \Gamma_{Fk}}{t_f}} \quad (N, mm) \quad (4)$$

$\gamma_{f,d} = 1$
$E_f = 227 \cdot 10^3 MPa$

$$\Gamma_{Fk} = 0.03 k_b \sqrt{f_{ck} \cdot f_{ccm}} \quad (N, mm) \quad (2)$$

$$k_b = \sqrt{\frac{2 - w_f/p_f}{1 + w_f/400}} \geq 1 \quad (3)$$

k_b (cont.)

$w_f = 305mm$

$p_f = 356mm$

$k_b = \sqrt{\frac{2 - 305/356}{1 + 305/400}} = .81 \neq 1$

$\therefore k_b = 1.0$

$f_{ck} = 29.3 MPa$

$f_{ctm} = 0.27 R_{ck}^{2/3} = 0.27(36.6)^{2/3} = 2.98 MPa$

R_{ck} = CUBIC STRENGTH = $\frac{\text{CYLINDRICAL}}{0.8}$ (BSI)

$= \frac{29.3 MPa}{0.8} = 36.6 MPa$

$\Gamma_{Fk} = 0.03(1.0)\sqrt{29.3 MPa (2.9 MPa)} = .28$

$t_f = 0.165mm$

$f_{dd} = \frac{0.80}{1}\sqrt{\frac{2(227 \times 10^3 MPa).27}{0.165mm}} = 702 MPa$

β = FIBER ANGLE = 90°

$h_w = 1219mm - 152mm = 1067mm$

$0.9d = 0.9(1150mm) = 1035mm$ CONTROLS

$l_e = \sqrt{\frac{E_f t_f}{2 f_{ctm}}} = \sqrt{\frac{227 \times 10^3 MPa \cdot 0.165mm}{2(2.98 MPa)}} = 79 mm$

$f_{fed} = 702 MPa\left[1 - \frac{1}{3}\left(\frac{79mm \cdot \sin 90°}{1035mm}\right)\right] = 685 MPa$

$V_{Rd,f} = \frac{1}{1}(1035mm)(685 MPa)(2 \cdot 0.165mm)(\cot 45° + \cot 90°)\frac{305mm}{356mm}$

$V_{Rd,f} = \underline{200 kN}$

$V_{Rd} = 348 kN + 368 kN + 200 kN = \boxed{916 kN}$

$V_{ACTUAL} = 1145 kN$ (DIFFERENCE = 21%)

CHECK: $V_{Rd,max} = 0.9 d b_w \nu f_{cd}(\cot\theta + \cot\beta_{sf})/(1+\cot^2\theta)$ (23)

$\nu = 0.6[1 - f_{ck}/250] = 0.6[1 - 29.3 MPa/250] = .53$

$f_{cd} = f_{ck}/\gamma_c = 29.3 MPa/1.0 = 29.3$

$V_{Rd,max} = 0.9(1150mm)(356mm)(0.53)(29.3 MPa)(\cot 45° + \cot 90°)/(1+\cot^2 45°) = 5724 kN$

Response 2000 (R2K) Design Capacity Calculations

Test specimen 1IT01

input		
E_f	227	Gpa
t_f	0.165	mm
f_{ck}	29.3	MPa
w_f	305	mm
p_f	356	mm
d	1150	mm
h_w	1067	mm
b_w	356	mm
n_{st}	2	
A_{st}	129	mm^2
s_{st}	254	mm
f_{yd}	350	MPa
θ_{actual}	37	deg
$\theta_{theoretical}$	45	deg
β	90	deg
V_{test}	1145	kN
V_{dead}	11.4	kN
V_{R2K}	934	kN

$V_{actual\theta}$	
V_{FRP}	222
V_{steel}	488
$V_{concrete}$	446

E_f = FRP sheet elastic modulus

t_f = sheet thickness

f_{ck} = concrete characteristic cylindrical strength

w_f = FRP strip width measured orthogonally to β

p_f = FRP strip spacing measured orthogonally to β

d = beam effective depth

h_w = beam web depth

b_w = web section width

n_{st} = transverse reinforcement arm number

A_{st} = area (one arm) of transverse reinforcement

s_{st} = spacing of transverse reinforcement

f_{yd} = design steel yield strength

$A_{sl(total)}$ = area of longitudinal steel reinforcement

θ_{actual} = actual crack angle as measured in test

$\theta_{theoretical}$ = assumed crack angle as measured from the beam axis

β = angle of strip or sheet to the beam axis

V_{test} = applied failure load

Test specimen 1IT02

input		
E_f	227	Gpa
t_f	0.165	mm
f_{ck}	26.34	MPa
w_f	305	mm
p_f	356	mm
d	1150	mm
h_w	1067	mm
b_w	356	mm
n_{st}	2	
A_{st}	129	mm^2
s_{st}	254	mm
f_{yd}	350	MPa
θ_{actual}	37	deg
$\theta_{theoretical}$	45	deg
β	90	deg
V_{test}	1112	kN
V_{dead}	12.7	kN
V_{R2K}	907	kN

$V_{actual\theta}$	
V_{FRP}	218
V_{steel}	488
$V_{concrete}$	419

E_f = FRP sheet elastic modulus

t_f = sheet thickness

f_{ck} = concrete characteristic cylindrical strength

w_f = FRP strip width measured orthogonally to β

p_f = FRP strip spacing measured orthogonally to β

d = beam effective depth

h_w = beam web depth

b_w = web section width

n_{st} = transverse reinforcement arm number

A_{st} = area (one arm) of transverse reinforcement

s_{st} = spacing of transverse reinforcement

f_{yd} = design steel yield strength

$A_{sl(total)}$ = area of longitudinal steel reinforcement

θ_{actual} = actual crack angle as measured in test

$\theta_{theoretical}$ = assumed crack angle as measured from the beam axis

β = angle of strip or sheet to the beam axis

V_{test} = applied failure load

Test specimen 2T03

input		
E_f	227	Gpa
t_f	0.33	mm
f_{ck}	25.4	MPa
w_f	254	mm
p_f	356	mm
d	1096	mm
b_w	356	mm
n_{st}	2	
A_{st}	129	mm^2
s_{st}	508	mm
f_{yd}	350	MPa
θ_{actual}	90	deg
$\theta_{theoretical}$	45	deg
β	90	deg
V_{test}	956	kN
V_{dead}	0	kN
V_{R2K}	681	kN

$V_{actual\theta}$	
V_{FRP}	275
V_{steel}	0
$V_{concrete}$	681

E_f = FRP sheet elastic modulus

t_f = sheet thickness

f_{ck} = concrete characteristic cylindrical strength

w_f = FRP strip width measured orthogonally to β

p_f = FRP strip spacing measured orthogonally to β

d = beam effective depth

b_w = web section width

n_{st} = transverse reinforcement arm number

A_{st} = area (one arm) of transverse reinforcement

s_{st} = spacing of transverse reinforcement

f_{yd} = design steel yield strength

$A_{sl(total)}$ = area of longitudinal steel reinforcement

θ_{actual} = actual crack angle as measured in test

$\theta_{theoretical}$ = assumed crack angle as measured from the beam axis

β = angle of strip or sheet to the beam axis

V_{test} = applied failure load

Test specimen 2T04

input		
E_f	227	Gpa
t_f	0.33	mm
f_{ck}	29.37	MPa
w_f	254	mm
p_f	356	mm
d	1096	mm
b_w	356	mm
n_{st}	2	
A_{st}	129	mm^2
s_{st}	508	mm
f_{yd}	350	MPa
θ_{actual}	40	deg
$\theta_{theoretical}$	45	deg
β	90	deg
V_{test}	1225	kN
V_{dead}	18.3	kN
V_{R2K}	677	kN

$V_{actual\theta}$	
V_{FRP}	566
V_{steel}	209
$V_{concrete}$	468

E_f = FRP sheet elastic modulus

t_f = sheet thickness

f_{ck} = concrete characteristic cylindrical strength

w_f = FRP strip width measured orthogonally to β

p_f = FRP strip spacing measured orthogonally to β

d = beam effective depth

b_w = web section width

n_{st} = transverse reinforcement arm number

A_{st} = area (one arm) of transverse reinforcement

s_{st} = spacing of transverse reinforcement

f_{yd} = design steel yield strength

$A_{sl(total)}$ = area of longitudinal steel reinforcement

θ_{actual} = actual crack angle as measured in test

$\theta_{theoretical}$ = assumed crack angle as measured from the beam axis

β = angle of strip or sheet to the beam axis

V_{test} = applied failure load

Test specimen 3IT05

input		
E_f	227	Gpa
t_f	0.165	mm
f_{ck}	25.39	MPa
w_f	305	mm
p_f	356	mm
d	1150	mm
h_w	1067	mm
b_w	356	mm
n_{st}	2	
A_{st}	129	mm^2
s_{st}	254	mm
f_{yd}	350	MPa
θ_{actual}	45	deg
$\theta_{theoretical}$	45	deg
β	90	deg
V_{test}	1134	kN
V_{dead}	13	kN
V_{R2K}	906	kN

$V_{actual0}$	
V_{FRP}	241
V_{steel}	368
$V_{concrete}$	538

E_f = FRP sheet elastic modulus

t_f = sheet thickness

f_{ck} = concrete characteristic cylindrical strength

w_f = FRP strip width measured orthogonally to β

p_f = FRP strip spacing measured orthogonally to β

d = beam effective depth

h_w = beam web depth

b_w = web section width

n_{st} = transverse reinforcement arm number

A_{st} = area (one arm) of transverse reinforcement

s_{st} = spacing of transverse reinforcement

f_{yd} = design steel yield strength

$A_{sl(total)}$ = area of longitudinal steel reinforcement

θ_{actual} = actual crack angle as measured in test

$\theta_{theoretical}$ = assumed crack angle as measured from the beam axis

β = angle of strip or sheet to the beam axis

V_{test} = applied failure load

Test specimen 3IT06

input		
E_f	227	Gpa
t_f	0.165	mm
f_{ck}	23.33	MPa
w_f	305	mm
p_f	356	mm
d	1150	mm
h_w	1067	mm
b_w	356	mm
n_{st}	2	
A_{st}	129	mm^2
s_{st}	254	mm
f_{yd}	350	MPa
θ_{actual}	39	deg
$\theta_{theoretical}$	45	deg
β	90	deg
V_{test}	1116	kN
V_{dead}	9.3	kN
V_{R2K}	899	kN

$V_{actual\theta}$	
V_{FRP}	226
V_{steel}	454
$V_{concrete}$	445

E_f = FRP sheet elastic modulus

t_f = sheet thickness

f_{ck} = concrete characteristic cylindrical strength

w_f = FRP strip width measured orthogonally to β

p_f = FRP strip spacing measured orthogonally to β

d = beam effective depth

h_w = beam web depth

b_w = web section width

n_{st} = transverse reinforcement arm number

A_{st} = area (one arm) of transverse reinforcement

s_{st} = spacing of transverse reinforcement

f_{yd} = design steel yield strength

$A_{sl(total)}$ = area of longitudinal steel reinforcement

θ_{actual} = actual crack angle as measured in test

$\theta_{theoretical}$ = assumed crack angle as measured from the beam axis

β = angle of strip or sheet to the beam axis

V_{test} = applied failure load

Test specimen 4IT07

input		
E_f	227	Gpa
t_f	0.33	mm
f_{ck}	26.27	MPa
w_f	305	mm
p_f	356	mm
d	1150	mm
h_w	1067	mm
b_w	356	mm
n_{st}	2	
A_{st}	129	mm^2
s_{st}	254	mm
f_{yd}	350	MPa
θ_{actual}	44	deg
$\theta_{theoretical}$	45	deg
β	90	deg
V_{test}	1110	kN
V_{dead}	9.2	kN
V_{R2K}	909	kN

$V_{actual\theta}$	
V_{FRP}	210
V_{steel}	381
$V_{concrete}$	528

E_f = FRP sheet elastic modulus

t_f = sheet thickness

f_{ck} = concrete characteristic cylindrical strength

w_f = FRP strip width measured orthogonally to β

p_f = FRP strip spacing measured orthogonally to β

d = beam effective depth

h_w = beam web depth

b_w = web section width

n_{st} = transverse reinforcement arm number

A_{st} = area (one arm) of transverse reinforcement

s_{st} = spacing of transverse reinforcement

f_{yd} = design steel yield strength

$A_{sl(total)}$ = area of longitudinal steel reinforcement

θ_{actual} = actual crack angle as measured in test

$\theta_{theoretical}$ = assumed crack angle as measured from the beam axis

β = angle of strip or sheet to the beam axis

V_{test} = applied failure load

References

ACI 318-05 (2005). "Building Code Requirements for Structural Concrete." American Concrete Institute. Farmington Hills, Michigan.

ACI 440.2R-02 (2002). "Guide for the Design and Construction of Externally Bonded FRP Systems for Strengthening Concrete Structures." American Concrete Institute. Farmington Hills, Michigan.

BS EN 1992-1-1 (2004). "Eurocode 2: Design of Concrete Structures – Part 1-1: General Rules and Rules for Buildings." (British Standard). European Committee for Standardization (CEN). Brussels.

CSA S806-02 (2002). "Design and Construction of Building Components with Fibre-Reinforced Polymers." Canadian Standards Association. Toronto, Ontario, Canada.

FIB Bulletin 14 (2001). "Externally Bonded FRP reinforcement for RC Structures." Prepared by Task Group 9.3 of the International Federation for Structural Concrete. Lausanne, Switzerland.

Higgins, C., Miller, T.H., Rosowsky, D.V., Yim, S.C., Potisuk, T., Daniels, T.K., Nicholas, B.S., Robelo, M.J., Lee, A-Y, and R.W. Forrest, (2004). "Assessment Methodology for Diagonally Cracked Reinforced Concrete Deck Girders." *Report No. FHWA-OR-RD-05-04*, Federal Highway Administration, Washington, D. C.

JSCE #41 (2001). "Recommendation for Upgrading of Concrete Structures with Use of Continuous Fiber Sheets." Japan Society of Civil Engineers. Concrete Engineering Series. http://www.jsce-int.org/.

Miyauchi, K., S. Inoue, S. Nishibayashi, and Y, Tanaka, (1997). "Shear Behavior of Reinforced Concrete Beam Strengthened with CFRP Sheet." *Transactions of the Japan Concrete Institute*, Vol.19, pp. 97-104.

Monti, G. and M.A. Liotta, (2005). "FRP-Strengthening in Shear: Tests and Design Equations." *Proceedings of the 7th International Symposium on Fiber-Reinforced Polymer (FRP) Reinforcement for Concrete Structures*, Vol. 1, pp. 543-562.

Tumialan, G., K. Nakano, H. Fukuyama, and A. Nanni, (2001). "Japanese and North American Guidelines for Strengthening Concrete Structures with FRP: A Comparative Review of Shear Provisions." Non-metallic Reinforcement for Concrete Structures-FRPRCS-5, Cambridge, UK

APPENDIX G: APPLICATION OF CFRP FOR SHEAR STRENGTHENING OF AN ODOT BRIDGE

Application of CFRP for Shear Strengthening of an ODOT Bridge

The case study is performed for bridge #07743A on Interstate 5 southbound (ADTT >5000). The bridge drawings are shown in Fig. AppG1. Based on field inspection of the bridge, diagonal cracking was observed in the main girders at a location 4 ft from the centerline of the bent cap on the main span (between the bents). This section of the main girders was considered for CFRP shear strengthening to meet ODOT Table 4 permit loads. Due to the configuration of the bridge, both positive and negative moments are generated at the section. The LRFR approach was used to compute the capacity and demands on the section. Capacity was determined using MCFT with the available stirrup and flexural steel at the section. The moment and shear demands on the section were determined using the ODOT rating vehicles that represent Table 4 loads as shown in Fig. AppG2. For the rating vehicle case, the LRFR uses single lane loaded distribution factors and load factors that reflect the condition that the single-trip permit will be mixed with traffic. The following input parameters were determined and used for the bridge at the section 4 ft from the bent.:

LOADS
Self-weight of Components DC=1.25 kip/ft
Self-weight of wearing surface DW=0.3 kip/ft
Distribution factors for shear g_v=0.695 based on single lane loaded (lever rule case)
Distribution factors for moment g_m=0.695 based on single lane loaded (lever rule case)
Dead load factor for weight of components γ_{DC}= 1.25
Dead load factor weight of wearing surface γ_{DW} = 1.5
Vehicle load factor γ_L = 1.5 for STP mixed with traffic in ADTT>5000
Impact factor = 1.20 (applied to vehicle load effects only)

RESISTANCE
Concrete compressive strength =3300 psi
Steel yield = 40,000 psi (intermediate grade ASTM A305)
Available flexural steel in deck =5.38 in^2
Available flexural steel in web =4.43 in^2
Stirrup size = #4
Stirrup spacing = 12 in.
Stem width = 13 in.
Moment arm for shear with deck in compression = 31.6 in.
Moment arm for shear with deck in tension = 31.1 in.
Resistance factor for moment and shear ϕ=0.9
Condition factor = ϕ_c=0.85 for “significantly cracked”

The shear-moment capacity envelope and the factored shear-moment load effects from the Table 4 vehicle models (combined with factored dead loads) are shown in Fig. AppG3. As seen in this figure, there is not adequate capacity to carry Table 4 STP (exaggerated due to the use of the condition factor). An additional 13 kips of shear capacity is required.

To develop an additional 13 kips of shear capacity, CFRP strips will be bonded to the surface of the stem. The ACI 440 approach will be used to determine the capacity of the CFRP. The

concrete and steel contributions are more precisely computed using the MCFT procedure followed above. The following CFRP properties were used:

Material = Mbrace CF 130
E_f = 33,000,000 psi
ε_{fu} = 0.017 in/in
t_f = 0.0065 in.
Select strip width w_f = 6 in. (strips come in 24 in. wide rolls so use integer multiple that does not waste material i.e. 2, 4, 6, or 12 in. wide strips)

For the FRP strip width selected (6 in.), the gap between strips can be estimated for an assumed 45° crack angle at failure, to ensure the crack will be crossed by ***at least*** one strip at midheight of the web. The spacing between strips to ensure this condition is:

$$g = \frac{1}{2}\left(\frac{h_w}{\tan\theta} - 3w_f \right) \qquad \text{[1.AppG]}$$

where g (in.) is the gap spacing between FRP strips, h_w (in.) is the height of the web, θ is the crack angle, and w_f (in.) is the FRP strip width. The required gap was 6 in. This results in CFRP strip spacing of 12 in. The gap permits inspection and/or monitoring of the concrete condition in the area of the CFRP strengthening.

The FRP contribution to the shear capacity was computed as:

$$V_f\,(lb) = \frac{A_{fv} f_{fe} (\sin\alpha + \cos\alpha) d_f}{s_f} \qquad \text{[2.AppG]}$$

where α is the angle of inclination of the FRP stirrups (=90^o) , d_f (in.) is the depth of FRP shear reinforcement as defined in Fig. AppG4 (=26.4 in. from deck soffitt to center of gravity of tension steel in web), s_f (in.) is the spacing of the FRP strips (12 in.), and A_{fv} (in.^{2}) is the area of the FRP shear reinforcement and is calculated as:

$$A_{fv} = 2nt_f w_f \qquad \text{[2.1.AppG]}$$

where n is the number of FRP plies (=1) and t_f (in.) is the nominal thickness of one ply of the FRP reinforcement (=0.0065 in.), and w_f (in.) is the width of the FRP reinforcing plies (=6 in.), A_{fv} was computed as 0.078 in^2;

f_{fe} (psi) is the effective stress in the FRP (i.e. the stress magnitude at failure) and was calculated as:

$$f_{fe} = \varepsilon_{fe} E_f \qquad \text{[2.2.AppG]}$$

where ε_{fe} (in./in.) is the strain level in the FRP, and is calculated, for bonded u-wraps or face plies as:

$$\varepsilon_{fe} = \kappa_v \varepsilon_{fu} \le 0.004 \qquad \text{[2.2.1.AppG]}$$

where κ_v is the bond dependent coefficient for shear calculated as:

$$\kappa_v = \frac{k_1 k_2 L_e}{468\varepsilon_{fu}} \le 0.75 \qquad \text{[2.2.1.1.AppG]}$$

where k_1 is the modification factor applied to κ_v to account for the concrete strength and is calculated as:

$$k_1 = \left(\frac{f_c'}{4000}\right)^{\frac{2}{3}} \qquad \text{[2.2.1.1a.AppG]}$$

where f'_c (psi) is the specified compressive strength of concrete; and where k_2 is the modification factor applied to κ_v to account for the wrapping scheme and is calculated as:

$$k_2 = \frac{d_f - L_e}{d_f} \qquad \text{[2.2.1.1b.AppG]}$$

where L_e (in.) is the active bond length of FRP laminate and is calculated as:

$$L_e = \frac{2500}{\left(nt_f E_f\right)^{0.58}} \qquad \text{[2.2.1.1c.AppG]}$$

where E_f (psi) is the tensile modulus of elasticity of FRP. Applying these formulae, the following were calculated:
L_e = 2.02 in.
k_2 = 0.923
k_1 = 0.880
κ_v = 0.206
ε_{fe} = 0.0035 < 0.004 in/in
f_{fe} = 115.8 ksi

The total CFRP shear contribution was then computed as V_f = 19.8 kips which is greater than the required 13 kips. No significant refinement is needed. The strips should not be spaced any wider or the spacing limits of Eq. 1.AppG will be violated.

The resulting CFRP strip design was applied over a length of +/- one half of the overall girder height centered about the location considered (4 ft from bent) and the design sketch is shown in Fig. AppG5a. As seen in this sketch, the design appears reasonable, and if cracks form in this area not exactly at the section considered, the cracks will be crossed by at least one strip as illustrated in Fig. AppG5b.

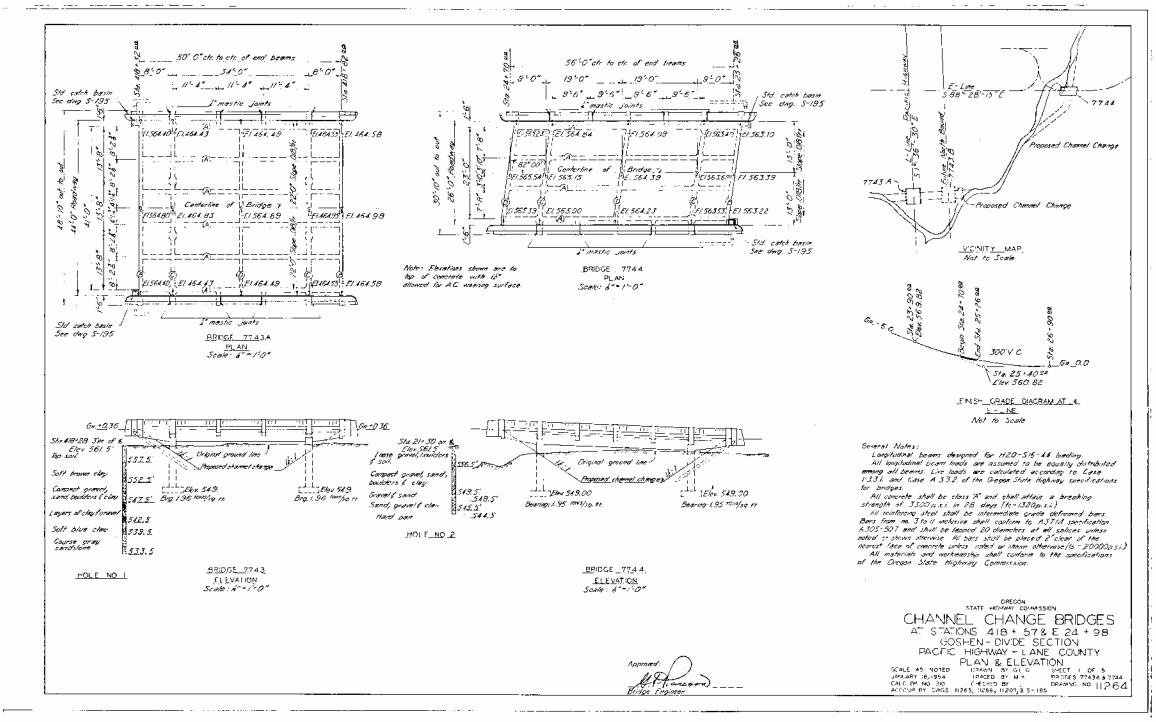

Fig. AppG1a – Overall view of bridge # 07743A (Drawing 11264).

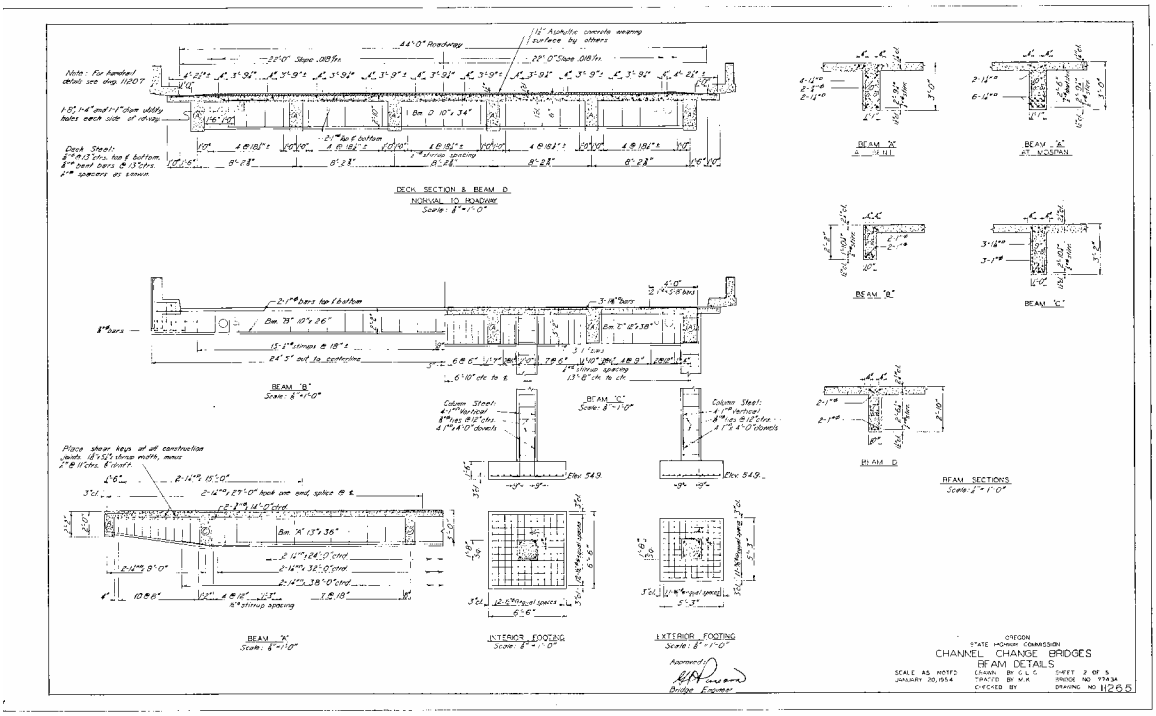

Fig. AppG1b – Girder details for bridge # 07743A (Drawing 11265).

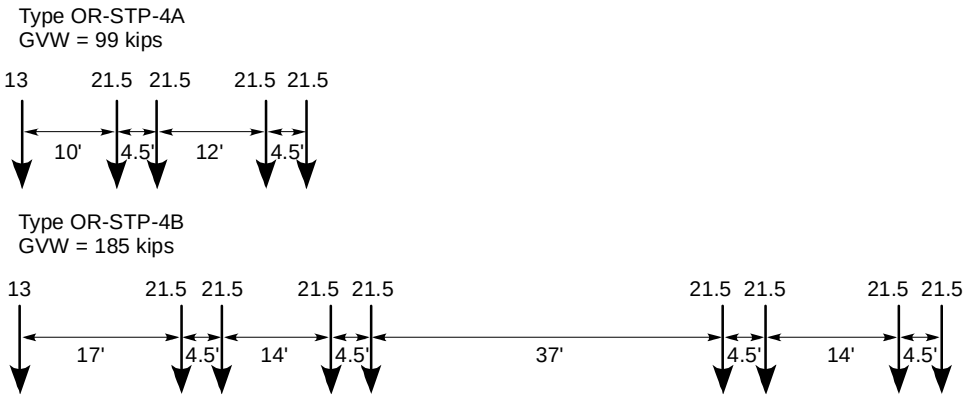

Fig. AppG2 – ODOT rating vehicles representing weight table 4.

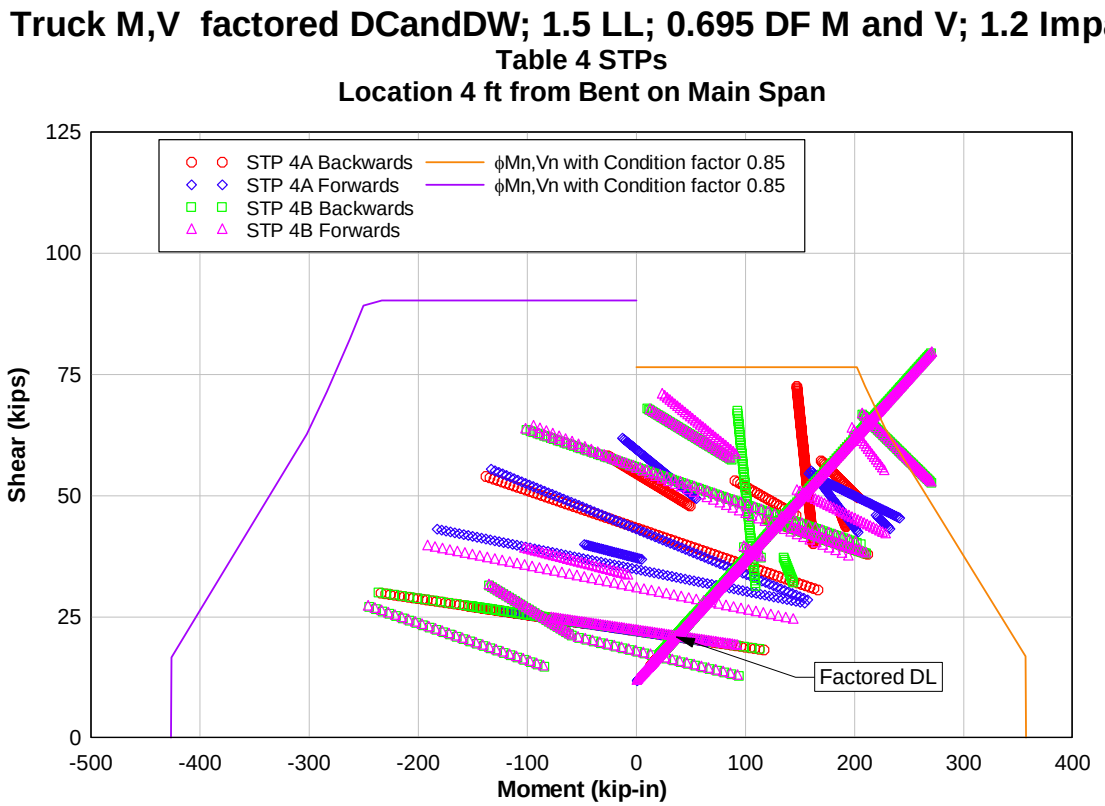

Fig. AppG3 – Factored moment-shear interactions and MCFT resistance.

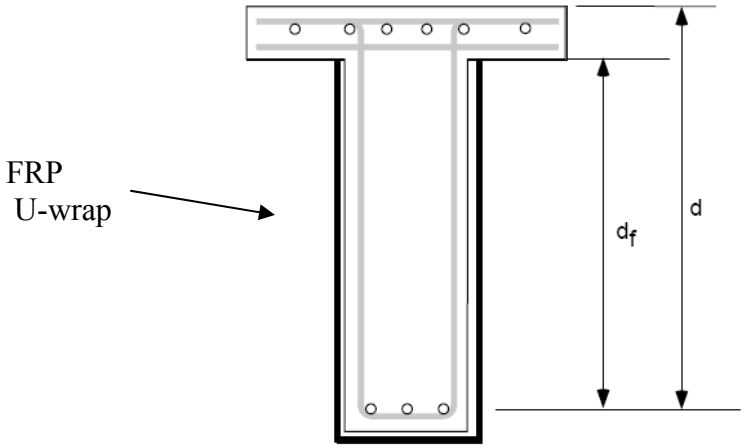

Fig. AppG4 - Graphical definition of d_f from ACI-440.

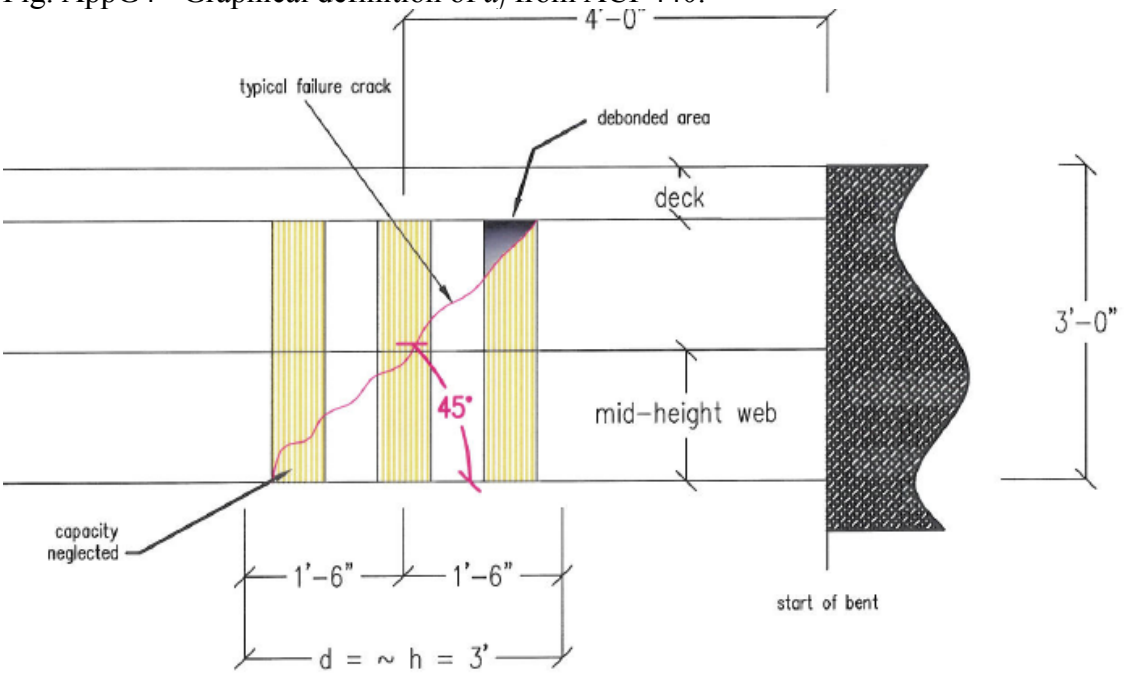

Fig. AppG5a – Design sketch of CFRP strengthening of main girder section 4 ft from bent.

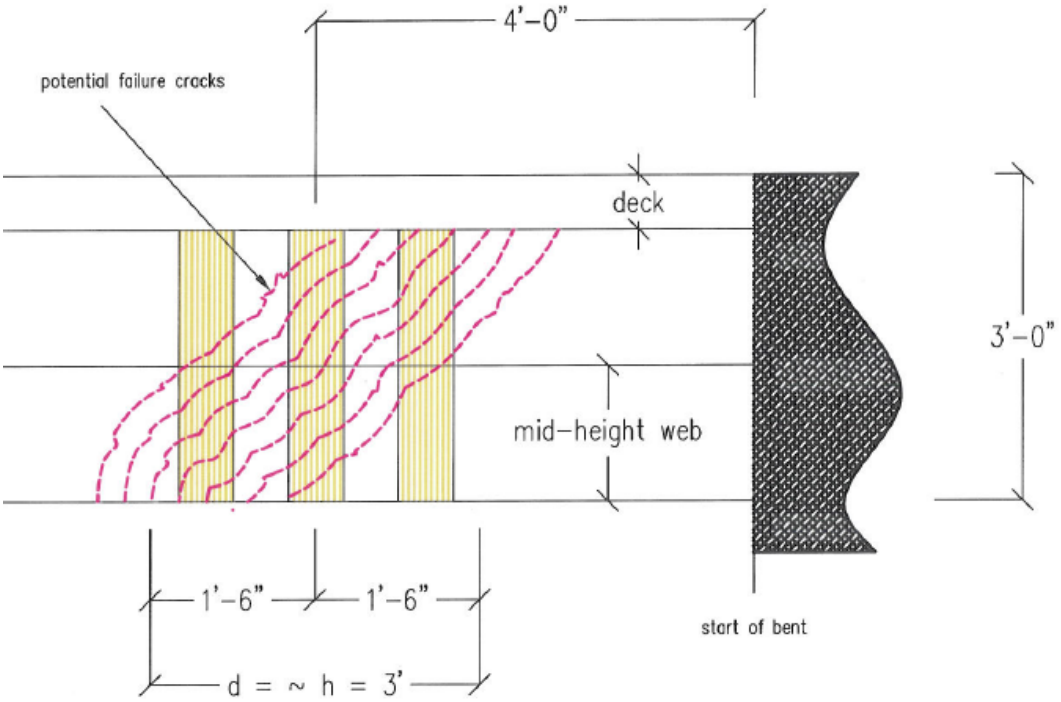

Fig. AppG5b – Illustration of CFRP design providing at least 1 strip crossing potential diagonal cracks at midheight of the stem near section 4 ft from bent.